



life

Prostate Cancer

Edited by
Ana Faustino and Paula A. Oliveira
Printed Edition of the Special Issue Published in *Life*

Prostate Cancer

Prostate Cancer

Editors

Ana Faustino

Paula A. Oliveira

MDPI • Basel • Beijing • Wuhan • Barcelona • Belgrade • Manchester • Tokyo • Cluj • Tianjin



Editors

Ana Faustino

Department of Zootechnics

University of Évora

Évora

Portugal

Paula A. Oliveira

Departamento de Ciências

Veterinárias

Universidade de

Trás-os-Montes e Alto Douro

Vila Real

Portugal

Editorial Office

MDPI

St. Alban-Anlage 66

4052 Basel, Switzerland

This is a reprint of articles from the Special Issue published online in the open access journal *Life* (ISSN 2075-1729) (available at: www.mdpi.com/journal/life/special_issues/pros.can).

For citation purposes, cite each article independently as indicated on the article page online and as indicated below:

LastName, A.A.; LastName, B.B.; LastName, C.C. Article Title. *Journal Name* **Year**, Volume Number, Page Range.

ISBN 978-3-0365-7085-3 (Hbk)

ISBN 978-3-0365-7084-6 (PDF)

© 2023 by the authors. Articles in this book are Open Access and distributed under the Creative Commons Attribution (CC BY) license, which allows users to download, copy and build upon published articles, as long as the author and publisher are properly credited, which ensures maximum dissemination and a wider impact of our publications.

The book as a whole is distributed by MDPI under the terms and conditions of the Creative Commons license CC BY-NC-ND.

Contents

Laura Nalleli Garrido Castillo, Arnaud Mejean, Philippe Vielh, Julien Anract, Alessandra Decina and Bertrand Nalpas et al. Predictive Value of Circulating Tumor Cells Detected by ISET® in Patients with Non-Metastatic Prostate Cancer Undergoing Radical Prostatectomy Reprinted from: <i>Life</i> 2022 , <i>12</i> , 165, doi:10.3390/life12020165	1
Sandra M. Rocha, Inês Sousa, Inês M. Gomes, Patrícia Arinto, Pedro Costa-Pinheiro and Eduarda Coutinho et al. Promoter Demethylation Upregulates <i>STEAP1</i> Gene Expression in Human Prostate Cancer: In Vitro and In Silico Analysis Reprinted from: <i>Life</i> 2021 , <i>11</i> , 1251, doi:10.3390/life11111251	15
Richard Y. Ball, Ryan Cardenas, Mark S. Winterbone, Marcelino Y. Hanna, Chris Parker and Rachel Hurst et al. The Urine Biomarker PUR-4 Is Positively Associated with the Amount of Gleason 4 in Human Prostate Cancers Reprinted from: <i>Life</i> 2021 , <i>11</i> , 1172, doi:10.3390/life11111172	27
Bruno Mendes, Inês Domingues, Augusto Silva and João Santos Prostate Cancer Aggressiveness Prediction Using CT Images Reprinted from: <i>Life</i> 2021 , <i>11</i> , 1164, doi:10.3390/life11111164	39
Zachary Kaplan, Steven P. Zielske, Kristina G. Ibrahim and Frank C. Cackowski Wnt and -Catenin Signaling in the Bone Metastasis of Prostate Cancer Reprinted from: <i>Life</i> 2021 , <i>11</i> , 1099, doi:10.3390/life11101099	55
Gerit Theil, Carlotta Lindner, Joanna Bialek and Paolo Fornara Association of Circulating Tumor Cells with Inflammatory and Biomarkers in the Blood of Patients with Metastatic Castration-Resistant Prostate Cancer Reprinted from: <i>Life</i> 2021 , <i>11</i> , 664, doi:10.3390/life11070664	65
Ivana Samaržija Site-Specific and Common Prostate Cancer Metastasis Genes as Suggested by Meta-Analysis of Gene Expression Data Reprinted from: <i>Life</i> 2021 , <i>11</i> , 636, doi:10.3390/life11070636	81
Bartosz Małkiewicz, Kuba Ptaszkowski, Klaudia Knecht, Adam Gurwin, Karol Wilk and Paweł Kielb et al. External Validation of the Briganti Nomogram to Predict Lymph Node Invasion in Prostate Cancer—Setting a New Threshold Value Reprinted from: <i>Life</i> 2021 , <i>11</i> , 479, doi:10.3390/life11060479	97
Hana Sedláčková, Olga Dolejšová, Milan Hora, Jiří Ferda, Ondřej Hes and Ondřej Topolčan et al. Prostate Cancer Diagnostic Algorithm as a “Road Map” from the First Stratification of the Patient to the Final Treatment Decision Reprinted from: <i>Life</i> 2021 , <i>11</i> , 324, doi:10.3390/life11040324	107
Diana Nitusca, Anca Marcu, Alis Dema, Loredana Balacescu, Ovidiu Balacescu and Razvan Bardan et al. Long Noncoding RNA NEAT1 as a Potential Candidate Biomarker for Prostate Cancer Reprinted from: <i>Life</i> 2021 , <i>11</i> , 320, doi:10.3390/life11040320	117

**Vanessa Sánchez-Martínez, Cristina Buigues, Rut Navarro-Martínez, Laura García-Villodre,
Noura Jeghalef and María Serrano-Carrascosa et al.**

Analysis of Brain Functions in Men with Prostate Cancer under Androgen Deprivation
Therapy: A One-Year Longitudinal Study

Reprinted from: *Life* **2021**, *11*, 227, doi:10.3390/life11030227 **127**

Communication

Predictive Value of Circulating Tumor Cells Detected by ISET[®] in Patients with Non-Metastatic Prostate Cancer Undergoing Radical Prostatectomy

Laura Nalleli Garrido Castillo ^{1,2,†}, Arnaud Mejean ^{3,†}, Philippe Vielh ^{4,†} , Julien Anract ^{1,5}, Alessandra Decina ⁶, Bertrand Nalpas ⁷, Naoual Benali-Furet ², Isabelle Desitter ⁶ and Patrizia Paterlini-Bréchot ^{1,6,8,*} 

- ¹ Institut Necker Enfants Malades (INEM), INSERM U1151, Faculté de Médecine, Université de Paris, 75015 Paris, France; laura.garrido-castillo@inserm.fr (L.N.G.C.); julien.anract@aphp.fr (J.A.)
² INSERM U807, Faculté de Médecine, Université de Paris, 75015 Paris, France; naoual.furet@bbox.fr
³ Service d'Urologie, Hôpital Européen Georges Pompidou, 75015 Paris, France; arnaud.mejean@aphp.fr
⁴ Medipath and American Hospital of Paris, 92200 Paris, France; ph.vielh@outlook.com
⁵ Service d'Urologie, Hôpital Cochin, 75005 Paris, France
⁶ Rarecells Diagnostics, 75280 Paris, France; alessandra.decina@rarecells.com (A.D.); isabelle.desitter@rarecells.com (I.D.)
⁷ Service d'addictologie, Université de Montpellier, 34090 Montpellier, France; bertrand.nalpas@inserm.fr
⁸ Laboratoires de Biochimie Hôpital Necker-Enfants Malades, 75015 Paris, France
* Correspondence: patrizia.paterlini@inserm.fr
† These authors contributed equally to this work.

Citation: Garrido Castillo, L.N.; Mejean, A.; Vielh, P.; Anract, J.; Decina, A.; Nalpas, B.; Benali-Furet, N.; Desitter, I.; Paterlini-Bréchot, P. Predictive Value of Circulating Tumor Cells Detected by ISET[®] in Patients with Non-Metastatic Prostate Cancer Undergoing Radical Prostatectomy. *Life* **2022**, *12*, 165. <https://doi.org/10.3390/life12020165>

Academic Editors: Ana Faustino and Paula A. Oliveira

Received: 10 January 2022

Accepted: 20 January 2022

Published: 22 January 2022

Publisher's Note: MDPI stays neutral with regard to jurisdictional claims in published maps and institutional affiliations.



Copyright: © 2022 by the authors. Licensee MDPI, Basel, Switzerland. This article is an open access article distributed under the terms and conditions of the Creative Commons Attribution (CC BY) license (<https://creativecommons.org/licenses/by/4.0/>).

Abstract: There is an unmet need for reliable biomarkers to predict prostate cancer recurrence after prostatectomy in order to better guide the choice of surgical treatment. We have evaluated the predictive value of the preoperative detection of Circulating Tumor Cells (CTC) for prostate cancer recurrence after surgery. A cohort of 108 patients with non-metastatic prostate adenocarcinoma undergoing radical prostatectomy was tested for the presence of CTC before prostatectomy using ISET[®]. Disease recurrence was assessed by the increase in serum PSA level after prostatectomy. The following factors were assessed for statistical association with prostate cancer recurrence: the presence of CTC, serum PSA, Gleason score, and pT stage using univariate and multivariate analyses, with a mean follow-up of 34.9 months. Prostate cancer recurrence was significantly associated with the presence of at least 1 CTC at the preoperative time point ($p < 0.001$; Predictive value = 0.83). Conversely, the absence of prostate cancer recurrence was significantly associated with the lack of CTC detection at diagnosis (Predictive value = 1). Our multivariate analysis shows that only CTC presence is an independent risk factor associated with prostate cancer recurrence after prostatectomy ($p < 0.001$). Our results suggest that CTC detection by ISET[®] before surgery is an interesting candidate predictive marker for cancer recurrence in patients with non-metastatic PCa.

Keywords: Circulating Tumor Cell (CTC); prostate cancer (PCa); liquid biopsy; cancer recurrence

1. Introduction

According to GLOBOCAN 2020, prostate cancer (PCa) is the third cause of cancer-related death among men over 65 years. Most of the patients have an organ-confined tumor at diagnosis. Despite efforts to diagnose and treat it at early stages, biochemical recurrence (BCR) occurs in approximately 30% of patients after prostatectomy [1]. BCR is defined as a re-increase in serum PSA above >0.2 ng/mL after radical prostatectomy (RP) or <1 ng/mL after radiotherapy [2]. BCR could be due to incomplete surgical resection or small metastases in distant organs. However, BCR can occur in patients with cancer-free surgical margins, raising the hypothesis that Circulating Tumor Cells (CTC) could have been spread in the blood before prostatectomy and created micrometastases able to secrete PSA in the serum. CTC are metastatic precursors shed from primary tumors or metastasis

into the bloodstream or lymphatic system [3]. Prediction of the risk of PCa recurrence after surgery is critical for the choice of surgical option versus non-surgical approaches. Given the known drawbacks and risks of prostatectomy (e.g., sexual impotence, urinary incontinence, etc.), new markers are needed to be able to predict when the surgical resection of the prostate is able to eradicate the PCa. Currently, a restricted number of tests are used as predictors of recurrence, such as preoperative serum PSA, patient age, biopsy-based Gleason score, and number of positive biopsy cores, all of them with limited accuracy [4,5].

Patients with intermediate or high-risk localized PCa undergo systematic staging imaging (computed tomography (CT), associated with bone scintigraphy or positron emission tomography (PET), or magnetic resonance imaging (MRI)) to detect locally advanced or metastatic diseases. Patients with locally advanced or metastatic diseases do not benefit from prostatectomy [6]. However, none of these imaging techniques is predictive such as CTC could do [7]. CTC could be a useful preoperative marker for cancer recurrence after surgery, and it could allow us to better select patients who will benefit from prostatectomy and help identify those patients who should be strictly monitored and treated with adjuvant therapies after surgery to avoid BCR.

The aim of this study was to assess, in a proof of principle approach, the potential clinical value of CTC as a pre-surgery marker to help identify patients at risk of developing recurrence after surgery, thus helping patients' stratification for surgical treatment and adjuvant treatment after surgery.

Several strategies have been developed to isolate and detect CTC either by marker-dependent or marker-independent approaches. Marker-dependent methods may lead to selection biases, false positive and false negative results, due to CTC heterogeneity (cells with either epithelial or mesenchymal phenotype or undergoing a transformation from an epithelial to a mesenchymal phenotype). CellSearch[®] system, which is a marker-dependent method, is currently the FDA-cleared method for CTC enumeration (CTC cut off of ≥ 5 CTCs in 7.5 mL blood) to predict progression-free survival and overall survival in patients with metastatic PCa. Despite this, CellSearch's clinical value in non-metastatic PCa is debated [8]. In this work, we used the Isolation by Size of Tumor cells (ISET[®]) technology (Rarecells Diagnostics, Paris, France), a label-free approach, to assess whether the preoperative presence of CTC in the blood is associated with disease recurrence after surgery in patients diagnosed with non-metastatic prostate cancer.

2. Patients and Methods

2.1. Study Patient Cohort

A total of 108 patients with non-metastatic PCa undergoing radical prostatectomy were consecutively included in this study and recruited at the Necker and HEGP hospitals in Paris. See Table 1 for baseline patients' characteristics, including the administered postoperative treatments, and Figure 1 for the consort flow diagram. All patients were tested for the presence of CTC using ISET[®] before surgery and before, or at least three weeks after, any medical invasive procedure (digital rectal examination, transrectal ultrasound, biopsy, etc.) which could iatrogenically spread CTC in blood. All patients had been diagnosed with PCa by biopsy. Inclusion criteria were: patients with newly diagnosed, untreated prostate cancer undergoing prostatectomy; not having been diagnosed with a different tumor before the inclusion; agreeing to participate in the study; having the French Social Security affiliation.

Seventy-seven patients (72.6%) had PSA ≥ 15 ng/mL at diagnosis. The majority of patients had a Gleason score of 7 or more at the biopsy (58/107 = 54.2%). The majority of patients had pT stage T2b or higher (87/108 = 80.6%) at the pathologic analysis after prostatectomy (Table 1).

Table 1. Patient clinical and pathological baseline characteristics.

Clinical Parameter		Number (%) or Median (Range)
Total patients		108 (100%)
Age (yrs)		65.1 (\pm 8.6)
Preoperative serum PSA (ng/mL)		
Mean		13.92
Median		10.0
Range		1.83–93.00
<15 ng/mL		77 (77/106 = 72.6%)
\geq 15 ng/mL		29 (29/106 = 27.4%)
Unknown		2 (2/108 = 1.9%)
Gleason Score		
\leq 6		49 (49/107 = 45.8%)
7		48 (48/107 = 44.9%)
\geq 8		10 (10/107 = 9.3%)
Unknown		1 (1/108 = 0.9%)
Pathological Stage—pT Staging		
T	T2a	21 (19.4%)
	T2b	44 (40.7%)
	T3a	23 (21.3%)
	T3b	20 (18.5%)
N	N0	103 (95.4%)
	N1	5 (4.6%)
M	M0	107 (99.1%)
	M1	1 (0.9%)
Initial treatment		
Radical prostatectomy		108 (100%)
Postoperative Treatments		
Radiotherapy + chemotherapy + ADT *		74 (68.5%)
Hormonal therapy (ADT)		10 (9.3%)
Radiotherapy		8 (7.4%)
None		16 (14.8%)

* ADT: Androgen-deprivation therapy.

The majority of patients, 92 (85.2%), were treated by radiotherapy plus chemotherapy plus androgen-deprivation therapy (ADT), while the rest of the patients received either ADT, radiotherapy or no treatment (Table 1).

The data about the prostate volume could not be collected.

Disease recurrence was defined by an increase in serum PSA level post-surgery to 0.2 ng/mL or higher in two independent tests, defined as biochemical recurrence (BCR). Patients with BCR could also be studied, in a case-by-case manner, with imaging (CT, or PET, or MRI). The median follow-up after prostatectomy was 34.9 months (range 6.3–75 months).

Fifty healthy controls were included in this study: men aged 55 to 75 yrs, without known pathology, including without BPH (Benign Prostatic Hyperplasia), agreeing to participate in the study, having the French Social Security affiliation.

Men with BPH were excluded because of the frequent association of BPH with prostate cancer.

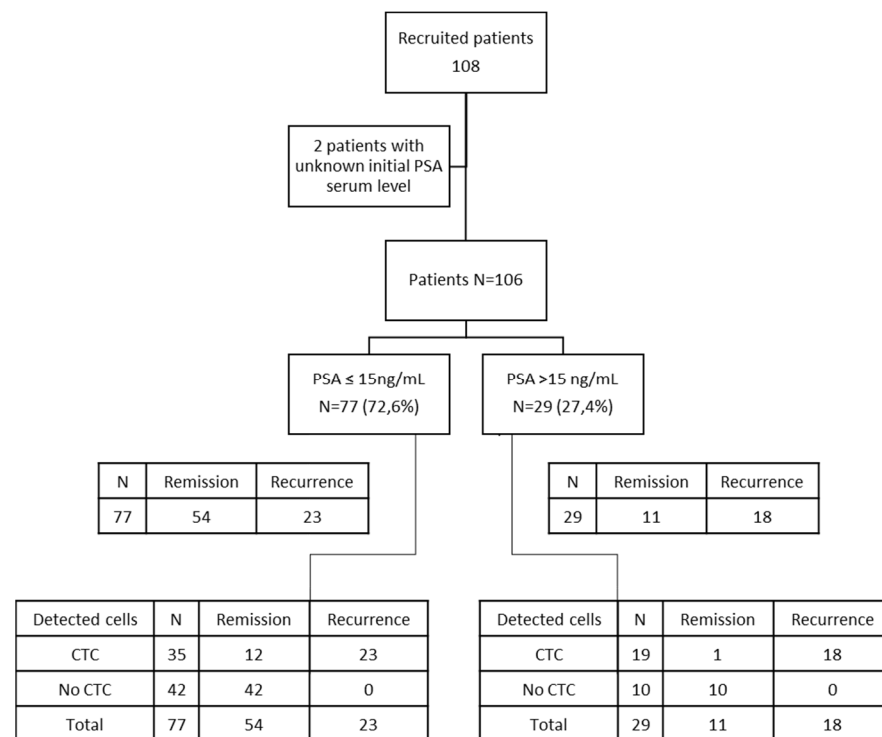


Figure 1. Consort flow diagram showing the CTC results and baseline PSA values in 106 out of 108 patients.

2.2. Circulating Tumor Cells Analysis

To evaluate the presence of CTC, peripheral blood samples (6 mL) were collected in EDTA tubes before prostatectomy far (see above) from any possible iatrogenic cause of CTC spreading. Blood was filtered using ISET[®] as described previously [9]. Briefly, blood samples were diluted with ISET[®] Buffer 1:10 and, after incubation (10 min), were filtered using the ISET[®] platform. ISET[®] membranes were then washed (PBS), dried, and stored at $-20\text{ }^{\circ}\text{C}$. Hematoxylin and eosin staining was done directly on ISET[®] membranes for cytomorphologic analysis. The blood (6 mL) from healthy controls was filtered and analyzed in the same manner.

The isolated circulating rare cells were analyzed to identify cells with fully malignant characteristics allowing us to diagnose them as Circulating Tumor Cells (CTC). The following criteria were used to characterize cell malignancy: nucleus larger than 3 calibrated pore size of the membrane ($>24\text{ }\mu\text{m}$), irregular nuclear borders, anisonucleosis, nuclear hyperchromatism, high nucleocytoplasmic ratio (ratio > 0.5), size and number of nucleoli, and presence of tridimensional sheets. CTC was then defined by the presence of at least three of these criteria [10]. Pathologists (PV and NB (acknowledged)) agreed on these criteria and did not report any discordant cell diagnosis).

2.3. Statistical Analysis

Continuous variables were compared using Student’s test or a non-parametric (Mann–Whitney) test when their distribution was skewed. Categorical variables were compared using Chi-square or the Fisher’s exact test. Multivariate analysis was done using the logistic regression method. The association of serum PSA, Gleason scores, and CTC with cancer relapse was evaluated by univariate and multivariate analysis. The cumulative survival rates were analyzed using the Kaplan–Meier method, and curves were compared using the log-rank test. All analyses were conducted in R (R Development Core Team, 2021). A p -value < 0.05 was considered statistically significant for all statistical analyses.

3. Results

Based on cytopathological analysis of the cells enriched by ISET[®], we detected CTC in 55 out of 108 (50.9%) patients, and in 0 out of 50 healthy controls. The cytopathological analysis of cells isolated by ISET[®] allowed us to categorize patients into three groups based on the number of detected CTC (0, 1 to 3, and more than 3 cancer cells) per 6 mL of blood. Table 2 shows the outcome of remission or recurrence according to the three different groups. The average CTC count in patients was 1.6 cells per 6 mL of blood, ranging from 1 to 14.

Table 2. CTC remission and recurrence according to CTC count in the 108 patients undergoing prostatectomy.

CTC Count	N	Remission	Recurrence
No CTC	53	53	0
1–3 CTC	39	7	32
>3 CTC	16	0	16

Cytopathologists noted the presence of cells having a tumor-like nucleus, damaged cytoplasm, or often incomplete criteria of malignancy. These cells, collectively named CFTC (Circulating Fragile Tumor Cells), were identified and counted. However, classical cytopathological criteria do not take them into account. Figure 2 shows an example of CTC and a CFTC.

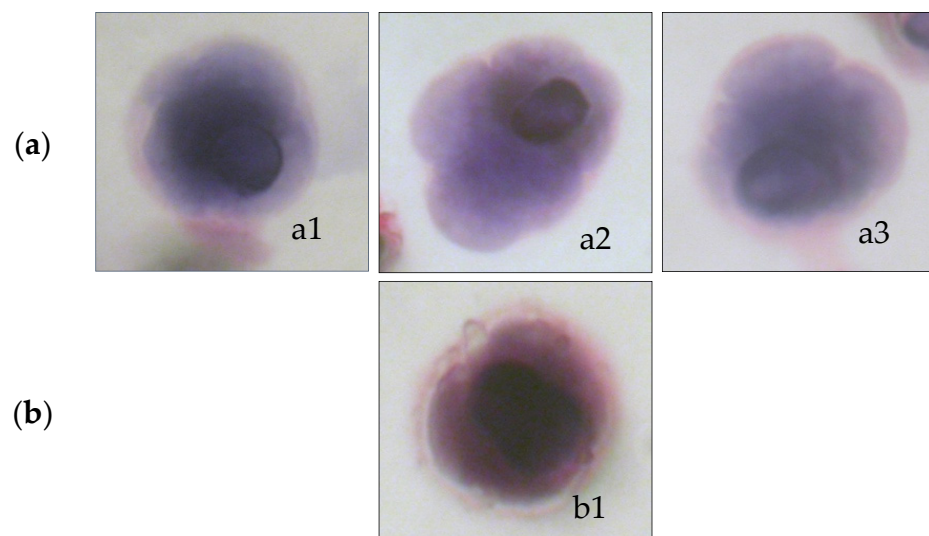


Figure 2. Cytomorphological analysis of cells isolated by ISET[®]: (a) a1, a2, and a3 illustrate circulating tumor cells (CTC) with full characteristics of tumor cells, and (b) b1 illustrates a circulating fragile tumor cell (CFTC) with a tumor-like nucleus and damaged cytoplasm.

A survival without recurrence curve analysis was performed to look at the correlation of CTC numbers and PCa recurrence. Both subgroups with CTC (1 to 3 and >3 CTC per 6 mL of blood) were associated with a significantly higher PCa recurrence than CTC free patients ($p < 0.0001$).

Figure 3 shows the survival without recurrence curve analysis depicting the correlation of CTC positivity with PCa recurrence after surgery. The correlation is statistically highly significant ($p < 0.0001$). Figure 3 (bottom) also shows the number of censored patients and recurrent cases.

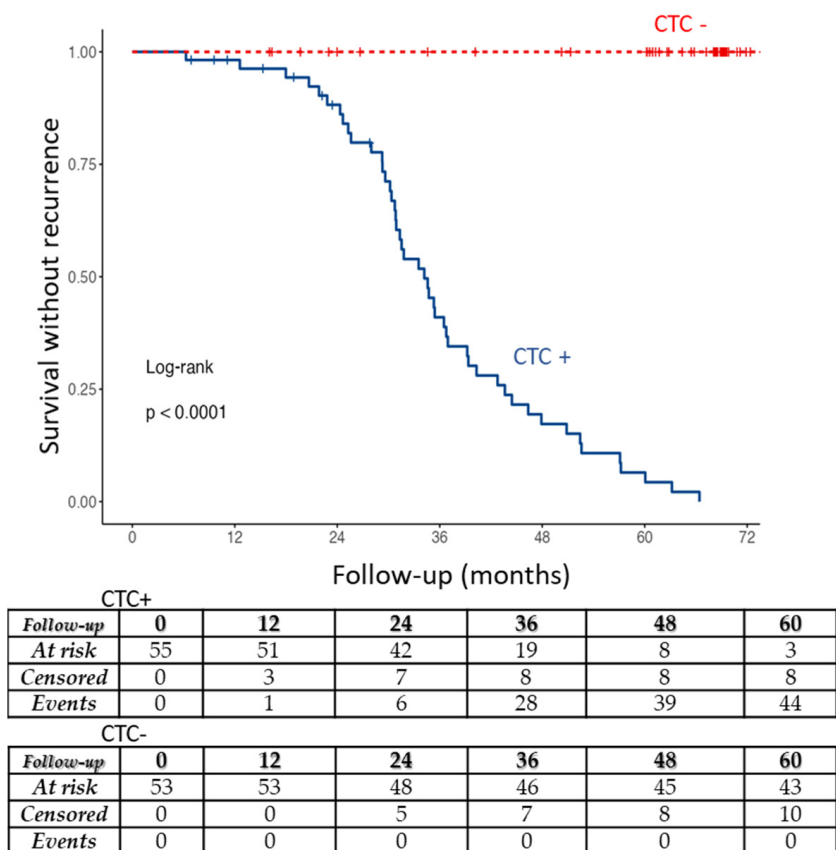


Figure 3. Survival without recurrence curve. Subgroups of patients: with CTC (CTC+), and without CTC (CTC-). The table at the bottom shows CTC+ and CTC- patients at risk of recurrence (At risk), censored patients and cases of PCa recurrence (Events) at 0, 12, 24, 36, 48, and 60 months during follow-up after prostatectomy. Risk of recurrence was highly significantly associated with CTC positivity: $p < 0.0001$. CFTC were not taken into account for this analysis.

PCa recurrence was thus significantly associated with the presence of at least 1 CTC detected before surgery ($p < 0.001$; positive predictive value = 0.83, 46/55), and the absence of recurrence was significantly associated with the lack of CTC detection (negative predictive value = 1, 53/53).

Concerning CFTC, 89 out of 108 (75.9%) patients were positive before prostatectomy. The average CFTC count in these positive individuals was 2.1, ranging from 1 to 14. Both CFTC and CTC were detected in 52 patients and only CFTC in 37 patients. Their presence was often detected along with CTC presence as only 3 patients had CTC only (without CFTC). An absence of CFTC was found in 19 patients. The predictive value for recurrence of CFTC is 0.48, far less than the value of CTC (0.83), supporting the view that they are probably dying cells not able to generate metastases, consistent with the cytopathological view.

We did not find a correlation between serum PSA at baseline and the presence or absence of CTC ($p = 0.079$). We also did not find a correlation between PSA and CTC count, taking into account all patients together ($p = 0.099$) or the two subpopulations of patients (CTC+ and CTC-) ($p = 0.553$). Figure 4 shows the scatterplot of serum PSA and CTC count (patients were divided into two categories CTC positive and CTC negative).

We observed that PSA level ≥ 15 ng/mL is significantly associated with PCa recurrence ($p = 0.002$), while Gleason score ≥ 7 was not ($p = 0.27$).

We studied the correlation between the pT staging and the presence of CTC. Patients with T2a tumors had a lower CTC positivity rate (4 CTC positive patients out of 21 T2a) ($p = 0.013$). Patients with T2b tumors or higher stage had a significantly higher CTC positivity rate (51 CTC positive patients out of 87 ($p < 0.001$)). No significant difference

in CTC frequency was found among patients with T2b, T3a, and T3b stages (T2b-59.1%, T3a-60.9%, T3b-55.0%).

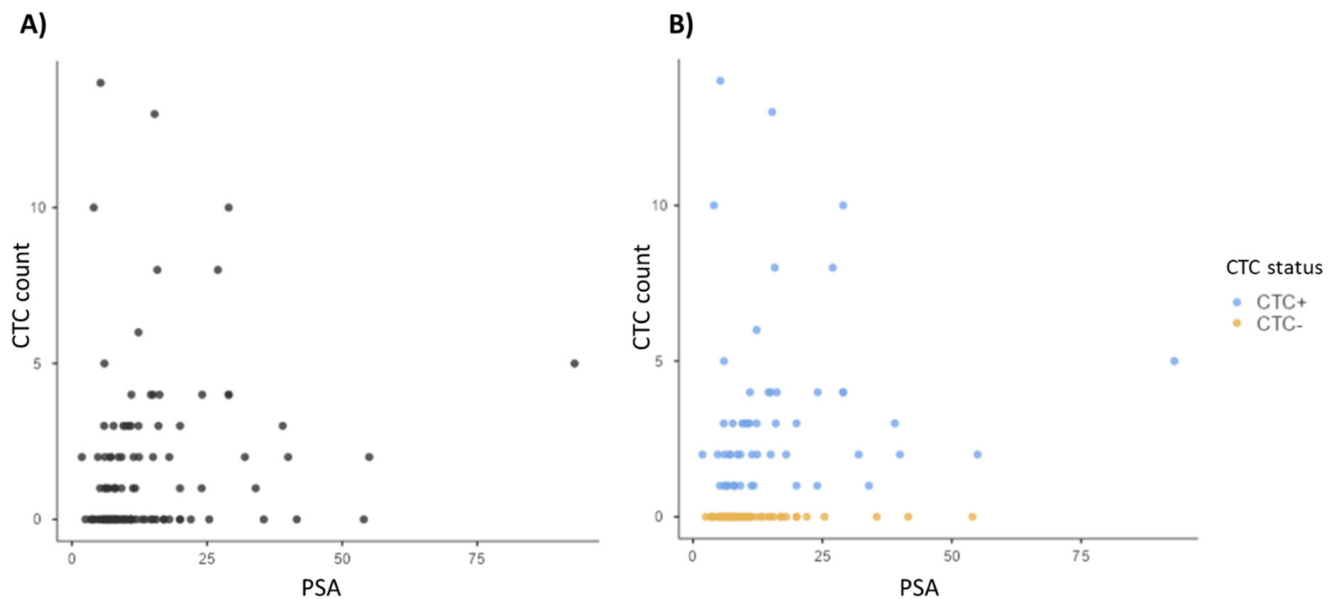


Figure 4. Scatterplots showing (A) no correlation ($p = 0.099$) between serum PSA level at baseline (ng/mL) and the CTC count (N° of CTC per 6 mL of blood) in all patients and, (B) no correlation ($p = 0.553$) between serum PSA level at baseline (ng/mL) and CTC count (N° of CTC per 6 mL of blood) in CTC positive (blue dots) and CTC negative (orange dots) patients.

To note, the CTC predictive value for the diagnosis of a tumor stage equal or greater than T2b is 0.93. In fact, out of 55 CTC positive patients, 51 were classified as stage T2b or higher. We also found that patients with tumor stage equal to or higher than T2b had a significantly higher frequency of recurrence ($p = 0.038$).

Table 3 shows the results of the statistical univariate and multivariate analysis for the association of different parameters with PCa recurrence. In the multivariate analysis, we studied the three parameters available before prostatectomy (CTC, PSA value, and Gleason score) and the pT stage obtained from the pathological analysis of the surgical sample. Only preoperative CTC detection was found to be an independent risk factor associated with PCa recurrence ($p < 0.001$).

Table 3. Statistical association of different parameters and PCa recurrence.

Prognostic Factor	<i>p</i> Value
Univariate analysis	
Gleason score 7/>7	0.27
PSA, >15 ng/mL	=0.002
Presence of CTC	<0.001 (predictive value = 0.83)
CTC positive patients in treated group	<0.001
CTC positive patients in non-treated group	0.007
≥T2b tumors (pT staging)	0.038
Multivariate analysis	
CTC presence	<0.001
PSA	0.497
Gleason score	0.172
pT stage	0.177

Notes: significant values are marked in bold. In multivariate analysis (serum PSA, Gleason, CTC, and pT stage) only preoperative CTC detection was an independent risk factor associated with PCa recurrence ($p < 0.001$).

4. Discussion

In this study, we evaluated the clinical impact of CTC detected by ISET[®] in patients with PCa undergoing prostatectomy. It is worth pointing out that ISET[®] was used to assess the cytomorphological characteristics of CTC and count them using a universally recognized diagnostic approach. Few studies evaluated the clinical impact of CTC in patients with non-metastatic PCa [8,11]. So far, the relationship between CTC before prostatectomy and PCa recurrence has not been reliably estimated due to the rarity of CTC in the blood at early cancer stages, the variable sensitivity of the methods used, and the lack of diagnostic approaches used to identify CTC. Thus, we thought of applying ISET[®], known for its extremely high sensitivity [12] and diagnostic approach to counting the CTC, to this field.

Our results show that ISET[®] could find CTC in 55 (50.9%) of the patients before prostatectomy, showing that the ISET[®] technology allows CTC enrichment at early PCa stages. Survival without recurrence curves showed that the presence of CTC, without difference between 1 to 3 CTC and more than 3 CTC per 6 mL of blood, was highly significantly associated with the risk of recurrence ($p < 0.001$).

By studying, in a multivariate analysis, all parameters which are available before prostatectomy (CTC, PSA, and Gleason score) and the pT stage, we have observed a strong correlation between the presence of CTC and cancer recurrence, with CTC being an independent risk factor significantly associated ($p < 0.001$) with PCa recurrence after prostatectomy. PCa recurrence was thus significantly associated with the presence of at least 1 CTC detected before surgery (positive predictive value = 0.83), and the absence of recurrence was significantly associated with the lack of CTC detection (negative predictive value = 1).

These very interesting results can presumably be explained by the fact that we used a marker-independent method to extract CTC from blood with high sensitivity, proven to detect CTC at early stages in prostate and other cancer types [7,13,14] and a diagnostic method to diagnose CTC.

The use of CTC as a biomarker for localized and locally advanced PCa has been limited due to technical challenges related to the CTC rarity and heterogeneity. Table 4 shows previous studies analyzing CTC presence and number in patients with non-metastatic PCa and the methods used. CTC isolation methods based on a surface marker, mainly CellSearch, are less sensitive and have lower CTC detection rates than marker-independent approaches. As we can see in Table 4, 9 out of 15 studies used a marker-dependent approach and 8 of 9 used CellSearch. A total of 4 of the 9 studies included a follow-up after surgery, and none reported a statistically significant correlation of CTC detection with PCa recurrence. However, as mentioned, marker dependent methods show a lower rate of CTC positive patients.

As a matter of fact, several publications have shown the superior sensitivity of ISET[®] (marker independent) as compared with CellSearch (marker dependent) when applied to prostate cancer and other types of cancer [15–21]. Detection rates in blood samples were: 50% vs 39% [16]; 75% vs 32% [17]; 93% vs 40% [19]; and 80% vs 23% [20], using ISET[®] and CellSearch, respectively.

Among 6 studies [22–27] using marker-dependent CTC isolation methods and reporting a CTC detection rate equal or higher than 50%, 3 did not show correlation between CTC and clinical variables, or have a follow-up. Among the remaining three studies with follow-up (from 14.2 months to 5 years), Todenhöfer et al. [22] did not study the correlation of CTC with PCa recurrence, Salami et al. [23] did not find a correlation between baseline CTC and BCR ($p = 0.10$), and Murray et al. [24] found a significant correlation of BCR with PSA, Gleason score, T3 stage, CTC positivity, and higher CTC counts ($p < 0.05$). Thus, our study confirms the results obtained by Murray et al. Furthermore, our study found a stronger association of CTC presence with BCR ($p < 0.001$), which is probably related to the specificity of the cytopathological method used to identify the CTC.

Table 4. Published studies assessing CTC counts in localized PCa.

Study	No. Patients	pT Stage	CTC Detection Method	Cutoff	CTC+ Patients (%)	Blood Sample Size	Results
(Davis et al., 2008) [28]	97	78 T2 19 T3	CellSearch	≥1 CTC/22.5 mL	20/97 (21%)	30 mL	No correlation between the number of CTC and tumor volume, pathological stage, and Gleason score.
(Maestro LM et al., 2009) [29]	24	Uninformed	CellSearch	≥2 CTC/7.5 mL	4 (14%)	10 mL	No correlation between CTC presence and tumor stage.
(Thalgott et al., 2015) [30]	20	locally advanced high risk	CellSearch	≥1 CTC	1 (5%)	7.5 mL before neoadjuvant therapy and RP	No difference in patients CTC counts compared to controls. Follow-up 8–16 weeks following RP.
(Kolostova et al., 2014) [31]	55	45 T2 10 T3	MetaCell® filtration	≥1 CTC	28 (52%)	8 mL	No correlation found with Gleason score or tumor stage.
(Shao et al., 2014) [25]	40	26 T2 13 T3 1 Tx	Near-infrared dyes	≥1 CTC	39 (97.5%)	7.5 mL	No correlation found with Gleason score, tumor stage, or PSA level.
(Pal et al., 2015) [32]	35	32 T1–T2, 3 T3	Ficoll- CellSearch	≥1 CTC	16 (49%)	30 mL	No association with clinical parameters. Median follow-up 510 days.
(Murray et al., 2016) [24]	269	Unknown	differential centrifugation + ICC	≥1 CTC	211 (79%)	8 mL	BCR was associated with PSA, Gleason score, T3 disease, CTC positivity, and higher CTC counts ($p < 0.05$). Median follow-up 5 years.
(Kuske et al., 2016) [26]	86	37 T1 45 T2 4 T3	CellSearch EPISPOT CellCollector	≥1 CTC	–37% CellSearch –54.9% CellCollect –58.7% EPISPOT	–7.5 mL-Directly from the vein –13–15 mL	CTC detected by EPISPOT correlated with tumor stage.
(Todenhöfer et al., 2016) [22]	50	37 T2 13 T3	Microfluidic device	≥1 CTC/2 mL	25 (50%)	2 mL	No correlation found with Gleason score, tumor stage, or PSA level. PCa recurrence was not studied. Median follow-up 48 months.
(Tsumura et al., 2017) [33]	59	26 T1c–T2a, 15 T2b–c, 17 T3, 1 T4	CellSearch	≥1 CTC/7.5 mL	0% (0/59) before and 11.8% (7/59) after surgery	10 mL	No correlation found with Gleason score, tumor stage, or PSA level. Median follow-up 18 months.
(Puche-Sanz et al., 2017) [34]	86	Unknown	Immune-magnetic	≥1 CTC/10 mL	16 (18.6%)	10 mL	No correlation with CTC counts. However, AR expression in tumor tissue correlated with CTC presence.
(Salami et al., 2019) [23]	26	2 pT2 15 pT3a9 pT3b	Epic Sciences	≥1	19 (73%)	10 mL	Metastasis ($p = 0.03$) was associated with baseline CTC detection while BCR ($p = 0.10$) was not. Median follow-up 14.2 months.
(Liu et al., 2020) [27]	80	5 T1c 37 T2a 11 T2b 23 T2c 4 T3a	CanPatrolTM	≥1 CTC/5 mL	44 (55%)	5 mL, before surgery	PSA levels and Gleason score had no correlation with CTC counts.
(Zapatero et al., 2020) [35]	65	1 T1 17 T2 47 T3	CellSearch	≥1 CTC	65 (7.5%) before treatment	7.5 mL	CTC status was not significantly associated with any clinical or pathologic factors. Detection of CTCs was not significantly associated with overall survival.
(Knipper et al., 2021) [36]	20	8 pT2 4 pT3a 7 pT3b 1 unknown	CellSearch	2–3 CTCs/7.5 mL	3 (15%)	7.5 mL	CTC-positive correlated with BCR-free survival (BFS). Median follow-up of 10.1 months.

Consistently with previous studies which have reported that CTC is not detectable in blood samples from healthy donors using the ISET[®] approach [7,9,10,37–48], we did not detect CTC in 50 healthy volunteers.

It is important to note that we did not include patients with BPH in the control group because BPH and prostate cancer are considered to be linked by common physiopathological factors [49] and frequently coexist in men aged < 65 years, as was shown in studies using transurethral prostatic resection [50].

Cytopathology is known to be extremely specific. As a matter of fact, to this date, 539 healthy volunteers and 200 patients with benign diseases have been tested by ISET[®] in 16 studies, setting the specificity of ISET blood cytopathology at 98.6% (10/739) [7,9,10,37–48,51]. However, its sensitivity is hard to assess, especially in the setting of circulating tumor cells analysis. A blind study that analyzed CTC in renal cell carcinomas carrying VHL mutation found the VHL mutation in all the CTCs isolated from the blood using ISET[®]. Results revealed that all the cells diagnosed as CTC by the cytopathological analysis carried the VHL mutation detected in the corresponding tumor tissue. Conversely, 104 out of 125 cells, defined as having uncertain malignant features according to pathological criteria, were, in fact, CTCs as they carried the identical VHL mutation also identified in the corresponding tumor tissue [52]. According to this study, the specificity of cytopathology was 100%, while the sensitivity was 72%.

This type of study is not possible yet in patients with prostate cancer due to the lack of suitable molecular markers. Some of them have been described as predictors of therapy response or ways of helping to guide therapies such as TMPRSS2-ERG fusion, PTEN status, presence of AR-V7 splice variant, mutations in DNA-repair genes such as BRCA2/1, etc. [53] in metastatic prostate cancer patients. However, we still do not know the genetic markers of prostate cancer that are present in all the tumor cells from the different prostate tumor types. Thus, the same type of comparative molecular versus morphological analysis that we have done in patients with kidney cancer cannot be performed in patients with prostate cancer. We are confident, anyway, that these diagnostic molecular markers will emerge in the near future.

In this study, we did not perform genetic analysis of patient DNA, nor of tumor or CTC DNA. Alterations in DNA repair pathways, such as single-nucleotide polymorphisms (SNPs) or germline mutations, are associated with PCa development, aggressiveness, and progression. Unfortunately, the rate of patients harboring these alterations at early-stage PCa is low (7–12%) [54].

Invasive tests based on genomic classifiers from tumor tissue, such as Oncotype DX Genomic Prostate Score and Decipher, are now commercially available as nomograms guiding PCa treatments and predicting metastasis and cancer mortality. Reports using those tests for predicting BCR showed that higher scores were independently associated with BCR (HR/5 units 1.14, 95% CI 1.03–1.26, $p = 0.01$) [55] with an accuracy of around 80% [56]. However, these tests require the DNA from the tumor tissue and cannot be used non-invasively and pre-surgery.

CTC characterization or subtyping by different biomarkers might help the applications of CTC in routine PCa management. Some cell markers such as EGFR, PSMA, PSA, AR [57], CD133 (stem cell marker), and E-cadherin (EMT) [31] have been used without a clear association to predict cancer outcomes. Other markers such as vimentin, PSA, and PSMA can be used for CTC characterization. However, if the expression of these markers is low or barely detectable, the CTC characterization fails. It is well known that PSA expression is specific to prostate cells but not of prostate tumor cells, and PSMA, as well as PSA, is not expressed in all prostate tumor cells. In our study, we did not perform immunolabelling of cells isolated by ISET[®], as labelling may hinder the cytopathological characteristics which have to be examined carefully by the cytopathologist to diagnose the presence of CTC. Our results show that, in our study targeting patients with newly diagnosed PCa, CTC detection by cytopathology without any other cell characterization is able to identify patients at higher risk of recurrence after prostatectomy.

An interesting point is the observation of CFTC in 75.9% of patients. We may hypothesize that the CFTCs we observed are CTCs detached from the tumor, dying because of anoikis, i.e., programmed cell death that occurs in cells upon loss of attachment to the surrounding extracellular matrix and neighboring cells. Thus, the nuclear characteristics remain “tumor-like” but the cell morphology is rapidly affected. In general, cytopathologists do not take into consideration cells that do not have a fully visible cytoplasm. However, it is natural to speculate that those possibly dying tumor cells do not have a real clinical impact on the disease outcome because of their presumed lack of viability. CFTC could derive from damages related to mechanical stress and cell–cell interactions [58]. Moreover, technical factors could have an impact on cellular morphology. Thus, more exhaustive studies have to be carried out in order to clarify the origin of the CFTCs and their significance. For now, we just want to attract attention to this finding hoping that more studies will be planned in the future targeting cells previously not described by the pathologists because they lack cellular integrity.

To conclude, our results show that CTC detection by ISET[®] before prostatectomy could be a reliable biomarker for PCa recurrence, with better predictive value than serum PSA before surgery. Studies of larger cohorts of patients with localized prostate cancer tested before prostatectomy are needed to further validate our findings.

Author Contributions: Conceptualization, P.P.-B., A.M., and P.V.; methodology, P.P.-B., P.V., N.B.-F., I.D., and B.N.; software, B.N. and A.D.; validation, P.P.-B., A.M., and P.V.; formal analysis, B.N. and A.D.; writing—original draft preparation, L.N.G.C. and P.P.-B.; writing—review and editing, L.N.G.C., J.A., and P.P.-B.; supervision, P.P.-B.; funding acquisition, P.P.-B. All authors have read and agreed to the published version of the manuscript.

Funding: This research was funded by INSERM (Institut national de la santé et de la recherche médicale).

Institutional Review Board Statement: This study was conducted according to the guidelines of the Declaration of Helsinki and approved by both the Ethical Committee of Ile de France XI (approval reference number CCP02002, approval date 11 April 2002) and the local ethics committee.

Informed Consent Statement: Informed consent was obtained from all subjects involved in the study.

Acknowledgments: We thank Nicole Brousse for her advice and contribution to the cytopathological analysis.

Conflicts of Interest: Patrizia Paterlini-Brechot is co-inventor of ISET[®] patents belonging to University Paris Descartes, INSERM, and Assistance Publique Hopitaux de Paris, exclusively licensed to Rarecells Diagnostics, France. The present study was conducted independently by academic research teams.

References

1. Pak, S.; You, D.; Jeong, I.G.; Kim, Y.S.; Hong, J.H.; Kim, C.-S.; Ahn, H. Time to biochemical relapse after radical prostatectomy and efficacy of salvage radiotherapy in patients with prostate cancer. *Int. J. Clin. Oncol.* **2019**, *24*, 1238–1246. [CrossRef] [PubMed]
2. Cornford, P.; Bellmunt, J.; Bolla, M.; Briers, E.; De Santis, M.; Gross, T.; Henry, A.M.; Joniau, S.; Lam, T.B.; Mason, M.D.; et al. EAU-ESTRO-SIOG Guidelines on Prostate Cancer. Part II: Treatment of Relapsing, Metastatic, and Castration-Resistant Prostate Cancer. *Eur. Urol.* **2017**, *71*, 630–642. [CrossRef]
3. Yang, C.; Xia, B.-R.; Jin, W.-L.; Lou, G. Circulating tumor cells in precision oncology: Clinical applications in liquid biopsy and 3D organoid model. *Cancer Cell Int.* **2019**, *19*, 341. [CrossRef]
4. Murata, Y.; Tatsugami, K.; Yoshikawa, M.; Hamaguchi, M.; Yamada, S.; Hayakawa, Y.; Ueda, K.; Momosaki, S.; Sakamoto, N. Predictive factors of biochemical recurrence after radical prostatectomy for high-risk prostate cancer. *Int. J. Urol.* **2018**, *25*, 284–289. [CrossRef] [PubMed]
5. Negishi, T.; Kuroiwa, K.; Hori, Y.; Tomoda, T.; Uchino, H.; Tokuda, N.; Furubayashi, N.; Nagase, K.; Iwai, H.; Nakamura, M. Predictive factors of late biochemical recurrence after radical prostatectomy. *Jpn. J. Clin. Oncol.* **2017**, *47*, 233–238. [CrossRef]
6. Professionals, S.-O. AU Guidelines: Prostate Cancer. Uroweb. Available online: <https://uroweb.org/guideline/prostate-cancer/> (accessed on 16 December 2021).
7. Ilie, M.; Hofman, V.; Long-Mira, E.; Selva, E.; Vignaud, J.-M.; Padovani, B.; Mouroux, J.; Marquette, C.-H.; Hofman, P. “Sentinel” Circulating Tumor Cells Allow Early Diagnosis of Lung Cancer in Patients with Chronic Obstructive Pulmonary Disease. *PLoS ONE* **2014**, *9*, e111597. [CrossRef]









8. Cao, L.; Hao, P.; Lin, D.; Li, Y.; Hu, T.; Cai, T.; Cui, S.; Wu, T. Application of Primary/Secondary Circulating Tumor Cells for the Prediction of Biochemical Recurrence in Nonmetastatic Prostate Cancer Patients following Radical Prostatectomy or Radiotherapy: A Meta-Analysis. *BioMed Res. Int.* **2021**, *2021*, 1–10. [CrossRef] [PubMed]
9. Vona, G.; Sabile, A.; Louha, M.; Sitruk, V.; Romana, S.; Schütze, K.; Capron, F.; Franco, D.; Pazzagli, M.; Vekemans, M.; et al. Isolation by Size of Epithelial Tumor Cells. *Am. J. Pathol.* **2000**, *156*, 57–63. [CrossRef]
10. Hofman, V.J.; Ilie, M.I.; Bonnetaud, C.; Selva, E.; Long, E.; Molina, T.; Vignaud, J.M.; Fléjou, J.F.; Lantuejoul, S.; Piaton, E.; et al. Cytopathologic Detection of Circulating Tumor Cells Using the Isolation by Size of Epithelial Tumor Cell Method: Promises and Pitfalls. *Am. J. Clin. Pathol.* **2011**, *135*, 146–156. [CrossRef] [PubMed]
11. Broncy, L.; Paterlini-Bréchet, P. Clinical Impact of Circulating Tumor Cells in Patients with Localized Prostate Cancer. *Cells* **2019**, *8*, 676. [CrossRef]
12. Laget, S.; Broncy, L.; Hormigos, K.; Dhingra, D.M.; BenMohamed, F.; Capiod, T.; Osteras, M.; Farinelli, L.; Jackson, S.; Paterlini-Bréchet, P. Technical Insights into Highly Sensitive Isolation and Molecular Characterization of Fixed and Live Circulating Tumor Cells for Early Detection of Tumor Invasion. *PLoS ONE* **2017**, *12*, e0169427. [CrossRef] [PubMed]
13. Ried, K.; Eng, P.; Sali, A. Screening for Circulating Tumour Cells Allows Early Detection of Cancer and Monitoring of Treatment Effectiveness: An Observational Study. *Asian Pac. J. Cancer Prev.* **2017**, *18*, 2275. [CrossRef] [PubMed]
14. Ried, K.; Tamanna, T.; Matthews, S.; Eng, P.; Sali, A. New Screening Test Improves Detection of Prostate Cancer Using Circulating Tumor Cells and Prostate-Specific Markers. *Front. Oncol.* **2020**, *10*, 582. [CrossRef] [PubMed]
15. Farace, F.; Massard, C.; Vimond, N.; Drusch, F.; Jacques, N.; Billiot, F.; Laplanche, A.; Chauchereau, A.; Lacroix, L.; Planchar, D.; et al. A direct comparison of CellSearch and ISET for circulating tumour-cell detection in patients with metastatic carcinomas. *Br. J. Cancer* **2011**, *105*, 847–853. [CrossRef]
16. Hofman, V.; Ilie, M.I.; Long, E.; Selva, E.; Bonnetaud, C.; Molina, T.; Vénissac, N.; Mouroux, J.; Vielh, P.; Hofman, P. Detection of circulating tumor cells as a prognostic factor in patients undergoing radical surgery for non-small-cell lung carcinoma: Comparison of the efficacy of the CellSearch AssayTM and the isolation by size of epithelial tumor cell method. *Int. J. Cancer* **2011**, *129*, 1651–1660. [CrossRef]
17. Ilie, M.; Szafer-Glusman, E.; Hofman, V.; Long-Mira, E.; Suttman, R.; Darbonne, W.; Butori, C.; Lalvée, S.; Fayada, J.; Selva, E.; et al. Expression of MET in circulating tumor cells correlates with expression in tumor tissue from advanced-stage lung cancer patients. *Oncotarget* **2017**, *8*, 26112–26121. [CrossRef]
18. Kallergi, G.; Politaki, E.; Alkhatani, S.; Stournaras, C.; Georgoulas, V. Evaluation of Isolation Methods for Circulating Tumor Cells (CTCs). *Cell. Physiol. Biochem.* **2016**, *40*, 411–419. [CrossRef] [PubMed]
19. Khoja, L.; Backen, A.; Sloane, R.; Menasce, L.; Ryder, D.; Krebs, M.; Board, R.; Clack, G.; Hughes, A.; Blackhall, F.; et al. A pilot study to explore circulating tumour cells in pancreatic cancer as a novel biomarker. *Br. J. Cancer* **2012**, *106*, 508–516. [CrossRef]
20. Krebs, M.G.; Hou, J.-M.; Sloane, R.; Lancashire, L.; Priest, L.; Nonaka, D.; Ward, T.H.; Backen, A.; Clack, G.; Hughes, A.; et al. Analysis of Circulating Tumor Cells in Patients with Non-small Cell Lung Cancer Using Epithelial Marker-Dependent and -Independent Approaches. *J. Thorac. Oncol.* **2012**, *7*, 306–315. [CrossRef] [PubMed]
21. Tamminga, M.; Andree, K.C.; Hiltermann, T.J.N.; Jayat, M.; Schuur, E.; van den Bos, H.; Spierings, D.C.J.; Lansdorp, P.M.; Timens, W.; Terstappen, L.W.M.M.; et al. Detection of Circulating Tumor Cells in the Diagnostic Leukapheresis Product of Non-Small-Cell Lung Cancer Patients Comparing CellSearch[®] and ISET. *Cancers* **2020**, *12*, 896. [CrossRef] [PubMed]
22. Todenhöfer, T.; Park, E.S.; Duffy, S.; Deng, X.; Jin, C.; Abdi, H.; Ma, H.; Black, P.C. Microfluidic enrichment of circulating tumor cells in patients with clinically localized prostate cancer. *Urol. Oncol. Semin. Orig. Investig.* **2016**, *34*, e9–e483. [CrossRef]
23. Salami, S.S.; Singhal, U.; Spratt, D.E.; Palapattu, G.S.; Hollenbeck, B.K.; Schonhoft, J.D.; Graf, R.; Louw, J.; Jendrisak, A.; Dugan, L.; et al. Circulating Tumor Cells as a Predictor of Treatment Response in Clinically Localized Prostate Cancer. *JCO Precis. Oncol.* **2019**, *3*, 1–9. [CrossRef] [PubMed]
24. Murray, N.P.; Aedo, S.; Fuentealba, C.; Jacob, O.; Reyes, E.; Novoa, C.; Orellana, S.; Orellana, N. Limited improvement of incorporating primary circulating prostate cells with the CAPRA score to predict biochemical failure-free outcome of radical prostatectomy for prostate cancer. *Urol. Oncol. Semin. Orig. Investig.* **2016**, *34*, e17–e430. [CrossRef]
25. Shao, C.; Liao, C.-P.; Hu, P.; Chu, C.-Y.; Zhang, L.; Bui, M.H.T.; Ng, C.S.; Josephson, D.Y.; Knudsen, B.; Tighiouart, M.; et al. Detection of Live Circulating Tumor Cells by a Class of Near-Infrared Heptamethine Carbocyanine Dyes in Patients with Localized and Metastatic Prostate Cancer. *PLoS ONE* **2014**, *9*, e88967. [CrossRef]
26. Kuske, A.; Gorges, T.M.; Tennstedt, P.; Tiebel, A.-K.; Pompe, R.; Preißer, F.; Prues, S.; Mazel, M.; Markou, A.; Lianidou, E.; et al. Improved detection of circulating tumor cells in non-metastatic high-risk prostate cancer patients. *Sci. Rep.* **2016**, *6*, 39736. [CrossRef]
27. Liu, H.; Ding, J.; Wu, Y.; Wu, D.; Qi, J. Prospective Study of the Clinical Impact of Epithelial and Mesenchymal Circulating Tumor Cells in Localized Prostate Cancer. *Cancer Manag. Res.* **2020**, *12*, 4549–4560. [CrossRef] [PubMed]
28. Davis, J.W.; Nakanishi, H.; Kumar, V.S.; Bhadkamkar, V.A.; McCormack, R.; Fritsche, H.A.; Handy, B.; Gornet, T.; Babaian, R.J. Circulating Tumor Cells in Peripheral Blood Samples From Patients With Increased Serum Prostate Specific Antigen: Initial Results in Early Prostate Cancer. *J. Urol.* **2008**, *179*, 2187–2191. [CrossRef] [PubMed]
29. Maestro, L.M.; Sastre, J.; Rafael, S.B.; Veganzones, S.B.; Vidaurreta, M.; Martin, M.; Olivier, C.; De La Orden, V.B.; Garcia-Saenz, J.A.; Alfonso, R.; et al. Circulating tumor cells in solid tumor in metastatic and localized stages. *Anticancer Res.* **2009**, *29*, 4839–4843.

30. Thalgott, M.; Rack, B.; Horn, T.; Heck, M.M.; Eiber, M.; Kübler, H.; Retz, M.; Gschwend, J.E.; Andergassen, U.; Nawroth, R. Detection of Circulating Tumor Cells in Locally Advanced High-risk Prostate Cancer during Neoadjuvant Chemotherapy and Radical Prostatectomy. *Anticancer Res.* **2015**, *35*, 5679–5685. [PubMed]
31. Kolostova, K.; Broul, M.; Schraml, J.; Cegan, M.; Matkowski, R.; Fiutowski, M.; Bobek, V. Circulating tumor cells in localized prostate cancer: Isolation, cultivation in vitro and relationship to T-stage and Gleason score. *Anticancer Res.* **2014**, *34*, 3641–3646.
32. Pal, S.K.; He, M.; Wilson, T.; Liu, X.; Zhang, K.; Carmichael, C.; Torres, A.; Hernandez, S.; Lau, C.; Agarwal, N.; et al. Detection and Phenotyping of Circulating Tumor Cells in High-Risk Localized Prostate Cancer. *Clin. Genitourin. Cancer* **2015**, *13*, 130–136. [CrossRef] [PubMed]
33. Tsumura, H.; Satoh, T.; Ishiyama, H.; Tabata, K.; Takenaka, K.; Sekiguchi, A.; Nakamura, M.; Kitano, M.; Hayakawa, K.; Iwamura, M. Perioperative Search for Circulating Tumor Cells in Patients Undergoing Prostate Brachytherapy for Clinically Nonmetastatic Prostate Cancer. *Int. J. Mol. Sci.* **2017**, *18*, 128. [CrossRef]
34. Puche-Sanz, I.; Alvarez-Cubero, M.J.; Pascual-Geler, M.; Rodríguez-Martínez, A.; Delgado-Rodríguez, M.; García-Puche, J.L.; Expósito, J.; Robles-Fernández, I.; Entrala-Bernal, C.; Lorente, J.A.; et al. A comprehensive study of circulating tumour cells at the moment of prostate cancer diagnosis: Biological and clinical implications of EGFR, AR and SNPs. *Oncotarget* **2017**, *8*, 70472–70480. [CrossRef] [PubMed]
35. Zapatero, A.; Gómez-Caamaño, A.; Cabeza Rodriguez, M.Á.; Muínelo-Romay, L.; Martín de Vidales, C.; Abalo, A.; Calvo Crespo, P.; Leon Mateos, L.; Olivier, C.; Vega Piris, L.V. Detection and dynamics of circulating tumor cells in patients with high-risk prostate cancer treated with radiotherapy and hormones: A prospective phase II study. *Radiat. Oncol.* **2020**, *15*, 137. [CrossRef]
36. Knipper, S.; Riethdorf, S.; Werner, S.; Tilki, D.; Graefen, M.; Pantel, K.; Maurer, T. Possible Role of Circulating Tumour Cells for Prediction of Salvage Lymph Node Dissection Outcome in Patients with Early Prostate Cancer Recurrence. *Eur. Urol. Open Sci.* **2021**, *34*, 55–58. [CrossRef] [PubMed]
37. Abdallah, E.A.; Souza e Silva, V.; Braun, A.C.; Gasparini, V.A.; Kupper, B.E.C.; Tariki, M.S.; Tarazona, J.G.R.; Takahashi, R.M.; Aguiar Júnior, S.; Chinen, L.T.D. A higher platelet-to-lymphocyte ratio is prevalent in the presence of circulating tumor microemboli and is a potential prognostic factor for non-metastatic colon cancer. *Transl. Oncol.* **2021**, *14*, 100932. [CrossRef] [PubMed]
38. Chinen, L.; Mello, C.; Abdallah, E.; Ocea, L.; Buim, M.; Mingues, N.; Gasparini Junior, J.; Fanelli, M.; Paterlini, P. Isolation, detection, and immunomorphological characterization of circulating tumor cells (CTCs) from patients with different types of sarcoma using isolation by size of tumor cells: A window on sarcoma-cell invasion. *Oncotargets Ther.* **2014**, *7*, 1609. [CrossRef] [PubMed]
39. De Giorgi, V.; Pinzani, P.; Salvianti, F.; Panelos, J.; Paglierani, M.; Janowska, A.; Grazzini, M.; Wechsler, J.; Orlando, C.; Santucci, M.; et al. Application of a Filtration- and Isolation-by-Size Technique for the Detection of Circulating Tumor Cells in Cutaneous Melanoma. *J. Investig. Dermatol.* **2010**, *130*, 2440–2447. [CrossRef]
40. Fina, E.; Federico, D.; Novellis, P.; Dieci, E.; Monterisi, S.; Cioffi, F.; Mangiameli, G.; Finocchiaro, G.; Alloisio, M.; Veronesi, G. Subpopulations of Circulating Cells with Morphological Features of Malignancy Are Preoperatively Detected and Have Differential Prognostic Significance in Non-Small Cell Lung Cancer. *Cancers* **2021**, *13*, 4488. [CrossRef] [PubMed]
41. Hofman, V.; Bonnetaud, C.; Ilie, M.I.; Vielh, P.; Vignaud, J.M.; Fléjou, J.F.; Lantuejoul, S.; Piaton, E.; Mourad, N.; Butori, C.; et al. Preoperative Circulating Tumor Cell Detection Using the Isolation by Size of Epithelial Tumor Cell Method for Patients with Lung Cancer Is a New Prognostic Biomarker. *Clin. Cancer Res.* **2011**, *17*, 827–835. [CrossRef]
42. Hofman, V.; Long, E.; Ilie, M.; Bonnetaud, C.; Vignaud, J.M.; Fléjou, J.F.; Lantuejoul, S.; Piaton, E.; Mourad, N.; Butori, C.; et al. Morphological analysis of circulating tumour cells in patients undergoing surgery for non-small cell lung carcinoma using the isolation by size of epithelial tumour cell (ISET) method: Circulating tumour cells and cytological analysis. *Cytopathology* **2012**, *23*, 30–38. [CrossRef] [PubMed]
43. Ilie, M.; Hofman, V.; Leroy, S.; Cohen, C.; Heeke, S.; Cattet, F.; Bence, C.; Lalive, S.; Mouroux, J.; Marquette, C.-H.; et al. Use of circulating tumor cells in prospective clinical trials for NSCLC patients – standardization of the pre-analytical conditions. *Clin. Chem. Lab. Med.* **2018**, *56*, 980–989. [CrossRef]
44. Lecharpentier, A.; Vielh, P.; Perez-Moreno, P.; Planchard, D.; Soria, J.C.; Farace, F. Detection of circulating tumour cells with a hybrid (epithelial/mesenchymal) phenotype in patients with metastatic non-small cell lung cancer. *Br. J. Cancer* **2011**, *105*, 1338–1341. [CrossRef]
45. Long, E.; Ilie, M.; Bence, C.; Butori, C.; Selva, E.; Lalive, S.; Bonnetaud, C.; Poissonnet, G.; Lacour, J.-P.; Bahadoran, P.; et al. High expression of TRF2, SOX10, and CD10 in circulating tumor microemboli detected in metastatic melanoma patients. A potential impact for the assessment of disease aggressiveness. *Cancer Med.* **2016**, *5*, 1022–1030. [CrossRef] [PubMed]
46. Pinzani, P.; Mazzini, C.; Salvianti, F.; Massi, D.; Grifoni, R.; Paoletti, C.; Ucci, F.; Molinara, E.; Orlando, C.; Pazzagli, M.; et al. Tyrosinase mRNA levels in the blood of uveal melanoma patients: Correlation with the number of circulating tumor cells and tumor progression. *Melanoma Res.* **2010**, *20*, 303–310. [CrossRef] [PubMed]
47. Salvianti, F.; Orlando, C.; Massi, D.; De Giorgi, V.; Grazzini, M.; Pazzagli, M.; Pinzani, P. Tumor-Related Methylated Cell-Free DNA and Circulating Tumor Cells in Melanoma. *Front. Mol. Biosci.* **2016**, *2*, 76. [CrossRef]
48. Yu, J.; Gemenetzi, G.; Kinny-Köster, B.; Habib, J.R.; Groot, V.P.; Teinor, J.; Yin, L.; Pu, N.; Hasanain, A.; van Oosten, F.; et al. Pancreatic circulating tumor cell detection by targeted single-cell next-generation sequencing. *Cancer Lett.* **2020**, *493*, 245–253. [CrossRef] [PubMed]

49. Miah, S.; Catto, J. BPH and prostate cancer risk. *Indian J. Urol.* **2014**, *30*, 214. [CrossRef]
50. Perera, M.; Lawrentschuk, N.; Perera, N.; Bolton, D.; Clouston, D. Incidental prostate cancer in transurethral resection of prostate specimens in men aged up to 65 years. *Prostate Int.* **2016**, *4*, 11–14. [CrossRef]
51. Vona, G.; Estepa, L.; Bérout, C.; Damotte, D.; Capron, F.; Nalpas, B.; Mineur, A.; Franco, D.; Lacour, B.; Pol, S.; et al. Impact of cytomorphological detection of circulating tumor cells in patients with liver cancer. *Hepatology* **2004**, *39*, 792–797. [CrossRef]
52. Broncy, L.; Njima, B.B.; Méjean, A.; Bérout, C.; Ben Romdhane, K.; Ilie, M.; Hofman, V.; Muret, J.; Hofman, P.; Chaabouni Bouhamed, H.; et al. Single-cell genetic analysis validates cytopathological identification of circulating cancer cells in patients with clear cell renal cell carcinoma. *Oncotarget* **2018**, *9*, 20058–20074. [CrossRef]
53. Morrison, G.J.; Goldkorn, A. Development and Application of Liquid Biopsies in Metastatic Prostate Cancer. *Curr. Oncol. Rep.* **2018**, *20*, 35. [CrossRef] [PubMed]
54. Schiewer, M.J.; Knudsen, K.E. DNA Damage Response in Prostate Cancer. *Cold Spring Harb. Perspect. Med.* **2019**, *9*, a030486. [CrossRef] [PubMed]
55. Kornberg, Z.; Cooperberg, M.R.; Cowan, J.E.; Chan, J.M.; Shinohara, K.; Simko, J.P.; Tenggara, I.; Carroll, P.R. A 17-Gene Genomic Prostate Score as a Predictor of Adverse Pathology in Men on Active Surveillance. *J. Urol.* **2019**, *202*, 702–709. [CrossRef]
56. Berlin, A.; Murgic, J.; Hosni, A.; Pintilie, M.; Salcedo, A.; Fraser, M.; Kamel-Reid, S.; Zhang, J.; Wang, Q.; Ch'ng, C.; et al. Genomic Classifier for Guiding Treatment of Intermediate-Risk Prostate Cancers to Dose-Escalated Image Guided Radiation Therapy Without Hormone Therapy. *Int. J. Radiat. Oncol. Biol. Phys.* **2019**, *103*, 84–91. [CrossRef] [PubMed]
57. Palermo, G.; Bassi, P.; Racioppi, M.; Recupero, S.M.; Sacco, E.; Campetella, M.; Canu, G.; Pinto, F. Circulating tumor cells as prognostic biological marker in different stages prostate cancer and the effect of different therapeutic approaches on their expression. *Minerva Urol. E Nefrol.* **2020**, *72*, 214–222. [CrossRef]
58. Osmulski, P.A.; Cunsolo, A.; Chen, M.; Qian, Y.; Lin, C.-L.; Hung, C.-N.; Mahalingam, D.; Kirma, N.B.; Chen, C.-L.; Taverna, J.A.; et al. Contacts with Macrophages Promote an Aggressive Nanomechanical Phenotype of Circulating Tumor Cells in Prostate Cancer. *Cancer Res.* **2021**, *81*, 4110–4123. [CrossRef]

Article

Promoter Demethylation Upregulates *STEAP1* Gene Expression in Human Prostate Cancer: In Vitro and In Silico Analysis

Sandra M. Rocha ¹, Inês Sousa ^{1,2}, Inês M. Gomes ¹, Patrícia Arinto ¹, Pedro Costa-Pinheiro ³, Eduarda Coutinho ¹, Cecília R. Santos ¹, Carmen Jerónimo ^{3,4}, Manuel C. Lemos ^{1,5}, Luís A. Passarinha ^{1,6,7,8}, Sílvia Socorro ¹ and Cláudio J. Maia ^{1,5,*}

- ¹ CICS-UBI-Health Sciences Research Center, Universidade da Beira Interior, 6201-506 Covilhã, Portugal; sandra.rocha@ubi.pt (S.M.R.); inesmmsousa@ua.pt (I.S.); inesgomes@fcsaude.ubi.pt (I.M.G.); patricia_arinto@hotmail.com (P.A.); ecoutinho@fcsaude.ubi.pt (E.C.); csantos@fcsaude.ubi.pt (C.R.S.); mclemos@fcsaude.ubi.pt (M.C.L.); lpassarinha@fcsaude.ubi.pt (L.A.P.); ssocorro@fcsaude.ubi.pt (S.S.)
- ² Department of Medical Sciences, Institute of Biomedicine—iBiMED, Universidade de Aveiro, 3810-193 Aveiro, Portugal
- ³ Cancer Biology and Epigenetics Group, IPO Porto Research Center (CI-IPOP), Portuguese Oncology Institute of Porto (IPO Porto), 4200-072 Porto, Portugal; pedro.dacostapinheiro@pennmedicine.upenn.edu (P.C.-P.); carmenjeronimo@ipoporto.min-saude.pt (C.J.)
- ⁴ Department of Pathology and Molecular Immunology, School of Medicine and Biomedical Sciences, Universidade do Porto (ICBAS-UP), 4050-513 Porto, Portugal
- ⁵ C4-UBI, Cloud Computing Competence Center, Universidade da Beira Interior, 6200-501 Covilhã, Portugal
- ⁶ Associate Laboratory i4HB-Institute for Health and Bioeconomy, NOVA School of Science and Technology, Universidade NOVA de Lisboa, 2819-516 Caparica, Portugal
- ⁷ UCIBIO-Applied Molecular Biosciences Unit, Department of Chemistry, NOVA School of Science and Technology, Universidade NOVA de Lisboa, 2819-516 Caparica, Portugal
- ⁸ Laboratório de Fármaco-Toxicologia-UBIMedical, Universidade da Beira Interior, 6201-284 Covilhã, Portugal
- * Correspondence: cmaia@fcsaude.ubi.pt; Tel.: +351-275-329-069

Citation: Rocha, S.M.; Sousa, I.; Gomes, I.M.; Arinto, P.; Costa-Pinheiro, P.; Coutinho, E.; Santos, C.R.; Jerónimo, C.; Lemos, M.C.; Passarinha, L.A.; et al. Promoter Demethylation Upregulates *STEAP1* Gene Expression in Human Prostate Cancer: In Vitro and In Silico Analysis. *Life* **2021**, *11*, 1251. <https://doi.org/10.3390/life11111251>

Academic Editor: Joo-Mi Yi

Received: 30 September 2021

Accepted: 15 November 2021

Published: 17 November 2021

Publisher's Note: MDPI stays neutral with regard to jurisdictional claims in published maps and institutional affiliations.

Abstract: The Six Transmembrane Epithelial Antigen of the Prostate (*STEAP1*) is an oncogene overexpressed in several human tumors, particularly in prostate cancer (PCa). However, the mechanisms involved in its overexpression remain unknown. It is well known that epigenetic modifications may result in abnormal gene expression patterns, contributing to tumor initiation and progression. Therefore, this study aimed to analyze the methylation pattern of the *STEAP1* gene in PCa versus non-neoplastic cells. Bisulfite amplicon sequencing of the CpG island at the *STEAP1* gene promoter showed a higher methylation level in non-neoplastic PNT1A prostate cells than in human PCa samples. Bioinformatic analysis of the GEO datasets also showed the *STEAP1* gene promoter as being demethylated in human PCa, and a negative association with *STEAP1* mRNA expression was observed. These results are supported by the treatment of non-neoplastic PNT1A cells with DNMT and HDAC inhibitors, which induced a significant increase in *STEAP1* mRNA expression. In addition, the involvement of HDAC in the regulation of *STEAP1* mRNA expression was corroborated by a negative association between *STEAP1* mRNA expression and *HDAC4,5,7* and *9* in human PCa. In conclusion, our work indicates that *STEAP1* overexpression in PCa can be driven by the hypomethylation of *STEAP1* gene promoter.

Keywords: prostate cancer; *STEAP1*; DNA methylation; histone deacetylation; bioinformatics



Copyright: © 2021 by the authors. Licensee MDPI, Basel, Switzerland. This article is an open access article distributed under the terms and conditions of the Creative Commons Attribution (CC BY) license (<https://creativecommons.org/licenses/by/4.0/>).

1. Introduction

Prostate cancer (PCa) is the second most common cancer worldwide, and it is the sixth leading cause of cancer death globally [1]. Prostatic carcinogenesis arises from precursor preneoplastic lesions that have the distinct molecular characteristics of normal prostate cells, and may give rise to localized cancer and eventually acquire the potential of invasion and metastasis [2]. The molecular alterations underpinning these cellular events include mutations, gene deletions and amplifications, chromosomal rearrangements and epigenetic

modifications in key genes controlling cell fate [3–5]. The main epigenetic mechanisms are DNA methylation and histone modifications, the main function of which is to ensure the proper regulation of gene expression by changing the chromatin structure [6]. DNA methylation is catalyzed by the family of enzymes known as DNA methyltransferases (DNMTs) and by histone modifications, including mainly histone acetylation, which is regulated by two groups of enzymes exerting opposite effects, histone acetyltransferases (HATs) and histone deacetylases (HDACs) [5,6].

In tumor cells, hypermethylation is observed in promoters of specific genes, particularly tumor suppressor genes, and a global hypomethylation contributes to genomic instability and the activation of oncogenes [7]. The disruption of epigenetic mechanisms may conduct the deregulation of gene expression, leading to tumor development and progression [6].

The Six Transmembrane Epithelial Antigen of the Prostate 1 (*STEAP1*) gene was identified as overexpressed in PCa compared to non-malignant tissues [8]. The *STEAP1* protein is mainly located in the plasma membrane of epithelial cells, particularly at cell–cell junctions where it may act as an ion channel or transporter protein [8]. In fact, it was reported that *STEAP1* may allow the transport of small molecules between adjacent cells, indicating that *STEAP1* may be involved in intercellular communication [9,10]. Several studies have demonstrated the role of *STEAP1* in cancer. In Ewing tumors, *STEAP1* protein seems to promote cell growth and invasiveness by increasing intracellular reactive oxygen species levels. The oxidative stress that results from *STEAP1* overexpression may enhance tumor aggressiveness through the activation of genes involved in cell proliferation and invasion [11]. Additionally, in gastric tumors, it was demonstrated that the upregulation of *STEAP1* increased cell proliferation, migration and invasion [12]. In human ovarian and lung cancers, the *STEAP1* gene is highly expressed, and it is associated with metastasis and epithelial–mesenchymal transition [12–14]. It was also demonstrated that the knockdown of *STEAP1* expression on prostate tumor cells is associated with antitumor effects, such as enhanced apoptosis, and reduced proliferation, migration and invasion [12–15]. Previously, it was shown that post-transcriptional and post-translational modifications may contribute to *STEAP1* overexpression, as *STEAP1* mRNA and protein stability are higher in neoplastic LNCaP cells than in non-neoplastic PNT1A cells [16]. However, these alterations do not justify the overexpression of *STEAP1* in tumor cells, suggesting that other mechanisms may be involved. Thus, we hypothesized that epigenetic alterations of the *STEAP1* gene result in its overexpression in PCa. The present study aimed to analyze the methylation pattern of the *STEAP1* gene in PCa cells. Therefore, we analyzed the methylation levels of the *STEAP1* gene promoter in prostate cell lines and human samples of PCa. In addition, we analyzed the association between methylation levels of *STEAP1* and gene expression using publicly available datasets. Additionally, non-neoplastic PNT1A cells were used to demonstrate that demethylation of the *STEAP1* gene, as well as a synergistic effect between DNA demethylation and inhibition of class I and II HDACs, induces *STEAP1* overexpression.

2. Materials and Methods

2.1. Prostate Cell Lines and Treatments

The human LNCaP PCa cell line and the immortalized non-neoplastic PNT1A prostate epithelial cell line were purchased from the European Collection of Cell Cultures (ECACC, Salisbury, UK). LNCaP and PNT1A cell lines were cultured at 37 °C in a 5% CO₂ atmosphere with RPMI 1640 phenol-red medium (Sigma-Aldrich, St. Louis, MO, USA) supplemented with 10% fetal bovine serum (FBS, Sigma-Aldrich, USA) and 1% penicillin/streptomycin (Sigma-Aldrich, USA). For the treatment with the demethylation and the histone deacetylation drug (epidrugs), approximately 3×10^5 PNT1A cells were seeded in six-well plates until reaching about 60% confluence. After that, PNT1A cells were exposed to one treatment with 5 μM 5-aza-dC (Sigma-Aldrich, USA) for 72 h, and the other with 5 μM 5-aza-dC for 48 h followed by 24 h with 1 μM TSA (Sigma-Aldrich, USA). In the control group, the medium was replaced by RPMI medium with DMSO for 72 h.

2.2. Patients and Tissue Sample Collection

Prostate tissue samples from five patients diagnosed with clinically localized PCa and primary treatment with radical prostatectomy, at the Portuguese Oncology Institute of Porto (IPO-Porto), were used in this study. Informed consent was obtained from all participants, according to institutional regulations. This study was approved by the institutional review board (Comissão de Ética para a Saúde-(IRB-CES-IPOFG-EPE 019/08)) of IPO-Porto.

2.3. DNA Extraction and Bisulfite Conversion

DNA extraction from PNT1A and LNCaP cells and clinical samples was carried out using the Genra Puregene Cell Kit (Qiagen, Hilden, Germany) according to the manufacturer's instructions. To evaluate the methylation pattern, 1 µg of genomic DNA was modified using the EZ DNA Methylation-Gold kit (ZYMO RESEARCH, Irvine, CA, USA) according to the manufacturer's instructions. The modified DNA was stored at −80 °C.

2.4. Polymerase Chain Reaction (PCR) Amplification and Cloning Products

PCR reactions were performed using 200 ng of bisulfite-modified DNA in 25 µL reaction containing 1 U of TrueStart Hot Start Taq DNA Polymerase (Thermo Scientific, Waltham, MA, USA), 2.5 mM of MgCl₂, 10 mM dNTPs and 300 nM of each primer (−338 fw/+74 rv). The primer sequences and characteristics are described in Table 1. The PCR products were purified using NucleoSpin Gel and the PCR Clean-up kit (Macherey-Nagel, Germany) according to the manufacturer's instructions, cloned into a pNZY28 vector and transformed in NZYStar Competent Cells. After heat shock, the cells were plated onto LB agar plates containing 100 µg/mL ampicillin, 80 µg/mL X-gal and 0.5 mM IPTG and incubated at 37 °C overnight. All components used in cloning and transformation were purchased from Nzytech, Portugal.

Table 1. Primer sequences and respective amplicon size used for amplification of the modified DNA from cell lines or human samples, and for the quantitative real-time PCR.

Primers	Accession Number	Sequence	Amplicon Size (bp)	Target
STEAP1_−338 fw STEAP1_+74 rv	NC_000007.14	5' AAAGTGTGATTGGGAATGTTTT 3' 5' TTTTAAAGTTAGTTGTAGGTTTT 3'	412	Modified DNA
hSTEAP1_619 fw hSTEAP1_747 rv	NM_012449.3	5' GGCGATCCTACAGATACAAGTTGC 3' 5' CCAATCCCACAATTCCCAGAGAC 3'	128	mRNA
hGAPDH_74 fw hGAPDH_149 rv	NM_002046.7	5' CGCCAGCCGAGCCACATC 3' 5' CGC CCA ATA CGA CCA AAT CCG 3'	75	mRNA
hβ2M_347 fw hβ2M_439 rv	NM_004048.4	5' ATGAGTATGCCTGCCGTGTG 3' 5' CAAACCTCCATGATGCTGCTTAC 3'	92	mRNA

2.5. DNA Sequencing

Colony screening was performed by PCR, with standard vector primers (T7 and M13), to confirm and amplify the DNA insert. Thus, white colonies were selected and incubated in 10 µL TE buffer at 100 °C for 2 min. Afterwards, 1 µL was used for PCR reaction with Speedy NZYTaq 2x Green Master Mix (Nzytech, Portugal). Sequencing of PCR products was carried out using the CEQ Dye Terminator Cycle Sequencing Quick Start Kit (Beckman Coulter, Fullerton, USA) according to the manufacturer's instructions. For each sample, the DNA sequencing reaction was performed in both strands with universal sequencing primers (T7 and M13). The sequencing products were separated on an automated capillary DNA sequencer (GenomeLab™ GeXP, Genetic Analysis System; Beckman Coulter, Fullerton, CA, USA). The sequencing data analysis was performed using the Clustal Omega software to align the PCR product sequences with the sequence of STEAP1 gene modified DNA.

2.6. Datasets and Bioinformatic Analysis

Three PCa datasets (GSE52955, GSE76938 and GSE38240) were downloaded from the public repository NCBI Gene Expression Omnibus (GEO) databases (<https://www.ncbi.nlm.nih.gov/geo/>, assessed on 12 November 2021). All these datasets were based on the GPL13534 platform (Illumina HumanMethylation450 BeadChip). For each dataset, only the samples associated with prostate were selected. Methylation status was determined through the interactive web tool GEO2R, which allows the comparison of the two groups defined, pathologic condition and normal. The methylation status varies between 0 and 1, where 0 means a low degree of methylation and 1 indicates a high degree of methylation. The results were exported, and graphs were constructed with GraphPad Prism 8.0.1. The details of each dataset used in the present study are described in Table 2. The correlation of DNA methylation status with *STEAP1* mRNA expression was assessed using another public repository, the Prostate Adenocarcinoma (TCGA, Cell 2015) [17] dataset, available from cBioPortal for Cancer Genomic (<https://www.cbioportal.org/>, assessed on 12 November 2021). This dataset comprises data from 333 primary prostate carcinomas.

Table 2. Dataset used to evaluate the *STEAP1* gene methylation profiling.

Dataset	Platform	Sample Type	Disease Condition (n)	Normal Tissue (n)	Reference
GSE52955	GLP13534	Frozen tissue	Cancer (25)	5 *	[18]
GSE76938	GLP13534		Cancer (73)	Adjacent Tissue (63)	[19]
GSE38240	GLP13534		Cancer Metastasis (8)	4 #	[20]

* Obtained from patients submitted to cystoprostatectomy due to bladder cancer. # Obtained from organ donor with no evidence of prostate cancer.

2.7. Total RNA Extraction, cDNA Synthesis and Quantitative Real-Time PCR (qPCR)

Total RNA extraction from PNT1A cells treated with epidrugs (5-aza-dC and TSA) was carried out using TRI reagent (Sigma-Aldrich, USA) according to the manufacturer's instructions. cDNA synthesis was performed using the NZY First-Strand cDNA Synthesis KIT (Nzytech, Portugal) according to the manufacturer's instructions, and qPCR was carried out to evaluate the expression of *STEAP1* mRNA (*hSTEAP1*) in PNT1A cells treated with 5-aza-dC alone and 5-aza-dC plus TSA. To normalize the expression of the *STEAP1* gene, human GAPDH (*hGAPDH*) and human beta-2-microglobulin (*hβ2M*) primers were used as internal controls. qPCR reactions were carried out using 1 μL of cDNA synthesized in a 20 μL reaction containing 10 μL of Maxima SYBR Green/Fluorescein qPCR Master Mix (Thermo Scientific) and 300 nM of primer for each gene. Fold differences were calculated following the mathematical model proposed by Pfaffl using the formula: $2^{-\Delta\Delta Ct}$ [21]. The primer sequence for each gene and respective amplicon sizes used in qPCR are described in Table 1.

2.8. Statistical Analysis

Data analysis was performed using GraphPad Prism version 8.0.1. for Windows (GraphPad Software, San Diego, CA, USA). The statistical significance of differences in *STEAP1* mRNA expression for the treatment with 5-aza-dC and TSA in non-neoplastic PNT1A cells was assessed by student's *t*-test. Significant differences were considered when $p < 0.05$ compared to control values. All experimental data are shown as mean \pm SEM.

3. Results

3.1. Methylation Analysis of *STEAP1* Gene in Neoplastic Tissue/Cells Compared with Non-Neoplastic Cells

To evaluate if DNA methylation plays a role in *STEAP1* gene regulation and if there are alterations in PCa, the methylation pattern of *STEAP1* was determined in PCa tissue samples, LNCaP and PNT1A cells. For this purpose, cytosine-rich regions of *STEAP1* gene promoter and primer design were performed using the Methyl Primer Express Software v1.0 (Applied Biosystems). This analysis indicated that part of the promoter region and the first exon of the *STEAP1* gene contain a large CpG island containing 24 CpG dinucleotides (Figure 1), which could provide a large number of sites for the methylation modification of this gene.

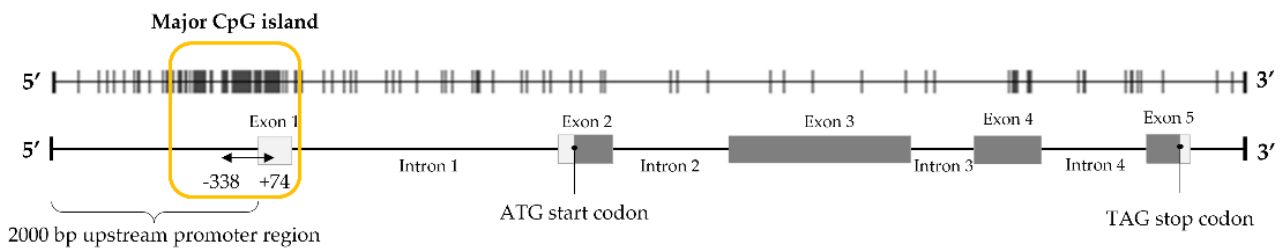


Figure 1. Schematic map of the predicted CpG island and indication of the region analyzed by bisulfite genomic sequencing within the exon–intron structure of *STEAP1* gene. Vertical bars represent the CG dinucleotides. Parameters used to find CpG islands: minimum length of island: 300 bp; maximum length of island: 2000 bp; C + Gs/total bases > 50%; CpG observed/CpG expected > 0.6.

The methylation pattern of the *STEAP1* was analyzed through the bisulfite sequencing PCR method from position -338 (promoter region) to $+74$ (exon 1). The analysis of the methylation pattern of *STEAP1* revealed some differences between neoplastic and non-neoplastic samples. In non-neoplastic PNT1A cells, the results show that some of the CpG dinucleotides located in the promoter region are methylated, but in PCa tissue or in neoplastic LNCaP cells the CpG dinucleotides are completely demethylated (Figure 2).

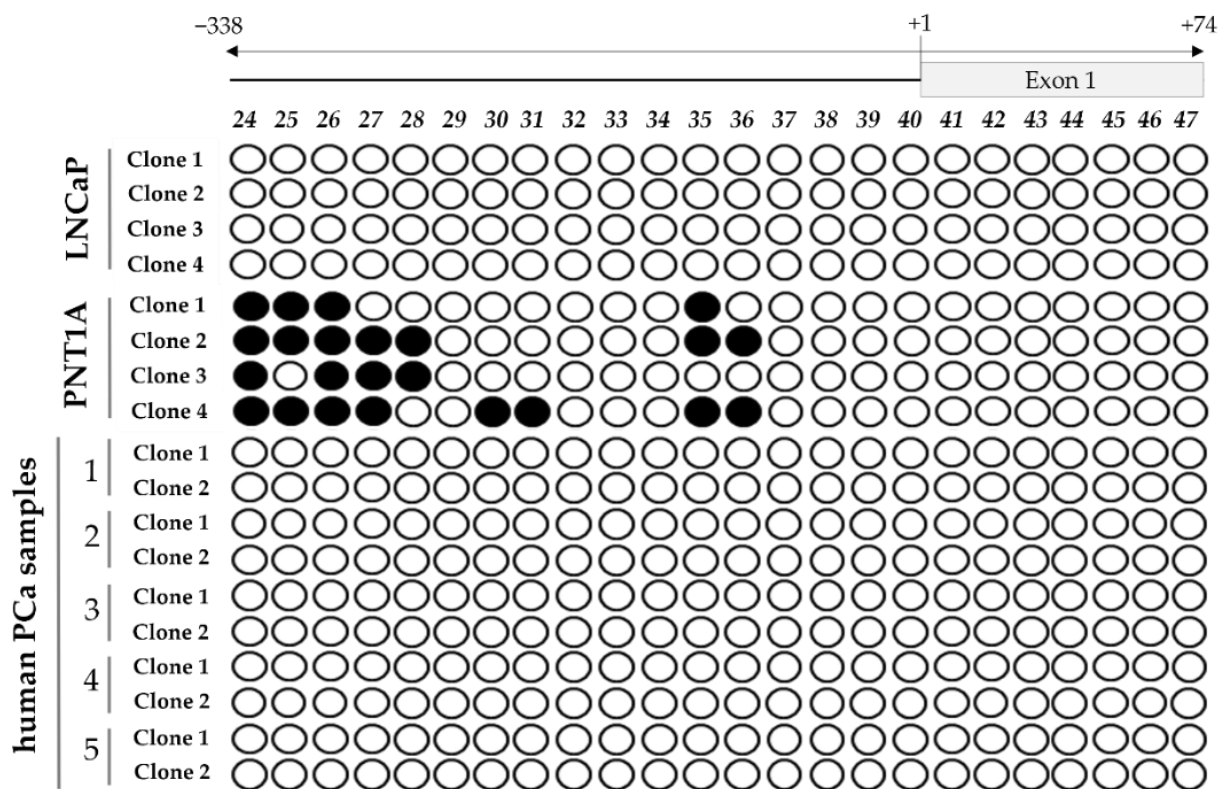


Figure 2. Evaluation of the *STEAP1* gene promoter methylation status in LNCaP and PNT1A cells, and human PCa samples. Each circle represents a CpG dinucleotide present in the CpG island identified, and on the top is the position of each CpG site relative to the beginning of the CpG island identified (● methylated CpG and ○ demethylated CpG). Each row represents a different clone.

3.2. Analysis of *STEAP1* Promoter Methylation Levels in PCa and Normal Prostate Tissues from the GEO Database

In order to support and validate the results above, the methylation pattern of *STEAP1* gene promoter methylation was evaluated in datasets from public PCa databases. The GSE52955, GSE76938 and GSE38240 datasets were downloaded and analyzed by GEO2R online software. Four CpG probes on the *STEAP1* gene promoter were selected: cg15089950,

cg19317433, cg19532731 and cg24286372 located on -314 to -193 bp, -285 to -163 bp, -301 to -180 bp and -250 to -129 bp upstream of the transcription start, respectively. As shown in Figure 3, there were significant differences in the levels of CpG methylation between prostate tumor and normal tissue. In three datasets analyzed, the results reveal lower methylation levels of the *STEAP1* gene promoter in neoplastic tissue than in normal tissue.

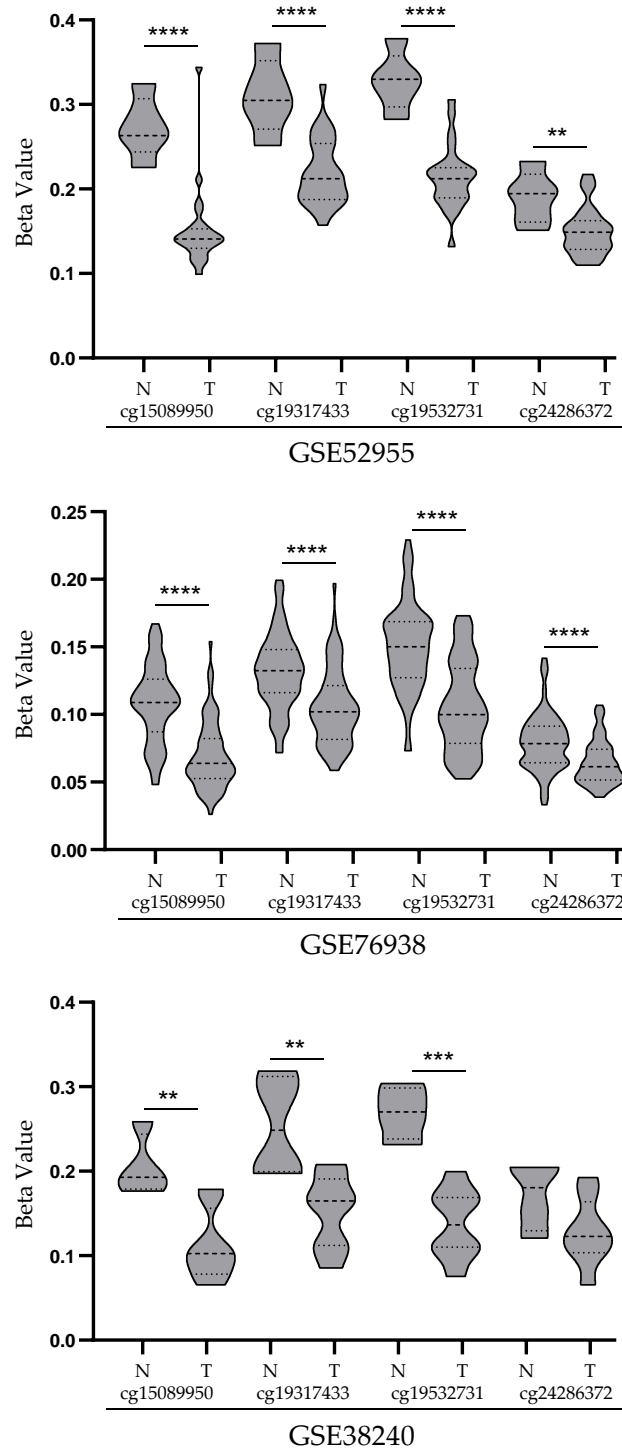


Figure 3. *STEAP1* promoter methylation levels (beta value) in GSE52955, GSE76938 and GSE38240 datasets. Each dataset represents methylation levels of *STEAP1* in prostate tumor tissue (T) and normal prostate tissue (N) for the four probes (cg15089950, cg19317433, cg19532731 and cg24286372). Violin plots were obtained with GraphPad Prism 8.0.1, and mean methylation levels between normal and tumor were compared with a student’s *t*-test. ** $p < 0.01$, *** $p < 0.001$ and **** $p < 0.0001$.

3.3. Correlation between *STEAP1* Gene Promoter Demethylation and Its Expression in PCa Tissue from the TCGA Database

In an attempt to better understand whether DNA methylation status may have an impact on *STEAP1* gene expression, the Prostate Adenocarcinoma dataset was analyzed from The Cancer Genome Atlas (TCGA, Cell 2015) [17], accessed through the cBioPortal. In this dataset, differential methylation levels between the unaltered ($n = 286$) and altered ($n = 43$) expression of the *STEAP1* gene were observed (Figure 4a). Additionally, a negative correlation (Spearman coefficient of -0.42 , and Pearson coefficient of -0.44) was observed between the methylation levels and the *STEAP1* gene expression (Figure 4b).

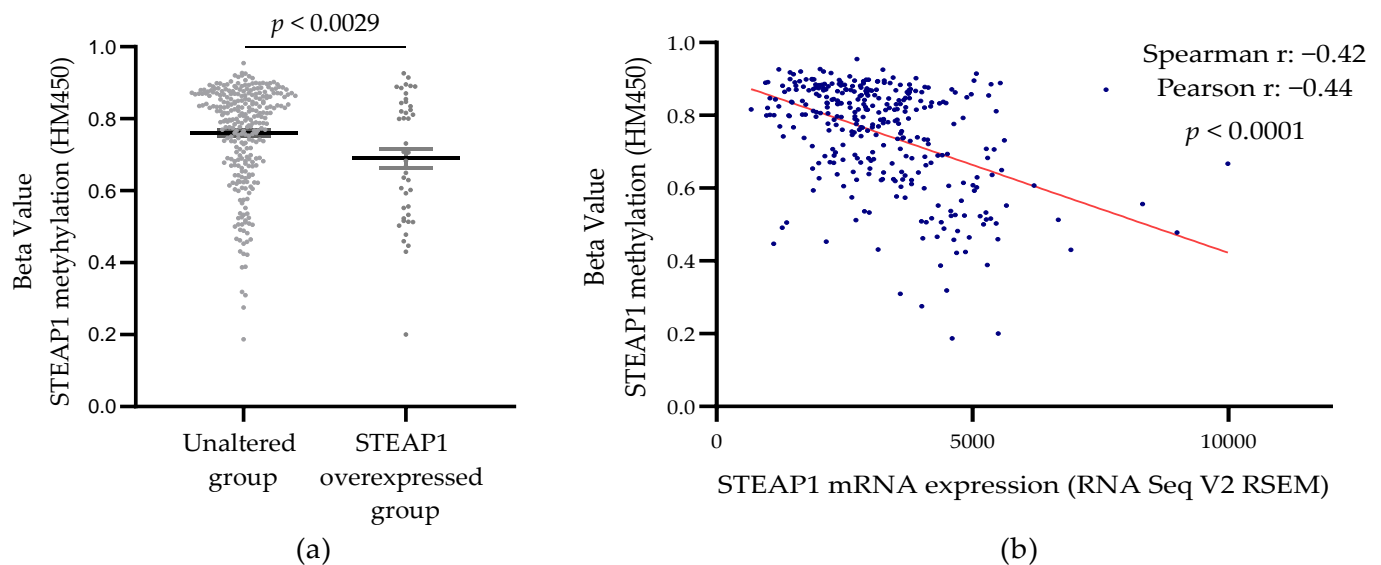


Figure 4. *STEAP1* methylation levels in PCa samples with normal and overexpression of *STEAP1* (a), and correlation between methylation levels and *STEAP1* mRNA expression (b) in Prostate Adenocarcinoma (TCGA, Cell 2015) [17] dataset ($n = 333$). Statistical analysis used a student's *t*-test (a) and Spearman and Pearson correlation (b).

3.4. Effect of Epigenetic-Modulating Drugs in *STEAP1* Gene Expression in Non-Neoplastic PNT1A Cells

In order to support that epigenetic modifications contribute to the regulation of *STEAP1* expression, non-neoplastic PNT1A cells were used to evaluate the effect of DNMT and HDAC inhibitors (5-aza-dC and TSA, respectively) on *STEAP1* mRNA expression by qPCR. As shown in Figure 5, treatment with the demethylation agent 5-aza-dC induced a three-fold increase in *STEAP1* mRNA levels when compared to the control group ($p < 0.01$). Moreover, treatment with both epidrugs (5-aza-dC + TSA), which contributes to demethylation and histone hyperacetylation, induced a strong increase (15-fold variation relative to control, $p < 0.001$) in *STEAP1* mRNA levels.

3.5. Analysis of Co-Expression between *STEAP1* mRNA Expression and HDACs

The TSA drug is a potent and specific inhibitor of HDAC classes I and II, which include ten isoforms (HDAC1–HDAC10) [22]. Considering that the results above suggest a negative association between histone deacetylation and *STEAP1* mRNA expression, we intended to analyze the association between *STEAP1* mRNA expression and HDAC mRNA expression, using the Prostate Adenocarcinoma (TCGA, Cell 2015) [17] dataset. Of the ten isoforms analyzed, *STEAP1* mRNA expression showed a positive association with *HDAC8*, as highlighted in Table 3. On the other hand, *STEAP1* mRNA expression was negatively associated with *HDAC4,5,7* and *9* (Table 3).

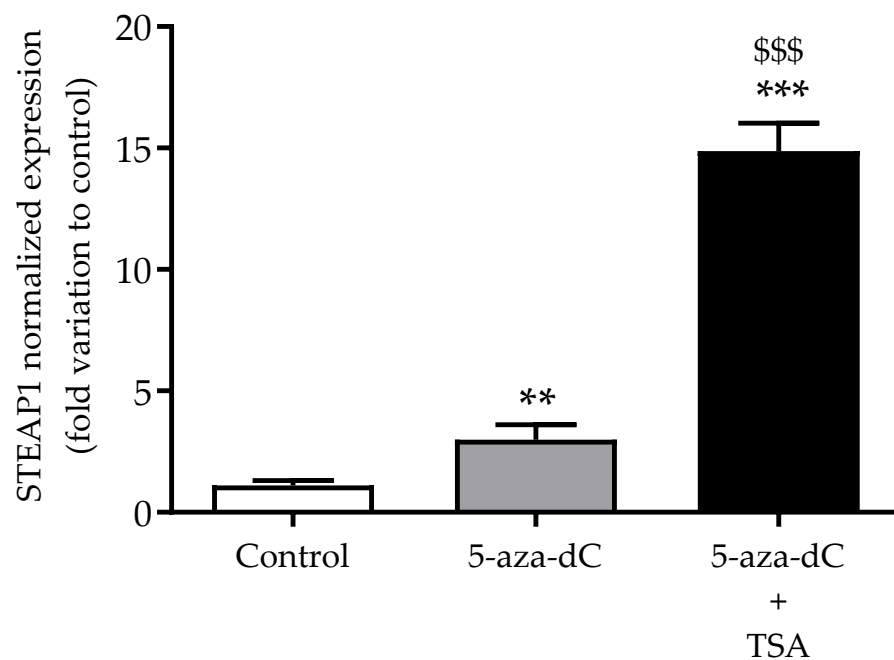


Figure 5. Effect of treatment with 5-aza-dC and TSA (DNMT and HDAC inhibitors, respectively) on *STEAP1* mRNA expression in PNT1A cells. Relative *STEAP1* mRNA expression was determined by qPCR analysis after normalization with the GAPDH and β 2M housekeeping genes. Results are expressed as fold-variation relative to the control group. Error bars indicate mean \pm SEM ($n = 6$). ** $p < 0.01$ and *** $p < 0.001$ relative to control. \$\$\$ $p < 0.001$ relative to 5-aza-dC.

Table 3. Association of *STEAP1* mRNA expression with class I and II HDACs, showing spearman's rank for each comparison and the respective p -value. The associations with significant values are highlighted in bold.

<i>STEAP1</i> Correlated	Spearman's Correlation	p -Value
HDAC1	−0.011	0.834
HDAC2	−0.005	0.929
HDAC3	0.089	0.105
HDAC4	−0.242	8.07×10^{-6}
HDAC5	−0.305	1.35×10^{-8}
HDAC6	0.049	0.366
HDAC7	−0.336	3.31×10^{-10}
HDAC8	0.255	2.34×10^{-6}
HDAC9	−0.294	4.53×10^{-8}
HDAC10	−0.064	0.245

4. Discussion

The methylation pattern observed in normal tissues undergoes relevant modifications in cancer, leading to changes in the regulation of the transcription of numerous genes [23]. Recent studies have shown that *STEAP1* acts as an oncogene, showing that its overexpression in several human cancers contributes to tumor progression and aggressiveness through the inhibition of apoptosis and stimulation of cell proliferation, invasion and epithelial–mesenchymal transition [11–15]. Although the stability of the *STEAP1* gene and protein is higher in LNCaP PCa cells than in PNT1A cells, contributing to *STEAP1* overexpression, other mechanisms underlying its overexpression in cancer must be involved. As epigenetics has been pointed out as a major hallmark in cancer, affecting genes involved in all cellular pathways [24,25], our main goal was to assess whether epigenetic mechanisms are involved in the regulation of the *STEAP1* gene expression in PCa, and if there are changes between normal and PCa cells.

As a first approach, two different cell lines were chosen, neoplastic LNCaP and non-neoplastic PNT1A, which express high and low levels of *STEAP1*, respectively [16], to analyze the methylation status of the *STEAP1* gene. Furthermore, five human PCa samples were also analyzed. The major CpG island located from position –338 of the promoter region to position +74 of the first exon of *STEAP1* revealed differences in the methylation status. While in non-neoplastic PNT1A cells, the CpG dinucleotides near the transcription start site are methylated, in neoplastic LNCaP cells and PCa samples these are demethylated. This result suggests that demethylation of the *STEAP1* gene promoter may lead to its overexpression in PCa. Hypomethylation/demethylation-dependent overexpression of several oncogenes has already been described in several cancer types. In PCa cells, Wingless-related MMTV integration site 5A, S100 calcium-binding protein P and cysteine-rich protein 1 were found to be hypomethylated [26]. hsa-miR-191 was also hypomethylated in 63% of hepatocellular carcinoma tissue samples, associated with its increased expression [27], and demethylation of the miR-128a promoter region drives the upregulation of miR-128a expression in the human T lymphocyte Jurkat cell line [28].

The possibility that demethylation of the *STEAP1* gene promoter may be involved in its overexpression in PCa was also corroborated by a bioinformatic analysis, using public datasets from the GEO database and cBioPortal platform. This analysis showed that CpG dinucleotides in the *STEAP1* gene of PCa samples have low levels of methylation, negatively correlated with *STEAP1* mRNA expression. These results suggest, once more, that demethylation of the *STEAP1* gene promoter may contribute to its overexpression in PCa. Our results are in line with other studies that also analyzed genes of the *STEAP* family, which showed that epigenetic alterations may be responsible for changes in gene expression. Using combined analysis of GEO and TCGA datasets, it was shown that *STEAP3* is hypomethylated and consequently upregulated in glioblastoma, and may be used as a potential methylation-based prognostic biomarker. In addition, the authors suggested that *STEAP3* is a potential target for glioblastoma treatment [29]. Another gene that was also reported to be deregulated due to epigenetic changes is the *STEAP4* gene. Tamura et al. showed no CpG methylation in the *STEAP4* promoter region in LNCaP cells, suggesting that demethylation may activate the expression of the *STEAP4* gene in PCa cells [30]. On the other hand, a more recent study showed that *STEAP4* was hypermethylated and downregulated in the hepatocellular carcinoma when compared to the non-tumor liver tissues [31]. This study also demonstrated that expression of *STEAP4* was restored with a DNA methyltransferase (DNMTs) inhibitor and a histone deacetylase (HDACs) inhibitor, suggesting that aberrant DNA methylation suppressed the expression of the *STEAP4* gene [31].

It is well established that there is a crosstalk between DNA methylation and histone modifications in the control of gene expression [32,33]. Aberrant CpG-island methylation by recruiting DNMTs and HDACs might be directly targeted by consequence of gene expression alterations [34]. Therefore, it was hypothesized that treatment with both DNMT and HDAC inhibitors might enhance *STEAP1* expression in cells with reduced levels of *STEAP1*. Thus, the non-neoplastic PNT1A cell line was used to evaluate the effects of 5-aza-dC (DNMT inhibitor) plus TSA (HDAC inhibitor) on the expression of *STEAP1*. The results indicate an increase in *STEAP1* gene expression in response to treatment with DNMT and HDAC inhibitors, suggesting a synergistic effect of combined hypomethylation and histone hyperacetylation.

HDACs are enzymes that remove acetyl groups from the tails of histones, resulting in a more closed chromatin structure and repression of gene expression [22,35,36]. Class I of the HDAC family includes HDAC1, 2, 3 and 8; class II includes HDAC4, 5, 6, 7, 9 and 10 [36]. To the best of our knowledge, the role played by both HDAC class I and II enzymes in the regulation of *STEAP1* gene expression is still unknown. So, we aimed to explore the association between HDAC and *STEAP1* gene expression. Our results reveal a positive association of *HDAC8* and a negative association of *HDAC4,5,7* and *9* with *STEAP1* mRNA expression. In fact, the HDAC family modulates several genes involved in cancer

development/progression via angiogenesis, cell adhesion, migration and invasion [22]. Some studies support our results, showing that increased expression of autotaxin in PCa cell lines is mediated by the downregulation of *HDAC7* and *HDAC3* [37]; additionally, *HDAC5* is downregulated in human cancer, namely PCa [38], and decreased expression of *HDAC4* increases the growth of PCa cells [39]. On the other hand, there are also studies showing an overexpression of HDAC in several types of cancer, suggesting the use of HDAC inhibitors as a promising class of compounds for cancer treatment [40–43]. Thus, the effects that can be triggered by these inhibitors on oncogenes should not be ignored and more studies are required to clarify their effectiveness in cancer treatment.

To summarize, this study showed that the *STEAP1* gene is hypomethylated in PCa cells when compared to non-neoplastic cells, contributing to the overexpression of *STEAP1* in PCa. Furthermore, our results suggest a putative involvement of *HDCA4,5,7* and *9* in the regulation of *STEAP1* in PCa. Considering the complexity of the mechanisms associated with HDAC, more studies are required to clarify their role in *STEAP1* regulation, as well as to elucidate this association with PCa development and progression.

Author Contributions: Conceptualization, S.M.R. and C.J.M.; methodology, S.M.R., I.S., I.M.G. and P.A.; formal analysis, P.C.-P. and E.C.; investigation, S.M.R., I.S., I.M.G., P.A. and C.J.M.; resources, C.J. and M.C.L.; writing—original draft preparation, S.M.R.; writing—review and editing, C.R.S., C.J., M.C.L., L.A.P., S.S. and C.J.M.; visualization, S.M.R., I.S., I.M.G., P.A., P.C.-P., E.C., C.R.S., C.J., M.C.L., L.A.P., S.S. and C.J.M.; supervision, L.A.P., S.S. and C.J.M. All authors have read and agreed to the published version of the manuscript.

Funding: This work was supported by FEDER funds through the POCI-COMPETE 2020-Operational Program Competitiveness and Internationalization in Axis I-Strengthening research, technological development and innovation (Project No. 007491; Project No 029114), National Funds by FCT-Foundation for Science and Technology (Project UIDB/00709/2020) and Applied Molecular Biosciences Unit UCIBIO (UIDB/04378/2020 and UIDP/04378/2020) and the Associate Laboratory Institute for Health and Bioeconomy-i4HB (project LA/P/0140/2020), which are financed by National Funds from FCT/MCTES. This work was also supported by the European Regional Development Fund through the “Programa Operacional Regional do Centro (Centro 2020)-Sistema de Apoio à Investigação Científica e Tecnológica-Programas Integrados de IC&DT” (Project Centro-01-0145-FEDER-000019-C4-Centro de Competências em Cloud Computing).

Institutional Review Board Statement: The study was conducted according to the guidelines of the Declaration of Helsinki, and approved by the Institutional Review Board (Comissão de Ética para a Saúde) of Portuguese Oncology Institute of Porto, Portugal (CES-IPOPFG-EPE 205/2013).

Informed Consent Statement: Informed consent was obtained from all participants involved in the study, according to institutional regulations.

Acknowledgments: Sandra M. Rocha (SFRH/BD/115693/2016) and Luís A. Passarinha (SFRH/BSAB/150376/2019) wish to thank Fundação para a Ciência e Tecnologia for their Ph.D. and sabbatical grants, respectively.

Conflicts of Interest: The authors declare no conflict of interest.

References



1. Culp, M.B.B.; Soerjomataram, I.; Efstathiou, J.A.; Bray, F.; Jemal, A. Recent Global Patterns in Prostate Cancer Incidence and Mortality Rates. In *European Urology*; Elsevier BV: Amsterdam, The Netherlands, 2020; Volume 77, pp. 38–52.
2. Gonzalgo, M.L.; Isaacs, W.B. Molecular Pathways to Prostate Cancer. *J. Urol.* **2003**, *170*, 2444–2452. [CrossRef]
3. Reynolds, M.A. Molecular alterations in prostate cancer. *Cancer Lett.* **2008**, *271*, 13–24. [CrossRef]
4. Joshua, A.M.; Evans, A.; Van der Kwast, T.; Zielenska, M.; Meeker, A.K.; Chinnaiyan, A.; Squire, J.A. Prostatic preneoplasia and beyond. *Biochim. Biophys. Acta.* **2008**, *1785*, 156–181. [CrossRef]
5. Nelson, W.G.; De Marzo, A.M.; Yegnasubramanian, S. Epigenetic alterations in human prostate cancers. *Endocrinology* **2009**, *150*, 3991–4002. [CrossRef]
6. Wang, R.; Liu, X. Epigenetic regulation of prostate cancer. *Genes Dis.* **2019**, *7*, 606–613. [CrossRef] [PubMed]
7. Kulis, M.; Esteller, M. DNA methylation and cancer. *Adv. Genet.* **2010**, *70*, 27–56. [PubMed]

8. Hubert, R.S.; Vivanco, I.; Chen, E.; Rastegar, S.; Leong, K.; Mitchell, S.C.; Madraswala, R.; Zhou, Y.; Kuo, J.; Raitano, A.B.; et al. STEAP: A prostate-specific cell-surface antigen highly expressed in human prostate tumors. *Proc. Natl. Acad. Sci. USA* **1999**, *96*, 14523–14528. [CrossRef] [PubMed]
9. Yamamoto, T.; Tamura, Y.; Kobayashi, J.-I.; Kamiguchi, K.; Hirohashi, Y.; Miyazaki, A.; Torigoe, T.; Asanuma, H.; Hiratsuka, H.; Sato, N. Six-transmembrane epithelial antigen of the prostate-1 plays a role for in vivo tumor growth via intercellular communication. *Exp. Cell Res.* **2013**, *319*, 2617–2626. [CrossRef]
10. Challita-Eid, P.M.; Morrison, K.; Etesami, S.; An, Z.; Morrison, K.J.; Perez-Villar, J.J.; Raitano, A.B.; Jia, X.C.; Gudas, J.M.; Kanner, S.B.; et al. Monoclonal antibodies to six-transmembrane epithelial antigen of the prostate-1 inhibit intercellular communication in vitro and growth of human tumor xenografts in vivo. *Cancer Res.* **2007**, *67*, 5798–5805. [CrossRef] [PubMed]
11. Grunewald, T.G.P.; Diebold, I.; Esposito, I.; Plehm, S.; Hauer, K.; Thiel, U.; Da Silva-Buttkus, P.; Neff, F.; Unland, R.; Müller-Tidow, C.; et al. STEAP1 is associated with the invasive and oxidative stress phenotype of ewing tumors. *Mol. Cancer Res.* **2012**, *10*, 52–65. [CrossRef]
12. Zhang, Z.; Hou, W.; Zhang, C.; Tan, Y.; Zhang, D.; An, W.; Pan, S.; Wu, W.; Chen, Q.; Xu, H. A research of STEAP1 regulated gastric cancer cell proliferation, migration and invasion in vitro and in vivos. *J. Cell. Mol. Med.* **2020**, *24*, 14217–14230. [CrossRef]
13. Huo, S.-F.; Shang, W.-L.; Yu, M.; Ren, X.-P.; Wen, H.-X.; Chai, C.-Y.; Sun, L.; Hui, K.; Liu, L.-H.; Wei, S.-H.; et al. STEAP1 facilitates metastasis and epithelial-mesenchymal transition of lung adenocarcinoma via the JAK2/STAT3 signaling pathway. *Biosci. Rep.* **2020**, *40*, BSR20193169. [CrossRef] [PubMed]
14. Jiao, Z.; Huang, L.; Sun, J.; Xie, J.; Wang, T.; Yin, X.; Zhang, H.; Chen, J. Six-transmembrane epithelial antigen of the prostate 1 expression promotes ovarian cancer metastasis by aiding progression of epithelial-to-mesenchymal transition. *Histochem. Cell Biol.* **2020**, *154*, 215–230. [CrossRef] [PubMed]
15. Gomes, I.M.; Rocha, S.; Gaspar, C.; Alvelos, M.I.; Santos, C.R.; Socorro, S.; Maia, C.J. Knockdown of STEAP1 inhibits cell growth and induces apoptosis in LNCaP prostate cancer cells counteracting the effect of androgens. *Med. Oncol.* **2018**, *35*, 40. [CrossRef]
16. Gomes, I.M.; Santos, C.R.; Maia, C.J. Expression of STEAP1 and STEAP1B in prostate cell lines, and the putative regulation of STEAP1 by post-transcriptional and post-translational mechanisms. *Genes Cancer* **2014**, *5*, 142–151. [CrossRef] [PubMed]
17. The Cancer Genome Atlas Research Network. The Molecular Taxonomy of Primary Prostate Cancer. *Cell* **2015**, *163*, 1011–1025. [CrossRef]
18. Ramalho-Carvalho, J.; Gonçalves, C.; Graça, I.; Bidarra, D.; Pereira-Silva, E.; Salta, S.; Godinho, M.I.; Gomez, A.; Esteller, M.; Costa, B.; et al. A multiplatform approach identifies miR-152-3p as a common epigenetically regulated onco-suppressor in prostate cancer targeting TMEM97. *Clin. Epigenetics* **2018**, *10*, 40. [CrossRef]
19. Kirby, M.K.; Ramaker, R.C.; Roberts, B.S.; Lasseigne, B.N.; Gunther, D.S.; Burwell, T.C.; Davis, N.S.; Gulzar, Z.G.; Absher, D.M.; Cooper, S.J.; et al. Genome-wide DNA methylation measurements in prostate tissues uncovers novel prostate cancer diagnostic biomarkers and transcription factor binding patterns. *BMC Cancer* **2017**, *17*, 273. [CrossRef] [PubMed]
20. Aryee, M.J.; Liu, W.; Engelmann, J.C.; Nuhn, P.; Gurel, M.; Haffner, M.C.; Esopi, D.; Irazarry, R.A.; Getzenberg, R.H.; Nelson, W.G.; et al. DNA methylation alterations exhibit intra-individual stability and inter-individual heterogeneity in prostate cancer metastases. *Sci. Transl. Med.* **2013**, *5*, 169ra10. [CrossRef] [PubMed]
21. Pfaffl, M.W. A new mathematical model for relative quantification in real-time RT-PCR. *Nucleic Acids Res.* **2001**, *29*, e45. [CrossRef]
22. Abbas, A.; Gupta, S. The role of histone deacetylases in prostate cancer. *Epigenetics* **2008**, *3*, 300–309. [CrossRef] [PubMed]
23. Sharma, S.; Kelly, T.K.; Jones, P.A. Epigenetics in cancer. *Carcinogenesis* **2010**, *31*, 27–36. [CrossRef] [PubMed]
24. Kukkonen, K.; Taavitsainen, S.; Huhtala, L.; Uusi-Makela, J.; Granberg, K.; Nykter, M.; Urbanucci, A. Chromatin and Epigenetic Dysregulation of Prostate Cancer Development, Progression, and Therapeutic Response. *Cancers* **2021**, *13*, 3325. [CrossRef]
25. Darwiche, N. Epigenetic mechanisms and the hallmarks of cancer: An intimate affair. *Am. J. Cancer Res.* **2020**, *10*, 1954–1978. [PubMed]
26. Wang, Q.; Williamson, M.; Bott, S.; Brookman-Amisshah, N.; Freeman, A.; Nariculam, J.; Hubank, M.; Ahmed, A.; Masters, J.R. Hypomethylation of WNT5A, CRIP1 and S100P in prostate cancer. *Oncogene* **2007**, *26*, 6560–6565. [CrossRef]
27. He, Y.; Cui, Y.; Wang, W.; Gu, J.; Guo, S.; Ma, K.; Luo, X. Hypomethylation of the hsa-miR-191 locus causes high expression of hsa-mir-191 and promotes the epithelial-to-mesenchymal transition in hepatocellular carcinoma. *Neoplasia* **2011**, *13*, 841–853. [CrossRef]
28. Yamada, N.; Noguchi, S.; Kumazaki, M.; Shinohara, H.; Miki, K.; Naoe, T.; Akao, Y. Epigenetic regulation of microRNA-128a expression contributes to the apoptosis-resistance of human T-cell leukaemia jurkat cells by modulating expression of fas-associated protein with death domain (FADD). *Biochim. Biophys. Acta.* **2014**, *1843*, 590–602. [CrossRef]
29. Zhang, M.; Lv, X.; Jiang, Y.; Li, G.; Qiao, Q. Identification of aberrantly methylated differentially expressed genes in glioblastoma multiforme and their association with patient survival. *Exp. Ther. Med.* **2019**, *18*, 2140–2152. [CrossRef]
30. Tamura, T.; Chiba, J. STEAP4 regulates focal adhesion kinase activation and CpG motifs within STEAP4 promoter region are frequently methylated in DU145, human androgen-independent prostate cancer cells. *Int. J. Mol. Med.* **2009**, *24*, 599–604. [CrossRef]
31. Yamada, N.; Yasui, K.; Dohi, O.; Gen, Y.; Tomie, A.; Kitaichi, T.; Iwai, N.; Mitsuyoshi, H.; Sumida, Y.; Moriguchi, M.; et al. Genome-wide DNA methylation analysis in hepatocellular carcinoma. *Oncol. Rep.* **2016**, *35*, 2228–2236. [CrossRef]
32. Esteller, M. Cancer epigenomics: DNA methylomes and histone-modification maps. *Nat. Rev. Genet.* **2007**, *8*, 286–298. [CrossRef] [PubMed]

33. Di Croce, L.; Raker, V.A.; Corsaro, M.; Fazi, F.; Fanelli, M.; Faretta, M.; Fuks, F.; Lo Coco, F.; Kouzarides, T.; Nervi, C.; et al. Methyltransferase recruitment and DNA hypermethylation of target promoters by an oncogenic transcription factor. *Science* **2002**, *295*, 1079–1082. [CrossRef] [PubMed]
34. D'Alessio, A.C.; Szyf, M. Epigenetic tête-à-tête: The bilateral relationship between chromatin modifications and DNA methylation. *Biochem. Cell Biol.* **2006**, *84*, 463–476. [CrossRef]
35. Minucci, S.; Pelicci, P.G. Histone deacetylase inhibitors and the promise of epigenetic (and more) treatments for cancer. *Nat. Rev. Cancer* **2006**, *6*, 38–51. [CrossRef] [PubMed]
36. Park, S.-Y.; Kim, J.-S. A short guide to histone deacetylases including recent progress on class II enzymes. *Exp. Mol. Med.* **2020**, *52*, 204–212. [CrossRef] [PubMed]
37. Li, S.; Wang, B.; Xu, Y.; Zhang, J. Autotaxin is induced by TSA through HDAC3 and HDAC7 inhibition and antagonizes the TSA-induced cell apoptosis. *Mol. Cancer* **2011**, *10*, 18. [CrossRef]
38. Zhou, Y.; Jin, X.; Ma, J.; Ding, D.; Huang, Z.; Sheng, H.; Yan, Y.; Pan, Y.; Wei, T.; Wang, L.; et al. HDAC5 Loss Impairs RB Repression of Pro-Oncogenic Genes and Confers CDK4/6 Inhibitor Resistance in Cancer. *Cancer Res.* **2021**, *81*, 1486–1499. [CrossRef]
39. Yang, Y.; Tse, A.K.-W.; Li, P.; Ma, Q.; Xiang, S.; Nicosia, S.V.; Seto, E.; Zhang, X.; Bai, W. Inhibition of androgen receptor activity by histone deacetylase 4 through receptor SUMOylation. *Oncogene* **2011**, *30*, 2207–2218. [CrossRef]
40. Hontecillas-Prieto, L.; Flores-Campos, R.; Silver, A.; De Álava, E.; Hajji, N.; García-Domínguez, D.J. Synergistic Enhancement of Cancer Therapy Using HDAC Inhibitors: Opportunity for Clinical Trials. *Front. Genet.* **2020**, *11*, 1113. [CrossRef]
41. Pacheco, M.B.; Camilo, V.; Lopes, N.; Moreira-Silva, F.; Correia, M.P.; Henrique, R.; Jerónimo, C. Hydralazine and Panobinostat Attenuate Malignant Properties of Prostate Cancer Cell Lines. *Pharmaceuticals* **2021**, *14*, 670. [CrossRef]
42. Lakshmaiah, K.C.; Jacob, L.A.; Aparna, S.; Lokanatha, D.; Saldanha, S.C. Epigenetic therapy of cancer with histone deacetylase in-hibitors. *J. Cancer Res. Ther.* **2014**, *10*, 469–478. [PubMed]
43. Rana, Z.; Diermeier, S.; Hanif, M.; Rosengren, R.J. Understanding Failure and Improving Treatment Using HDAC Inhibitors for Prostate Cancer. *Biomedicines* **2020**, *8*, 22. [CrossRef] [PubMed]

Article

The Urine Biomarker PUR-4 Is Positively Associated with the Amount of Gleason 4 in Human Prostate Cancers

Richard Y. Ball ¹, Ryan Cardenas ², Mark S. Winterbone ², Marcelino Y. Hanna ³, Chris Parker ^{4,5}, Rachel Hurst ², Daniel S. Brewer ^{2,6}, Lauren D'Sa ¹, Rob Mills ¹, Colin S. Cooper ² and Jeremy Clark ^{2,*}

- ¹ Norfolk and Norwich University Hospitals NHS Foundation Trust, Norwich NR4 7UY, UK; richard.ball@nnuh.nhs.uk (R.Y.B.); lauren.dsa@doctors.org.uk (L.D.); robert.mills@nnuh.nhs.uk (R.M.)
- ² Norwich Medical School, University of East Anglia, Norwich NR4 7TJ, UK; R.Cardenas@uea.ac.uk (R.C.); Mark.Winterbone@uea.ac.uk (M.S.W.); R.Hurst1@uea.ac.uk (R.H.); D.Brewer@uea.ac.uk (D.S.B.); Colin.Cooper@uea.ac.uk (C.S.C.)
- ³ Urology Department Castle Hill, Hull University Teaching Hospital, Castle Rd, Cottingham HU16 5JQ, UK; marcelino.hanna1@nhs.net
- ⁴ Institute of Cancer Research, Sutton SM2 5NG, UK; Chris.Parker@icr.ac.uk
- ⁵ Royal Marsden Hospital, Sutton SM2 5PT, UK
- ⁶ Earlham Institute, Norwich NR4 7UZ, UK
- * Correspondence: jeremy.clark@uea.ac.uk

Abstract: The Prostate Urine Risk (PUR) biomarker is a four-group classifier for predicting outcome in patients prior to biopsy and for men on active surveillance. The four categories correspond to the probabilities of the presence of normal tissue (PUR-1), D'Amico low-risk (PUR-2), intermediate-risk (PUR-3), and high-risk (PUR-4) prostate cancer. In the current study we investigate how the PUR-4 status is linked to Gleason grade, prostate volume, and tumor volume as assessed from biopsy ($n = 215$) and prostatectomy ($n = 9$) samples. For biopsy data PUR-4 status alone was linked to Gleason Grade group (GG) (Spearman's, $\rho = 0.58$, $p < 0.001$ trend). To assess the impact of tumor volume each GG was dichotomized into Small and Large volume cancers relative to median volume. For GG1 (Gleason Pattern 3 + 3) cancers volume had no impact on PUR-4 status. In contrast for GG2 (3 + 4) and GG3 (4 + 3) cancers PUR-4 levels increased in large volume cancers with statistical significance observed for GG2 ($p = 0.005$; Games-Howell). These data indicated that PUR-4 status is linked to the presence of Gleason Pattern 4. To test this observation tumor burden and Gleason Pattern were assessed in nine surgically removed and sectioned prostates allowing reconstruction of 3D maps. PUR-4 was not correlated with Gleason Pattern 3 amount, total tumor volume or prostate size. A strong correlation was observed between amount of Gleason Pattern 4 tumor and PUR-4 signature ($r = 0.71$, $p = 0.034$, Pearson's). These observations shed light on the biological significance of the PUR biomarker and support its use as a non-invasive means of assessing the presence of clinically significant prostate cancer.

Keywords: prostate; cancer; urine; PUR; PUR-4; Gleason pattern 4

Citation: Ball, R.Y.; Cardenas, R.; Winterbone, M.S.; Hanna, M.Y.; Parker, C.; Hurst, R.; Brewer, D.S.; D'Sa, L.; Mills, R.; Cooper, C.S.; et al. The Urine Biomarker PUR-4 Is Positively Associated with the Amount of Gleason 4 in Human Prostate Cancers. *Life* **2021**, *11*, 1172. <https://doi.org/10.3390/life11111172>

Academic Editors: Ana Faustino and Paula A. Oliveira

Received: 30 September 2021
Accepted: 20 October 2021
Published: 3 November 2021

Publisher's Note: MDPI stays neutral with regard to jurisdictional claims in published maps and institutional affiliations.



Copyright: © 2021 by the authors. Licensee MDPI, Basel, Switzerland. This article is an open access article distributed under the terms and conditions of the Creative Commons Attribution (CC BY) license (<https://creativecommons.org/licenses/by/4.0/>).

1. Introduction

Prostate cancer (PCa) diagnosis and prognosis are based on histopathological interpretation of biopsy cores to assess the grade and volume of cancer present as well as the relative proportions of the various Gleason patterns (GP) present. A number of studies have investigated the importance of amount of GP4 on the patient's prognosis and survival. Stark et al. [1] indicated that Gleason Grade group (GG) 3 cancers which have a majority of GP4 cancer were associated with a three-fold higher rate of lethal outcome compared to GG2 cancers [1] which have a majority of GP3 cancer. Additional studies have highlighted that a binary cut-off for relative amount of GP4 cancer as used for defining GG2 and GG3, whilst useful, is not sufficient for complete prognostic discrimination. Specifically Choy et al. [2] reported that an increase in the percentage of tumor in radical prostatectomy (RPx)

samples that is GP4 or greater is associated with an increase in biochemical recurrence (BCR)—ranging from 16% BCR in men where GP4 content was 1–20% to 68% BCR where GP4 was >70% [2]. The percentage of biopsy cores positive for tumor has also been found to link to prognosis [3] and is factored into the CAPRA (Cancer of the Prostate Risk Assessment) score [4]. There is further complexity in that tumor foci in up to 87% of RPx can contain multiple Gleason patterns [5–7].

Most tumors arise in the peripheral and transitional zones of the prostate, which are secretory in nature. Prostatic secretions carry tumor biomarkers into the urethra from where they can be harvested in urine. PCa-biomarkers in urine have shown utility in assessing prognosis. PCa-specific RNA transcripts such as *TMPRSS2:ERG* are detectable in urine from men with prostate cancer [8] and there has been much interest in development of a urine diagnostic test. The majority of such biomarker tests, including the PCA3 test (*PCA3* and *KLK3*), MiPS (serum PSA plus urine *TMPRSS2:ERG* and *PCA3*) and ExosomeDX Prostate Intelliscore (*ERG*, *PCA3*, *SPDEF*), rely on detecting transcripts from a very small number of genes which may not be expressed in every cancer [9–11]. In contrast we have developed the Prostate Urine Risk (PUR) signatures using a NanoString panel of 36 gene probes [12]. PUR detected PCa in urine samples that were negative for *PCA3* and/or *TMPRSS2:ERG*. The PUR signatures were designed to correspond to patients in four clinical groups: those with no evidence of cancer (NEC, PUR-1), and three D’Amico categories of PCa: low-(PUR-2), intermediate-(PUR-3) and high-risk PCa (PUR-4). The PUR-4 signature could detect intermediate and high-risk disease (AUC = 0.77, 95% confidence interval [CI] 0.70–0.84) and was able to predict disease progression in men on an active surveillance monitoring regime up to 5 years after a single urine sample was collected (HR 8.23, 95% CI 3.26–20.81; $p < 0.001$). To understand how PUR-4 related to the structure of the cancerous prostate we now examine its relationship to the amounts and grade of tumor in biopsy-sampled prostates and in a series of radical prostatectomy specimens.

2. Materials and Methods

2.1. Urine RNA Extraction and PUR Signatures

All urine samples (≤ 30 mL) were collected from 295 men who attended urology clinics at the Norfolk and Norwich University Hospitals NHS Foundation Trust (NNUH) UK ($n = 214$) and at the Royal Marsden Hospital (RMH) UK ($n = 81$) between September 2012 to September 2014 [12]. Ethical approval for this study was gained from the Health Research Authority and the NRES Committee East of England in 2012, REC reference: 12/EE/0058, IRAS project ID: 196199. Informed consent was obtained from all subjects involved in the study. All urine samples (≤ 30 mL) were collected pre-biopsy. Urine cell-free RNA (cfRNA) was extracted and the PUR signatures were generated from NanoString (NanoString Technologies Inc, Seattle, WA, USA) expression analysis as per Connell et al. (2019) [12].

2.2. Biopsy Tissue Analyses

Full biopsy data required for tumor volume analysis (prostate volume, total number of cores taken and number of cores positive for PCa) were available for 215/295 patients (Table 1). The majority of the biopsies were trans-rectal ultrasound guided (TRUS) with a range of 2–23 cores taken per prostate (median 9, mean 9). Biopsy data were recorded as part of a standard biopsy assessment for PCa diagnosis at the NNUH and the RMH. Ultrasound prostate volumes ranged from 5.5–353.9 g (mean 53.9, SD 41.9). For clinical characteristics of Gleason grade groups divided into small and large tumors see Supplementary Table S1.

Table 1. Clinical characteristics and PUR scores for biopsy cases. All data presented as: ‘Median (IQR)’.

	NEC	GG1	GG2	GG3	GG4	GG5
Total (%)	62 (22.4%)	93 (33.6%)	61 (22.0%)	38 (13.7%)	12 (4.3%)	11 (4.0%)
Age in years	66 (17)	67 (6.5)	68 (9)	73 (8.25)	71 (12.25)	69 (8.5)
PSA ng/mL	1.2 (2)	7.3 (5.5)	7.8 (4.5)	11.35 (11.03)	13.45 (12.7)	18.7 (45.95)
Prostate volume US	NA	23 (7.5)	42.43 (24.7)	49.03 (28.4)	50.39 (22.9)	55.93 (24.97)
PSAD	NA	0.292 (0.31)	0.179 (0.12)	0.256 (0.22)	0.287 (0.38)	0.31 (0.56)
Biopsy Cores taken	NA	11 (4)	9 (2)	8 (6)	5.5 (5.25)	4 (6.5)
Biopsy Cores positive	NA	1 (1)	3 (3)	3.5 (2.75)	3.5 (3.5)	4 (5)
% biopsy cores positive	NA	12.5 (16.67)	37.5 (42.5)	50 (58.57)	50 (36.39)	100 (0)
% biopsy cores positive/US	NA	0.003 (0.004)	0.001 (0.001)	0.001 (0.001)	0.001 (0.001)	0.001 (0.002)
PUR-1	0.358 (0.206)	0.119 (0.165)	0.078 (0.145)	0.03 (0.119)	0.059 (0.04)	0.07 (0.059)
PUR-2	0.321 (0.036)	0.302 (0.078)	0.275 (0.151)	0.187 (0.217)	0.248 (0.07)	0.201 (0.124)
PUR-3	0.256 (0.129)	0.442 (0.15)	0.452 (0.116)	0.475 (0.119)	0.506 (0.032)	0.489 (0.073)
PUR-4	0.049 (0.036)	0.126 (0.09)	0.162 (0.18)	0.255 (0.269)	0.188 (0.075)	0.171 (0.146)

Abbreviations: IQR, interquartile range; GG, Gleason Grade; NEC, No Evidence of Cancer; US, Ultrasound; Age and PSA at time of urine collection; PSA, prostate specific antigen; PSAD, PSA density (PSA/US prostate volume). PUR-1–4, Prostate urine risk signatures 1–4, NA, Not applicable.

2.3. Radical Prostatectomy Analyses

Nine men had a radical prostatectomy (RPx) within 4 months of their biopsy, and these were analyzed in detail. The RPx were fixed, embedded, sectioned at ~5mm intervals and megablock slides were stained with hematoxylin and eosin (H&E) as part of the standard histopathological reporting process for the NNUH. The H&E stained megablock sections were re-examined for this study by two NNUH histopathologists (RYB, LDS) and marked to indicate all areas of tumor. Each tumor focus was given a Gleason grade (GG) and an estimate for the percentage of Gleason Pattern (GP) 3 and 4 present (see main text and Figure 1). GG2 and GG3 tumor foci were then divided into 6 groups, depending on the percent of Gleason 4 present (see Figures 1 and 2). The tumor-marked H & E-stained slides were scanned on a flatbed scanner at 300 dpi, and Fiji software (Image J version 1.42 q, <https://imagej.net/software/fiji/>) was used to analyze the images and measure the areas of prostate and of each focus of cancer. Prior to analysis of each tissue section Fiji was calibrated using the known width of the H&E slide in the scanned image. Total areas of GP3 and GP4 tumor in each prostate were calculated by multiplying area of each tumor foci by the percentage of GP3 or GP4 present.

2.4. Statistical Analyses

R (v4.0.3) was utilized to perform all statistical analyses. Prior to test selection data were checked for appropriateness for normality and variance using QQ-plots and flinger/shapiro tests, respectively, using the base R package. The Rstatix package was used to perform Kruskal-Wallis rank sum test and Games Howell post-hoc test. All correlation analyses were performed using base R and used Cohen’s effect sizes [13]. Plots were developed using ‘ggplot’ in combination with multiple package extensions including ‘ggsci’, ‘ggrepel’ and ‘ggpubr’. The collection of ‘tidyverse’ packages were utilized for data manipulation. Default options were opted for unless otherwise stated.

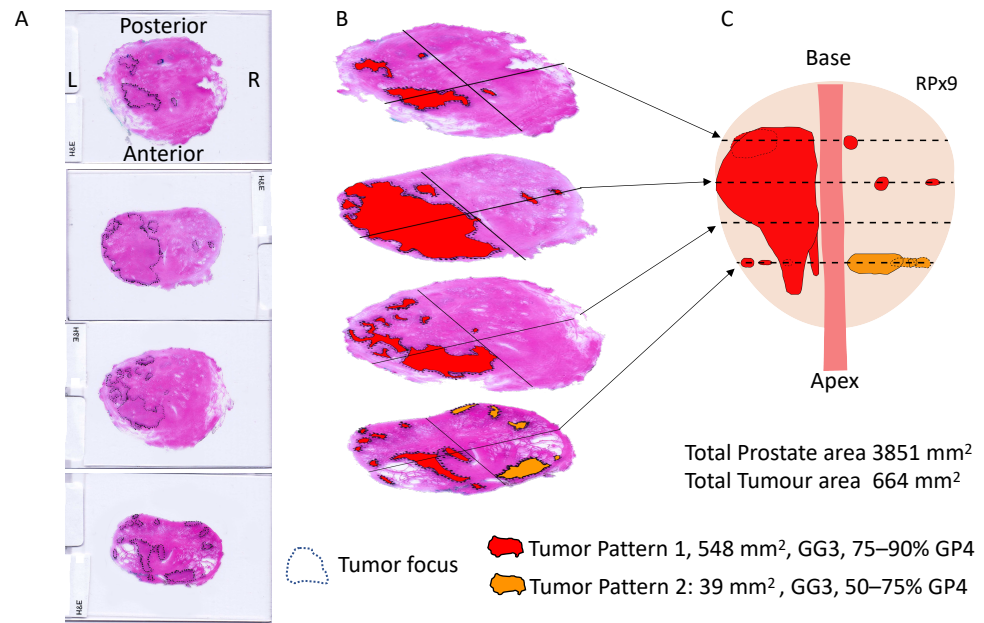


Figure 1. Assessment of prostatectomy RPx9. (A) RPx9 was cut into 4 sections, for which H&E slides were prepared and areas of tumor marked up. (B) the sections are arranged for viewing from base to apex. The PCa areas have been colored to correspond to the Gleason Grade Group (GG) and % GP4 found: red indicates GG3 with 75–90% GP4, orange indicates GG3 with 50–75% GP4 (see Figure 2). (C) the information in ‘B’ was used to create a 3D projection of what the prostate and tumor may have looked like. Dotted tumor indicates a tumor focus behind a more anterior tumor.

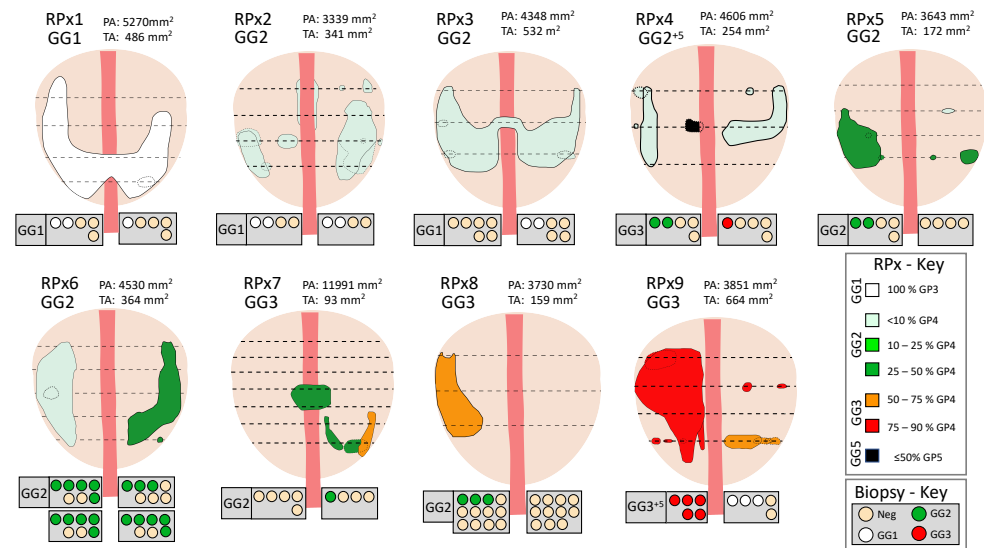


Figure 2. Image projections of tumor content for 9 radical prostatectomies (RPx1–9). Images were constructed for each prostate as shown in Figure 1. The different colors correspond to the % GP4 detected (RPx-Key). PA: prostate area summed for all slices. TA: Tumor Area. ‘+5’ indicates a tertiary region of GP5 tumor. Dotted tumor indicates a tumor focus behind a more anterior tumor. Horizontal dotted lines indicate approximate positions of H&E sections examined. The grey boxes underneath each 3D construct contain the biopsy data taken prior to prostatectomy, including the highest GG found on biopsy. Each circle represents a core taken, data is divided up into left and right cores and also into anterior (upper boxes) and posterior (lower boxes) for one prostate (RPx6).

3. Results

3.1. Analyses of Prostate Needle Biopsy Tissue

PUR signatures (PUR-1 to PUR-4) were generated as published in Connell et al. [12] from urine cell-free-RNA NanoString expression data (36 NanoString gene probes) collected from patients with a suspicion of prostate cancer (Movember cohort, $n = 535$). PUR signatures represent the probability of membership of each of the following clinical groups: PUR-1, NEC (No clinical Evidence of Cancer, PSA normal for age); and PUR-2 to 4, respectively the three D’Amico risk categories low-(PUR-2), intermediate-(PUR-3) and high-risk (PUR-4) [12]. Each sample is represented by a readout in all four PUR signatures with the sum adding up to ‘1’ (see Figure 3A for examples).

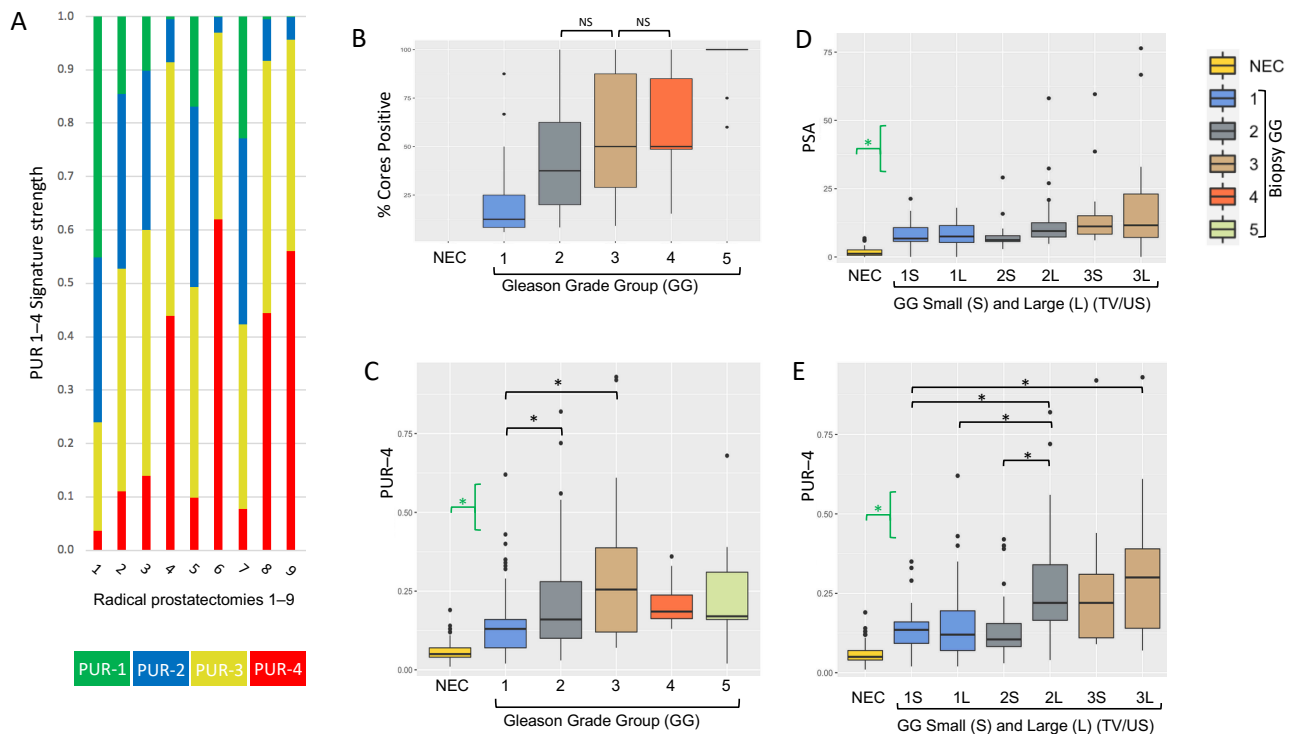


Figure 3. PUR status in biopsy samples. (A) Distribution of the four PUR signatures from nine patients that were subsequently treated by radical prostatectomy. See Figures 1 and 2 for the cancer maps corresponding to these cases. PUR-1 (green), PUR-2 (blue), PUR-3 (yellow), PUR-4 (red). The sum of PUR-1-4 in each sample is ‘1’. (B–D) Data were analyzed using a non-parametric Kruskal-Wallis analysis of variance followed by Games-Howell post-hoc analysis. (B) % Biopsy cores positive also referred to as tumor volume (TV) was calculated as PCa-positive cores/total cores taken. The clinical categories are ‘NEC’: No Evidence of Cancer ($n = 62$) and Biopsy Gleason Grade (GG) groups GG1 ($n = 93$), GG2 ($n = 61$), GG3 ($n = 38$), GG4 ($n = 12$), GG5 ($n = 11$). ‘NS’ indicates ‘Not Significant’ difference in pair-wise analysis of the groups, all other pairwise comparisons were significant ($p < 0.05$). (C) PUR-4 signature for samples in Figure 3B. * indicates a significant difference between groups. Green brackets indicate that a significant difference was found between NEC patient samples and each of the GG patient groups. (D) Serum PSA in GG 1, 2, 3 samples dichotomized based on tumor volume/ultrasound prostate volume (TV/US) into small (S) and large (L) groups, only pairwise comparisons with NEC were significant. No significant differences between GG (S) and (L) groups were found. (E) PUR-4 signal for samples dichotomized as ‘D’ above.

The ‘Biopsy cohort’ consisted of men with PCa detected on biopsy in the Movember cohort for whom full biopsy data were available: number of cores positive; Gleason score; pre-biopsy PSA; and prostate ultrasound volume, $n = 215$. Additionally, 62 men designated as NEC from the Movember cohort were used in comparisons of PUR values. PUR-4 correlated with increasing D’Amico risk group (Supplementary Figure S1), and PUR-4 was significantly different in pairwise comparisons between NEC, D’Amico low, and intermediate-risk groups. PSA also correlated with increasing D’Amico risk group and was significantly different in pairwise comparisons between all clinical categories (Figure S1).

Comparison of PUR-4 to DRE data was not performed due to unreliability of data (see discussion). As expected, the percentage of cores positive for prostate cancer correlated with Gleason Grade group (GG) (Spearman's coefficient of rank correlation $\rho = 0.63$, $p = 1.77 \times 10^{-25}$, Figure 3B). PUR-4 signature values showed a significant positive correlation with increasing GG (Spearman's correlation $\rho = 0.58$, $p = 3.5 \times 10^{-24}$, Figure 3C). When intercomparing the different clinical groups, PUR-4 was significantly different between NEC and each individual GG (all $p < 0.00035$); GG1 cancers were significantly different to both GG2 (Games-Howell post-hoc test, $p = 0.003$) and GG3 tumors ($p = 0.036$). There was no significant difference in tumor volume or PUR-4 between GG2 and GG3 tumors (both $p > 0.05$; Games-Howell post-hoc test).

We next examined the relationships between PUR-4 value and tumor volume. To achieve this the results for each GG were divided into large (L) and small (S) volume cancers relative to the median tumor volume. Tumor volume was calculated as the number of PCa-positive cores/total number of cores taken, with individual values corrected for their patient's prostate volume determined by ultrasound (US). GG4 ($n = 12$) and GG5 groups ($n = 11$) were not subdivided due to the small numbers of samples. There were no significant differences in PSA between (S) and (L) groups for GG1, GG2 or GG3 (Figure 3D, Games-Howell post-hoc test, all $p > 0.05$). There was no difference in PUR-4 values comparing GG1(S) and GG1(L) (Games-Howell post-hoc test, $p = 0.98$, Figure 3E). Since GG1 cancers contain only Gleason Pattern 3 cancer this observation showed that the volume of Gleason Pattern 3 cancer present had no impact on PUR-4 values. PUR-4 for GG2 (L) was significantly greater than for GG2 (S) ($p = 0.005$; Games-Howell post-hoc test), while PUR-4 values for GG3 (L) were greater than for GG3 (S) but did not reach significance (Figure 3E). Since GG2 and GG3 contain both Gleason Pattern 3 and 4 cancer these observations suggest that Gleason Pattern 4 cancer may be contributing to PUR4 status.

3.2. Prostatectomy Analyses

Nine radical prostatectomy specimens were chosen for histopathological re-examination; three GG1, four GG2, and two GG3 based on pre-surgical histopathological assessment of biopsies. H&E analysis was carried out on all individual sections from each RPx as shown in Figure 1 allowing construction of 3D cancer maps (Figure 2). Each section was examined independently by 2 histopathologists (RYB and LD) and areas of cancers were marked depending on the estimated percentage of GP4 present: (i) <10% GP4; (ii) 10–25% GP4; (iii) 26–50% GP4; (iv) 51–75% GP4; (v) 76–90% GP4; and (vi) >90% GP4 (Figures 1 and 2). For each focus of tumor the range midpoint was multiplied by the focus area to provide an estimated amount of GP3 and GP4. These values were summed for each prostate (Table 2, biopsy data for RPx1-9 are presented in Supplementary Table S2).

No significant correlation was observed between PUR-4 score and PSA (Figure S1), or the size of the prostate as measured by ultrasound or H&E tissue area (Figure 4), (Pearson's correlation, $r = -0.33$ $p = 0.4$; $r = -0.47$ $p = 0.2$; $r = -0.3$ $p > 0.4$ respectively). No significant associations were identified between PUR-4 scores and the total area of tumor or the area of GP3 tumor with or without adjustment for prostate size (Pearson's correlation all $p \geq 0.48$) (Figure 4). The amount of GP4 tumor was found to have a strong significant positive correlation with PUR-4 score ($r = 0.71$, $p = 0.035$; Pearson's correlation; Figure 4D), and similar strong associations were found after adjustment for total prostate area on H&E slides ($r = 0.72$, $p = 0.028$; Figure 4E) or for ultrasound prostate volume ($r = 0.73$, $p = 0.024$).

Table 2. Clinical characteristics for the 9 radical prostatectomy (RPx) cases examined.

	GG	Majority GG, %GP4	Prostate Area (mm ²)	Tumor Area (mm ²)	GP3 Area	GP4 Area	Age	PSA	PUR-4
RPx 1	GG1	GG1 ⁺⁴	5269.9	486.4	481.6	4.8	54	5.5	0.04
RPx 2	GG2	GG2, <10% GP4	3339.0	341.2	324.1	17.1	64	15	0.11
RPx 3	GG2	GG2, <10% GP4	4347.6	531.8	505.2	26.6	52	5.8	0.14
RPx 4	GG2 ⁺⁵	GG2, <10% GP4	4606.0	254.5	233.9	20.5	70	8.4	0.44
RPx 5	GG2	GG2, 10–25% GP4	3643.2	172.1	143.3	28.8	66	5.2	0.10
RPx 6	GG2	GG2, <10% GP4	4529.7	364.0	302.0	62.0	68	6.7	0.62
RPx 7	GG3	GG2, 25–50% GP4	11,991.1	92.9	54.8	38.0	67	10.3	0.08
RPx 8	GG3	GG3, 50–75% GP4	3729.6	158.7	60.3	98.4	65	7.4	0.44
RPx 9	GG3	GG3, 75–90% GP4	3851.4	664.4	122.2	542.2	75	2.9	0.56

GG = Gleason Grade group; Majority, data for most common GG found in each prostate; GP3, GP4, GP5, Gleason Pattern 3, 4, 5 respectively; Age, age at recruitment; US, Ultrasound; PCa, prostate cancer; All areas measured from scans of H&E slides (see methods); for GP3 and GP4 amount calculation see results; GG2⁺⁵ indicates GG2 cancer with a tertiary GP5 (<5% of all PCa), similarly GG1⁺⁴ indicates a GG1 cancer with tertiary GP4; PUR-4, Prostate urine risk signatures 4.

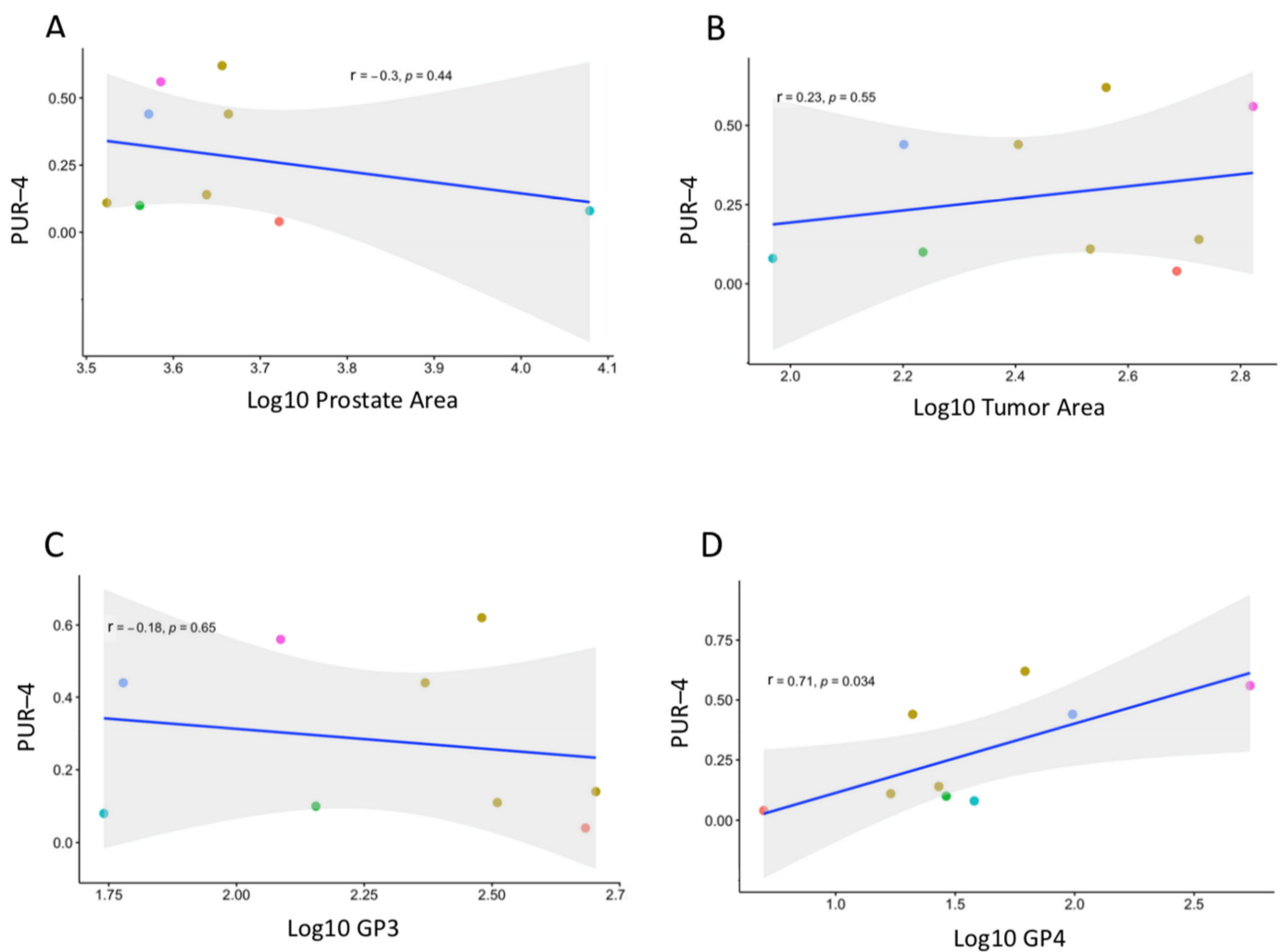


Figure 4. Cont.

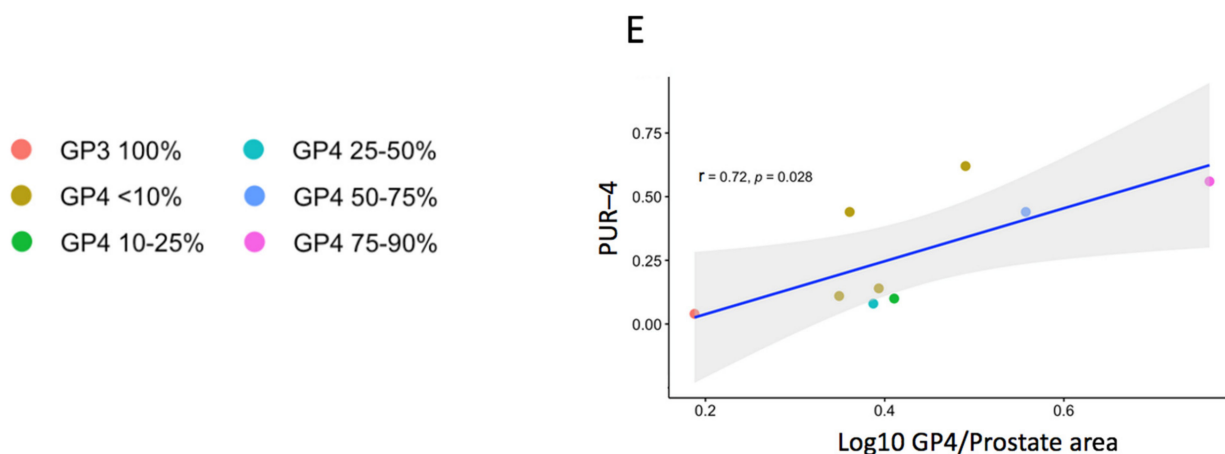


Figure 4. Correlation of PUR-4 with prostate parameters. Measurements were taken from the 9 whole mount prostate H&E sections shown in Figure 2. Each sample is colored by the Gleason score of the predominant tumor area (see key). No correlation was found between PUR-4 and (A) prostate area of the H&E sections, (B) tumor area, (C) amount of Gleason pattern 3. (D) PUR-4 correlated with amount of Gleason pattern 4 cancer both before, and (E) after adjustment for prostate area (see body text for details). ‘*r*’ is the Pearson’s correlation coefficient, an ‘*r*’ > 0.7 indicates a strong correlation, ‘*p*’ = probability that the correlation has not arisen by chance.

4. Discussion

When estimating Gleason Grade Evans et al. [14] reported that only 55% of cases were concordant between biopsy and radical prostatectomy, while Yang et al. [15] and Epstein et al. [16] reported upgrading in 30–36% of RPxs. Comparably we found disease upgrading in 55% (5 of 9) prostatectomy specimens (Figure 2). Two out of three RPx reported as GG1 on biopsy had GP4 in their RPxs, 2/4 biopsy GG2 were upgraded to GG3, and GP5 was found in one prostate (RPx4). As the interval between biopsy and prostatectomy was ≤ 4 months for all samples, these Gleason differences were inferred to be due to biopsy sampling issues. Despite potential limitations of the tumor volume assessment, our results support the hypothesis that there is a relationship between increasing amounts of GP4 PCa and increasing PUR-4 signal in GG2 and GG3 tumors both in biopsy specimens and for prostatectomies. The importance of detecting and estimating the amount of Gleason pattern 4 tumor is highly relevant to risk stratification and selecting the appropriate treatment pathway for a patient [17–19].

No difference in PUR-4 signals were observed between GG2 (S) and the GG1 (S) and GG1 (L) subgroups ($p > 0.05$). We have previously shown that a PUR-4 signature of < 0.174 identified a subgroup of men whose disease did not progress to require treatment intervention up to 5 years later (HR 8.23, 95% CI 3.26–20.81; $p < 0.001$) [12]. Significantly, 80% of the GG2 (S) tumors were below the 0.174 PUR-4 cutoff, and the vast majority of these (83%) had $< 30\%$ PCa-positive cores (average 21%, median 19%), a figure comparable to that found in the GG1 cancers (94% $< 30\%$ cores positive, median 13%, average 15%). These results suggest that PUR-4 may be identifying a group of low tumor-volume GG2 men who could benefit from an active surveillance monitoring regime.

One limitation of this study is that we could not interrogate an increase in PUR-4 in patients with GG4 and GG5 disease due to the small sample numbers involved. Anecdotally the PUR-4 signature for RPx4 which was found to have an area of GP4+5 on RPx was much higher than expected for the volume of GP4 calculated in this largely GG2 $< 10\%$ GP4 cancer, which may imply that PUR-4 can respond to disease that is becoming more aggressive.

PUR-4 increases with D’Amico risk group, and D’Amico categorization includes data from Gleason, PSA and DRE. However, while PSA increased with D’Amico risk group, there were no differences in PSA between the GG (S) and GG (L) groups. In addition, there was no correlation between PSA and PUR-4 for the 9 RPx. When taken together these

results indicate that PUR-4 does not appear to mirror serum PSA. DRE information was not considered reliable data for this cohort, DRE data is considered to be subjective, for example Gosselaar et al. [20] found that suspicion of cancer on DRE by 6 clinicians varied from 4–28%, while Ankerst [21] found that 70% of abnormal DREs were DRE-normal the following year. A meta-analysis by Naji et al. [22] of 8217 studies led them to the conclusion that there was no evidence for the efficacy of using a DRE to detect prostate cancer [22]. The percentage of cores positive was considered to be a more solid assessment of extent of tumor, and as approximately equal numbers of cores were taken on each side of the prostate, a figure of >50% cancer positive would indicate disease on both sides of the prostate.

We propose that the PUR urine test could help in the diagnostic pathway for patients who are worried about their risk of prostate cancer and those with suspected prostate cancer. mpMRI has aided the diagnosis of significant disease, but negative aspects of mpMRI are that it can miss significant cancers ($GP \geq 4$) [23], identify insignificant cancers (GG1) [24], and has been reported to have a high false-positive rate of around 50% [23], with problems of interoperator inconsistencies [25]. We believe that the PUR test could add to the information from multiparametric magnetic resonance imaging (mpMRI) and aid decision making on whether a biopsy is necessary.

5. Conclusions

A strong association was observed between an increasing amount of Gleason pattern 4 cancer and increasing PUR-4 signal. These data suggest that the PUR-4 signature could provide useful additional information in determining the amount of clinically significant tumor within a prostate and thereby help guide the patient treatment pathway with essential information for triage, improved management and prognostic utility.

Supplementary Materials: The following are available online at <https://www.mdpi.com/article/10.3390/life11111172/s1>, Figure S1: PSA and PUR-4 data in biopsy patients categorized on D'Amico and PSA in the nine RPx men, Table S1: Clinical characteristics and PUR scores for biopsy cases categorized by Gleason Grade and subcategorized by % biopsy cores positive, Table S2: Combined RPx and Biopsy clinical characteristics for the 9 radical prostatectomy (RPx) cases examined.

Author Contributions: Conceptualization, J.C. and R.Y.B.; methodology, J.C. and R.Y.B.; software, J.C. and R.C.; formal analysis, M.S.W. and R.C.; resources, R.Y.B., L.D., R.M., R.H., C.P. and M.Y.H.; data curation, D.S.B.; writing—original draft preparation, J.C.; writing—review & editing, J.C., C.S.C., D.S.B., R.H., R.Y.B., R.C. and M.S.W.; visualization, J.C. and R.C.; supervision, J.C., C.S.C. and D.S.B.; project administration, J.C.; funding acquisition, C.S.C. and D.S.B. All authors have read and agreed to the published version of the manuscript.

Funding: This study was possible thanks to the Movember Foundation GAP1 Urine Biomarker project, Prostate Cancer UK, The Masonic Charitable Foundation, The Bob Champion Cancer Trust, the King family, Big C Cancer Charity, The Andy Ripley Memorial Fund and the Stephen Hargrave Trust. The sponsors had no role in the design, execution, interpretation, or writing of the study.

Institutional Review Board Statement: The study was conducted according to the guidelines of the Declaration of Helsinki, and approved by the Health Research Authority and the NRES Committee East of England Ethics Committee, 2012. REC reference: 12/EE/0058, IRAS project ID: 196199.

Informed Consent Statement: Informed consent was obtained from all subjects involved in the study.

Data Availability Statement: Data is contained within the article or supplementary material.

Conflicts of Interest: A patent application has been filed by C.S.C., J.C. and D.S.B. for the use of the PUR biomarkers in prostate cancer diagnosis and prognosis. There are no other conflicts of interest to disclose.

References

1. Stark, J.R.; Perner, S.; Stampfer, M.J.; Sinnott, J.A.; Finn, S.; Eisenstein, A.S.; Ma, J.; Fiorentino, M.; Kurth, T.; Loda, M.; et al. Gleason score and lethal prostate cancer: Does $3 + 4 = 4 + 3$? *J. Clin. Oncol.* **2009**, *27*, 3459–3464. [CrossRef] [PubMed]
2. Choy, B.; Pearce, S.M.; Anderson, B.B.; Shalhav, A.L.; Zagaja, G.; Eggener, S.E.; Paner, G.P. Prognostic Significance of Percentage and Architectural Types of Contemporary Gleason Pattern 4 Prostate Cancer in Radical Prostatectomy. *Am. J. Surg. Pathol.* **2016**, *40*, 1400–1406. [CrossRef]
3. Spalding, A.C.; Daignault, S.; Sandler, H.M.; Shah, R.B.; Pan, C.C.; Ray, M.E. Percent positive biopsy cores as a prognostic factor for prostate cancer treated with external beam radiation. *Urology* **2007**, *69*, 936–940. [CrossRef] [PubMed]
4. Cooperberg, M.R.; Freedland, S.J.; Pasta, D.J.; Elkin, E.P.; Presti, J.C.; Amling, C.L.; Terris, M.K.; Aronson, W.J.; Kane, C.J.; Carroll, P.R. Multiinstitutional validation of the UCSF cancer of the prostate risk assessment for prediction of recurrence after radical prostatectomy. *Cancer* **2006**, *107*, 2384–2391. [CrossRef]
5. Arora, R.; Koch, M.O.; Eble, J.N.; Ulbright, T.M.; Li, L.; Cheng, L. Heterogeneity of Gleason grade in multifocal adenocarcinoma of the prostate. *Cancer* **2004**, *100*, 2362–2366. [CrossRef] [PubMed]
6. Le, J.D.; Tan, N.; Shkoliar, E.; Lu, D.Y.; Kwan, L.; Marks, L.S.; Huang, J.; Margolis, D.J.A.; Raman, S.S.; Reiter, R.E. Multifocality and prostate cancer detection by multiparametric magnetic resonance imaging: Correlation with whole-mount histopathology. *Eur. Urol.* **2015**, *67*, 569–576. [CrossRef] [PubMed]
7. Cooper, C.S.; Eeles, R.; Wedge, D.C.; Van Loo, P.; Gundem, G.; Alexandrov, L.B.; Kremeyer, B.; Butler, A.; Lynch, A.G.; Camacho, N.; et al. Analysis of the genetic phylogeny of multifocal prostate cancer identifies multiple independent clonal expansions in neoplastic and morphologically normal prostate tissue. *Nat. Genet.* **2015**, *47*, 367–372. [CrossRef] [PubMed]
8. Nguyen, P.-N.; Violette, P.; Chan, S.; Tanguay, S.; Kassouf, W.; Aprikian, A.; Chen, J.Z. A Panel of TMPRSS2:ERG Fusion Transcript Markers for Urine-Based Prostate Cancer Detection with High Specificity and Sensitivity. *Eur. Urol.* **2010**, *59*, 407–414. [CrossRef] [PubMed]
9. Groskopf, J.; Aubin, S.M.J.; Deras, I.L.; Blase, A.; Bodrug, S.; Clark, C.; Brentano, S.; Mathis, J.; Pham, J.; Meyer, T.; et al. APTIMA PCA3 molecular urine test: Development of a method to aid in the diagnosis of prostate cancer. *Clin. Chem.* **2006**, *52*, 1089–1095. [CrossRef] [PubMed]
10. Tomlins, S.A.; Day, J.R.; Lonigro, R.J.; Hovelson, D.H.; Siddiqui, J.; Kunju, L.P.; Dunn, R.L.; Meyer, S.; Hodge, P.; Groskopf, J.; et al. Urine TMPRSS2:ERG Plus PCA3 for Individualized Prostate Cancer Risk Assessment. *Eur. Urol.* **2016**, *70*, 45–53. [CrossRef] [PubMed]
11. McKiernan, J.; Donovan, M.J.; Margolis, E.; Partin, A.; Carter, B.; Brown, G.; Torkler, P.; Noerholm, M.; Skog, J.; Shore, N.; et al. A Prospective Adaptive Utility Trial to Validate Performance of a Novel Urine Exosome Gene Expression Assay to Predict High-grade Prostate Cancer in Patients with Prostate-specific Antigen 2–10 ng/mL at Initial Biopsy. *Eur. Urol.* **2018**, *74*, 731–738. [CrossRef] [PubMed]
12. Connell, S.P.; Hanna, M.; McCarthy, F.; Hurst, R.; Webb, M.; Curley, H.; Walker, H.; Mills, R.; Ball, R.Y.; Sanda, M.G.; et al. A Four-Group Urine Risk Classifier for Predicting Outcome in Prostate Cancer Patients. *BJU Int.* **2019**, *124*, 609–620. [CrossRef] [PubMed]
13. Cohen, J. *Statistical Power Analysis for the Behavioral Sciences*; Academic Press: Cambridge, MA, USA, 2013.
14. Evans, S.M.; Bandarage, V.P.; Kronborg, C.; Earnest, A.; Millar, J.; Clouston, D. Gleason group concordance between biopsy and radical prostatectomy specimens: A cohort study from Prostate Cancer Outcome Registry-Victoria. *Prostate Int.* **2016**, *4*, 145–151. [CrossRef] [PubMed]
15. Yang, D.D.; Mahal, B.A.; Muralidhar, V.; Nezelosky, M.D.; Vastola, M.E.; Labe, S.A.; Boldbaatar, N.; King, M.T.; Martin, N.E.; Orio, P.F., 3rd; et al. Risk of Upgrading and Upstaging Among 10,000 Patients with Gleason 3 + 4 Favorable Intermediate-risk Prostate Cancer. *Eur. Urol. Focus* **2019**, *5*, 69–76. [CrossRef]
16. Epstein, J.I.; Feng, Z.; Trock, B.J.; Pierorazio, P.M. Upgrading and Downgrading of Prostate Cancer from Biopsy to Radical Prostatectomy: Incidence and Predictive Factors Using the Modified Gleason Grading System and Factoring in Tertiary Grades. *Eur. Urol.* **2012**, *61*, 1019–1024. [CrossRef] [PubMed]
17. Kane, C.J.; Eggener, S.E.; Shindel, A.W.; Andriole, G.L. Variability in Outcomes for Patients with Intermediate-risk Prostate Cancer (Gleason Score 7, International Society of Urological Pathology Gleason Group 2–3) and Implications for Risk Stratification: A Systematic Review. *Eur. Urol. Focus* **2017**, *3*, 487–497. [CrossRef] [PubMed]
18. Sanda, M.G.; Cadeddu, J.A.; Kirkby, E.; Chen, R.C.; Crispino, T.; Fontanarosa, J.; Freedland, S.J.; Greene, K.; Klotz, L.H.; Makarov, D.V.; et al. Clinically Localized Prostate Cancer: AUA/ASTRO/SUO Guideline. Part I: Risk Stratification, Shared Decision Making, and Care Options. *J. Urol.* **2017**, *199*, 683–690. [CrossRef]
19. Zumsteg, Z.S.; Zelefsky, M.J. Short-term androgen deprivation therapy for patients with intermediate-risk prostate cancer undergoing dose-escalated radiotherapy: The standard of care? *Lancet Oncol.* **2012**, *13*, e259–e269. [CrossRef]
20. Gosselaar, C.; Kranse, R.; Roobol, M.J.; Roemeling, S.; Schröder, F.H. The interobserver variability of digital rectal examination in a large randomized trial for the screening of prostate cancer. *Prostate* **2008**, *68*, 985–993. [CrossRef]
21. Ankerst, D.P.; Miyamoto, R.; Nair, P.V.; Pollock, B.H.; Thompson, I.M.; Parekh, D.J. Yearly prostate specific antigen and digital rectal examination fluctuations in a screened population. *J. Urol.* **2009**, *181*, 2071–2076. [CrossRef] [PubMed]

22. Naji, L.; Randhawa, H.; Sohani, Z.; Dennis, B.; Lautenbach, D.; Kavanagh, O.; Bawor, M.; Banfield, L.; Profetto, J. Digital Rectal Examination for Prostate Cancer Screening in Primary Care: A Systematic Review and Meta-Analysis. *Ann. Fam. Med.* **2018**, *16*, 149–154. [CrossRef] [PubMed]
23. Ahmed, H.U.; El-Shater Bosaily, A.; Brown, L.C.; Gabe, R.; Kaplan, R.; Parmar, M.K.; Collaco-Moraes, Y.; Ward, K.; Hindley, R.G.; Freeman, A.; et al. Diagnostic accuracy of multi-parametric MRI and TRUS biopsy in prostate cancer (PROMIS): A paired validating confirmatory study. *Lancet* **2017**, *25*, 815–822. [CrossRef]
24. Eldred-Evans, D.; Burak, P.; Connor, M.J.; Day, E.; Evans, M.; Fiorentino, F.; Gammon, M.; Hosking-Jervis, F.; Klimowska-Nassar, N.; McGuire, W.; et al. Population-Based Prostate Cancer Screening with Magnetic Resonance Imaging or Ultrasonography. *JAMA Oncol.* **2021**, *7*, 395–402. [CrossRef] [PubMed]
25. Walz, J. The “PROMIS” of Magnetic Resonance Imaging Cost Effectiveness in Prostate Cancer Diagnosis? *Eur. Urol.* **2018**, *73*, 31–32. [CrossRef] [PubMed]

Prostate Cancer Aggressiveness Prediction Using CT Images

Bruno Mendes ^{1,2,*} , Inês Domingues ^{1,3} , Augusto Silva ⁴  and João Santos ^{1,5} 

- ¹ Centro de Investigação do Instituto Português de Oncologia do Porto (CI-IPOP), Grupo de Física Médica, Radiobiologia e Protecção Radiológica, 4200-072 Porto, Portugal; inesdomingues@gmail.com (I.D.); j.a.miranda.santos@gmail.com (J.S.)
- ² Faculdade de Engenharia da Universidade do Porto (FEUP), 4200-465 Porto, Portugal
- ³ Instituto Superior de Engenharia de Coimbra (ISEC), 3030-199 Coimbra, Portugal
- ⁴ IEETA, Universidade de Aveiro (UA), 3810-193 Aveiro, Portugal; augusto.silva@ua.pt
- ⁵ Instituto de Ciências Biomédicas Abel Salazar (ICBAS), 4050-313 Porto, Portugal
- * Correspondence: brunomendes81@gmail.com

Abstract: Prostate Cancer (PCa) is mostly asymptomatic at an early stage and often painless requiring active surveillance screening. Transrectal Ultrasound Guided Biopsy (TRUS) is the principal method to diagnose PCa following a histological examination by observing cell pattern irregularities and assigning the Gleason Score (GS) according to the recommended guidelines. This procedure presents sampling errors and, being invasive may cause complications to the patients. External Beam Radiotherapy Treatment (EBRT) is presented as curative option for localised and locally advanced disease, as a palliative option for metastatic low-volume disease or after prostatectomy for prostate bed and pelvic nodes salvage. In the EBRT workflow a Computed Tomography (CT) scan is performed as the basis for dose calculations and volume delineations. In this work, we evaluated the use of data-characterization algorithms (radiomics) from CT images for PCa aggressiveness assessment. The fundamental motivation relies on the wide availability of CT images and the need to provide tools to assess EBRT effectiveness. We used Pyradiomics and Local Image Features Extraction (LIFEx) to extract features and search for a radiomic signature within CT images. Finally, when applying Principal Component Analysis (PCA) to the features, we were able to show promising results.

Citation: Mendes, B.; Domingues, I.; Silva, A.; Santos, J. Prostate Cancer Aggressiveness Prediction Using CT Images. *Life* **2021**, *11*, 1164. <https://doi.org/10.3390/life11111164>

Academic Editor: Antonio Bellastella

Received: 30 September 2021

Accepted: 26 October 2021

Published: 31 October 2021

Publisher's Note: MDPI stays neutral with regard to jurisdictional claims in published maps and institutional affiliations.



Copyright: © 2021 by the authors. Licensee MDPI, Basel, Switzerland. This article is an open access article distributed under the terms and conditions of the Creative Commons Attribution (CC BY) license (<https://creativecommons.org/licenses/by/4.0/>).

Keywords: prostate cancer; radiomic features; classification; risk stratification; computed tomography

1. Introduction

The first described Prostate Cancer (PCa) case goes back to 1853, when John Adams, a surgeon at the London Hospital, followed a histological examination for cirrhosis of the prostate gland. He reported the condition as an orphan disease. In 2020, it was the second most frequent malignancy, with 1.414.259 new cases and responsible for 7.3% of all cancer deaths in men [1].

The prostate gland is part of the male reproductive system and about the size of a walnut. It is located in the pelvis surrounding the prostatic urethra and below the bladder [2]. Histologically and clinically, it is a heterogeneous organ divided into four anatomic regions [3]. The central zone encompasses the ejaculatory duct and is relatively immune to cancer. The main body of the prostate gland is the peripheral zone, located posteriorly to the rectum. Most carcinomas arise here [3]. The transitional zone surrounds the urethra and the anterior fibromuscular stroma is non-glandular with no pathological interest [3].

PCa is usually asymptomatic at an early stage and screened by Digital Rectal Examination (DRE) and Prostate Specific Antigen (PSA) blood test. The principal method to diagnose PCa is the Transrectal Ultrasound Guided Biopsy (TRUS) with samples taken mainly from the peripheral zone [4]. The pathologist identifies the two most predominant sets of patterns. He then assigns a score of 1 if prostate cells are uniformly packed, up to a grade of 5 depending on pattern irregularity. The sum of both is designated the Gleason Score (GS) and is proportional

to PCa aggressiveness. Several studies showed that a GS of 7 = 4 + 3 has the worst prognosis than a GS of 7 = 3 + 4. Taking this into account, Epstein et al. [5] proposed a new stratification by Grade Group (GG), as shown in Figure 1. This new grading system provides the potential to reduce the overtreatment of indolent cancer and reflects the high heterogeneity of PCa [5].

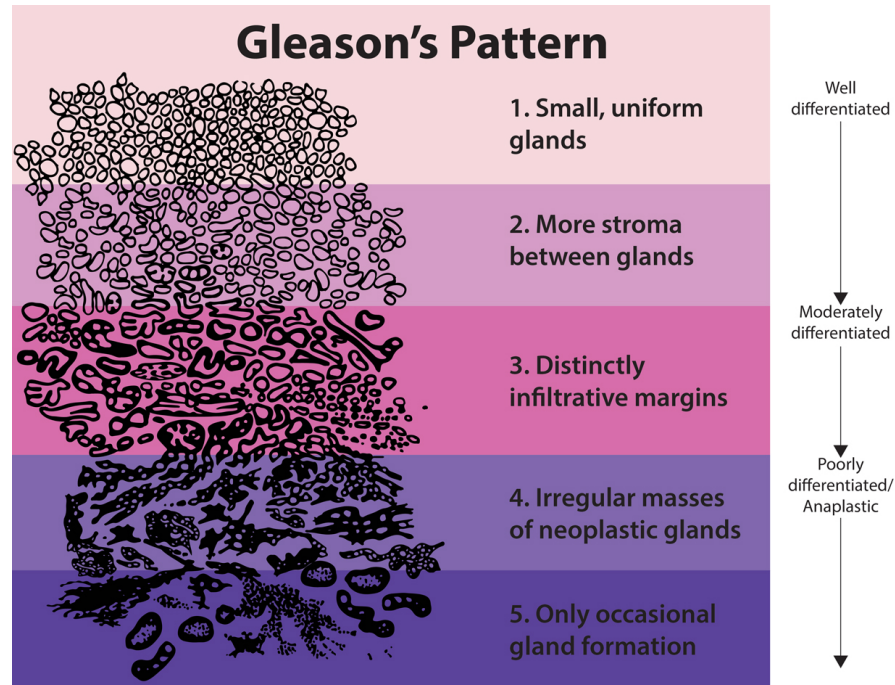


Figure 1. Stratification by Risk Group (RG). Adapted from [5].

Theoretically GS ranges from 2 to 10 but in practice scores < 6 are never assigned. Table 1 shows the stratification by risk groups.

Table 1. Stratification by risk groups.

Risk Group	Grade Group	GS
Low/Very Low	1	≤6
Intermediate	2	7 (3+4)
(Favorable/Unfavorable)	3	7 (4+3)
High/Very High	4	8
	5	9–10

Grading PCa plays a crucial role in treatment decision outcomes. External Beam Radiotherapy Treatment (EBRT) is a curative option for localised and locally advanced diseases. Also, as a palliative option for metastatic low-volume disease or after prostatectomy for prostate bed and pelvic nodes salvage [6].

In the treatment workflow, patients usually do a Computed Tomography (CT) scan providing the anatomical basics for EBRT planning. In this stage, experts define tumour and tissue-related volumes. According to the International Commission on Radiation Units and Measurements (ICRU) guidelines, Organs At Risk (OARs) are structures or tissues that may suffer morbidity if irradiated. For PCa, the OARs are, by order of priority, rectum, bladder, bowel bag and femoral heads (right and left). The Gross Tumour Volume (GTV) is the gross demonstrable extent and location of the tumour. It may also include regional lymph nodes and distant metastasis if they are indistinguishable from the primary tumour. The Clinical Target Volume (CTV) is a volume that contains a GTV and a margin that reflects the probability of subclinical disease occurrence. The dose prescription is to the CTV plus a clinically acceptable margin that includes organ motion and setup variations (Planning Target Volume (PTV)) [7].

During or after treatment, the tumour marker used to evaluate the effectiveness is the PSA. PSA is an enzyme produced in the prostatic epithelium aiding in the mobility of sperm cells and fertilization. High levels of PSA may indicate the presence of PCa [8], although it may also be associated with BPH, enlarged prostate gland [9]. The traditional PSA level of 4.0 ng/ml is usually the threshold for further evaluation, but this value remains controversial [4,10].

Heterogeneous solid cancers may limit invasive biopsies but open an opportunity to medical imaging. Particularly when significant differences in protein expression patterns proved to correlate to radiographic findings [11]. CT images have a higher spatial resolution than Magnetic Resonance Imaging (MRI) allowing the evaluation of density, shape and texture characteristics. Radiomics, the extraction of features from radiographic images using data-characterization algorithms, may provide a valuable tool for PCa grading during EBRT. The hypothesis behind radiomics is that quantitative analysis of medical images may provide a similar prognosis power as phenotypes and gene protein signatures.

Most studies seem focused on the initial and diagnosis stage of PCa. Therefore, the preferred imaging modality for radiomic studies is MRI, the *de facto* standard for PCa staging and grading. The present study aims to evaluate the potential use of radiomic features extracted from CT images and provide the baseline for a classifier that predicts PCa aggressiveness during treatment. Such a tool may improve decision outcomes and avoid overdiagnosis and overtreatment.

In this work, we evaluated the extraction of radiomic features from pyradiomics and Local Image Features Extraction (LIFEx) platforms. We searched for a radiomic signature that could predict prostate cancer aggressiveness. However, the lack of characteristic metabolic manifestation of CT proved to be a challenge. Using Principal Component Analysis (PCA) and several variations, we computed Area Under the Receiver Operating Characteristic (AUROC) values using a One-vs-Rest (OvR) Classifier with a linear kernel and obtained promising results.

Following this introductory section, we have Section 2 that presents the state-of-the-art radiomics in prostate cancer. Section 3 hands over the image database and proposed stratification according to the RG. It also shows the proposed method to overcome the lack of CT radiomic signatures for PCa aggressiveness assessment. Section 4 shows the obtained results and grounds the methodology, and finally, Section 5 extends the main conclusions of this work.

2. Related Work

PCa diagnosis, staging and grading presents several challenges to overcome. Radiomics, the extraction of quantitative features from medical images using data characterization algorithms, have the ability to provide more relevant information, improving decision outcomes and avoiding overdiagnosis and/or overtreatment.

TRUS is usually used for PCa diagnosis but it may present sampling errors due to the randomness in needle positioning [4]. Besides it is an invasive procedure and can cause complications to the patient such as hematuria, hematospermia and inflammation [12]. The addition of radiomic features to ultrasound images may provide the ability to diagnose PCa without any of these issues. The power of radiomic features to distinguish clinically significant PCa based on ultrasound images has been addressed by Wildeboer et al. [13], Liang et al. [14] with promising results. Liang et al. [14] also added clinical parameters as age, prostate volume, PSA and others. Both studies provided the baseline for deeper analysis using ultrasound images revealing also the potential to use radiomics in an early stage of PCa evaluation.

Multi-parametric Magnetic Resonance Imaging (mpMRI) is considered the gold standard for PCa assessment. And, with no wonder, most of the radiomic studies found are based on this imaging modality. Prostate Imaging Reporting and Data System (PIRADS) also provides an already established system to enable performance comparisons. In fact, PIRADS 3 score raises some doubts as it defines clinically significant PCa as equivocal.

Hou et al. [15] addressed this issue in order to identify clinically significant PCa in PIRADS 3 patients with success. Giambelluca et al. [16] added texture analysis also with PIRADS 3 patients to successfully identify PCa. Chen et al. [17] compared the performance of radiomic-based model with PIRADS. All selected patients had undergone a TRUS and histologically confirmed PCa, GS was available, mpMRI and no prior surgery or EBRT. The same baseline as PIRADS. After statistically selecting six radiomic features the models built from different mpMRI sequences, all outperformed PIRADS predicting PCa.

Biochemical Recurrence (BCR) is also worth mentioning because it is not taken into account by PIRADS. BCR is usually defined as a rise in PSA level after radical prostatectomy or EBRT, although this definition is somewhat controversial. Not all patients with elevated PSA values will develop metastases [18]. In an attempt to predict BCR prior to treatment, Shiradkar et al. [19] identified a set of radiomic features highly predictive of BCR compared to GS, PSA and PIRADS. But the first study to externally validate a radiomics predictive model for high risk PCa with prostatectomy only, was Bourbonne et al. [20] with 88 patients from an external institution. The radiomic model based on Apparent Diffusion Coefficient (ADC) maps achieved an accuracy on the external validation dataset of 76% in predicting BCR. In a pioneer study, Bosetti et al. [21] suggested that energy and kurtosis features from Cone Beam Computed Tomography (CBCT) are predictive of BCR with an AUROC of 0.84.

Recently, Providência et al. [22] has developed a specially designed algorithm to classify hotspots from bone scintigraphy images. They extracted hand-crafted intensity features and used a pretrained Convolutional Neural Network (CNN) for high-level features following a semisupervised approach, claiming an AUROC of 0.66.

Grading can be challenging for radiomic analysis because the endpoint to address aggressiveness derives from histological findings (GS). But Abraham and Nair [23] proved otherwise. Introducing texture features and a Stacked Sparse AutoEncoder (SSAE) for PCa grade group prediction, Abraham and Nair [23] topped the PROSTATEx-2 challenge with a quadratic-weighted kappa score of 0.2772. Introducing peri-tumoral radiomic features for PCa stratification Algohary et al. [24] also achieved great results with an improvement of 3–6% compared to intra-tumoral features alone. Osman et al. [25] was able to distinguish between $GS \leq 6$ and $GS \geq 7$ with an AUROC of 0.90 and $GS 7(3 + 4)$ versus $GS 7(4 + 3)$ with an AUROC of 0.98 from CT images.

The mentioned previous studies sustain the idea that the addition of radiomics to already well-established guidelines offer benefits. With the phenotypic and predictive power of radiomic features and the wide availability of CT images, we may provide a tool to assess treatment responses, increasing effectiveness and survival rates.

3. Materials and Methods

This work is retrospective research that used treatment plans available at Instituto Português de Oncologia do Porto Francisco Gentil (IPO-PORTO). All patients had undergone a CT scan as part of the EBRT treatment and had the GS available. Section 3.1 presents the image database. In Section 3.3 and Section 3.4 are the methods used to extract and select features, and finally, in Section 3.5 the methods used to build the classifier.

3.1. The Image Dataset

The image dataset has CT images from 44 patients following a 3-fold GS risk group stratification, as suggested by Epstein et al. [5] and presented in Table 2. All studies ranged from 2015 to 2019 with curative intent, and patients were between 48 and 58 years old. Two 16 slices CT scanners from General Electric, GE Optima 580 and LightspeedRT16, available at the IPO-PORTO, were used, with 2.5 mm slice thickness, 120 Kvp and automatic tube current modulation.

CT images have a higher spatial resolution than MRI, allowing the evaluation of density, shape and texture characteristics. Although they lack characteristic manifestation [26] and seem to be a poor candidate for radiomic feature extraction, their use for volume delineation in the treatment planning stage makes them widely available.

All images were anonymized and had the approval of use from the ethics committee of IPO-PORTO.

Table 2. Number of cases and images per risk group.

Risk Group	Class	# Cases	# Images
Low/Very Low	0	3	56
Intermediate	1	31	664
High/Very High	2	10	209
Total		44	929

3.2. Volumes of Interest

In EBRT planning, tumor and tissue related volumes are defined by the ICRU. The recommended tool to shape absorbed dose distributions is to define the PTV. Knowledge of uncertainties and variations in tumor volume and machine parameters must be known a priori and thus this volume is very institution dependent. Modern EBRT treatment planning systems use priority rules and weights in the OARs in an optimization framework. The goal is to minimize dose at OARs while preserving the prescribed dose at the PTV [7]. For PCa the OARs are, by order of priority rectum, bladder, bowel bag and femoral heads (right and left). In the treatment planning system dose constrains for each OAR must be taken into account [7]. Figure 2 shows the volumes of interest for prostate adenocarcinoma.

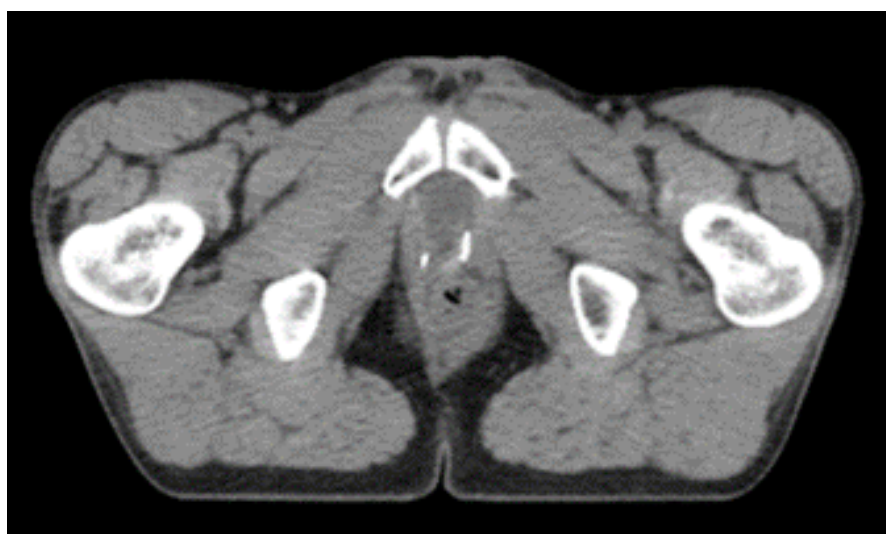


Figure 2. Volumes of interest for prostate adenocarcinoma treatment planning. In orange the CTV; in red the PTV; in green the rectum; the bladder in dark blue and in light blue the femoral heads. Adapted from Gregoire et al. [7].

Experts at the institution delineated all Volumes Of Interest (VOIs) and OARs following an ATLAS based semi-automatic approach. The CTV was chosen as the feature extraction region because it contains the most clinical and pathological information.

3.3. Feature Extraction

Radiomics are the extracting and quantifying image features in a given volume. Combined with other patient information and clinical outcomes, they can provide a potential tool for decision support models [27]. Radiomics extracts two types of features: semantic and agnostic. Semantic features describe lesions with prognostic values, such as size, shape or necrosis. Agnostic features provide first-order, second-order or higher-order statistics. First-order statistics focus on individual voxels reducing the volume to a single value. Second-order descriptors are texture features grouping voxels with similar statistics and

are very useful to measure tumour heterogeneity. Higher-order statistics search for pattern repetitions in the volume [27]. Table 3 shows some of the features that can be extracted.

Table 3. Examples of radiomic features.

First-order	Mean, Medium, Maximum, Minimum, Entropy, Skewness, Kurtosis, ...
Second-order	Autocorrelation, Contrast, Difference Average, Difference Entropy, Inverse Difference Moment, ...
Higher-order	Coarseness, Busyness, Complexity, Strength, Gray Level Non-Uniformity, Gray Level Variance, ...

Features should comply with the Image Biomarker Standardisation Initiative (IBSI), an independent international collaboration that aims at standardizing the extraction of image biomarkers for high-throughput quantitative analysis (radiomics). With this in mind, we used two platforms for feature extraction: PyRadiomics [28], a highly tested and maintained open-source platform, and LIFEx [29], a freeware for radiomic feature calculation in multimodality imaging.

3.3.1. Pyradiomics

Pyradiomics is an open-source python package that allows feature extraction both in 2D or 3D. It is also available as an extension for the 3D Slicer platform [30].

Figure 3 shows the viewing layout of 3D Slicer. Axial, coronal and sagittal views are perfectly loaded and displayed in the platform as well as a 3D volumetric reconstruction of the OARs and the CTV. All structures and volumes are perfectly registered with the CT series with the z component of every element and planar orientation matching.

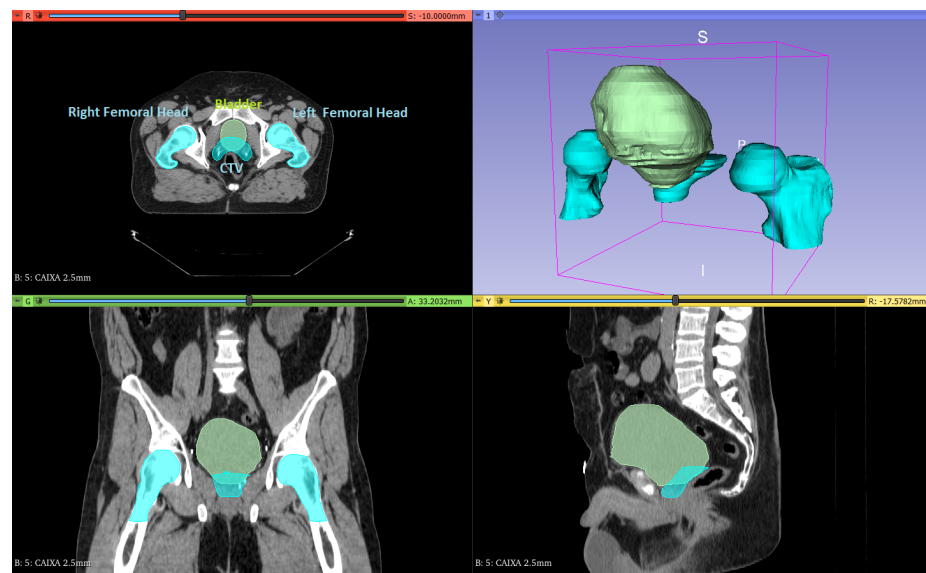


Figure 3. 3D Slicer Interface. Visualization of image series, OARs and CTV. **Top-left:** Axial view. **Top-right:** Volumetric reconstruction. **Bottom-left:** Coronal view. **Bottom-right:** Sagittal view.

Pyradiomics excluded some features due to mathematical similarities to the ones defined in IBSI. For example, the *Sum Variance* and the *Dissimilarity* are identical to the *Cluster Tendency* and *Difference Average* correspondingly [28]. It is important to note that shape descriptors are independent of the grey value and therefore extracted from the label mask. All other features can be retrieved from the original or derived (filtered) masked images. In this work, we did not consider filtered images. Results returned as an ordered dictionary with the unique feature name and additional information on the extraction [28].

3.3.2. LIFEx

LIFEx is a software developed for visualizing multiple imaging modalities and specially designed for feature extractions. It is currently at version 7.1.0 and being actively developed. It presents a very intuitive interface and massive and well-established documentation. It presents a Digital Imaging and Communications in Medicine (DICOM) browser to read images locally or from a network, and even non-DICOM formats are supported. The viewer displays axial, coronal and sagittal slices perfectly aligned and synchronized. A simple drag and drop interface allows to upload structures and desired VOIs [29].

The number of features is smaller when compared to pyradiomics because it is more oriented to Positron Emission Tomography (PET)/CT texture analysis and MRI. In fact, it presents a specific module for PET Standardized Uptake Value (SUV) calculation and another for MRI Perfusion. The results are saved in a csv file for further analysis.

Figure 4 shows the LIFEx interface displaying axial, coronal and sagittal views. The selected CTV is displayed in blue. The right menu presents several options for segmentation and measuring tools. The left menu with resampling and window-level adjustments and the top menu with all the available feature extraction modules.

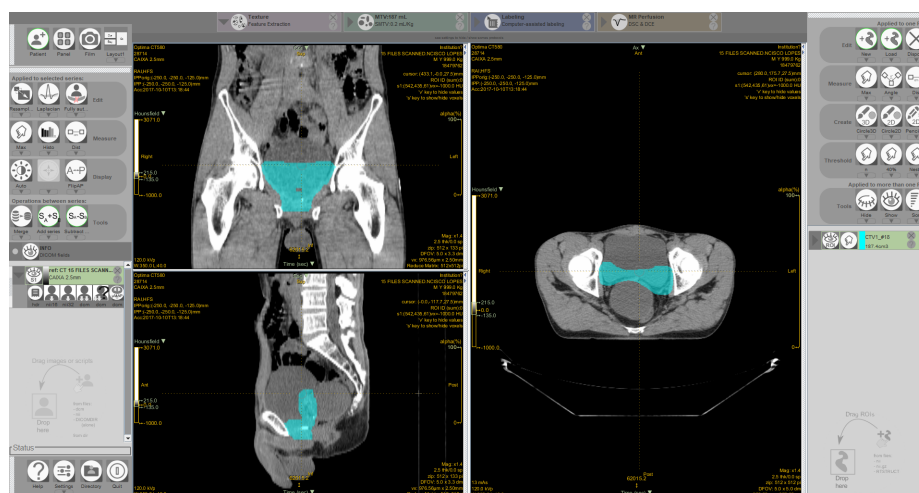


Figure 4. LIFEx Interface. Visualization of image series and CTV in blue.

For textural analysis, it allows customization of several parameters such as spatial resampling, intensity discretization and rescaling. It is a user-friendly software specially designed for radiomic features studies.

Both platforms, pyradiomics and LIFEx, offer the possibility to extract features from derived images. Wavelets allow overcoming non-rotational invariance. Laplacian of Gaussian (LoG) will emphasize areas of grey level change [28]. In this work, we only used original, non-derived images.

Table 4 summarizes the number of features per feature class possible to extract from pyradiomics and LIFEx.

Table 4. Pyradiomics and LIFEx feature classes.

Feature Class	# Features	
	Pyradiomics	LIFEx
First Order Statistics	19	12
Shape based	26	4
GLCM	24	6
GLRLM	16	—
GLRM	—	11
NGLDM	—	3
NGTDM	5	—
GLSZM	16	11
GLDM	14	—
Total	120	47

3.4. Dimensionality Reduction

Features were standardized by removing the mean and scaling to unit variance. Each image or volume descriptor represents a point in the feature space. But some are highly correlated, which means overlapped axis. To overcome this issue, we used PCA, which projects the data points to an uncorrelated and orthogonal axis to maximize variance [31]. Dimensionality reduction occurs with the selection of higher variance components.

For this task, we used Scikit-learn, a machine-learning python package [32]. It offers a few variations of PCA, such as linear dimensionality reduction using Singular Value Decomposition (SVD), non-linear dimensionality reduction using kernels (KernelPCA), sparse components that optimally reconstruct data, linear dimensionality reduction using truncated SVD and using the most significant singular vectors to project the data to a lower-dimensional space (IncrementalPCA) [32]. We tried all of these options searching for a combination that would maximize performance.

3.5. Model Building and Classification

The adopted methodology allows having a dataset with multiple image features labelled with a particular output, the GS. CT images are not the *de facto standard* for PCa evaluation, so we attempted a more conservative approach. We used an OvR multiclass strategy with an Support Vector Machine (SVM) as a baseline. With this approach, we fitted one classifier per class against all the others. To assess performance, we computed the AUROC curve. For this particular task, we used the python library Scikit-learn [32].

The model was built considering stratified randomized folds. The folds were made by preserving the percentage of samples for each class and the test size was 20% of all slices or volumes.

Our feature extraction pipeline encompasses several steps:

- (a) CT images from EBRT;
- (b) Manually delineated segmentation by professional experts;
- (c) Feature extraction from pyradiomics and LIFEx.

In Radiomic studies, the model is a radiomic signature that relates to a specific clinical endpoint. In our case, such a signature was not possible to find. The model was built with the components obtained from PCA as exemplified in Figure 5.

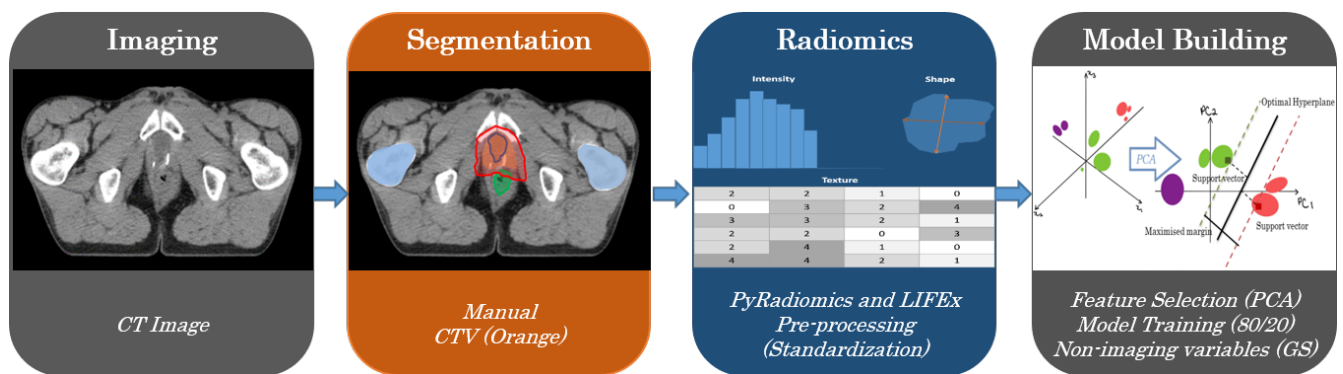


Figure 5. Radiomics Pipeline.

4. Results

CT images are an essential part of EBRT. Although mpMRI shows higher soft-tissue contrast and thus more PCa informative features, this also comes with a higher cost. In this work, we seek to find the potential of CT images for PCa grading and risk stratification.

4.1. What Are the More Grade Relevant Features?

The fundamental idea behind radiomics is to find a signature. In other words, a feature or a set of features that shows a high correlation with the GS.

We computed the heatmaps and dendrograms of all calculated features from pyradiomics and LIFEx. Using the nearest point algorithm and correlation metrics, we clustered all features based on the pairwise distances between observations [32]. Figures 6 and 7 show the obtained hierarchical cluster heatmaps for pyradiomics and LIFEx. The dendrogram reveals a high inter-correlation between features. Also, there is no apparent relation with the RG (represented between the dendrogram and the correlation matrix as Grade). The low soft-tissue contrast and the lack of metabolic manifestation of CT will provide a challenge for a possible radiomic signature.

For classification purposes, a high inter-correlation between features is not a desirable scenario. In radiomic studies, the number of extracted features does not allow adequate interpretability for clinical levels. In this particular case, feature selection seems unfeasible based on the analysis of Figures 6 and 7. There is no apparent pattern considering the clustering by RG following the correlation matrix. Besides, features reveal a low dissimilarity, observed by the close node distance in the dendrogram. To overcome this issue, we tried a dimensionality reduction technique mentioned in radiomic studies [26].



Figure 6. Hierarchical cluster heatmap for pyradiomics features.



Figure 7. Hierarchical cluster heatmap for LIFEx features.

4.2. PCA Variations

PCA allows the reduction of dimensionality of large datasets by projecting the most meaningful data to a lower-dimensional space. This reduction may come at the cost of accuracy but, it increases visualization and analysis and faster machine learning algorithms. The sklearn library provides several variations [32]:

- PCA: Linear dimensionality reduction using SVD;
- SparsePCA: Sparse components that can optimally reconstruct original data;
- KernelPCA: Non-linear dimensionality reduction using kernels;
- TruncatedSVD: linear dimensionality reduction by means of truncated SVD;
- IncrementalPCA: Linear dimensionality reduction using SVD but only keeping the most significant singular vectors.

In this work, we explored the differences in performance by computing AUROC values for each of the mentioned PCA methods, as well as the optimal number of components. Sklearn estimates the maximum number of components according to Equation (1).

$$\min((\#samples \times 0.8, \#features)) \tag{1}$$

For our dataset, the maximum number of components is 34. Figure 8 shows the obtained results for both sets of features (pyradiomics and LIFEx) and for PCA variations and number of components. The obtained values result from 30 runs of the classification pipeline. The multiple OvR classifiers were built with Support Vector Classification and a linear kernel.

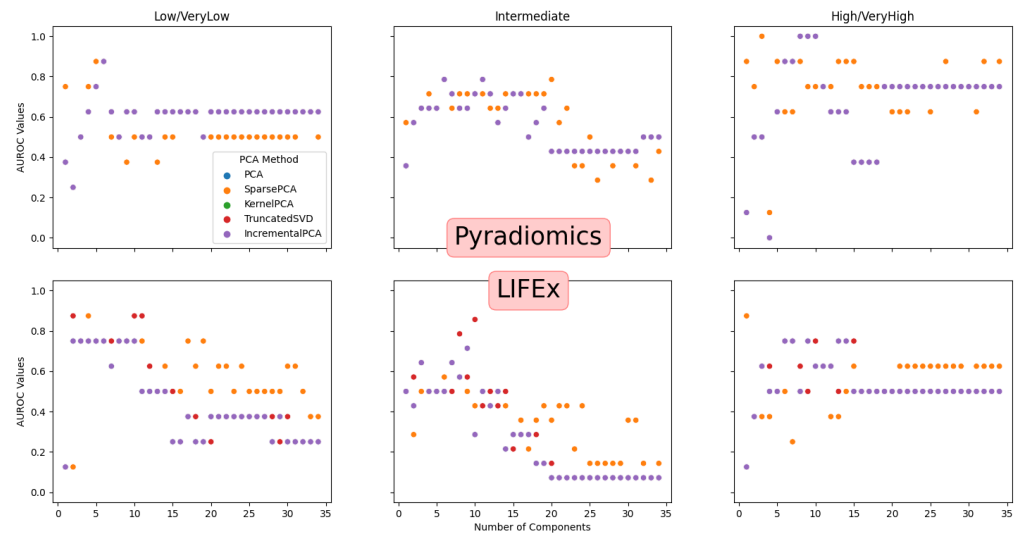


Figure 8. AUROC Values for multiple PCA variations and number of principal components.

Tables 5 and 6 show the best obtained values. On average, six components are enough to maximize performance (not shown for simplicity). The present study does not attempt to compare pyradiomics and LIFEx but to establish a baseline for deeper studies.

Table 5. Pyradiomics Best AUROC values.

	Low/Very Low	Intermediate	High/Very High
PCA	0.88	0.79	0.88
SparsePCA	0.88	0.79	0.88
KernelPCA	0.88	0.79	0.88
TruncatedSVD	0.88	0.79	0.88
IncrementalPCA	0.88	0.79	0.88

Table 6. LIFEx Best AUROC values.

	Low/Very Low	Intermediate	High/Very High
PCA	0.75	0.71	0.75
SparsePCA	0.88	0.64	0.88
KernelPCA	0.75	0.71	0.75
TruncatedSVD	0.88	0.86	0.75
IncrementalPCA	0.75	0.71	0.75

5. Discussion

The low soft-tissue contrast and the lack of metabolic manifestation on CT provides a challenge for a radiomic signature. The extracted features, either from pyradiomics or LIFEx, reveal a poor correlation with the RG. The stratification of patients is crucial to decide treatment workflows. The GS is a histological characterization of observed cell patterns. Several studies suggest improvements in the classification framework when adding radiomic intel. With this in mind, we applied several PCA methods, reducing dimensionality by projecting features to a more well-behaved space. The downside is that we lose the ability to identify a radiomic signature for CT to predict PCa aggressiveness.

This study does not intend to be a comparison of pyradiomics and LIFEx. Instead, it intends to be a baseline to provide deeper insights and a classification framework to evaluate EBRT responses. LIFEx seems more PET/CT, and MRI perfusion oriented, offering features that seem more optimized for such imaging modalities. Pyradiomics offers more features and is more imaging modality agnostic. A huge number of features may represent an issue. The results seem better overall using pyradiomics. Also, they seem almost invariant to the PCA method used.

The built models allow the establishment of three classifiers, one for each risk group. In our dataset, the “Low/VeryLow” class is under-represented. This issue will be addressed in the future with the addition of more cases. Also, this is quite an unbalanced dataset considering the distribution of the cases per class.

Both platforms, offer the ability to extract features from derived images, i.e., from wavelets and LoG filters. In our work, we only used the originals. In the future, derived images will be considered and may offer other insights.

6. Conclusions

PCa grading is a complex task with multiple variables to be evaluated. The present study provides the baseline to develop an accurate classifier to predict PCa aggressiveness during treatment using CT images. Such a tool may improve decision outcomes and avoid overdiagnosis and overtreatment.

CT images provide a challenge to find a radiomic signature to predict PCa aggressiveness. The application of PCA methods allows the development of a classifier capable of stratifying patients according to the RG.

The well-established guidelines like PIRADS do not take into account a treated prostate. With the biological and morphological changes induced by EBRT, reclassifying or regrading PCa is challenging. With the present study, we do not intend to perform a direct comparison with PIRADS and mpMRI. Instead, we aspire to provide a baseline for a framework capable of reevaluating PCa aggressiveness during treatment. In the EBRT workflow, an initial CT scan is mandatory to provide tissue attenuation coefficients for dose estimations and anatomical intel for volume delineation. The addition of radiomic information can increase the predictive power of CT images. Complemented with the valuable initial findings given by mpMRI, PET/CT and histology, we may walk towards ongoing treatment optimizations. CBCT is also freely available in the EBRT workflow for patient setup verifications. This study may provide the necessary methods to use CBCT as a restaging imaging modality for PCa during treatment.

In the future, we intend to contribute with a clinically implemented system capable of providing valuable intel on the effectiveness of EBRT, improving decision outcomes and survival rates.

Author Contributions: Conceptualization, B.M.; methodology, B.M. and I.D.; software, B.M. and A.S.; validation, B.M., I.D., A.S. and J.S.; formal analysis, B.M.; investigation, B.M.; resources, B.M., I.D., A.S. and J.S.; data curation, B.M. and I.D.; writing—original draft preparation, B.M.; writing—review and editing, B.M., I.D., A.S. and J.S.; supervision, I.D. and J.S. All authors have read and agreed to the published version of the manuscript.

Funding: This research received no external funding.

Institutional Review Board Statement: The study was conducted according to the guidelines of the Declaration of Helsinki. The study was approved by IPO Porto Healthcare Ethics Committee (protocol code CES.274/020 and date of approval 1 October 2020).

Informed Consent Statement: Informed consent was obtained from all subjects involved in the study.

Data Availability Statement: Not applicable.

Conflicts of Interest: The authors declare no conflict of interest.

Abbreviations

The following abbreviations are used in this manuscript:

ADC	Apparent Diffusion Coefficient
AUROC	Area Under the Receiver Operating Characteristic
BCR	Biochemical Recurrence
CBCT	Cone Beam Computed Tomography
CNN	Convolutional Neural Network.
CT	Computed Tomography
CTV	Clinical Target Volume
DICOM	Digital Imaging and Communications in Medicine
DRE	Digital Rectal Examination
EBRT	External Beam Radiotherapy Treatment
GG	Grade Group
GLCM	Gray Level Co-occurrence Matrix
GLDM	Gray Level Dependence Matrix
GLRLM	Gray Level Run Length Matrix
GLRM	Grey-Level Run Length Matrix
GLSZM	Gray Level Size Zone Matrix
GS	Gleason Score
GTV	Gross Tumour Volume
IBSI	Image Biomarker Standardisation Initiative
ICRU	International Commission on Radiation Units and Measurements
IPO-PORTO	Instituto Português de Oncologia do Porto Francisco Gentil
LIFEx	Local Image Features Extraction
LoG	Laplacian of Gaussian
mpMRI	Multi-parametric Magnetic Resonance Imaging
MRI	Magnetic Resonance Imaging
NGLDM	Neighborhood Grey-Level Difference Matrix
NGTDM	Neighbouring Gray Tone Difference Matrix
OAR	Organ At Risk
OvR	One-vs-Rest
PCA	Principal Component Analysis
PCa	Prostate Cancer
PET	Positron Emission Tomography
PIRADS	Prostate Imaging Reporting and Data System
PSA	Prostate Specific Antigen
PTV	Planning Target Volume

RG	Risk Group
SSAE	Stacked Sparse AutoEncoder
SUV	Standardized Uptake Value
SVD	Singular Value Decomposition
SVM	Support Vector Machine
TRUS	Transrectal Ultrasound Guided Biopsy
VOI	Volume Of Interest

References

- Sung, H.; Ferlay, J.; Siegel, R.L.; Laversanne, M.; Soerjomataram, I.; Jemal, A.; Bray, F. Global Cancer Statistics 2020: GLOBOCAN Estimates of Incidence and Mortality Worldwide for 36 Cancers in 185 Countries. *CA Cancer J. Clin.* **2021**, *71*, 209–249. [CrossRef] [PubMed]
- Singh, O.; Bolla, S.R. Anatomy, Abdomen and Pelvis, Prostate. *StatPearls [Internet]* **2019**.
- McNeal, J.E. The zonal anatomy of the prostate. *Prostate* **1981**, *2*, 35–49. [CrossRef]
- Descotes, J.L. Diagnosis of prostate cancer. *Asian J. Urol.* **2019**, *6*, 129–136. [CrossRef] [PubMed]
- Epstein, J.I.; Egevad, L.; Amin, M.B.; Delahunt, B.; Srigley, J.R.; Humphrey, P.A. The 2014 International Society of Urological Pathology (ISUP) consensus conference on Gleason grading of prostatic carcinoma. *Am. J. Surg. Pathol.* **2016**, *40*, 244–252. [CrossRef] [PubMed]
- Parker, C.; Castro, E.; Fizazi, K.; Heidenreich, A.; Ost, P.; Procopio, G.; Tombal, B.; Gillessen, S. Prostate cancer: ESMO Clinical Practice Guidelines for diagnosis, treatment and follow-up. *Ann. Oncol.* **2020**, *31*, 1119–1134. [CrossRef] [PubMed]
- Gregoire, V.; Mackie, T.; Neve, W. Prescribing, recording, and reporting photon-beam intensity-modulated radiation therapy (IMRT). *J. Int. Comm. Radiat. Units Meas. (J. ICRU)* **2010**, *10*, 1–106.
- Bath, M. The Prostate Gland. 2019. Available online: <https://teachmeanatomy.info/pelvis/the-male-reproductive-system/prostate-gland/> (accessed on 26 October 2021).
- Schröder, F.H.; Kruger, A.B.; Rietbergen, J.; Kranse, R.; Maas, P.v.d.; Beemsterboer, P.; Hoedemaeker, R. Evaluation of the digital rectal examination as a screening test for prostate cancer. *J. Natl. Cancer Inst.* **1998**, *90*, 1817–1823. [CrossRef] [PubMed]
- Wolf, A.M.; Wender, R.C.; Etzioni, R.B.; Thompson, I.M.; D’Amico, A.V.; Volk, R.J.; Brooks, D.D.; Dash, C.; Guessous, I.; Andrews, K. American Cancer Society guideline for the early detection of prostate cancer: Update 2010. *CA A Cancer J. Clin.* **2010**, *60*, 70–98. [CrossRef]
- Lambin, P.; Rios-Velazquez, E.; Leijenaar, R.; Carvalho, S.; Van Stiphout, R.G.; Granton, P.; Zegers, C.M.; Gillies, R.; Boellard, R.; Dekker, A. Radiomics: Extracting more information from medical images using advanced feature analysis. *Eur. J. Cancer* **2012**, *48*, 441–446. [CrossRef]
- Loeb, S.; Vellekoop, A.; Ahmed, H.U.; Catto, J.; Emberton, M.; Nam, R.; Rosario, D.J.; Scattoni, V.; Lotan, Y. Systematic review of complications of prostate biopsy. *Eur. Urol.* **2013**, *64*, 876–892. [CrossRef]
- Wildeboer, R.R.; van Sloun, R.J.; Huang, P.; Wijkstra, H.; Mischi, M. 3-D multi-parametric contrast-enhanced ultrasound for the prediction of prostate cancer. *Ultrasound Med. Biol.* **2019**, *45*, 2713–2724. [CrossRef]
- Liang, L.; Zhi, X.; Sun, Y.; Li, H.; Wang, J.; Xu, J.; Guo, J. A Nomogram Based on a Multiparametric Ultrasound Radiomics Model for Discrimination between Malignant and Benign Prostate Lesions. *Front. Oncol.* **2021**, *11*, 290.
- Hou, Y.; Bao, M.L.; Wu, C.J.; Zhang, J.; Zhang, Y.D.; Shi, H.B. A radiomics machine learning-based redefining score robustly identifies clinically significant prostate cancer in equivocal PI-RADS score 3 lesions. *Abdom. Radiol.* **2020**, *45*, 4223–4234. [CrossRef]
- Giambelluca, D.; Cannella, R.; Vernuccio, F.; Comelli, A.; Pavone, A.; Salvaggio, L.; Galia, M.; Midiri, M.; Lagalla, R.; Salvaggio, G. PI-RADS 3 lesions: Role of prostate MRI texture analysis in the identification of prostate cancer. *Curr. Probl. Diagn. Radiol.* **2021**, *50*, 175–185. [CrossRef]
- Chen, T.; Li, M.; Gu, Y.; Zhang, Y.; Yang, S.; Wei, C.; Wu, J.; Li, X.; Zhao, W.; Shen, J. Prostate cancer differentiation and aggressiveness: Assessment with a radiomic-based model vs. PI-RADS v2. *J. Magn. Reson. Imaging* **2019**, *49*, 875–884. [CrossRef] [PubMed]
- Stephenson, A.J.; Kattan, M.W.; Eastham, J.A.; Dotan, Z.A.; Bianco, F.J., Jr.; Lilja, H.; Scardino, P.T. Defining biochemical recurrence of prostate cancer after radical prostatectomy: A proposal for a standardized definition. *J. Clin. Oncol.* **2006**, *24*, 3973–3978. [CrossRef]
- Shiradkar, R.; Ghose, S.; Jambor, I.; Taimen, P.; Ettala, O.; Purysko, A.S.; Madabhushi, A. Radiomic features from pretreatment bi-parametric MRI predict prostate cancer biochemical recurrence: Preliminary findings. *J. Magn. Reson. Imaging* **2018**, *48*, 1626–1636. [CrossRef]
- Bourbonne, V.; Fournier, G.; Vallières, M.; Lucia, F.; Doucet, L.; Tissot, V.; Cuvelier, G.; Hue, S.; Le Penn Du, H.; Perdriel, L. External validation of an MRI-derived radiomics model to predict biochemical recurrence after surgery for high-risk prostate cancer. *Cancers* **2020**, *12*, 814. [CrossRef]
- Bosetti, D.G.; Ruinelli, L.; Piliero, M.A.; van der Gaag, L.C.; Pesce, G.A.; Valli, M.; Bosetti, M.; Presilla, S.; Richetti, A.; Deantonio, L. Cone-beam computed tomography-based radiomics in prostate cancer: A mono-institutional study. *Strahlenther. Und Onkol.* **2020**, *196*, 943–951. [CrossRef]

22. Providência, L.; Domingues, I.; Santos, J. An Iterative Algorithm for Semisupervised Classification of Hotspots on Bone Scintigraphies of Patients with Prostate Cancer. *J. Imaging* **2021**, *7*, 148. [CrossRef] [PubMed]
23. Abraham, B.; Nair, M.S. Computer-aided classification of prostate cancer grade groups from MRI images using texture features and stacked sparse autoencoder. *Comput. Med. Imaging Graph.* **2018**, *69*, 60–68. [CrossRef]
24. Algohary, A.; Shiradkar, R.; Pahwa, S.; Purysko, A.; Verma, S.; Moses, D.; Shnier, R.; Haynes, A.M.; Delprado, W.; Thompson, J. Combination of peri-tumoral and intra-tumoral radiomic features on bi-parametric MRI accurately stratifies prostate cancer risk: A multi-site study. *Cancers* **2020**, *12*, 2200. [CrossRef]
25. Osman, S.O.; Leijenaar, R.T.; Cole, A.J.; Lyons, C.A.; Hounsell, A.R.; Prise, K.M.; O’Sullivan, J.M.; Lambin, P.; McGarry, C.K.; Jain, S. Computed tomography-based radiomics for risk stratification in prostate cancer. *Int. J. Radiat. Oncol. Biol. Phys.* **2019**, *105*, 448–456. [CrossRef] [PubMed]
26. Yao, S.; Jiang, H.; Song, B. Radiomics in prostate cancer: Basic concepts and current state-of-the-art. *Chin. J. Acad. Radiol.* **2020**, *2*, 47–55. [CrossRef]
27. Gillies, R.J.; Kinahan, P.E.; Hricak, H. Radiomics: Images are more than pictures, they are data. *Radiology* **2016**, *278*, 563–577. [CrossRef] [PubMed]
28. Van Griethuysen, J.J.; Fedorov, A.; Parmar, C.; Hosny, A.; Aucoin, N.; Narayan, V.; Beets-Tan, R.G.; Fillion-Robin, J.C.; Pieper, S.; Aerts, H.J. Computational radiomics system to decode the radiographic phenotype. *Cancer Res.* **2017**, *77*, e104–e107. [CrossRef]
29. Nioche, C.; Orlhac, F.; Boughdad, S.; Reuzé, S.; Goya-Outi, J.; Robert, C.; Pellot-Barakat, C.; Soussan, M.; Frouin, F.; Buvat, I. LIFEX: A freeware for radiomic feature calculation in multimodality imaging to accelerate advances in the characterization of tumor heterogeneity. *Cancer Res.* **2018**, *78*, 4786–4789. [CrossRef]
30. Fedorov, A.; Beichel, R.; Kalpathy-Cramer, J.; Finet, J.; Fillion-Robin, J.C.; Pujol, S.; Bauer, C.; Jennings, D.; Fennessy, F.; Sonka, M. 3D Slicer as an image computing platform for the Quantitative Imaging Network. *Magn. Reson. Imaging* **2012**, *30*, 1323–1341. [CrossRef]
31. Lever, J.; Krzywinski, M.; Altman, N. Points of Significance: Principal Component Analysis. *Nat. Methods* **2017**, *14*, 641–643. [CrossRef]
32. Pedregosa, F.; Varoquaux, G.; Gramfort, A.; Michel, V.; Thirion, B.; Grisel, O.; Blondel, M.; Prettenhofer, P.; Weiss, R.; Dubourg, V.; et al. Scikit-learn: Machine Learning in Python. *J. Mach. Learn. Res.* **2011**, *12*, 2825–2830.

Review

Wnt and β -Catenin Signaling in the Bone Metastasis of Prostate Cancer

Zachary Kaplan ¹, Steven P. Zielske ², Kristina G. Ibrahim ² and Frank C. Cackowski ^{2,*} 

¹ College of Literature, Science, and the Arts, University of Michigan, Ann Arbor, MI 48109, USA; zkaplan@umich.edu

² Department of Oncology and Karmanos Cancer Institute, Wayne State University School of Medicine, Detroit, MI 48201, USA; steven.zielske@wayne.edu (S.P.Z.); KristinaIbrahim@wayne.edu (K.G.I.)

* Correspondence: cackowskif@karmanos.org

Abstract: Wnt family proteins and β -catenin are critical for the regulation of many developmental and oncogenic processes. Wnts are secreted protein ligands which signal using a canonical pathway, and involve the transcriptional co-activator β -catenin or non-canonical pathways that are independent of β -catenin. Bone metastasis is unfortunately a common occurrence in prostate cancer and can be conceptualized as a series of related steps or processes, most of which are regulated by Wnt ligands and/or β -catenin. At the primary tumor site, cancer cells often take on mesenchymal properties, termed epithelial mesenchymal transition (EMT), which are regulated in part by the Wnt receptor FZD4. Then, Wnt signaling, especially Wnt5A, is of importance as the cells circulate in the blood stream. Upon arriving in the bones, cancer cells migrate and take on stem-like or tumorigenic properties, as aided through Wnt or β -catenin signaling involving CHD11, CD24, and Wnt5A. Additionally, cancer cells can become dormant and evade therapy, in part due to regulation by Wnt5A. In the bones, E-selectin can aid in the reversal of EMT, a process termed mesenchymal epithelial transition (MET), as a part of metastatic tumorigenesis. Once bone tumors are established, Wnt/ β -catenin signaling is involved in the suppression of osteoblast function largely through DKK1.

Keywords: Wnt; β -catenin; bone metastasis; prostate cancer; Wnt5A; breast cancer; DKK1

Citation: Kaplan, Z.; Zielske, S.P.; Ibrahim, K.G.; Cackowski, F.C. Wnt and β -Catenin Signaling in the Bone Metastasis of Prostate Cancer. *Life* **2021**, *11*, 1099. <https://doi.org/10.3390/life11101099>

Academic Editors: Ana Faustino and Paula A. Oliveira

Received: 30 September 2021

Accepted: 14 October 2021

Published: 16 October 2021

Publisher's Note: MDPI stays neutral with regard to jurisdictional claims in published maps and institutional affiliations.



Copyright: © 2021 by the authors. Licensee MDPI, Basel, Switzerland. This article is an open access article distributed under the terms and conditions of the Creative Commons Attribution (CC BY) license (<https://creativecommons.org/licenses/by/4.0/>).

1. Introduction

Signaling pathways involving proteins of the Wnt family of secreted protein ligands and the adherens junction component and transcription cofactor, β -catenin (a product of the *CTNNB1* gene), play significant roles in cancer metastasis and other oncogenic processes. These pathways involve the complex interactions between 19 ligands of the Wnt family binding to 10 receptors of the Frizzled family, with co-receptors including RYK, LRP5, and ROR2. Wnt ligands share 27% to 83% of the same amino acid sequence and contain 23 or 24 conserved cysteine residues. All of the Wnt ligands are similar in size and are held in their folded states by multiple disulfide bonds. Included among the Wnt ligands is Wnt3a, typically a ligand of the canonical pathways, and Wnt5a, typically a ligand of the non-canonical pathways [1]. Signaling downstream of the Frizzled receptors occurs via two major modes or pathways: canonical, which involves β -catenin, and non-canonical, which signals independently of β -catenin (Figure 1). In the canonical signaling pathway, the binding of a Wnt ligand to a Frizzled receptor releases β -catenin from a cytoplasmic destruction complex, which allows it to translocate to the nucleus and act as a transcription cofactor. Conversely, in non-canonical Wnt signaling, binding of a Wnt ligand to a Frizzled receptor initiates signaling most commonly through either (1) a calcium-sensing pathway downstream of phospholipase C, or (2) the planar cell polarity pathway (PCP) involving the cytoskeleton and associated small GTPases, including RHOA and RAC1. The non-canonical pathway may also proceed through signaling involving protein kinase C (PKC), calcium/calmodulin-dependent protein kinase II (CaMKII), or the nuclear

factor of activated T cells (NFAT). A detailed discussion of the biochemistry and molecular biology of Wnt signaling is beyond the scope of the current work but has been the subject of multiple excellent reviews [2,3]. Here, we describe how Wnt and/or β -catenin signaling regulates prostate cancer metastasis to the bone and its growth in this new anatomic site. Although we focus our discussion on prostate cancer, we use examples from breast cancer and some other malignancies to illustrate key concepts.

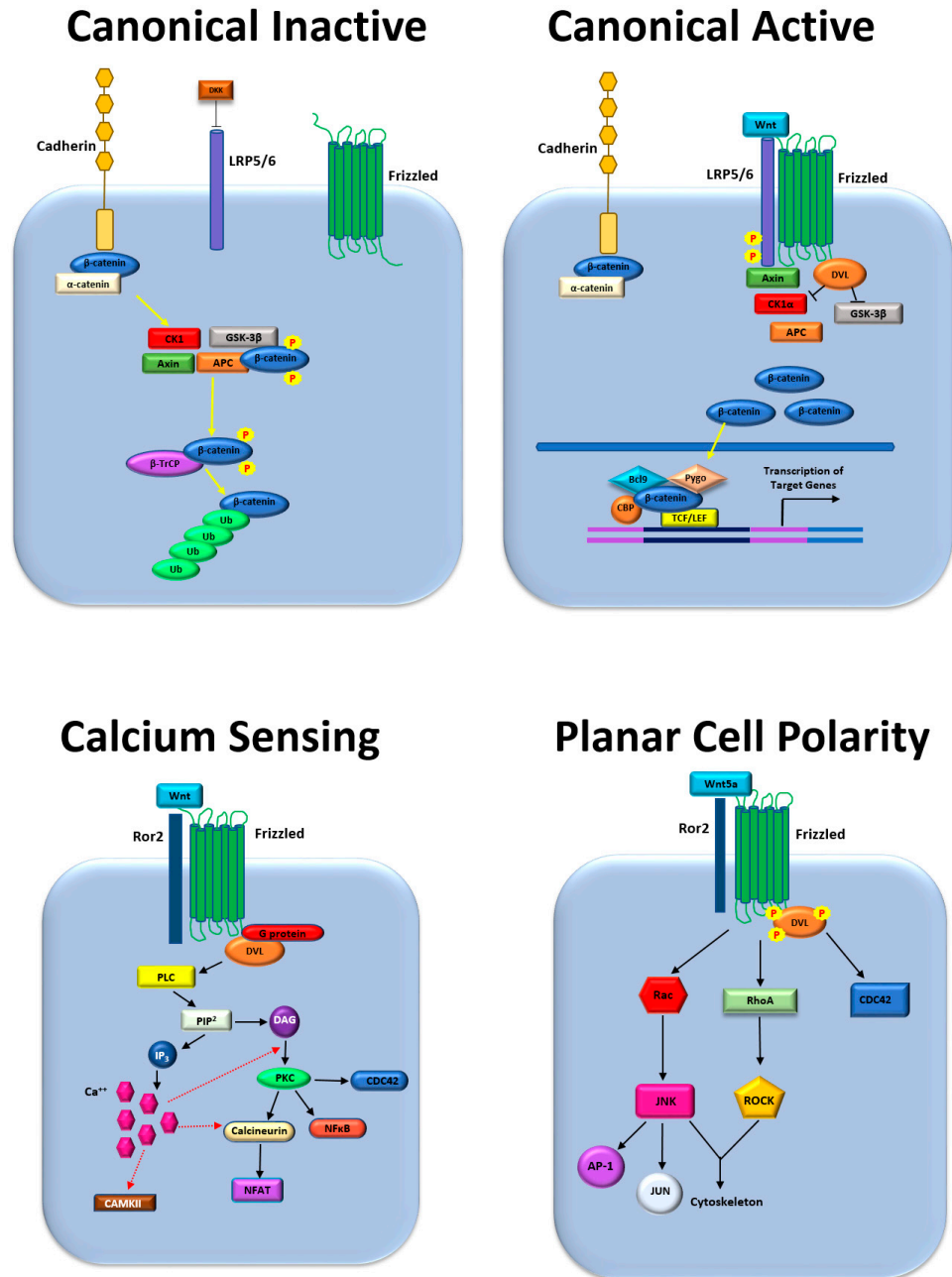


Figure 1. Wnt and β -catenin signaling pathways: Upper left, canonical pathway in the inactive state; Upper right, canonical pathway in the active state. Lower left, non-canonical calcium-sensing pathway; Lower right, non-canonical planar cell polarity pathway.

Cancer metastasis to the bone involves a series of related processes, most of which are regulated by Wnt and/or β -catenin signaling to some extent. Critical to successful metastatic spread is that cells maintain a degree of stemness and the ability to undergo tumorigenesis at the sites of dissemination. Cells often lose epithelial properties and gain

mesenchymal characteristics (epithelial to mesenchymal transition/EMT) as they detach from the primary tumor to migrate and disseminate and then revert to a more epithelial phenotype (mesenchymal to epithelial transition/MET) when they take residence in the metastatic site. Taking up residence in sites such as the bone requires complex interactions with bone, mesenchymal, and hematopoietic cells to remodel the new microenvironment, which aids tumor growth but causes dysfunction of the bone. In addition, metastasis requires the specific migration of cells into circulation and into tissues where they can remain dormant for years before the formation of gross metastatic tumors. Each step of this process, and the cell transitions undergone, have been shown to be influenced by the β -catenin pathway. Please refer to Figure 2 for a diagram of the highlights of this regulation. In this review, we concentrate on studies that have studied bone metastases directly but also include studies that do not address bone metastases directly, in order to allow an illustration of the entire bone metastatic cascade. An understanding of these processes could yield many therapeutic opportunities, especially because Wnt/ β -catenin was previously thought of as not druggable; however, therapeutic development targeting the pathway has met with much more success recently [4]. Therefore, we expect the regulation of prostate cancer bone metastases by Wnt and β -catenin to be a popular and fruitful area of research in the future.

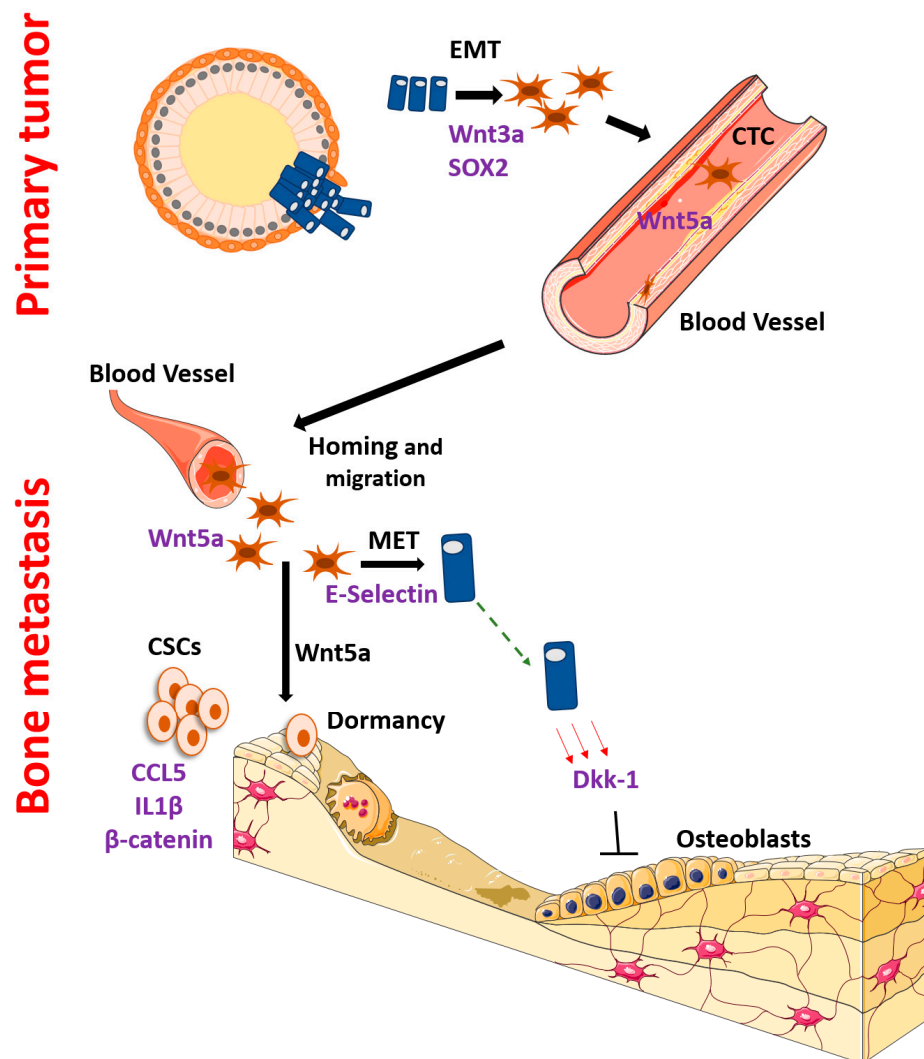


Figure 2. Key steps and molecules involved in the regulation of the bone metastatic cascade by Wnt and/or β -catenin signaling. Top, events at the primary tumor site; Bottom, events at the bone metastatic site.

2. Bone Metastasis Regulated by Wnt and β -Catenin

Below we describe cell biologic processes that carcinoma cells undergo in order to disseminate and grow in the bone, including migration, phenotypic plasticity, dormancy and tumorigenesis. Although we separated these topics for ease of presentation, there are many overlaps between them. For example, cancer stem-like cells have overlapping characteristics with mesenchymal phenotype (EMT) cells, and dormant disseminated tumor cells often upregulate the expression of transcription factors important for stem cells. Thus, we encourage the reader to consider how Wnt and/or β -catenin signaling might regulate more than one of these subprocesses to allow bone metastasis formation and growth.

3. EMT, Initial Dissemination and Homing

In order to seed bone metastases, a cancer cell must first loosen attachments with the surrounding cells, migrate, and enter the blood stream. At the same time, epithelial cancer cells often assume characteristics of mesenchymal cells (EMT), in part regulated by Wnt and/or β -catenin signaling. Nearly half of patients with prostate cancer have a translocation between the TMPRSS2 locus and ERG or another ETS family transcription factor, which places the transcription factor under the control of androgens [5,6]. In this large subset of prostate cancers, EMT is also regulated by β -catenin signaling. TMPRSS2 translocation-positive patients have an increased expression of Wnt receptors, especially FZD4. The upregulation of this Wnt receptor leads to oncogenic effects including EMT and decreased cell adhesion [7]. Curiously, in their work, Gupta and colleagues showed the upregulation of Wnt target genes and the activity of canonical β -catenin transcription factors TCF and LEF in a reporter assay but did not observe the upregulation of β -catenin activity itself. Further work also showed direct binding of the TMPRSS2-ERG protein to the promoter of the EMT transcription factor, ZEB1, thus illustrating the complexities of Wnt and β -catenin pathways [8]. Furthermore, Wnt and β -catenin regulate EMT in prostate cancers without TMPRSS2-ERG family translocations. For example, the transcription factor SOX2 binds to the promoter region of β -catenin to mediate EMT in the DU145 prostate cancer cell line, which lacks a TMPRSS2-ERG translocation [9], and also in breast cancer cell lines [10]. The expression of SOX2 negatively correlated with the expression of E-cadherin and positively correlated with α -SMA, a mesenchymal marker protein. Although TGF- β is often an important regulator of EMT, it was not involved in these model systems [10].

Similarly, in using a mouse model of HER2⁺ breast cancer, Harper and colleagues illustrated the importance of canonical β -catenin for the initial spread of cancer cells they termed “early disseminated cancer cells” (eDCCs) [11]. These cells showed more membrane/adherens junction-associated (inactive) β -catenin and had higher amounts of β -catenin-mediated transcription than the bulk cancer cell population. They had a low level of the epithelial marker E-cadherin (CDH1) and a high level of the EMT marker Twist1, but maintained a partial epithelial character including an expression of epithelial cytokeratins. These eDCCs were initially dormant and had low levels of phosphorylated p38, but were later able to escape dormancy and form metastases. Breast cancer cells that did not respond to the HER2-targeted drug, trastuzumab, showed an upregulation of Wnt3A when compared to normal breast cancer cells. The resistant cells also had higher levels of N-cadherin, which promotes EMT and deters MET [12,13]. This correlation provides evidence that Wnt signaling potentially promotes EMT-like phenotypes in trastuzumab-resistant breast cancer cells. In keeping with its typical role as a canonical ligand, Wnt3A acted through the nuclear translocation of β -catenin [12]. The knockdown of Wnt3A by siRNA increased expression levels of E-cadherin and decreased the expression of Slug and Twist, which promoted the reversal of EMT, i.e., mesenchymal epithelial transition (MET). Additionally, β -catenin can also transmit signals from other upstream molecules other than Wnt ligands and Frizzled receptors. Wu et al. showed that PI3K can signal through GSK3 β to β -catenin to induce ZEB1 expression, EMT and bone metastases in urothelial (bladder) carcinoma [14].

Because bones do not have lymphatics, almost all (if not all) cancer cells must metastasize to the bone through blood vessels. While in blood, cancer cells are often referred to as circulating tumor cells (CTCs). Especially for prostate cancer, investigators have shown the importance of the non-canonical ligand Wnt5A for CTC function. In a single cell RNA sequencing study of prostate cancer patient CTCs, Miyamoto and colleagues identified Wnt5A as a key regulator, especially for antiandrogen resistance [15]. Similarly, using a multiplex qRT-PCR approach, Singhal et al. found that Wnt5A was one of the three genes expressed in CTCs that independently predicted overall survival in metastatic castration-resistant patients [16]. However, while these studies showed the importance of non-canonical Wnt signaling in CTCs, they did not directly prove that there is a role for Wnt signaling in bone metastases.

In an extension of these studies, Wang et al. showed that Wnt5A was partially responsible for the anatomic distribution of bone metastases in mouse models [17]. To further dissect this mechanism, they showed that JNK, FZD4, and FZD8 were partially responsible for prostate cancer cell migration in this model. Previously, others found that both canonical and non-canonical Wnt signaling was increased in metastatic vs. localized prostate cancer [18]. They also found that the transcription factor PITX2 was especially upregulated in bone metastases as compared to soft tissue metastases, and that PITX2 was important for prostate cancer migration stimulated by the non-canonical ligand, Wnt5A [18]. Recently, Tseng and co-workers found that the non-canonical Wnt receptor ROR2 suppressed prostate cancer bone metastasis through PI3K signaling in model systems and was inversely correlated with bone metastasis in patient samples [19]. In addition, canonical signaling is important for the homing of prostate cancer to the bone as well. Li and coworkers showed that FZD8 promotes prostate cancer migration through β -catenin and that FZD8 knockdown inhibited bone metastases, specifically [20]. Specifically, they reported that the unusual expression of FZD8 in prostate cancer resulted in the hyperactivation of Wnt signaling by triggering a positive feedback loop of Wnt3A, a ligand of the canonical pathway that causes bone metastasis.

4. Dormancy, Recurrence and Mesenchymal Epithelial Transition

Cancers, especially prostate and breast cancers, can disseminate early in the disease process and lie dormant for years or decades, then relapse at distant sites such as the bone. Part of this process of recurrence can be a reversal of some of the mesenchymal properties that the cancer cells acquired at the time of initial dissemination, a process termed mesenchymal epithelial transition (MET). As prostate or other cancer cells arrive in the bone marrow, they often share similar niches as hematopoietic stem cells, which have been used as a model for understanding cancer dormancy and recurrence [21]. Here, they are exposed to a milieu of pro- and anti-proliferation factors. The maintenance of HSCs in a quiescent state in the bone marrow has been shown to be regulated by Wnt5a [22]. Similarly, a recent report found that Wnt5A induces the dormancy of prostate cancer cells in bone [23]. Although Wnt5A is often a non-canonical ligand, here it acted by the inhibition of β -catenin (i.e., canonical signaling) through a novel mechanism. Osteoblasts in the endosteal niche secreted Wnt5A to bind to ROR2 and activated the ubiquitin ligase SIAH2, which led to the degradation of β -catenin. These dormant cells were also resistant to the commonly used prostate cancer chemotherapy drug, docetaxel. Therefore, this work illustrates how, paradoxically, dormancy can work to the advantage of a cancer by protecting the disseminated cells from treatment and other stressors. Wnt signaling is also important for dormancy induction in breast cancer. As discussed above in the EMT section, canonical β -catenin signaling was critical for early dissemination and initial dormant behavior. These early disseminated cells had a partial EMT phenotype and were dormant upon arrival in the bone marrow. This dormant behavior was characterized by the activity of p38 MAPK, a key regulator of dormancy in multiple cancers [11]. Similarly, the reversal of EMT, mesenchymal epithelial transition (MET), can also be partial. Using both breast and prostate cancer models, Esposito and colleagues found that E-selectin binds to

disseminated cancer cells in the peri-vascular niche of the bone microenvironment and induces MET to promote bone metastasis [24]. However, this was not the usual type of MET, in that the usual transcription factors such as ZEB1 and SNAI1 were not affected. Rather, it was a partial MET process that induced canonical β -catenin signaling to induce E-selectin glycosylation and SOX2 and SOX9 expression to stimulate stem-like properties. This was through the expression of Wnt repressors such as DKK1, CTGF, and CYR61, which are all mesenchymal-related genes.

5. Stemness and Tumorigenesis

As discussed immediately above, dormancy and stemness are related and overlapping processes. Likewise, Wnt/ β -catenin signaling is critical for stemness and metastatic tumorigenesis in many malignant contexts, including bone metastases. Many of the studies discussed below did not study bone metastases specifically, but may provide invaluable insight into prostate cancer metastases in the bone.

CSCs can be induced through Wnt and/or β -catenin signaling pathways through the interaction with immune cells, which could be viewed as a stressor in the new environment. Wnt5A was found to recruit and regulate bone marrow macrophages through the subsequent secretion of CCL2 and BMP6, which aided in the development of prostate cancer castration resistance [25]. Hwang et al. subsequently showed that CCL5 secreted by macrophages stimulated the formation of prostate cancer CSCs through a β -catenin-dependent mechanism [26]. CSCs were assayed by dual positivity for CD133 and CD44 or Aldefluor positivity, in addition to functional assays *in vitro* and *in vivo*. They proposed that CCL2 acted through binding to CCR5, which subsequently stimulated β -catenin activity, which then stimulated STAT3 transcription. Similarly, in breast cancer, the inflammatory mediator IL-1 β secreted by bone marrow also stimulates CSC formation and bone metastatic tumorigenesis in a β -catenin-dependent fashion [27]. In this system, IL-1 β activates NF κ B/CREB signaling and Wnt ligand production, which stimulates colony formation.

Wnts and β -catenin also stimulate CSCs in bone metastases through non-immune-dependent mechanisms. CD24 induces metastasis to bone and cancer stemness by activating Wnt/ β -catenin signaling in prostate cancer *in vivo*. FH535, a Wnt signaling inhibitor, reduces prostate cancer cell migration *in vitro* which corroborates the notion that CD24-mediated Wnt/ β -catenin signaling controls cell migration and stemness. There is a positive correlation between the CD24 expression of Wnt-mediated bone metastasis of prostate cancer cells *in vitro* and *in vivo* [28]. Recently, Pan and colleagues reported a novel mechanism for prostate cancer CSC regulation [29]. Endothelial cell-specific molecule 1 (ESM1), normally a secreted proteoglycan, stimulated the formation of prostate cancer CSCs through β -catenin when localized in the nucleus. In turn, β -catenin stimulated the nuclear localization of ESM1. Stably overexpressing ESM1 resulted in the increased spheroid formation and enhanced self-renewal ability of PC3 cells *in vitro*. Similarly, when ESM1 was silenced in PC3 cells, spheroid formation decreased but was restored back to normal levels when ESM1 was rescued. When the group tested tumorigenicity *in vivo*, it was discovered that tumors overexpressing ESM1 grew larger than tumors injected with an empty vector control in immunodeficient mice. Furthermore, the presence of stem cell markers CD44 and CD133 was increased in ESM1-overexpressing cells versus the controls [29]. In another example of prostate cancer CSC formation stimulated by canonical signaling, Li et al. found that low levels of the circadian rhythm gene PER3 stimulated CSC formation through β -catenin using ALDH and CD44 positivity to define CSCs, in addition to functional assays [30]. Curiously, PER3 signaled to β -catenin through another clock-related gene, BMAL1. Overall, there are multiple mechanisms through both canonical and non-canonical Wnt pathways that regulate the formation of CSCs in prostate cancer.

6. Interactions with the Bone Microenvironment

After cancer cells have arrived in the bone and have formed macroscopic tumors, they interact with host bone cells to aid cancer growth, but unfortunately impair normal bone function. Much of this impairment is through the inhibition of the formation and/or the function of osteoblasts. DKK1, an inhibitor of Wnt/ β -catenin signaling, stimulates osteoclasts and inhibits the formation and differentiation of osteoblasts [31]. DKK1 expression is directly linked to the production of osteolytic lesions in animal models of metastatic breast and prostate cancers. Wnt/ β -catenin signaling continues in osteolytic cell lines such as PC3 and MDA-MB-231 because they express the DKK1 receptors, Kremen1 and Kremen2, at much lower levels than osteoblastic cell lines [32]. Noggin, similar to DKK1, acts as an antagonist to osteoinductive Wnt proteins in osteolytic cancer cells, and as expected, noggin is not expressed in osteoinductive cancer cell lines. Therefore, the expression of noggin and DKK1 has deleterious effects on the osteoblast response in the bone microenvironment [33,34]. In breast cancer cells, another antagonist of Wnt/ β -catenin, sclerostin, inhibits osteoblast differentiation. The cancer cells secrete sclerostin which interacts with osteoblasts in the bone microenvironment. Sclerostin is typically secreted by osteocytes, but breast cancer cells gain the ability to secrete the inhibitor when in the bone marrow niche by activating RUNX2/CBF β signaling [35].

Investigators have also worked out mechanisms involving multiple mediators working in concert to aid the growth of bone metastasis, but impair normal bone function. Dai et al. found that prostate cancer cells induce osteoblast differentiation in vitro through both canonical and non-canonical Wnt signaling and through BMP-dependent and BMP-independent mechanisms [36]. Wnt3A and Wnt5A stimulated BMP4 and BMP6 expression, which was blocked by DKK1. Noggin and DKK1 synergistically inhibited osteoblast differentiation induced by the prostate cancer cell-conditioned media. As expected, Wnt3A signaling was dependent on β -catenin, whereas Wnt5A signaling was dependent on JNK1. Non-coding RNAs are also involved in the effects of Wnt signaling on osteoblasts. For instance, miR-218 activates osteoblast differentiation and promotes osteogenesis by stimulating a positive Wnt signaling loop. Additionally, miR-218 downregulates three different Wnt inhibitors: sclerostin, DKK2, and secreted Frizzled-related protein2, and is also upregulated by Wnt signaling which forms a positive feedback loop. In metastatic breast cancer cells, miR-218 promotes osteomimicry by enhancing Wnt signaling and the expression of osteoblastic genes relating to homing and growth [37].

Furthermore, cancers can induce changes in the bone before any cells actually arrive at the metastatic site. Using the TRAMP-C1 model of localized prostate cancer, Ardura and colleagues found that tumors in the prostate increased osteoclast formation and function. Osteoblast formation was also increased through a β -catenin-dependent mechanism [38]. They found that these effects were predominantly through the secretion of Spondin-2. They found increased cancer cell adhesion in vitro and ex vivo, which might translate to the creation of a pre-metastatic niche more hospitable for bone metastasis formation. Additionally, prostate cancer cells in the bone microenvironment induce osteoblast differentiation through the PKC noncanonical pathway activated by Wnt7B. The knockdown of Wnt7B in C4-2B cells resulted in a decrease of the mRNA expression of the osteoblast differentiation markers, ALP and BSP, in the ST2 cells they were co-cultured with. When Wnt7B was overexpressed in C4-2B cells, co-cultured ST2 cells had increased ALP activity, mineralization, and ALP and BSP mRNA levels. The results of these experiments were then tested and confirmed with two other cell lines, LNCaP and LAPC4 [39].

Lastly, of particular interests to patients, Wnt signaling is also important for the transmission of bone pain [40]. He and colleagues found that Wnt5b and the co-receptor RYK had increased expression in the (sensory) dorsal root ganglia of bone tumor-bearing mice. Wnt5b increased pain sensation and RYK knockdown decreased indicators of pain. Furthermore, the process was blocked by a CaMKII inhibitor, thus indicating a non-canonical calcium-sensing pathway of Wnt signaling.

7. Conclusions

Wnt and β -catenin signaling pathways regulate multiple processes that impact bone metastasis. Microenvironmental cues act through these pathways to drive cells toward metastatic sites, maintain stemness and dormancy, and eventually drive cells to reactivate and form metastatic tumors. If any step of this process can be thwarted therapeutically, there is the potential to disrupt the seeding of metastatic tissues, to maintain dormancy indefinitely, or to eliminate the stemness/tumorigenic property of cells. Therefore, with the likely upcoming introduction of clinically effective drugs to target these pathways, Wnt and β -catenin pathways hold immense promise for the treatment of metastases to the bone and other sites. Furthermore, we expect that much biology is yet to be uncovered. For example, much of the existing work is centered on only three of the nineteen Wnt ligands: Wnt3A, Wnt5A, and Wnt7B. Future studies could uncover roles of additional ligands, which would improve our understanding of the regulation of bone metastases by Wnt and β -catenin signaling, and offer additional targets for pre-clinical and clinical approaches.

Author Contributions: All authors made substantial contributions to the conception and writing of this manuscript. F.C.C. and Z.K. were involved in all aspects of the manuscript. S.P.Z. participated in writing and revising. K.G.I. participated in writing, revising, and the design and creation of figures. All authors have read and agreed to the published version of the manuscript.

Funding: F.C.C. received support from the Prostate Cancer Foundation Young Investigator Award 18YOUN04 and the Department of Defense Prostate Cancer Research Program Physician Research Award W81XWH2010394, and start-up funds from Karmanos Cancer Institute.

Institutional Review Board Statement: Not applicable.

Informed Consent Statement: Not applicable.

Data Availability Statement: Not applicable.

Acknowledgments: Images from the Servier Image Bank were used for some elements in the figures.

Conflicts of Interest: The authors declare no conflict of interest.

References

1. Miller, J.R. The Wnts. *Genome Biol.* **2002**, *3*, 1–15. [CrossRef]
2. Xie, J.; Huang, L.; Lu, Y.-G.; Zheng, D.-L. Roles of the Wnt Signaling Pathway in Head and Neck Squamous Cell Carcinoma. *Front. Mol. Biosci.* **2020**, *7*, 590912. [CrossRef]
3. Valenta, T.; Hausmann, G.; Basler, K. The many faces and functions of β -catenin. *EMBO J.* **2012**, *31*, 2714–2736. [CrossRef]
4. Wang, Z.; Li, Z.; Ji, H. Direct targeting of beta-catenin in the Wnt signaling pathway: Current progress and perspectives. *Med. Res. Rev.* **2021**, *41*, 2109. [CrossRef]
5. Abeshouse, A.; Ahn, J.; Akbani, R.; Ally, A.; Amin, S.; Andry, C.D.; Annala, M.; Aprikian, A.; Armenia, J.; Arora, A.; et al. The Molecular Taxonomy of Primary Prostate Cancer. *Cell* **2015**, *163*, 1011–1025. [CrossRef]
6. Tomlins, S.A.; Rhodes, D.R.; Perner, S.; Dhanasekaran, S.M.; Mehra, R.; Sun, X.W.; Varambally, S.; Cao, X.; Tchinda, J.; Kuefer, R.; et al. Recurrent fusion of TMPRSS2 and ETS transcription factor genes in prostate cancer. *Science* **2005**, *310*, 644–648. [CrossRef]
7. Gupta, S.; Iljin, K.; Sara, H.; Mpindi, J.P.; Mirtti, T.; Vainio, P.; Rantala, J.; Alanen, K.; Nees, M.; Kallioniemi, O. FZD4 as a mediator of ERG oncogene-induced WNT signaling and epithelial-to-mesenchymal transition in human prostate cancer cells. *Cancer Res.* **2010**, *70*, 6735–6745. [CrossRef]
8. Leshem, O.; Madar, S.; Kogan-Sakin, I.; Kamer, I.; Goldstein, I.; Brosh, R.; Cohen, Y.; Jacob-Hirsch, J.; Ehrlich, M.; Ben-Sasson, S.; et al. TMPRSS2/ERG promotes epithelial to mesenchymal transition through the ZEB1/ZEB2 axis in a prostate cancer model. *PLoS ONE* **2011**, *6*, e21650. [CrossRef]
9. Mertz, K.D.; Setlur, S.R.; Dhanasekaran, S.M.; Demichelis, F.; Perner, S.; Tomlins, S.; Tchinda, J.; Laxman, B.; Vessella, R.L.; Beroukhimt, R.; et al. Molecular characterization of TMPRSS2-ERG gene fusion in the NCI-H660 prostate cancer cell line: A new perspective for an old model. *Neoplasia* **2007**, *9*, 200-IN3. [CrossRef]
10. Li, X.; Xu, Y.; Chen, Y.; Chen, S.; Jia, X.; Sun, T.; Liu, Y.; Li, X.; Xiang, R.; Li, N. SOX2 promotes tumor metastasis by stimulating epithelial-to-mesenchymal transition via regulation of WNT/ β -catenin signal network. *Cancer Lett.* **2013**, *336*, 379–389. [CrossRef]
11. Harper, K.L.; Sosa, M.S.; Entenberg, D.; Hosseini, H.; Cheung, J.F.; Nobre, R.; Avivar-Valderas, A.; Nagi, C.; Girmius, N.; Davis, R.J.; et al. Mechanism of early dissemination and metastasis in Her2+ mammary cancer. *Nature* **2016**, *540*, 588–592. [CrossRef]

12. Wu, Y.; Ginther, C.; Kim, J.; Mosher, N.; Chung, S.; Slamon, D.; Vadgama, J.V. Expression of Wnt3 Activates Wnt/ β -Catenin Pathway and Promotes EMT-like Phenotype in Trastuzumab-Resistant HER2-Overexpressing Breast Cancer Cells. *Mol. Cancer Res.* **2012**, *10*, 1597–1606. [CrossRef]
13. Loh, C.-Y.; Chai, J.Y.; Tang, T.F.; Wong, W.F.; Sethi, G.; Shanmugam, M.K.; Chong, P.P.; Looi, C.Y. The E-Cadherin and N-Cadherin Switch in Epithelial-to-Mesenchymal Transition: Signaling, Therapeutic Implications, and Challenges. *Cells* **2019**, *8*, 1118. [CrossRef]
14. Wu, K.; Fan, J.; Zhang, L.; Ning, Z.; Zeng, J.; Zhou, J.; Li, L.; Chen, Y.; Zhang, T.; Wang, X.; et al. PI3K/Akt to GSK3 β /beta-catenin signaling cascade coordinates cell colonization for bladder cancer bone metastasis through regulating ZEB1 transcription. *Cell. Signal.* **2012**, *24*, 2273–2282. [CrossRef]
15. Miyamoto, D.T.; Zheng, Y.; Wittner, B.S.; Lee, R.J.; Zhu, H.; Broderick, K.T.; Desai, R.; Fox, D.B.; Brannigan, B.W.; Trautwein, J.; et al. RNA-Seq of single prostate CTCs implicates noncanonical Wnt signaling in antiandrogen resistance. *Science* **2015**, *349*, 1351–1356. [CrossRef]
16. Singhal, U.; Wang, Y.; Henderson, J.; Niknafs, Y.S.; Qiao, Y.; Gursky, A.; Zaslavsky, A.; Chung, J.S.; Smith, D.C.; Karnes, R.J.; et al. Multigene Profiling of CTCs in mCRPC Identifies a Clinically Relevant Prognostic Signature. *Mol. Cancer Res.* **2018**, *16*, 643–654. [CrossRef]
17. Wang, Y.; Singhal, U.; Qiao, Y.; Kasputis, T.; Chung, J.-S.; Zhao, H.; Chammaa, F.; Belardo, J.A.; Roth, T.M.; Zhang, H.; et al. Wnt Signaling Drives Prostate Cancer Bone Metastatic Tropism and Invasion. *Transl. Oncol.* **2020**, *13*, 100747. [CrossRef]
18. Vela, I.; Morrissey, C.; Zhang, X.; Chen, S.; Corey, E.; Stratton, G.M.; Nelson, C.C.; Nicol, D.L.; Clements, J.A.; Gardiner, E.M. PITX2 and non-canonical Wnt pathway interaction in metastatic prostate cancer. *Clin. Exp. Metastasis* **2014**, *31*, 199–211. [CrossRef]
19. Tseng, J.-C.; Huang, S.-H.; Lin, C.-Y.; Wang, B.-J.; Huang, S.-F.; Shen, Y.-Y.; Chuu, C.-P. ROR2 suppresses metastasis of prostate cancer via regulation of miR-199a-5p–PIAS3–AKT2 signaling axis. *Cell Death Dis.* **2020**, *11*, 1–11. [CrossRef]
20. Li, Q.; Ye, L.; Zhang, X.; Wang, M.; Lin, C.; Huang, S.; Guo, W.; Lai, Y.; Du, H.; Li, J.; et al. FZD8, a target of p53, promotes bone metastasis in prostate cancer by activating canonical Wnt/ β -catenin signaling. *Cancer Lett.* **2017**, *402*, 166–176. [CrossRef]
21. Shiozawa, Y.; Pedersen, E.A.; Havens, A.M.; Jung, Y.; Mishra, A.; Joseph, J.; Kim, J.K.; Patel, L.R.; Ying, C.; Ziegler, A.M.; et al. Human prostate cancer metastases target the hematopoietic stem cell niche to establish footholds in mouse bone marrow. *J. Clin. Investig.* **2011**, *121*, 1298–1312. [CrossRef]
22. Nemeth, M.J.; Topol, L.; Anderson, S.M.; Yang, Y.; Bodine, D.M. Wnt5a inhibits canonical Wnt signaling in hematopoietic stem cells and enhances repopulation. *Proc. Natl. Acad. Sci. USA* **2007**, *104*, 15436–15441. [CrossRef]
23. Ren, D.; Dai, Y.; Yang, Q.; Zhang, X.; Guo, W.; Ye, L.; Huang, S.; Chen, X.; Lai, Y.; Du, H.; et al. Wnt5a induces and maintains prostate cancer cells dormancy in bone. *J. Exp. Med.* **2019**, *216*, 428–449. [CrossRef]
24. Esposito, M.; Mondal, N.; Greco, T.M.; Wei, Y.; Spadazzi, C.; Lin, S.-C.; Zheng, H.; Cheung, C.; Magnani, J.L.; Lin, S.-H.; et al. Bone vascular niche E-selectin induces mesenchymal–epithelial transition and Wnt activation in cancer cells to promote bone metastasis. *Nat. Cell Biol.* **2019**, *21*, 627–639. [CrossRef]
25. Lee, G.T.; Kwon, S.J.; Kim, J.; Kwon, Y.S.; Lee, N.; Hong, J.H.; Jamieson, C.; Kim, W.J.; Kim, I.Y. WNT5A induces castration-resistant prostate cancer via CCL2 and tumour-infiltrating macrophages. *Br. J. Cancer* **2018**, *118*, 670–678. [CrossRef]
26. Huang, R.; Wang, S.; Wang, N.; Zheng, Y.; Zhou, J.; Yang, B.; Wang, X.; Zhang, J.; Guo, L.; Wang, S.; et al. CCL5 derived from tumor-associated macrophages promotes prostate cancer stem cells and metastasis via activating beta-catenin/STAT3 signaling. *Cell Death Dis.* **2020**, *11*, 234. [CrossRef]
27. Eyre, R.; Alferes, D.G.; Santiago-Gomez, A.; Spence, K.; McConnell, J.C.; Hart, C.; Simoes, B.M.; Lefley, D.; Tulotta, C.; Storer, J.; et al. Microenvironmental IL1 β promotes breast cancer metastatic colonisation in the bone via activation of Wnt signalling. *Nat. Commun.* **2019**, *10*, 5016. [CrossRef]
28. Weng, C.-C.; Ding, P.-Y.; Liu, Y.-H.; Hawse, J.R.; Subramaniam, M.; Wu, C.-C.; Lin, Y.-C.; Chen, C.-Y.; Hung, W.-C.; Cheng, K.-H. Mutant Kras-induced upregulation of CD24 enhances prostate cancer stemness and bone metastasis. *Oncogene* **2019**, *38*, 2005–2019. [CrossRef]
29. Pan, K.F.; Lee, W.J.; Chou, C.C.; Yang, Y.C.; Chang, Y.C.; Chien, M.H.; Hsiao, M.; Hua, K.T. Direct interaction of beta-catenin with nuclear ESM1 supports stemness of metastatic prostate cancer. *EMBO J.* **2021**, *40*, e105450. [CrossRef]
30. Li, Q.; Xia, D.; Wang, Z.; Liu, B.; Zhang, J.; Peng, P.; Tang, Q.; Dong, J.; Guo, J.; Kuang, D.; et al. Circadian Rhythm Gene PER3 Negatively Regulates Stemness of Prostate Cancer Stem Cells via WNT/beta-Catenin Signaling in Tumor Microenvironment. *Front. Cell Dev. Biol.* **2021**, *9*, 656981. [CrossRef]
31. Kasoha, M.; Bohle, R.M.; Seibold, A.; Gerlinger, C.; Juhasz-Böss, I.; Solomayer, E.-F. Dickkopf-1 (Dkk1) protein expression in breast cancer with special reference to bone metastases. *Clin. Exp. Metastasis* **2018**, *35*, 763–775. [CrossRef]
32. Clines, K.L.; Clines, G.A. DKK1 and Kremen Expression Predicts the Osteoblastic Response to Bone Metastasis. *Transl. Oncol.* **2018**, *11*, 873–882. [CrossRef]
33. Schwaninger, R.; Rentsch, C.A.; Wetterwald, A.; van der Horst, G.; van Bezooijen, R.L.; van der Pluijm, G.; Löwik, C.W.G.M.; Ackermann, K.; Pyerin, W.; Hamdy, F.C.; et al. Lack of Noggin Expression by Cancer Cells Is a Determinant of the Osteoblast Response in Bone Metastases. *Am. J. Pathol.* **2007**, *170*, 160–175. [CrossRef]
34. Aufderklamm, S.; Hennenlotter, J.; Leidenberger, P.; Rausch, S.; Hohner, A.; Kühs, U.; Maas, M.; Schwentner, C.; Bedke, J.; Stenzl, A.; et al. Systemic Alterations of Wnt Inhibitors in Patients with Prostate Cancer and Bone Metastases. *Dis. Markers* **2018**, *2018*, 1874598. [CrossRef]

35. Mendoza-Villanueva, D.; Zeef, L.; Shore, P. Metastatic breast cancer cells inhibit osteoblast differentiation through the Runx2/CBF β -dependent expression of the Wnt antagonist, sclerostin. *Breast Cancer Res.* **2011**, *13*, R106. [CrossRef]
36. Dai, J.; Hall, C.L.; Escara-Wilke, J.; Mizokami, A.; Keller, J.M.; Keller, E.T. Prostate Cancer Induces Bone Metastasis through Wnt-Induced Bone Morphogenetic Protein-Dependent and Independent Mechanisms. *Cancer Res.* **2008**, *68*, 5785–5794. [CrossRef]
37. Hassan, M.Q.; Maeda, Y.; Taipaleenmaki, H.; Zhang, W.; Jafferji, M.; Gordon, J.A.R.; Li, Z.; Croce, C.M.; van Wijnen, A.J.; Stein, J.L.; et al. miR-218 directs a Wnt signaling circuit to promote differentiation of osteoblasts and osteomimicry of metastatic cancer cells. *J. Biol. Chem.* **2012**, *287*, 42084–42092. [CrossRef]
38. Ardura, J.A.; Alvarez-Carrion, L.; Gutierrez-Rojas, I.; Friedman, P.A.; Gortazar, A.R.; Alonso, V. MINDIN secretion by prostate tumors induces premetastatic changes in bone via beta-catenin. *Endocr. Relat. Cancer* **2020**, *27*, 441–456. [CrossRef]
39. Zheng, D.; Decker, K.F.; Zhou, T.; Chen, J.; Qi, Z.; Jacobs, K.; Weilbaecher, K.N.; Corey, E.; Long, F.; Jia, L. Role of WNT7B-induced noncanonical pathway in advanced prostate cancer. *Mol. Cancer Res.* **2013**, *11*, 482–493. [CrossRef]
40. He, J.J.; Wang, X.; Liang, C.; Yao, X.; Zhang, Z.S.; Yang, R.H.; Fang, D. Wnt5b/Ryk-mediated membrane trafficking of P2X3 receptors contributes to bone cancer pain. *Exp. Neurol.* **2020**, *334*, 113482. [CrossRef]

Article

Association of Circulating Tumor Cells with Inflammatory and Biomarkers in the Blood of Patients with Metastatic Castration-Resistant Prostate Cancer

Gerit Theil *, Carlotta Lindner, Joanna Bialek and Paolo Fornara

Medical Faculty of Martin Luther University Halle-Wittenberg, University Clinic and Outpatient Clinic for Urology, 06120 Halle (Saale), Germany; Carlotta.lindner@uk-halle.de (C.L.); joanna.bialek@uk-halle.de (J.B.); paolo.fornara@uk-halle.de (P.F.)

* Correspondence: Gerit.Theil@medizin.uni-halle.de

Abstract: The identification of specific biomarkers that recognize the functional drivers of heterogeneity in prostate cancer (PCa) and personalized treatment remain challenging in systemic medicine. Liquid biopsy allows for the detection and analysis of personalized predictive biomarkers in single blood samples and specifies the current stage of cancer. The aim of our preliminary study was to investigate the association between an elevated circulating tumor cell (CTC) count and the levels of inflammatory factors (IL-6 and IL-8) and biomarkers (DKK-1, PSA, sHER2, and CD44) in patients with metastasized castration-resistant PCa (mCPRC) under chemotherapy and those with localized PCa. Such an association could be used as a component of cancer progression monitoring. We compared the sensitivity and specificity of two CTC isolation platforms. Twenty-eight patients (12 mCRPC and 16 localized PCa patients) were enrolled. Over the study period, the CTC detection rates were 84% with CellCollector[®] and 73.5% with CellSearch[®] System in mCPRC patients. The CTC counts determined by the CellSearch[®] System (CTC_CS) were correlated significantly with the DKK-1, sHER-2, and PSA concentrations in mCRPC patients. The CTC counts captured by CellCollector[®] demonstrated no significant association with the concentrations of the tested blood-based biomarkers. The CTC_CS count (AUC = 0.9 (95% CI: 0.72–1.0)) and the PSA level (AUC = 0.95 (95% CI: 0.83–1.0)) presented approximately the same sensitivity and specificity for the overall survival of mCRPC patients. For better personalized characterization, further research on CTC phenotyping and their interactions with tumor-associated blood-released factors is needed.

Citation: Theil, G.; Lindner, C.; Bialek, J.; Fornara, P. Association of Circulating Tumor Cells with Inflammatory and Biomarkers in the Blood of Patients with Metastatic Castration-Resistant Prostate Cancer. *Life* **2021**, *11*, 664. <https://doi.org/10.3390/life11070664>

Academic Editors: Ana Faustino and Paula A. Oliveira

Received: 25 May 2021

Accepted: 4 July 2021

Published: 6 July 2021

Publisher's Note: MDPI stays neutral with regard to jurisdictional claims in published maps and institutional affiliations.



Copyright: © 2021 by the authors. Licensee MDPI, Basel, Switzerland. This article is an open access article distributed under the terms and conditions of the Creative Commons Attribution (CC BY) license (<https://creativecommons.org/licenses/by/4.0/>).

Keywords: biomarker; circulating tumor cells; prostate cancer

1. Introduction

Prostate cancer (PCa) is the fifth leading cause of cancer-related death worldwide [1]. The incidence increases with each decade of age, and thus, 59% of men over 79 years of age have PCa [2]. In an aging population, more PCa would be diagnosed. Furthermore, in men aged 75 years and older, the incidence of regional- and distant-stage disease increased from 2013 to 2016 [3]. For 28% of patients with distant metastasis, the estimated survival rate is approximately 5 years [4]. The majority of these patients have multifocal metastatic sites, such as bone and lymph nodes (particularly vertebrae and pelvis) [5]. Moreover, oligometastatic PCa has distinct biological states and harbors different mutations, which result in heterogeneous phenotypes. Metastatic progression requires certain characteristics of cancer cells, such as plasticity, motility, and colonization, as well as systemic physiological conditions, such as inflammation, which are drivers of metastasis and therapeutic resistance in PCa [6]. Drug resistance is a dynamic process in tumor cells, which includes molecular events such as genome modification and the regulation of diverse transcriptional states. Additionally, cancer cells undergo phenotype acquisition in the process of cellular rewiring [7]. In the last decade, innovations in treatments and combination therapeutic

strategies have been developed and have contributed to the therapeutic armamentarium, improving the outcomes from metastatic PCa [8,9].

Nevertheless, the determination of the optimal personalized drug sequence to minimize possible therapeutic resistance remains a challenge [10]. Therefore, personalized biomarkers of these characteristics are needed to determine treatment responses and facilitate decisions on the selection of agents.

Classic clinical factors, such as the blood levels of prostate-specific antigen (PSA), and pathological factors, such as Gleason grading and tumor, node, and metastasis (TNM) staging, are well-known prognostic markers in PCa [11]. However, these methods are often insufficient for accurate risk stratification, and do not adequately describe the metastatic process. One possibility is liquid biopsy, which includes (among others) circulating tumor cells (CTCs). CTCs detach from primary or metastatic tumors to enter the bloodstream, and a small CTC population has the ability to metastasize to multiple organs [12]. They provide characteristics of the current stage of the tumor or potential metastasis and allow for the real-time monitoring of therapeutic responses. CTCs' interplay with blood components is important for their survival and metastatic characteristics [13,14]. They may interact with neutrophils, platelets, leukocytes, monocytes, and macrophages in the circulation, which protect the CTCs from rapid clearance by natural killer cells and the physical shear stress of blood flow. These interactions promote the survival and extravasation of CTCs at distant sites [13].

The cytokines interleukin 8 (IL-8) and IL-6 are associated with inflammation contributing to PCa and progression to treatment resistance. IL-8 is secreted by monocytes, neutrophils, and endothelial cells. Its signaling in PCa cells is involved in regulating the transcriptional activity of the androgen receptor (AR), and substantiates the transition to an androgen independent proliferation of prostate cancer cells [15]. Furthermore, IL-8 overexpression by tumor cells is often induced in response to chemotherapeutic treatment and may be important in the tumor microenvironment [16,17].

IL-6 stimulates proliferation, promotes angiogenesis, and inhibits apoptosis of PCa cells and other tumor cells. These activities are due to the interaction of IL-6 with multiple signaling pathways, such as the Janus tyrosine family kinase (JAK)-signal transducer and activator of transcription (STAT) pathway and the extracellular signal-regulated kinase 1 and 2 (ERK1/2)-mitogen activated protein kinase (MAPK) pathway [18]. Additionally, IL-6 has been identified as a nonsteroidal compound of AR activation (N-terminus of AR), which is different from ligand activation [19,20]. IL-6 is also known to induce human epidermal growth factor receptor-2 (HER2) signaling through the MAPK pathways [21]. HER2 belongs to the epidermal growth receptor family, which regulates processes such as cell differentiation, migration, and survival. The activation of HER2 results in ligand-independence over homodimerization, heterodimerization with other receptors of the HER family, or proteolytic cleavage of the extracellular domain (sHER2 ECD) [22]. HER2 signaling promotes AR signaling through androgen ligand-independent mechanisms and supports the development of castration-resistant PCa (CRPC) [23,24]. Ma et al. [25] demonstrated that CD44 interacted with HER2 promotes DNA damage repair and radioresistance. Moreover, CD44 expression in cancer cells promotes bone metastases by enhancing tumorigenicity, cell migration, and progression [26,27].

CRPC patients mostly have bone metastasis, which results in skeletal-related events such as pathological fractures. Osteoblast function is dependent on Wnt signaling, controlled by the Wnt inhibitors sclerostin and Dickkopf1 (DKK-1) [28]. Furthermore, DKK-1 expression in tumor cells activated Wnt/ β -catenin signaling and demonstrated an interaction with AR signaling [29].

The aim of our preliminary study was to investigate the association of an elevated CTC count with inflammatory molecules (IL-6 and IL-8) and biomarkers (DKK-1, sHER2, and CD44) in patients with metastasized CRPC (mCRPC) under chemotherapy and localized PCa (PCa-I). Such an association could be used as a component of cancer progression monitoring.

2. Materials and Methods

2.1. Patient Cohorts

This is a retrospective analysis of a subpopulation of a prospectively planned clinical trial in the University Clinic and Outpatient Clinic for Urology, Medical Faculty of Martin Luther University Halle-Wittenberg [30]. All of the patients provided written informed consent and were enrolled in the study. This included blood sampling (4.5 mL serum) for future research. The protocol was approved by the medical faculty ethics committee of Martin Luther University Halle-Wittenberg (number of ethical approval: FSMW EPCAM-Prostata-M00, 2012-65). The men enrolled in the first group were patients with histologically confirmed prostate adenocarcinoma with progressive disease, despite castration levels of serum testosterone (<50 ng/dL). Only two of the patients achieved the castration-resistant stage in the second month of the study. All 12 patients were examined every month for 6 months, followed by visits in the 8th and 12th months, for a total of eight visits. CTC evaluation with CellCollector[®] and the CellSearch[®] System and blood sampling for additional biomarker analysis were taken before starting the chemotherapy or the bone-targeted therapy. The second group included patients with confirmed prostate adenocarcinoma, who had opted for radical prostatectomy (RP) in the observation period and were assessed three times within 12 months. The first visit was before the prostate removal. The next visits were 6 and 12 months after surgery.

2.2. Sample Collection

Additionally, 9 mL of blood serum was collected for the determination of the levels of PSA, C-reactive protein (CRP), and testosterone and for Luminex analysis. Samples were collected at each visit. The serum was processed within one hour after collection through centrifugation at $1300 \times g$ for 10 min. The samples were stored at $-80\text{ }^{\circ}\text{C}$.

2.3. CTC Isolation

We used two different methods for CTC isolation, the CellSearch[®] System (Silicon Biosystem, Menarini, Florence, Italy) and CellCollector[®] (GILUPI GmbH, Potsdam, Germany), at matched times. Both systems used an epithelial cell adhesion molecule (EpCAM) antibody to capture the CTCs, as previously described [30,31].

CellCollector[®], a medical wire, was carefully inserted into the patient's cubital vein via a 20G peripheral venous catheter until the tip of the wire (2 cm) was in the bloodstream of the vein. After 30 min, the wire was pulled out of the vein. In the first step, the captured cells were fixed with 100% acetone for 10 min at room temperature, blocked with 3% bovine serum albumin/PBS for 30 min, and then prepared for characterization.

For the CellSearch[®] System analysis, 7.5 mL of blood was collected in CellSave[®] Preservative Tubes. These samples remained stable for 96 h at room temperature and were sent overnight to the Department of Tumor Biology, University Medical Center Hamburg-Eppendorf, Hamburg, Germany.

2.4. CTC Characterization

The matched pair analysis requires the same identification criteria as that of the CTCs. The captured cells were stained with fluorescein isothiocyanate (FITC)-labeled antibodies against cytokeratin 8, 18, and 19 (eBioscience, Abcam) for the detection of epidermal cancer cells in the blood. CD45 staining (anti-CD45-A647, Exbio) was performed to exclude leucocytes. Additionally, the cells' nuclei were stained with Hoechst 33342. Cells were defined as CTCs when they met the following cytology-based FDA definition: (i) size $\geq 4\text{ }\mu\text{m}$, (ii) visible cytoplasm, (iii) high nuclear/cytoplasm ratio, and (iv) positive fluorescent staining, as described above [32,33].

The images were digitally processed with ImageJ software by altering the contrast and brightness in accordance with Nature Publishing Guidelines [34].

2.5. Detection of Circulating Biomarkers

The serum levels of sHER2, IL-8, IL-6, DKK-1, and CD44 were simultaneously determined by a custom-made configuration of the Luminex Screening Human Magnetic Assay (R&D Systems). The assays were conducted following the manufacturer's instructions and were performed on a Luminex 100™ Qiagen GmbH system (Hilden, Germany). All of the serum samples required a two-fold dilution in calibration diluent. For the analysis, we used a 96-well flat bottom microplate. The measurements for each sample were performed in duplicate, and the average of the two measurements was used. Limits of quantification were determined using the lowest or highest standard point and a percent CV (%CV = $100 \times \text{standard deviation}/\text{average}$) of less than 20%. PSA and CRP were determined with Immulite 100 (Siemens Healthcare Diagnostics GmbH, Eschborn, Germany), according to the manufacturer's instructions.

2.6. Statistical Analysis

All of the determined blood-based biomarkers or metabolites were normalized. The values obtained at the first visits were defined as 100%. The relative secretion values are shown in box plots with medians and interquartile ranges (IQRs). Whiskers represent the minimum and maximum values. Furthermore, all of the data were tested for normal distribution using the Shapiro–Wilk test, and the parameters are presented as the median \pm range.

Finally, for the identification of possible correlations between the different markers for the different study groups, Spearman's rank correlation coefficient (r_s) was determined and is represented in a heatmap. The reported p-values are two-sided, and ≤ 0.05 was considered significant. The accuracy of the selected biomarker levels was evaluated by receiver operating characteristic (ROC) analysis. For this analysis, we used no cut-offs, but the median was six visits performed for 24 months survival. The optimal cut-off for the Kaplan–Meier analysis of PSA based on the ROC curve was calculated by the largest value of the formula, sensitivity + specificity – 1, from the median PSA level for every mCRPC patient (likelihood ratio). The mean CTC count was determined based on the CTC counts of visits 1–8 (V1–V8). Kaplan–Meier analysis was used to analyze the overall survival (OS) depending on the mean CTC count. The survival estimates in different groups were compared using the log-rank (Mantel–Cox) test. All of the statistical analyses were performed using GraphPad Prism software versions 7 and 9.

3. Results

3.1. Study Design and Patient Data

A total of 28 patients (12 mCRPC patients and 16 PCa-I patients) were enrolled in the analysis. All of the study-related applications were identical in the groups. Age ($p = 0.09$) and body mass index ($p = 0.18$) were not significantly different between the groups (Mann-Whitney test). The median age was 68.5 years in the mCRPC patients and 63 years in the PCa-I patients. The median BMI was 27.5 in the mCRPC patients and 29.7 in the PCa-I patients. The Gleason score was significantly different ($p < 0.0001$) between the PCa-I and mCRPC groups (Mann-Whitney test). Ten patients (83.3%) received docetaxel in combination with prednisone as the first-line treatment for mCRPC, and three (25%) received cabazitaxel (one patient switched in the study period from docetaxel to cabazitaxel) in response to resistance to docetaxel. The PCa-I patients were treated after the first visit with laparoscopic RP (82.3%) or high-intensity focused ultrasound (HIFU) (11.76%). The other baseline characteristics are summarized in Table 1.

Table 1. Study population characteristic and demographics.

Characteristics	mCRPC	PCa-1
Patient (<i>n</i>)	12	16
Median (range), years	69 (53–72)	63 (56–75)
Median (range) BMI	27.5 (20.8–39)	29.7 (22.5–34.5)
Median PSA (range), ng/mL at baseline	25.6 (35–1200)	8.2 (0.64–38.8)
Median PSA (range), ng/mL at the last visit	44.95 (0.04–903)	0.04 (0.04–0.06)
Median CRP (range), mg/mL at baseline	7.3 (1.8–94.8)	2.3 (1–26.2)
Median HB (range), nmol/L at baseline	7 (6.3–9.5)	9.4 (7.9–10.5)
Gleason sum, <i>n</i> (%)		
≤7	2 (16.67)	11 (64.7)
>7	10 (83.33)	6 (35.3)
Sites of metastasis, <i>n</i> (%)		
Bone	12 (100)	
Visceral	4 (33.3)	
Nodal	10 (83.3)	
Prior treatments, <i>n</i> (%)		
TURP	5 (41.7)	
Androgen treatment	12 (100)	
Radiation	9 (75)	
Treatments between baseline and study end, <i>n</i> (%)		
TURP		
Surgery (RP)		14 (82.3)
HIFU		2 (11.8)
Radiation	10 (83.3)	
Bone-targeted therapy	12 (100)	
Chemotherapy		
Docetaxel	10 (83.3)	
Cabazitaxel	3 * (25)	

RP—radical prostatectomy; HB—hemoglobin; PSA—prostate-specific antigen; TURP—transurethral resection of the prostate; HIFU—high-intensity focused ultrasound; BMI—body mass index; CRP—C-reactive protein. 3 * one CRPC patient received docetaxel and switched to cabazitaxel during the study period.

3.2. Assessment of Different Serum and Blood Biomarkers

We isolated CTCs with two different EpCAM-based systems from the mCRPC ($n = 12$) and PCa-1 ($n = 16$) patients. Over the study period, the CTC detection rates were 84% with CellCollector[®] (CTC_CC) and 73.5% with the CellSearch[®] system (CTC_CS) in the mCRPC patients. Furthermore, the CTC-median in the mCRPC patients did not differ significantly ($p = 0.29$) between the two isolation platforms. A median of 4 CTCs (range 0–820) was captured by CellCollector[®], and 8.5 CTCs (range 0–1428) by the CellSearch[®] system (Figure 1a). The baseline CTC count was zero in one mCRPC patient with CellCollector[®] and in three patients with the CellSearch[®] system. At the first visit, seven patients (58.8%) had <5 CTCs and three (25%) had ≥5 CTCs, as determined with CellCollector[®]. When the CellSearch[®] system was used, one (8.3%) patient had <5 CTCs and nine (75%) patients had ≥5 CTCs.

The PCa-1 group had a median of 0 CTCs detected with both platforms at the first visit; 0–5 CTCs were achieved with CellCollector[®] and 0–1 CTCs were achieved with the CellSearch[®] system. In addition, in the cured patients, 0 CTCs were detected using the CellSearch[®] system. However, CellCollector[®] captured a median of 0 CTCs with a range of 0–9 at visits 6 and 12 months after RP (Figure 1b).

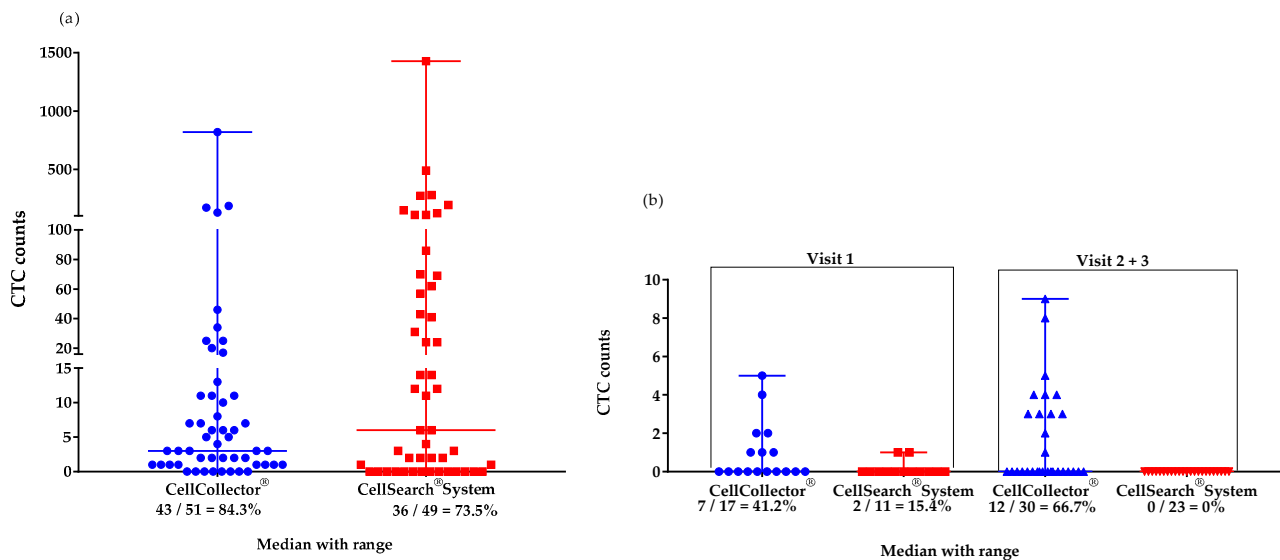


Figure 1. Median (range) values of CTCs isolated with the CellCollector® and CellSearch® Systems. (a) mCRPC patients ($n = 12$) in the study period of 12 months: CellCollector®, 4 CTCs (0–820), and CellSearch® System, 8.5 CTCs (0–1428); (b) PCa-I patients ($n = 16$) at visit 1 (before surgical removal): CellCollector®, 0 CTCs (0–5), and CellSearch® System, 0 CTCs (0–1) and at visits 2 and 3 (6 and 12 months after removal of prostate, respectively): CellCollector®, 0 CTCs (0–9), and CellSearch® System, 0 CTCs (0).

Biomarkers were measured until visit 6 (sixth month) in the study period. Unfortunately, data from visits 7 and 8 could not be included in the analysis because of an insufficient sample size. The serum levels of sHER2, IL-8, IL-6, Dkk-1, and CD44 did not show significant differences between the PCa-I and mCRPC patients (Table 2). The median levels of DKK-1 (4625 pg/mL), IL-6 (11.7 pg/mL), and IL-8 (20 pg/mL) in the mCRPC patients were higher than those in the PCa-I patients (3939 pg/mL, 5.6 pg/mL, and 10.8 pg/mL, respectively). Interestingly, the CD44 level in the mCRPC patients was the lowest in the study population. Moreover, the sHER level demonstrated a decreased concentration over six months in the mCRPC group. The median secretion levels were 3.3 ng/mL in the PCa-I group at visit 1 and 3.5 ng/mL at visits 2 and 3. The mCRPC patients had a median concentration of 3.3 ng/mL, which was approximately equal to the concentrations in the localized cancer stage groups. Interestingly, the sHER concentration had the widest range of 0.3–16.64 ng/mL in the mCRPC group. Significant differences were found for the PSA level ($p < 0.001$), CRP level ($p = 0.03$), and CTC count ($p < 0.001$) between the groups (Table 2).

We investigated the serial secretion of the biomarkers in the treatment follow-up at 6 months in the mCRPC patients (Figure 2). The first values were defined as 100%. The median relative CTC_SC count and the median relative secretion of PSA, IL-6, and IL-8 during the settlement period were the most dynamic markers (Figure 2a,c,e). The CTC count continually changed from 95 to 300% from visit 2 to visit 4. In contrast, the relative CTC_CC counts demonstrated a decreasing level during the period of analysis. The lowest relative CTC_CC count was reduced by 14% at visit 4 (Figure 2b). The median PSA level also showed variations with a range of 36% at visit 3 and 157% at visit 6. The DKK-1 protein showed a relatively constant secretion of 90.1–112.5%. IL-6 secretion remained relatively constant in the range of 126–117% until the fifth month. Interestingly, IL-6 secretion increased 440% in the 6th month. sHER-2 showed variations in a range of 96–66.8%, which revealed a continuous decrease in concentration under therapy. The serial change in IL-8 secretion demonstrated a variation of 66% in the third month to 156% in the 6th month. CD44 secretion was relatively constant over the observation period (104–86%).

Table 2. Serum levels of different biomarkers.

Median (Range)	mCRPC V1–V6	PCa-I V2 + V3	V1	p-Value
CD44 (pg/mL)	710 (205.9–4878)	777.1 (230.6–3382)	783.6 (386–2440)	0.70
DKK-1 (pg/mL)	4625 (566.9–8878)	3939 (1632–10937)	3976 (1273–7988)	0.80
sHer2 (ng/mL)	3.3 (0.83–16.46)	3.3 (1.1–7.7)	3.5 (1.27–8.4)	0.39
IL-6 (pg/mL)	11.7 (1.91–180)	5.6 (1.5–587.2)	8.2 (1.0–589)	0.24
IL-8 (pg/mL)	20 (1.98–112.7)	10.8 (4.8–1127)	13.2 (2.6–1216)	0.27
CTC_CC	4 (0–820)	0 (0–5)	0 (0–9)	<0.0001
CTC_CS	8.5 (0–1428)	0 (0–1)	0	<0.0001
PSA (ng/mL)	18.5 (1–1120)	8.2 (0.64–38.8)	0.04 (0.04–1.12)	<0.0001
CRP (ng/mL)	7.3 (1.8–94.8)	2.1 (1–26.4)	n.d.	0.03

CD44—cluster of differentiation 44; DKK-1—Dickkopf1; sHER2—soluble human epidermal growth factor receptor 2; IL-6, -8—interleukin-6, -8; CTC_CC—determined with CellCollector®; CTC_CS—determined with the CellSearch® system; PSA—prostate-specific antigen; CRP—C-reactive protein.

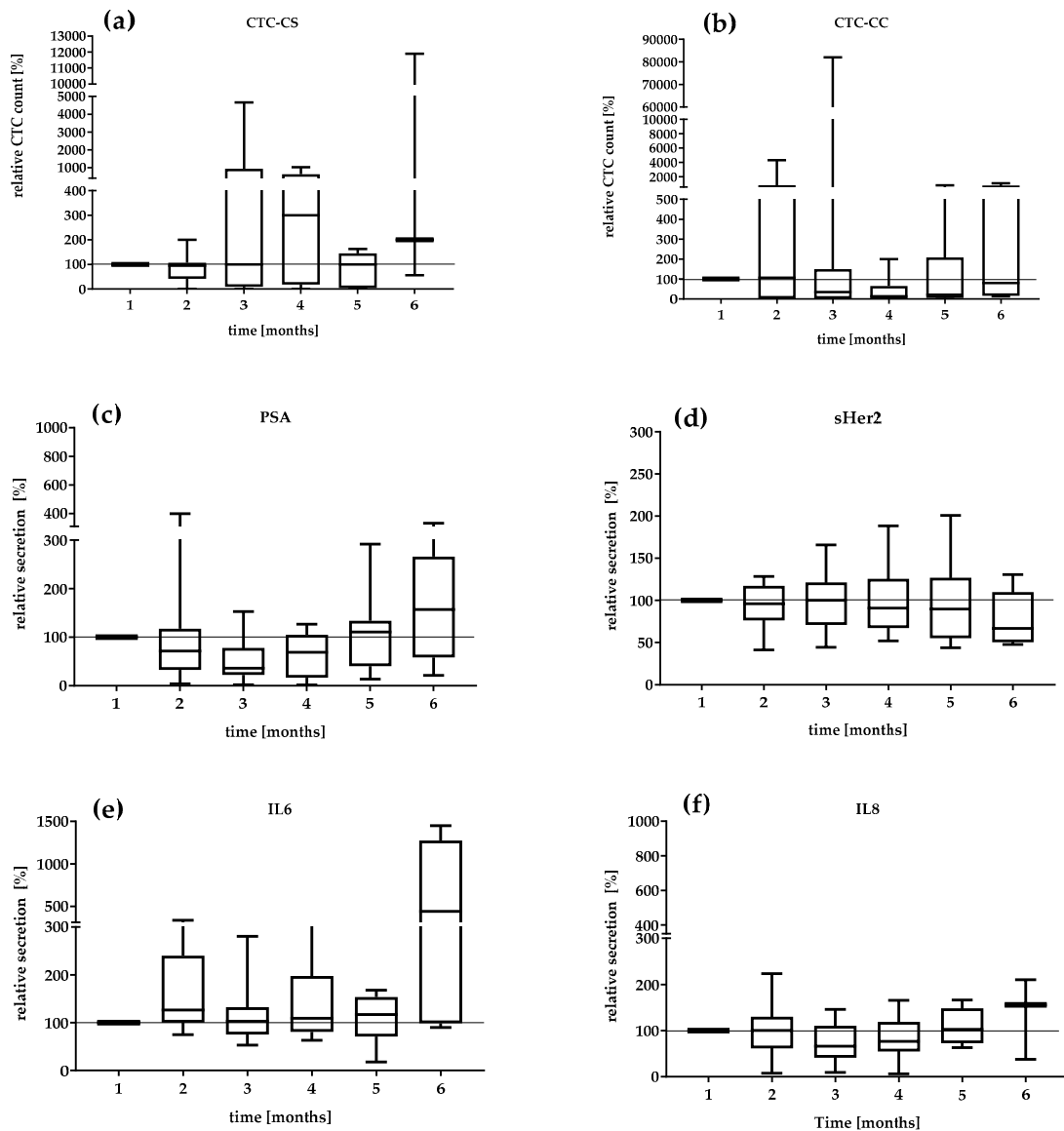


Figure 2. Cont.

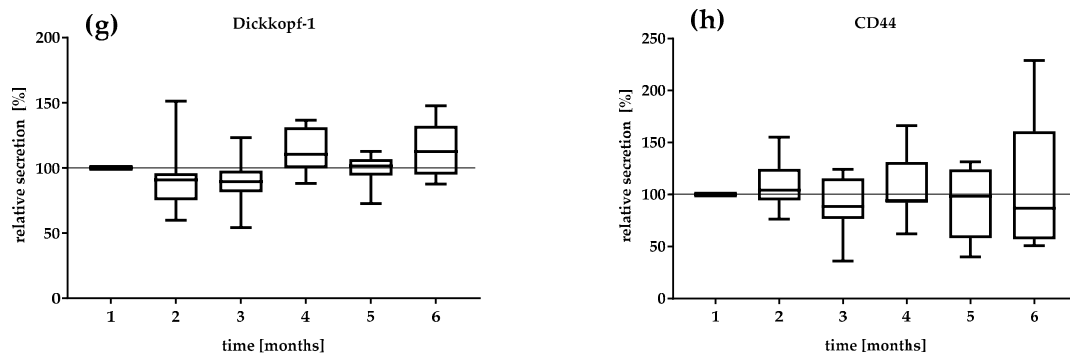


Figure 2. Relative value in percent of (a) CTC_CS count, (b) CTC_CC count, (c) PSA, (d) sHER2, (e) IL-6, (f) IL-8, (g) DKK-1, and (h) CD44 in the mCRPC patients during 6 months. The median relative secretion with minimum and maximum values. The value of the first visit was defined as 100%.

The correlation of serial CTC secretion between the serial secretion of biomarkers and inflammatory markers is shown in Figure 3. CTC counts determined with the CellSearch[®] system (CTC_CS) were moderately positively correlated with the concentrations of DKK-1 ($r_s = 0.35, p = 0.01$) and sHER-2 ($r_s = 0.41, p = 0.004$) in the mCRPC patients. A strong correlation was found between the CTC_CS count and the PSA concentration ($r_s = 0.75, p \leq 0.0001$) and the CTC counts of both platforms ($r_s = 0.78, p = 0.03$). Within regard to the CTC count captured by CellCollector[®] (CTC_CC), no significant association was observed with the concentrations of the other blood-based biomarkers. The CRP concentration was strongly positively, but not significantly correlated with the CTC count (CTC_CS $r_s = 0.60, p = 0.4$; CTC_CC $r_s = 0.78, p = 0.078$). Interestingly, we demonstrated a good correlation between PSA and sHer2 levels ($r_s = 0.55, p \leq 0.0001$) and PSA and IL-8 levels ($r_s = 0.47, p \leq 0.0001$) in our cohort. For IL-6, a good negative correlation was observed with DKK-1 ($r_s = -0.45$) and CD44 ($r_s = -0.54$).

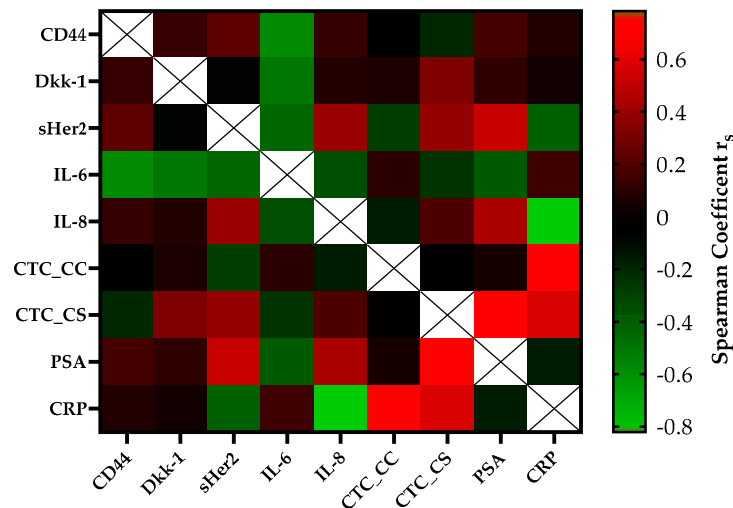


Figure 3. The heatmap of the correlation coefficients (Spearman) among biomarkers of the mCRPC patients. The color-coded correlation is on the left, where red demonstrates a strong positive correlation and light green indicates a strong negative correlation.

In the PCa-I patient group, no significant correlation was found between the CTC counts of either platform and the biomarker levels; however, the levels of markers prior to prostate removal were correlated (Supplementary Figure S1).

The sensitivity, specificity, and area under the curve (AUC) value were determined for CTC_CC, DKK-1, PSA, CTC_CS, and sHER2, which were correlated significantly with the

CTC_SC count. The results demonstrated that for a survival time of 24 months, the AUC values of these markers were 0.63, 0.62, 0.9, 0.95, and 0.79, respectively. The PSA level and the CTC_CS showed the strongest ability to predict survival for 24 months for the mCRPC patients. These results were calculated with the 6-month median level of the evaluated markers for every single mCRPC patient (Figure 4).

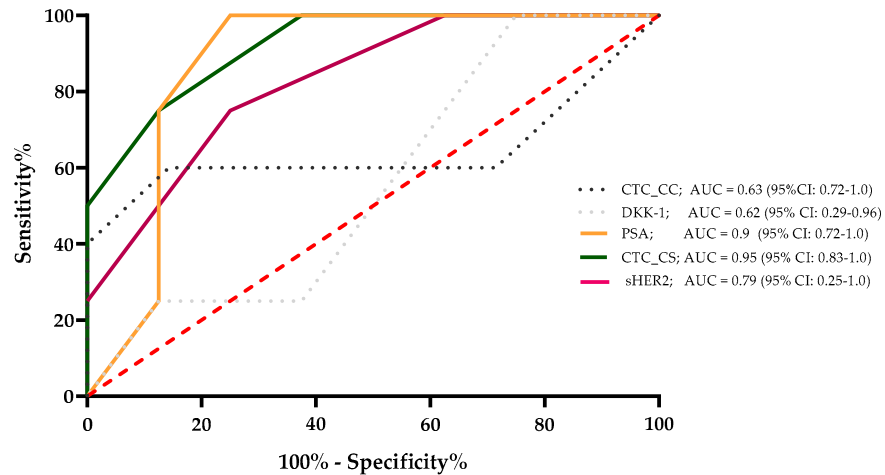


Figure 4. A survival ROC curve was plotted to evaluate the sensitivity, specificity, and AUC of serum concentrations of sHer2, PSA, DKK-1, CTC_CC, and CTC_CS and the 24-month survival.

3.3. The OS Value of CTC Count Versus PSA Level

We reached a follow-up time of 5 years in the study population, and compared the prognostic value of the median CTC count and the PSA concentration. In our analyses, we used the established CTC cutoff values of <5 or ≥ 5 CTCs [32]. For the PSA level, we used the estimated cutoff value of 53 ng/mL, which was calculated for the mCRPC patients in our study. In this study, the positive likelihood ratio was 8.0 (sensitivity 100%, specificity 87.5) for PSA cutoff values of 53 ng/mL.

Patients (75%) with evaluated CTC counts of <5 cells survived 34 months, with a median of 56 months. Patients (75%) with an evaluated CTC count of ≥ 5 cells survived 14 months, with a median survival time of 21.5 months. The hazard ratio (HR), referring to <5 or ≥ 5 CTCs, was 4.6 (95% confidence interval (CI): 1.2–17.03; Figure 5a).

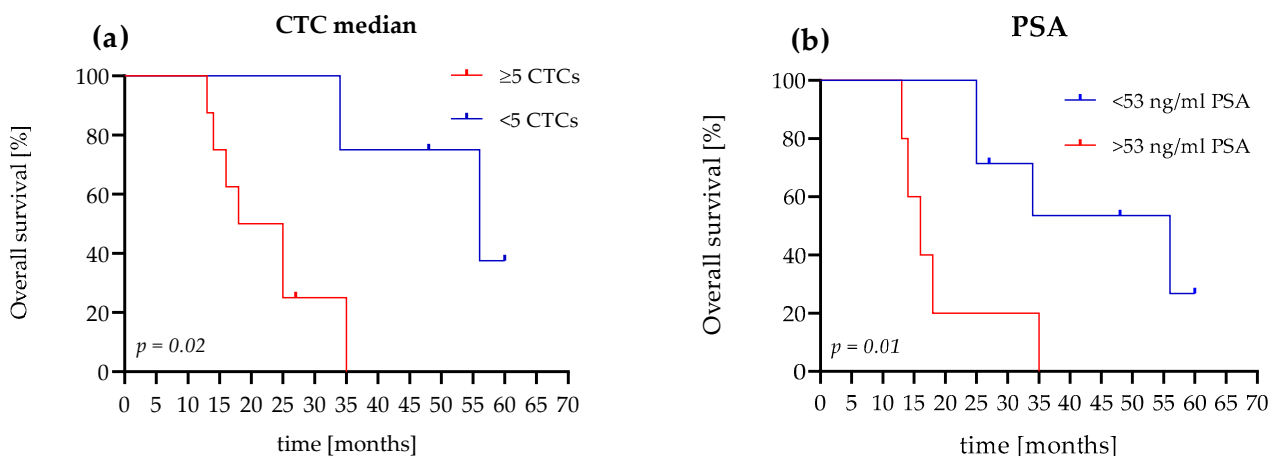


Figure 5. Comparison of Kaplan–Meier curves for OS according to the CTC count and PSA level of the mCRPC patients. (a) The patient shows <5 CTCs and a ≥ 5 CTC difference in OS (56 months versus 21.5 months (HR 4.6, 95% CI, 1.2–17)). (b) The patient shows a PSA level <53 ng/mL and a ≥ 53 ng/mL difference in OS (56 months versus 16 months (HR 4.4, 95% CI, 0.9–21)).

In comparison, with a PSA level <53 ng/mL, 71.5% of the patients survived 25 months with a median of 56 months. Patients (60%) with PSA levels >53 ng/mL survived 14 months and had a median survival time of 16 months. The HR, referred to as <53 ng/mL PSA or >53 ng/mL PSA, was 4.4 (95% CI: 0.9–21; Figure 5b).

4. Discussion

We analyzed the association between inflammatory markers and different biomarkers under therapy in a cohort of patients with PCa-I and mCRPC. Moreover, we compared two CTC isolation platforms for their sensitivity and specificity. There are many CTC isolation platforms; however, all of them have disadvantages and advantages [35,36]. We used CellCollector[®], an in vivo CTC isolation system [30,37], and the FDA-approved CellSearch[®] system [32]. Similarly, in both platforms, CTCs were captured using antibodies against the EpCAM protein and were further characterized. The CellSearch[®] system required a blood sample of 7.5 mL, while CellCollector[®] required a larger volume. The CellSearch[®] system detected a higher CTC count in the mCRPC group, although the detection rate of CellCollector[®] was 84% compared with 73.5% of the CellSearch[®] system. Nevertheless, a range of 0–9 CTCs detected using CellCollector[®] in PCa-I patients compared with a range of 0–1 CTCs detected using the CellSearch[®] system. These results indicated that CellCollector[®] might be more useful than the CellSearch[®] system in nonmetastatic PCa patients because of the higher CTC detection rate. A possible reason for the different results could be the different EpCAM antibodies with differences in the affinity to the EpCam molecule. Furthermore, the veins in localized PCa patients are sometimes better for the in vivo application of the CellCollector[®] as in mCRPC patients. Even if the number of detected CTCs in indolent localized patients is low and their clinical utility remains unclear, their better specified molecular characterization would be crucial for clinical application. Chen et al. [38] further assessed high-risk nonmetastatic PCa patients and described CellCollector[®] as an efficient CTC technology for monitoring cancer relapse in localized PCa, as well as for monitoring of the treatment response.

The CTC counts obtained with CellCollector could also be tested in metastatic castration-sensitive prostate cancer patients (mCSPC) as biomarkers for evaluation of the treatment with androgen-receptor-axis-targeted (ARAT) therapy compared with docetaxel to improve the outcome in mCSPC patients [39,40].

However, in a comparison of different CTC platforms (CellCollector[®], dual fluoro-EPISPOTPSA/FGF2, and the CellSearch[®] system), the CellSearch[®] system was the most accurate predictor of metastatic PCa (AUC 0.76, 95% CI: 0.631–0.908) [41]. Our ROC analysis showed an AUC of 0.95 (95% CI: 0.83–1.0) for the CellSearch[®] system, which confirmed the high sensitivity and specificity of this system. The PSA level, a classic marker in blood-based therapeutic monitoring of advanced PCa patients, demonstrated a comparatively high sensitivity and specificity with an AUC of 0.90 (95% CI: 0.72–1.0) in our mCRPC patient cohort (Figure 4). Interestingly, our results demonstrated a good correlation between the PSA level and the CTC count determined with the CellSearch[®] System. CTCs are prognostic parameters in mCRPC patients, but are usually independent of the PSA levels [32,42–44]. In our Kaplan–Meier OS analysis, a CTC count of ≥ 5 cells and >53 ng/mL PSA showed nearly identical HRs (CTC count HR = 4.6, $p = 0.02$ and PSA level HR = 4.4, $p = 0.01$). Our data showed that the CTC count and the PSA value in our cohort of mCRPC patients presented almost identical prognostic values. Nevertheless, CTCs can provide additional cancer-specific characteristics at the protein, mRNA, and DNA levels [35].

Furthermore, we found elevated serum levels of sHER2, DKK-1, IL-6, and IL-8 in the mCRPC patients and the PCa-I patients and found no significant difference between the groups (Table 2). Moreover, all of the analyzed markers were actively or passively involved in the bypassing of the AR signaling and might indicate active signaling in the blood. These factors may also influence the ability of CTCs to enhance inflammatory factors and biomarker release in blood circulation for possible crosstalk with cells.

Moreover, we found that the median DKK-1 serum level of 4625 pg/mL in the mCRPC patients was slightly increased compared with that in the PCa-I patients (3939 pg/mL), which may contribute to the development of osteoblastic metastasis. In addition, the higher DKK-1 concentration could indicate a possible switch in phenotype to the osteoblastic metastasis type [45]. In the serial measurements, a variation of 90.1–112.5% of DKK-1 was observed (Figure 3g). Interestingly, in the sixth month of systemic therapy, an increase of 112% was observed, as well as increases in the levels of PSA (157%), IL-6 (440%), CTC_CS (200%), and IL-8 (156%), which was consistent with the docetaxel treatment interruption (Figure 3). The doubling of the median CTC count suggests active cancer communication or micrometastatic progression. The increased serum level of DKK-1 could be due to the zoledronic acid treatment of the mCRPC patients, as shown by Thiele et al. [46] in an analysis of serum samples at different PCa stages. Our mCRPC cohort was under zoledronic acid treatment.

However, a good negative correlation of -0.45 ($p < 0.0001$) was demonstrated for DKK-1 and IL-6. This effect was described in inflamed joints of rheumatoid arthritis [47]. The median IL-6 and IL-8 concentrations in the serum of the mCRPC patients were substantially increased compared with those in the PCa-I group (Table 2). Culig [48] postulated in his review that serum IL-6 can act as an attractant for tumor cells and is linked to aggressive tumors. The IL-6 concentration of our cohort (11.7 pg/mL in the mCRPC group) was similar to that of the cohort of Nakashima et al. [49], and higher than 7 pg/mL. The increase of 440% in the sixth month of treatment could indicate active signaling pathways in PCa. Our results confirmed the findings from these studies, which concluded that higher IL-6 serum levels were correlated with the tumor stage and were inversely correlated with tumor survival and therapeutic response [18,48]. In the monitoring of mCRPC patients, the IL-8 level increased to 156% (visit at 6 months) compared with the baseline level (100%). Maynard et al. [50] reported that the high expression of IL-8 in the tumor microenvironment is associated with aggressive PCa and with the loss of the AR. Analysis of the IL-8 serum level of PCa-I patients found no correlation with diagnosis and aggressiveness [51]. We also detected lower IL-6 and IL-8 concentrations in the serum of the PCa-I group. In the mCRPC group, we could not demonstrate any significant correlation of interleukins 6 and 8 with the CTC count. One possible explanation could be the CTC status in the blood circulation and current tumor stage, which need to be explored in further studies. It is known that CTCs undergo a phenotype switch from epithelial to mesenchymal transition (EMT), and present a mesenchymal status [52]. Patients with newly diagnosed metastatic castration-sensitive PCa and positive for mesenchymal CTCs show a decline in resistance to androgen deprivation therapy compared with patients who are negative for EMT CTCs [53].

Interestingly the serum level of the sHER2 showed a significant ($p < 0.001$) moderate ($r_s = 0.41$) correlation with the CTC_SC count. Although we could detect sHER2 in the serum, the median concentration was equal in our groups, but the range (0.83–16.46 ng/mL) in the mCRPC group was much wider. This finding suggests that CTCs in the blood circulation express HER2, and that HER2 signaling is activated through the cleavage of sHER2 (ECD). The single patient profile shows an increasing sHER2 concentration in the fifth and sixth months (data not shown), which is consistent with chemotherapy interruption. Josefsson et al. [54] demonstrated a high correlation between HER2 expression in CTCs and metastatic samples, and emphasized the potential for CTC phenotyping for individualized therapy in metastatic PCa. Furthermore, it was demonstrated in 236 PCa patients that HER2 over expression is associated with a low expression of the tumor suppressor gene PTEN (phosphatase and tensin homologue) and reduced the cancer-specific survival [55]. Using the AdnaTest ProstateCancerSelect/Detect kit for CTC isolation from the PCa patients in their study, they captured CTCs with the EpCAM and HER2 protein [54]. The same kit was used for the analysis by Antonarakis et al. [56]. This group detected AR splice variant 7 mRNA (AR-V7) in the CTCs from patients with castration-resistant PCa. The CTCs also express HER2 and AR-V7. This variant of the AR in CTCs has no ligand-binding domain, but via an active HER2 signaling it can bypass the androgen signaling pathway. In

a recently published study, the expressions of AR-V7 and PTEN were determined in CTC. The authors demonstrated that more than two PTEN negative CTCs were associated with a 3.96 hazard ratio for progression or death compared with CRPC patients with less than two PTEN negative CTCs. Moreover, a high CTC AR-V7 positive count (0–20) was associated with a radiographic progression-free survival in ezalutamid-treated patients [57].

We determined the CD44 expression in the serum, but the median concentration in the mCRPC group was only slightly decreased compared with that in the PCa-I patients. However, the concentration range was much wider in this group than in the PCa-I group. Nevertheless, we could not observe any increase in the CD44 concentration after chemotherapy in the mCRPC group. Some patients demonstrated constant levels, and others had decreased levels after chemotherapy. Ma et al. [25] showed the interaction between CD44 and HER2 in PCa cell line, and linked this relationship to potential radio resistance PCa.

In this study, we showed that the CTC count determined with the CellSearch[®] system (CTC_CS) is more suitable for mCRPC patients than CellCollector, an *in vivo* isolation system. We identified a moderate correlation between the CTC counts and the biomarkers sHER2 and DKK-1, and a strong correlation with the PSA level. Additionally, we found that a CTC_CS count ≥ 5 cells and a PSA level > 53 ng/mL presented approximately the same diagnostic potency with regard to the sensitivity and specificity for OS in our mCRPC patients. Furthermore, for better personalized characterization, it is crucial to expand the research focused on CTC phenotyping, and the interactions of these cells with coexisting, tumor-associated blood-released factors.

The limitations of our preliminary investigations are of course the small number of patients and the heterogeneous group of mCRPC patients (first and second line of chemotherapy). Likewise, the CTC platforms used here capture CTCs with an EpCam antibody but not CTCs with a mesenchymal phenotype. Moreover, we included no independent cohorts such as age match healthy woman or man. A wider characterization might provide additional information about the association between CTC and other biomarkers [13]. Larger studies are needed to further validate our findings.

Supplementary Materials: The following are available online at <https://www.mdpi.com/article/10.3390/life11070664/s1>, Figure S1: Heatmap of non-significant correlation coefficients (Spearman) among biomarkers of localized prostate cancer patients.

Author Contributions: conceptualization, G.T. and C.L.; methodology, G.T.; software, J.B.; validation, G.T., J.B. and P.F.; formal analysis, C.L.; investigation, G.T.; resources, P.F.; data curation, J.B.; writing—original draft preparation, G.T.; writing—review and editing, J.B.; visualization, C.L.; supervision, P.F.; project administration, G.T.; funding acquisition, G.T. All authors have read and agreed to the published version of the manuscript.

Funding: This research was funded by GILUPI GMPH. They provided CellCollector and the patients received travel expenses.

Institutional Review Board Statement: The study was conducted according to the guidelines of the Declaration of Helsinki and was approved by the medical faculty ethics committee of Martin Luther University Halle-Wittenberg (protocol code SMW EPCAM-Prostata-M00 and approved on 01/2011).

Informed Consent Statement: Informed consent was obtained from all of the subjects involved in the study.

Acknowledgments: We acknowledge the financial support within the funding program Open Access Publishing by the German Research Foundation (DFG).

Conflicts of Interest: The authors declare no conflict of interest. The funders had no role in the design of the study; in the collection, analyses, or interpretation of data; in the writing of the manuscript; or in the decision to publish the results.

References


- Bray, F.; Ferlay, J.; Soerjomataram, I.; Siegel, R.L.; Torre, L.A.; Jemal, A. Global cancer statistics 2018: GLOBOCAN estimates of incidence and mortality worldwide for 36 cancers in 185 countries. *CA Cancer J. Clin.* **2018**, *68*, 394–424. [CrossRef]
- Bell, K.J.; Del Mar, C.; Wright, G.; Dickinson, J.; Glasziou, P. Prevalence of incidental prostate cancer: A systematic review of autopsy studies. *Int. J. Cancer* **2015**, *137*, 1749–1757. [CrossRef] [PubMed]
- Jemal, A.; Culp, M.B.; Ma, J.; Islami, F.; Fedewa, S. Prostate Cancer Incidence 5 Years After US Preventive Services Task Force Recommendations Against Screening. *J. Natl. Cancer Inst.* **2021**, *113*, 64–71. [CrossRef] [PubMed]
- Siegel, R.L.; Miller, K.D.; Jemal, A. Cancer statistics, 2019. *CA Cancer J. Clin.* **2019**, *69*, 7–34. [CrossRef]
- Gandaglia, G.; Abdollah, F.; Schiffmann, J.; Trudeau, V.; Shariat, S.F.; Kim, S.P.; Perrotte, P.; Montorsi, F.; Briganti, A.; Trinh, Q.-D.; et al. Distribution of metastatic sites in patients with prostate cancer: A population-based analysis. *Prostate* **2014**, *74*, 210–216. [CrossRef]
- Welch, D.R.; Hurst, D.R. Defining the Hallmarks of Metastasis. *Cancer Res.* **2019**, *79*, 3011–3027. [CrossRef]
- Carceles-Cordon, M.; Kelly, W.K.; Gomella, L.; Knudsen, K.E.; Rodriguez-Bravo, V.; Domingo-Domenech, J. Cellular rewiring in lethal prostate cancer: The architect of drug resistance. *Nat. Rev. Urol.* **2020**, *17*, 292–307. [CrossRef] [PubMed]
- Nuhn, P.; De Bono, J.S.; Fizazi, K.; Freedland, S.J.; Grilli, M.; Kantoff, P.W.; Sonpavde, G.; Sternberg, C.N.; Yegnasubramanian, S.; Antonarakis, E.S. Update on Systemic Prostate Cancer Therapies: Management of Metastatic Castration-resistant Prostate Cancer in the Era of Precision Oncology. *Eur. Urol.* **2019**, *75*, 88–99. [CrossRef]
- Lorente, D.; Ravi, P.; Mehra, N.; Pezaro, C.; Omlin, A.; Gilman, A.; Miranda, M.; Rescigno, P.; Kolinsky, M.; Porta, N.; et al. Interrogating Metastatic Prostate Cancer Treatment Switch Decisions: A Multi-institutional Survey. *Eur. Urol. Focus* **2018**, *4*, 235–244. [CrossRef]
- Caffo, O.; Maines, F.; Kinspergher, S.; Vecchia, A.; Messina, C. Sequencing strategies in the new treatment landscape of prostate cancer. *Futur. Oncol.* **2019**, *15*, 2967–2982. [CrossRef]
- Mottet, N.; van den Bergh, R.C.; Briers, E.; Van den Broeck, T.; Cumberbatch, M.G.; De Santis, M.; Cornford, P. *EAU—EANM—ESTRO—ESUR—SIOG Guidelines on Prostate Cancer*; European Association of Urology: Arnhem, The Netherlands, 2019.
- Massague, J.; Obenauf, A.C. Metastatic colonization by circulating tumour cells. *Nature* **2016**, *529*, 298–306. [CrossRef]
- Lambert, A.W.; Pattabiraman, D.R.; Weinberg, R.A. Emerging Biological Principles of Metastasis. *Cell* **2017**, *168*, 670–691. [CrossRef]
- Lozar, T.; Gersak, K.; Cemazar, M.; Kuhar, C.G.; Jesenko, T. The biology and clinical potential of circulating tumor cells. *Radiol. Oncol.* **2019**, *53*, 131–147. [CrossRef] [PubMed]
- Araki, S.; Omori, Y.; Lyn, D.; Singh, R.K.; Meinbach, D.M.; Sandman, Y.; Lokeshwar, V.B.; Lokeshwar, B.L. Interleukin-8 Is a Molecular Determinant of Androgen Independence and Progression in Prostate Cancer. *Cancer Res.* **2007**, *67*, 6854–6862. [CrossRef]
- Waugh, D.J.; Wilson, C. The interleukin-8 pathway in cancer. *Clin. Cancer Res.* **2008**, *14*, 6735–6741. [CrossRef] [PubMed]
- Aguilar-Saavedra, J.A.; Anjos, N.; Cantrill, R.; Carvalho, J.; Castro, N.F.; Conde Muiño, P. Search for magnetic monopoles in sqrt[s]=7 TeV pp collisions with the ATLAS detector. *Phys. Rev. Lett.* **2012**, *109*, 261803.
- Nguyen, D.P.; Li, J.; Tewari, A.K. Inflammation and prostate cancer: The role of interleukin 6 (IL-6). *BJU Int.* **2014**, *113*, 986–992. [CrossRef] [PubMed]
- Ueda, T.; Bruchovsky, N.; Sadar, M. Activation of the Androgen Receptor N-terminal Domain by Interleukin-6 via MAPK and STAT3 Signal Transduction Pathways. *J. Biol. Chem.* **2002**, *277*, 7076–7085. [CrossRef] [PubMed]
- Culig, Z. Interleukin-6 Function and Targeting in Prostate Cancer. *Adv. Exp. Med. Biol.* **2021**, *1290*, 1–8. [CrossRef]
- Qiu, Y.; Ravi, L.; Kung, H.-J. Requirement of ErbB2 for signalling by interleukin-6 in prostate carcinoma cells. *Nat. Cell Biol.* **1998**, *393*, 83–85. [CrossRef]
- Perrier, A.; Gligorov, J.; Lefevre, G.; Boissan, M. The extracellular domain of Her2 in serum as a biomarker of breast cancer. *Lab. Investig.* **2018**, *98*, 696–707. [CrossRef]
- Craft, N.; Shostak, Y.; Carey, M.; Sawyers, C.L. A mechanism for hormone-independent prostate cancer through modulation of androgen receptor signaling by the HER-2/neu tyrosine kinase. *Nat. Med.* **1999**, *5*, 280–285. [CrossRef]
- Miller, D.R.; Ingersoll, M.A.; Lin, M.-F. ErbB-2 signaling in advanced prostate cancer progression and potential therapy. *Endocrine-Relat. Cancer* **2019**, *26*, R195–R209. [CrossRef]
- Ma, J.-W.; Wang, X.; Chang, L.; Zhong, X.-Y.; Jing, H.; Zhu, X.; Wang, S.; Xiao, W. CD44 collaborates with ERBB2 mediate radiation resistance via p38 phosphorylation and DNA homologous recombination pathway in prostate cancer. *Exp. Cell Res.* **2018**, *370*, 58–67. [CrossRef]
- Hiraga, T.; Ito, S.; Nakamura, H. Cancer Stem-like Cell Marker CD44 Promotes Bone Metastases by Enhancing Tumorigenicity, Cell Motility, and Hyaluronan Production. *Cancer Res.* **2013**, *73*, 4112–4122. [CrossRef] [PubMed]
- Senbanjo, L.T.; Aljohani, H.; Majumdar, S.; Chellaiyah, M.A. Characterization of CD44 intracellular domain interaction with RUNX2 in PC3 human prostate cancer cells. *Cell Commun. Signal.* **2019**, *17*, 1–13. [CrossRef] [PubMed]
- Baron, R.; Rawadi, G. Targeting the Wnt/beta-catenin pathway to regulate bone formation in the adult skeleton. *Endocrinology* **2007**, *148*, 2635–2643. [CrossRef] [PubMed]
- Pakula, H.; Xiang, D.; Li, Z. A Tale of Two Signals: AR and WNT in Development and Tumorigenesis of Prostate and Mammary Gland. *Cancers* **2017**, *9*, 14. [CrossRef] [PubMed]

30. Theil, G.; Boehm, C.; Fischer, K.; Bialek, J.; Hoda, R.; Weber, E.; Schönburg, S.; Kawan, F.; Fornara, P. In vivo isolation of circulating tumor cells in patients with different stages of prostate cancer. *Oncol. Lett.* **2021**, *21*, 1–8. [CrossRef]
31. Kuske, A.; Gorges, T.M.; Tennstedt, P.; Tiebel, A.-K.; Pompe, R.S.; Preißer, F.; Prues, S.; Mazel, M.; Markou, A.; Lianidou, E.; et al. Improved detection of circulating tumor cells in non-metastatic high-risk prostate cancer patients. *Sci. Rep.* **2016**, *6*, 39736. [CrossRef]
32. De Bono, J.S.; Scher, H.I.; Montgomery, R.B.; Parker, C.; Miller, M.C.; Tissing, H.; Doyle, G.V.; Terstappen, L.; Pienta, K.; Raghavan, D. Circulating Tumor Cells Predict Survival Benefit from Treatment in Metastatic Castration-Resistant Prostate Cancer. *Clin. Cancer Res.* **2008**, *14*, 6302–6309. [CrossRef]
33. Allard, W.J.; Matera, J.; Miller, M.C.; Repollet, M.; Connelly, M.C.; Rao, C.; Tibbe, A.G.J.; Uhr, J.W.; Terstappen, L.W.M.M. Tumor cells circulate in the peripheral blood of all major carcinomas but not in healthy subjects or patients with nonmalignant diseases. *Clin. Cancer Res.* **2004**, *10*, 6897–6904. [CrossRef] [PubMed]
34. Llopis, P.M.; Senft, R.A.; Ross-Elliott, T.J.; Stephansky, R.; Keeley, D.P.; Koshar, P.; Marqués, G.; Gao, Y.-S.; Carlson, B.R.; Pengo, T.; et al. Best practices and tools for reporting reproducible fluorescence microscopy methods. *Nat. Methods* **2021**, 1–14. [CrossRef]
35. Theil, G.; Fornara, P.; Bialek, J. Position of Circulating Tumor Cells in the Clinical Routine in Prostate Cancer and Breast Cancer Patients. *Cancers* **2020**, *12*, 3782. [CrossRef]
36. Alix-Panabières, C.; Pantel, K. Technologies for detection of circulating tumor cells: Facts and vision. *Lab Chip* **2013**, *14*, 57–62. [CrossRef] [PubMed]
37. Saucedo-Zeni, N.; Mewes, S.; Niestroj, R.; Gasiorowski, L.; Murawa, D.; Nowaczyk, P.; Lücke, K. A novel method for the in vivo isolation of circulating tumor cells from peripheral blood of cancer patients using a functionalized and structured medical wire. *Int. J. Oncol.* **2012**, *41*, 1241–1250.
38. Chen, S.; Tauber, G.; Langsenlehner, T.; Schmolzer, L.M.; Pötscher, M.; Riethdorf, S.; Kuske, A.; Leitinger, G.; Kashofer, K.; Czyż, Z.T.; et al. In Vivo Detection of Circulating Tumor Cells in High-Risk Non-Metastatic Prostate Cancer Patients Undergoing Radiotherapy. *Cancers* **2019**, *11*, 933. [CrossRef]
39. Buonerba, C.; Ferro, M.; Dolce, P.; Crocetto, F.; Verde, A.; Lucarelli, G.; Scafuri, L.; Facchini, S.; Vaia, A.; Marinelli, A.; et al. Predictors of efficacy of androgen-receptor-axis-targeted therapies in patients with metastatic castration-sensitive prostate cancer: A systematic review and meta-analysis. *Crit. Rev. Oncol.* **2020**, *151*, 102992. [CrossRef]
40. Ferro, M.; Lucarelli, G.; Crocetto, F.; Dolce, P.; Verde, A.; La Civita, E.; Zappavigna, S.; de Cobelli, O.; Di Lorenzo, G.; Facchini, B.A.; et al. First-line systemic therapy for metastatic castration-sensitive prostate cancer: An updated systematic review with novel findings. *Crit. Rev. Oncol.* **2021**, *157*, 103198. [CrossRef]
41. Cieślakowski, W.A.; Budna-Tukan, J.; Świerczewska, M.; Ida, A.; Hrab, M.; Jankowiak, A.; Mazel, M.; Nowicki, M.; Milecki, P.; Pantel, K.; et al. Circulating Tumor Cells as a Marker of Disseminated Disease in Patients with Newly Diagnosed High-Risk Prostate Cancer. *Cancers* **2020**, *12*, 160. [CrossRef]
42. Lorente, D.; Olmos, D.; Mateo, J.; Dolling, D.; Bianchini, D.; Seed, G.; Flohr, P.; Crespo, M.; Figueiredo, I.; Miranda, S.; et al. Circulating tumour cell increase as a biomarker of disease progression in metastatic castration-resistant prostate cancer patients with low baseline CTC counts. *Ann. Oncol.* **2018**, *29*, 1554–1560. [CrossRef] [PubMed]
43. Scher, H.I.; Lu, D.; Schreiber, N.A.; Louw, J.; Graf, R.P.; Vargas, H.A.; Johnson, A.; Jendrisak, A.; Bambury, R.; Danila, D.; et al. Association of AR-V7 on Circulating Tumor Cells as a Treatment-Specific Biomarker with Outcomes and Survival in Castration-Resistant Prostate Cancer. *JAMA Oncol.* **2016**, *2*, 1441–1449. [CrossRef] [PubMed]
44. Scher, H.I.; Heller, G.; Molina, A.; Attard, G.; Danila, D.C.; Jia, X.; de Bono, J.S. Circulating tumor cell biomarker panel as an individual-level surrogate for survival in metastatic castration-resistant prostate cancer. *J. Clin. Oncol.* **2015**, *33*, 1348–1355. [CrossRef]
45. Aufderklamm, S.; Hennenlotter, J.; Leidenberger, P.; Rausch, S.; Hohneder, A.; Kühs, U.; Todenhöfer, T. Systemic Alterations of Wnt Inhibitors in Patients with Prostate Cancer and Bone Metastases. *Dis. Markers* **2018**, *2018*, 1874598. [CrossRef]
46. Thiele, S.; Rauner, M.; Goettsch, C.; Rachner, T.D.; Benad, P.; Fuessel, S.; Erdmann, K.; Hamann, C.; Baretton, G.B.; Wirth, M.P.; et al. Expression profile of WNT molecules in prostate cancer and its regulation by aminobisphosphonates. *J. Cell. Biochem.* **2011**, *112*, 1593–1600. [CrossRef]
47. Yeremenko, N.; Zwerina, K.; Rigter, G.; Pots, D.; Fonseca, J.E.; Zwerina, J.; Schett, G.; Baeten, D. Brief Report: Tumor Necrosis Factor and Interleukin-6 Differentially Regulate Dkk-1 in the Inflamed Arthritic Joint. *Arthritis Rheumatol.* **2015**, *67*, 2071–2075. [CrossRef] [PubMed]
48. Culig, Z. Proinflammatory cytokine interleukin-6 in prostate carcinogenesis. *Am. J. Clin. Exp. Urol.* **2014**, *2*, 231–238. [PubMed]
49. Nakashima, J.; Tachibana, M.; Horiguchi, Y.; Oya, M.; Ohigashi, T.; Asakura, H.; Murai, M. Serum interleukin 6 as a prognostic factor in patients with prostate cancer. *Clin. Cancer Res.* **2000**, *6*, 2702–2706. [PubMed]
50. Maynard, J.P.; Ertunc, O.; Kulac, I.; Del Valle, J.A.B.; De Marzo, A.M.; Sfanos, K.S. IL8 Expression Is Associated with Prostate Cancer Aggressiveness and Androgen Receptor Loss in Primary and Metastatic Prostate Cancer. *Mol. Cancer Res.* **2019**, *18*, 153–165. [CrossRef]
51. Roumeguere, T.; Legrand, F.; El Rassy, E.; Kaitouni, M.I.; Albisinni, S.; Rousseau, A.; Vanhaeverbeek, M.; Rorive, S.; De-caestecker, C.; Debeir, O.; et al. A prospective clinical study of the implications of IL-8 in the diagnosis, aggressiveness and prognosis of prostate cancer. *Futur. Sci. OA* **2018**, *4*, FSO266. [CrossRef]
52. Armstrong, A.J. Epithelial-mesenchymal transition in cancer progression. *Clin. Adv. Hematol. Oncol.* **2011**, *9*, 941–943.

53. Yang, Y.-J.; Kong, Y.-Y.; Li, G.-X.; Wang, Y.; Ye, D.-W.; Dai, B. Phenotypes of circulating tumour cells predict time to castration resistance in metastatic castration-sensitive prostate cancer. *BJU Int.* **2019**, *124*, 258–267. [CrossRef] [PubMed]
54. Josefsson, A.; Larsson, K.; Månsson, M.; Bjorkman, J.; Rohlová, E.; Åhs, D.; Brisby, H.; Damber, J.-E.; Welén, K. Circulating tumor cells mirror bone metastatic phenotype in prostate cancer. *Oncotarget* **2018**, *9*, 29403–29413. [CrossRef]
55. Ahmad, I.; Gao, M.; Patel, R.; Leung, H.Y. Modelling synergistic interactions between HER2, Sprouty2 and PTEN in driving prostate carcinogenesis. *Asian J. Androl.* **2013**, *15*, 323–327. [CrossRef] [PubMed]
56. Antonarakis, E.S.; Lu, C.; Wang, H.; Luber, B.; Nakazawa, M.; Roeser, J.C.; Chen, Y.; Mohammad, T.A.; Chen, Y.; Fedor, H.L.; et al. AR-V7 and Resistance to Enzalutamide and Abiraterone in Prostate Cancer. *N. Engl. J. Med.* **2014**, *371*, 1028–1038. [CrossRef] [PubMed]
57. Di Lorenzo, G.; Zappavigna, S.; Crocetto, F.; Giuliano, M.; Ribera, D.; Morra, R.; Buonerba, C. Assessment of Total, PTEN(-), and AR-V7(+) Circulating Tumor Cell Count by Flow Cytometry in Patients with Metastatic Castration-Resistant Prostate Cancer Receiving Enzalutamide. *Clin. Genitourin. Cancer* **2021**, in press.

Article

Site-Specific and Common Prostate Cancer Metastasis Genes as Suggested by Meta-Analysis of Gene Expression Data

Ivana Samaržija ^{1,2} 

¹ Laboratory for Epigenomics, Division of Molecular Medicine, Ruđer Bošković Institute, Bijenička 54, 10000 Zagreb, Croatia; Ivana.Samarzija@irb.hr

² Laboratory for Cell Biology and Signalling, Division of Molecular Biology, Ruđer Bošković Institute, Bijenička 54, 10000 Zagreb, Croatia

Abstract: Anticancer therapies mainly target primary tumor growth and little attention is given to the events driving metastasis formation. Metastatic prostate cancer, in comparison to localized disease, has a much worse prognosis. In the work presented here, groups of genes that are common to prostate cancer metastatic cells from bones, lymph nodes, and liver and those that are site-specific were delineated. The purpose of the study was to dissect potential markers and targets of anticancer therapies considering the common characteristics and differences in transcriptional programs of metastatic cells from different secondary sites. To that end, a meta-analysis of gene expression data of prostate cancer datasets from the GEO database was conducted. Genes with differential expression in all metastatic sites analyzed belong to the class of filaments, focal adhesion, and androgen receptor signaling. Bone metastases undergo the largest transcriptional changes that are highly enriched for the term of the chemokine signaling pathway, while lymph node metastasis show perturbation in signaling cascades. Liver metastases change the expression of genes in a way that is reminiscent of processes that take place in the target organ. Survival analysis for the common hub genes revealed involvements in prostate cancer prognosis and suggested potential biomarkers.

Citation: Samaržija, I. Site-Specific and Common Prostate Cancer Metastasis Genes as Suggested by Meta-Analysis of Gene Expression Data. *Life* **2021**, *11*, 636. <https://doi.org/10.3390/life11070636>

Keywords: prostate cancer; bone metastasis; lymph node metastasis; liver metastasis; gene expression; meta-analysis; focal adhesion; protein filament; androgen receptor signaling

Academic Editors: Ana Faustino and Paula A. Oliveira

Received: 15 May 2021

Accepted: 28 June 2021

Published: 30 June 2021

Publisher's Note: MDPI stays neutral with regard to jurisdictional claims in published maps and institutional affiliations.



Copyright: © 2021 by the author. Licensee MDPI, Basel, Switzerland. This article is an open access article distributed under the terms and conditions of the Creative Commons Attribution (CC BY) license (<https://creativecommons.org/licenses/by/4.0/>).

1. Introduction

The vast majority (90%) of cancer-related deaths is not caused by primary tumors but metastasis on distal organs [1]. Still, cancer chemotherapies are mainly designed in a way that they consider events that drive primary tumor growth only, and little attention is given to pathways governing metastatic outgrowth [2]. While the literature and research on gene expression differences between primary tumors and metastasis is abundant [3], little is known on which signaling pathways are shared among metastatic cells colonizing distinct secondary sites, and which strategies are site-specific. Several publications exist on such topics, including the recent reports by Hartung et al. [4,5]. This type of knowledge is essential to suggest signaling pathways that could be therapeutic targets in metastatic cells in cancer types that spread to multiple organs.

Prostate cancer (PCa) is the second most commonly occurring cancer in men and the fifth leading cause of death worldwide [6]. The 5-year survival rate of non-metastatic prostate cancer is 98.9%, but, the rate in patients who are initially diagnosed with metastatic prostate cancer is less than 30% and does not show improvements [7]. The most usual sites colonized by prostate cancer cells are bones, lymph nodes, lungs, liver, and brain while rare locations include adrenal glands, breasts, eyes, kidneys, muscles, pancreas, salivary glands, and spleen. Recently, it was shown that patients with liver-only metastasis have worse cancer-specific and overall survival than patients with bone-only and lung-only metastasis [8].

The driving events in prostate cancer dissemination include entangled actions of several signaling pathways that are potentiated by changes in gene expression, genetic alterations [9], and post-translational modifications [10]. To better understand signaling events that are site-specific and common to prostate cancer metastasis, herein a meta-analysis of publicly available GEO gene expression datasets that consist of primary prostate cancer samples as well as samples of metastasis from bones, lymph nodes, and liver was conducted. Differentially expressed genes that are shared among all sites analyzed are presented. A substantial number of differentially expressed genes are secondary site-specific which emphasizes the need to study metastasis separately according to the secondary site. Survival analysis for hub genes found among the genes commonly changed in all metastatic sites was conducted and has revealed potential biomarkers.

2. Materials and Methods

2.1. Gene Expression Datasets

The list and description of gene expression datasets downloaded from the GEO database [11] and used in the meta-analysis are provided in Table 1. All the datasets are from microarray chips. The samples within datasets belong to four categories: primary tumors, bone metastasis (51 samples versus 175 primary tumor samples, from three datasets), lymph node metastasis (103 samples versus 232 primary tumor samples, from four datasets), and liver metastasis (26 samples versus 83 primary tumor samples, from two datasets). Depending on the platform, the annotation was either downloaded from the file deposited on the GEO database or obtained using gProfiler [12].

Table 1. Description of datasets used in this study.

GEO Set	Reference	Platform	Samples			
			Primary Tumors	LN Met.	Liver Met.	Bone Met.
GSE6605, GSE6606	Chandran et al. 2007 [13]	GPL8300	61	15	5	-
GSE21034	Taylor et al. 2010 [14]	GPL10264	131	7	-	2
GSE32269	Cai et al. 2013 [15]	GPL96	22	-	-	29
GSE59745	Böttcher et al. 2015 [16]	GPL5175	18	12	-	-
GSE77930	Kumar et al. 2016 [17]	GPL15659	22	69	21	20

2.2. Meta-Analysis of Gene Expression Data and Enrichment Analysis

Meta-analysis of the gene expression data was performed using ImaGEO software that displayed good performance in the comprehensive gene expression meta-analysis [18]. The *p*-value method (minP) and default settings were used. This meta-analysis method was chosen as combining *p*-values provides an advantage over effect size combination for standardization of the associations from genomic studies to a common scale allowing to compare very heterogeneous datasets, for example, datasets from different tissues [18]. The criteria for differential gene expression were false discovery rate (FDR) *p*-value < 0.05 and $|\log_2\text{fold change}| > 1$. The intersection and the list of genes differentially expressed among bone, lymph node, and liver metastasis were obtained using GeneVenn [19]. Overview of enrichment analysis was obtained by Enrichr [20] using default settings and GO Biological Process (BP), GO Cellular Component (CC), GO Molecular Function (MF), KEGG (Kyoto Encyclopedia of Genes and Genomes), and WikiPathways data are presented. The top five processes are listed. The background used is set by default by Enrichr software, as Enrichr cannot upload a background list [20].

2.3. Visualization of Metastasis Genes Networks and Identification of the Hub Genes

The networks representing up-regulated and down-regulated genes among the 434 shared metastasis genes were retrieved by STRING [21] with default settings (default medium confidence 0.4) and visualized in Cytoscape [22]. The genes that showed interactions are depicted as a network, while the genes with no connections were omitted

from the Figures. Twenty hub genes from a set of 434 genes that are shared among all metastatic sites were detected with the use of cytoHubba application [23].

2.4. Survival and Expression Analysis for the Hub Genes

The prognostic significance of each hub gene was performed by gene expression profiling interactive analysis (GEPIA [24]) taking into account disease-free survival. $p < 0.05$ was considered to indicate a statistically significant difference.

The analysis of mRNA expression for the first 10 hub genes was performed using GEPIA software, including TCGA (The Cancer Genome Atlas) and GTEx (Genotype-Tissue Expression) data.

3. Results

3.1. The Top Ten Most Changed Genes Shared by Metastasis from All Analyzed Sites Belong to the Class of Filaments and Proteins Involved in Bone and Prostate Biology

As shown in Table 2, a substantial proportion (40 of 260) of genes that are among the 50 most up-regulated or 50 most down-regulated in prostate cancer bone, lymph node, and liver metastasis groups are shared at least between two groups (30 genes) or between all three groups (10 genes). It is interesting to note that all 40 genes that are found overlapping in two or three groups change in the same direction (up- or down-regulated), adding to the hypothesis that the change in their expression is functional, “driving” change rather than “passenger” change. The ten genes found in all groups are SPP1 (up-regulated) and MYH11, MSMB, ACTG2, CNN1, PCP4, KRT15, NEFH, DES, and CHRDL1 (down-regulated).

Table 2. 50 most up- (first row) and down-regulated (second row) genes in prostate cancer metastasis originating from bones, lymph nodes, and liver. The genes are ordered by decreasing |fold change|. Genes shared among three lists are depicted in red; genes shared among bone and LN metastasis are depicted in blue; genes shared among bone and liver metastasis are depicted in orange; genes shared among LN and liver metastasis are depicted in green.

Bone Metastasis	Lymph Node Metastases	Liver Metastasis
COL11A1, SPP1, HBB, IBSP, HBD, FABP4, MMP13, TNFAIP6, COL5A2, LRRC15, S100A8, MMP9, PTX3, TOP2A, FMO3, AKR1C3, COL1A1, SLPI, CA1, COL3A1, ENPEP, GMFG, COL1A2, CD36, LPL, OMD, APOE, SERPINE2, CFH, IGF2BP2, AHSP, TPX2, OLFML2B, CYP26A1, KIF20A, MEPE, COL10A1, MKI67, CTSZ, BUB1, DMP1, DPT, COL5A1, PPBP, IFI27, SULT1B1, COL4A1, STAB1, KIF4A, ALAS2	CDKN3, THOC5, CCNE2, PPP3CA, TPH1, RFC5, UBE2C, HIST1H4L, FABP4, PAK2, PMAIP1, ESM1, MPHOSPH9, RAD23B, MVD, CENPF, SLC26A3, CD36, SPP1, RIPK2, RFPL3S, HMGCS1, TIMM8A, VDR, KCTD20, ATP8A2, NTNG1, BUB1, MAGEA12, CDC6, TOP2A, UBFD1, PTTG1, OSGIN2, COL9A3, KRR1, COL11A1, EZH2, ANGPT2, THBS2, FGF12, FOXM1, MYL4, KIF3A, CDKN2A, TPX2, NCBP1, MLF1, SEL1L, LMNB1	FGB, FGG, PCK1, GC, FABP1, CRP, HP, CFHR4, APOC3, TM4SF4, CDKN3, APOB, APOA1, FGL1, RBP4, PEG10, HPGD, UGT2B7, ARG1, PLG, F2, FGA, SERPINC1, HBD, ALDOB, ALB, AMBP, SLC1A2, HIST1H4L, SPP1, AKR1C4, KNG1, KIF11, NMU, SERPINA1, COL9A3, APC5, IGFBP1, CPS1, F9, AADAC, MKNK2, UBE2C, ASGR2, AHSG, C4BPA, KIF23, C8A, SAA1, HSPA6
ACADL, PGM3, SORD, MT1E, ANXA3, SMARCA1, KIAA1324, CHRDL1, MYBPC1, RLN1, PAK1IP1, ANPEP, GULP1, ACTA2, JMJD1C, NR4A2, LIFR, HSD17B6, DHRS7, KLF6, EPHX2, KIF5C, SFRP1, IQGAP2, MYLK, DMXL1, NCAPD3, CPE, SLC4A4, GREB1, FOS, ALDH1A3, ZFP36, HGD, DES, AZGP1, NEFH, DPP4, ABCCC4, TRPM8, KRT15, FOSB, MEIS2, SORBS1, PCP4, CNN1, MAOB, ACTG2, MSMB, MYH11	LTF, FBLN1, EGR2, AKAP5, ABCA8, SLC20A2, EGR3, FHL1, KRT5, PAMR1, MYLK, BDNF, EYA4, CHRDL1, EPHB6, NR4A2, HDAC9, GPM6B, EYA1, ATP1A2, EDNRA, CXCL11, PTGS2, FGFR2, PTPRD, KRT15, IGFBP6, PLN, SPOCK3, RLN1, DKK1, MFAP4, PTN, MOXD1, MSMB, PTGDS, MMP7, MEIS1, FOXF1, SYNM, CNTN1, DES, TCF21, CNN1, PCP4, OLFM4, NEFH, PAGE4, ACTG2, MYH11	NT5E, PHF14, SPOCK3, VWF, NOV, CPM, NR4A3, COL16A1, EGR2, FGFR2, DYNC111, VPS13D, DDR2, PLA2G4A, TAC1, EGR3, CDH11, KRT15, FRZB, ATP1A2, SFRP1, SULF1, FOXF1, EDNRA, MYL9, PCP4, SPARCL1, UBE2K, CHRDL1, IGFBP6, DES, MFAP4, PTGDS, ACTC1, KLK11, SLC20A2, PAGE4, KLRD1, FBLN1, NEFH, MSMB, CNN1, KLK2, HDAC9, RLN2, CNTN1, PKP2, ACTG2, F3, MYH11

According to the KEGG enrichment analysis of the nine shared down-regulated genes MYH11 and ACTG2 belong to the enriched process of vascular smooth muscle contraction (p -value = 0.0015). Additionally, five of those nine genes are also either filaments or they are involved in their processes, as listed below. CNN1 is a thin filament-associated protein

that is also implicated in the regulation and modulation of smooth muscle contraction. DES is a muscle-specific type III intermediate filament essential for proper muscular structure and function. NEFH is an intermediate filament protein, part of neurofilaments. KRT15 is a keratin that belongs to intermediate filament proteins responsible for the structural integrity of epithelial cells. PCP4 is a calmodulin regulator protein that functions as a modulator of calcium-binding by calmodulin. Among other roles, it was shown that Ca²⁺ and calmodulin regulate the binding of FLNA to actin filaments [25]. In summary, MYH11 and ACTG2 genes belong to genes involved in the assembly of actin fibers, while CNN1 and PCP4 are proteins capable of binding actin or influence its association with partner proteins. KRT15, NEFH, and DES belong to the three (keratins, neurofilaments, and desmin, respectively) of five classes of intermediate filaments.

SPP1 gene codes for osteopontin, the protein that is involved in the attachment of osteoclasts to the mineralized bone matrix. CHRDL1 protein has recently been shown to improve osteogenesis of bone marrow mesenchymal stem cells [26]. CNN1 gene also plays a role in osteoblast and osteoclast function and formation [27].

MSMB is one of the three major proteins secreted by the epithelial cells of the prostate. It is also secreted by epithelial cells in many other organs. The protein inhibits the growth of cancer cells in an experimental model of prostate cancer, but this property was shown to be cell line-specific [28].

3.2. Reorganization of Focal Adhesions and Changes in Androgen Receptor Signaling Are Common Characteristics of Prostate Cancer Metastasis Regardless of the Target Organ

As shown in Figure 1, the meta-analysis revealed that the intersection of differentially expressed genes among prostate cancer bone, lymph node, and liver metastasis consists of 434 genes. This gene list was analyzed to establish prostate cancer metastasis “core transcriptional program”. Table 3 is listing the results of enrichment analysis for all 434 shared genes. It is clear from Table 3 that “Focal adhesion” is the most changed enrichment term in the intersection of metastasis from all sites as it is among the top enriched terms from the three lists—KEGG, WikiPathways, and GO CC. The up-regulated and down-regulated gene networks are depicted in Figures 2 and 3, respectively.

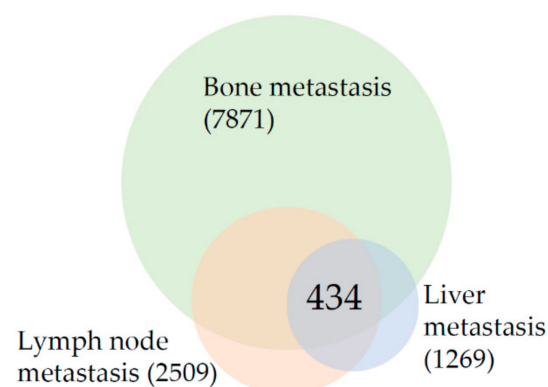


Figure 1. Venn diagram of differentially expressed genes in prostate cancer bone, lymph node, and liver metastasis in comparison to primary prostate tumors. The number in parenthesis indicates the total number of differentially expressed genes and the number in the intersection indicates the number of overlapping genes.

The enrichment term “Prostate cancer” with 10/97 genes, “miRNA regulation of prostate cancer signaling pathways” with 8/33 genes, and “Androgen receptor” (12/90) are also among the most changed enrichment terms (Table 3) confirming the specificity of the results.

Table 3. Gene ontology and pathway enrichment analysis of the genes common to all metastatic sites analyzed.

Category	Term	Count	Adj. <i>p</i> -Value
BP	Platelet aggregation (GO:0070527)	8/33	0.0010
	Negative regulation of cellular macromolecule biosynthetic process (GO:2000113)	30/512	0.0011
	Homotypic cell-cell adhesion (GO:0034109)	8/38	0.0011
	Regulation of retinoic acid receptor signaling pathway (GO:0048385)	5/13	0.0027
	Neutrophil degranulation (GO:0043312)	27/479	0.0027
CC	Cytoskeleton (GO:0005856)	32/520	3.37×10^{-5}
	Focal adhesion (GO:0005925)	24/356	1.31×10^{-4}
	Ficolin-1-rich granule (GO:0101002)	15/184	9.15×10^{-4}
	Microtubule cytoskeleton (GO:0015630)	23/388	9.15×10^{-4}
	Chromatin (GO:0000785)	19/296	0.0014
MF	Kinase binding (GO:0019900)	30/418	5.99×10^{-6}
	Protein kinase binding (GO:0019901)	30/495	1.22×10^{-4}
	Cadherin binding (GO:0045296)	19/313	0.0103
	Metal ion binding (GO:0046872)	23/442	0.0143
	Kinesin binding (GO:0019894)	5/28	0.0268
KEGG	Focal adhesion	20/199	3.7×10^{-6}
	Cell cycle	14/124	6.72×10^{-5}
	Prostate cancer	10/97	0.0042
	Glycolysis/Gluconeogenesis	8/68	0.0071
	p53 signaling pathway	8/72	0.0085
WikiPathways	Focal Adhesion WP306	19/198	2.17×10^{-5}
	Cell Cycle WP179	14/120	4.16×10^{-5}
	miRNA regulation of prostate cancer signaling pathways WP3981	8/33	4.16×10^{-5}
	Androgen receptor signaling pathway WP138	12/90	4.37×10^{-5}
	DNA Damage Response WP707	10/68	1.24×10^{-4}

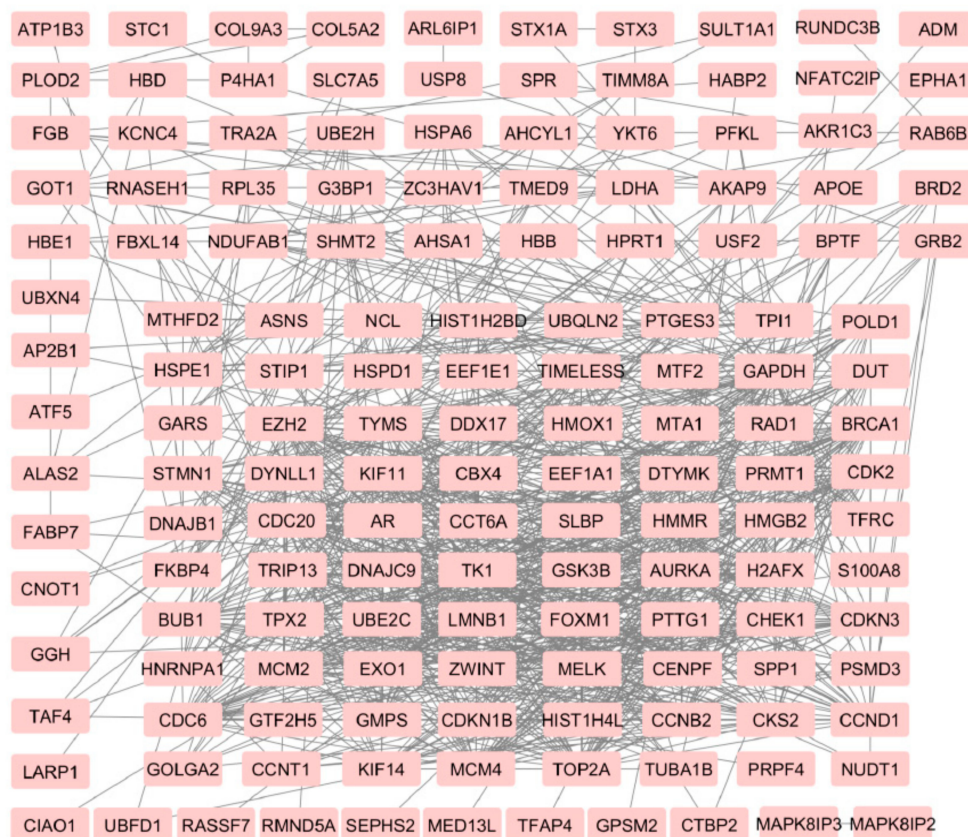


Figure 2. Network of up-regulated genes in prostate cancer metastasis from an intersection of bone, lymph node, and liver metastasis.

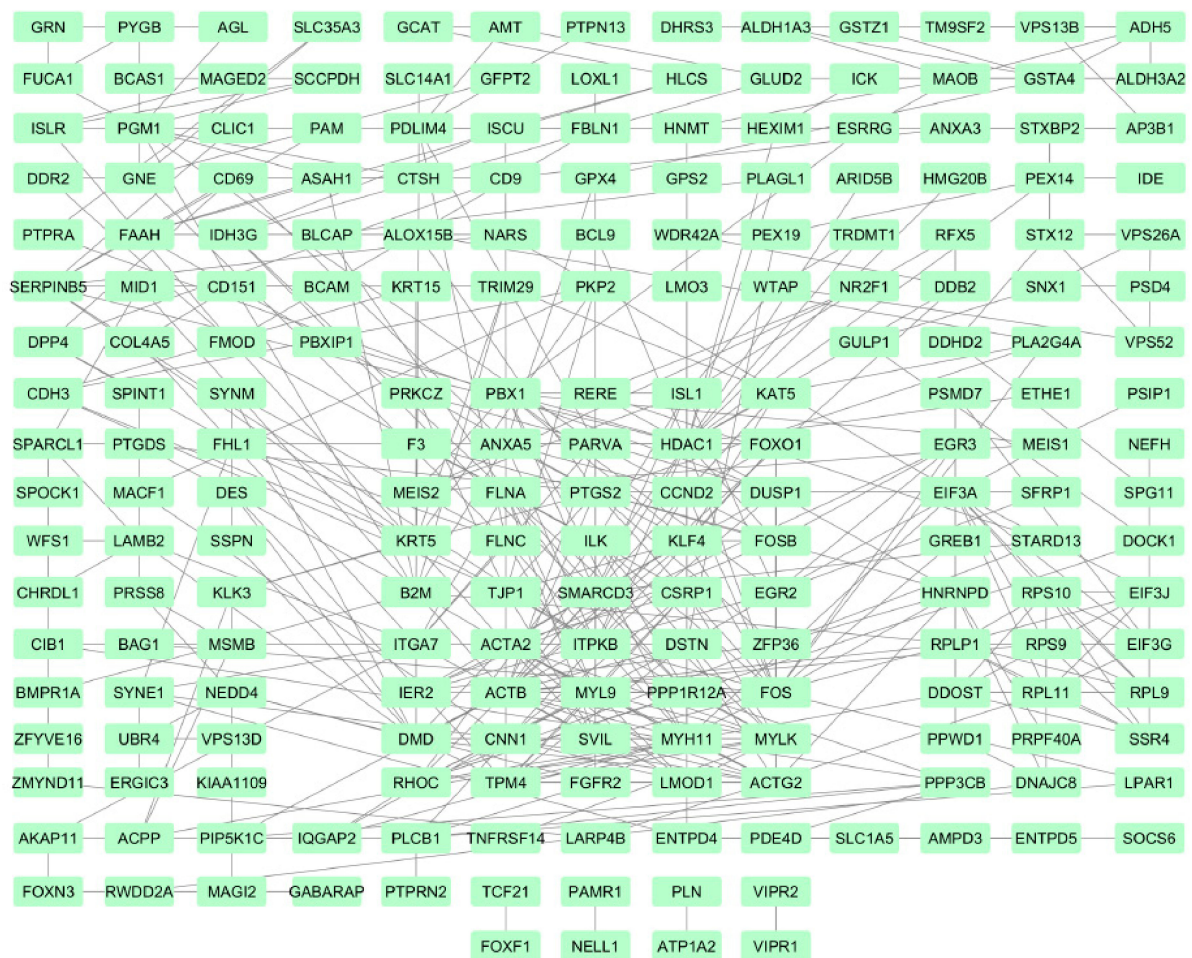


Figure 3. Network of down-regulated genes in prostate cancer metastasis from an intersection of bone, lymph node, and liver metastasis.

3.3. Results Suggest That Transcriptional Landscape of Bone Metastasis Is Profoundly Rewired in Comparison to Lymph Node and Liver Metastasis

In comparison to the number of genes differentially expressed in lymph nodes (2509) and liver (1269) metastasis, the changes in bone (7871 genes) metastasis are several times higher, suggesting the profound change in the transcriptional repertoire. Enrichment analysis was done for all the genes that are changed in bone metastasis (Table 4). On the top of the list of genes whose expression changes in bones is the term “VEGFA-VEGFR2 signaling pathway” followed by genes from focal adhesions and other signaling pathways. The BP category showed enrichment in genes involved in neutrophil biology. The top of the enrichment list of differentially expressed genes found in bone metastasis only (data not shown) is dominated by genes involved in immune system function, especially “Chemokine signaling pathway”, “T-Cell antigen receptor signaling pathway” and “B-cell receptor signaling pathway”.

The enrichment analysis of 100 most up- or down-regulated genes (Table 2) in bone metastasis revealed enriched term of “Regulators of bone mineralization” (IBSP, COL4A1, and SPP1) being on the top of the list (BioCarta 2016).

3.4. Lymph Node Metastasis Are Characterized by Changes in Signaling Networks While the Liver Metastasis Transcriptional Program Is Reminiscent of Processes That Take Place in the Target Organ

On the top of the list of genes that are changed in lymph node metastasis (Table 5) is the term “VEGFA-VEGFR2 signaling pathway”, followed by “Focal adhesion”. This was found to be similar to the result of the genes differentially expressed in bone metastasis.

Other signaling pathways whose components are found to have significant differential expression in lymph node metastasis include PI3K-Akt, EGF/EGFR, MAPK, and TGF-beta signaling pathways.

Table 4. Gene ontology and pathway enrichment analysis of the genes differentially expressed in bone metastasis.

Category	Term	Count	Adj. <i>p</i> -Value
BP	Cellular protein modification process (GO:0006464)	582/1001	3.21×10^{-31}
	Neutrophil activation involved in immune response (GO:0002283)	320/483	2.26×10^{-30}
	Neutrophil mediated immunity (GO:0002446)	322/487	2.26×10^{-30}
	Neutrophil degranulation (GO:0043312)	317/479	4.20×10^{-30}
	Positive regulation of gene expression (GO:0010628)	459/771	7.62×10^{-28}
CC	Focal adhesion (GO:0005925)	245/356	3.51×10^{-27}
	Secretory granule lumen (GO:0034774)	217/317	1.00×10^{-23}
	Nuclear body (GO:0016604)	350/618	1.37×10^{-16}
	Mitochondrion (GO:0005739)	537/1026	4.30×10^{-16}
	Nucleolus (GO:0005730)	375/676	4.63×10^{-16}
MF	RNA binding (GO:0003723)	794/1387	2.90×10^{-41}
	Cadherin binding (GO:0045296)	221/313	9.62×10^{-27}
	Protein kinase activity (GO:0004672)	308/513	3.11×10^{-19}
	Protein homodimerization activity (GO:0042803)	380/664	6.99×10^{-19}
	Protein kinase binding (GO:0019901)	295/495	6.33×10^{-18}
KEGG	Pathways in cancer	335/530	7.73×10^{-27}
	Human T-cell leukemia virus 1 infection	155/219	4.57×10^{-19}
	Human papillomavirus infection	214/330	3.89×10^{-19}
	PI3K-Akt signaling pathway	222/354	2.39×10^{-17}
	Protein processing in the endoplasmic reticulum	121/165	3.98×10^{-17}
WikiPathways	VEGFA-VEGFR2 Signaling Pathway WP3888	166/236	1.57×10^{-19}
	Focal Adhesion-PI3K-Akt-mTOR-signaling pathway WP3932	198/303	7.32×10^{-18}
	Focal Adhesion WP306	141/198	1.17×10^{-17}
	EGF/EGFR Signaling Pathway WP437	120/162	2.70×10^{-17}
	TGF-beta Signaling Pathway WP366	102/132	5.84×10^{-17}

Table 5. Gene ontology and pathway enrichment analysis of the genes differentially expressed in lymph node metastasis.

Category	Term	Count	Adj. <i>p</i> -Value
BP	Regulation of transcription from RNA polymerase II promoter (GO:0006357)	303/1478	9.34×10^{-16}
	Positive regulation of transcription, DNA-templated (GO:0045893)	241/1120	8.53×10^{-15}
	Positive regulation of transcription from RNA polymerase II promoter (GO:0045944)	195/848	8.73×10^{-15}
	Negative regulation of apoptotic process (GO:0043066)	130/485	9.64×10^{-15}
	Regulation of cell migration (GO:0030334)	96/316	2.69×10^{-14}
CC	Focal adhesion (GO:0005925)	110/356	1.26×10^{-17}
	Cytoskeleton (GO:0005856)	127/520	8.73×10^{-12}
	Membrane raft (GO:0045121)	46/119	5.95×10^{-11}
	Perinuclear region of cytoplasm (GO:0048471)	96/378	5.33×10^{-10}
	Platelet alpha granule (GO:0031091)	36/90	3.67×10^{-9}
MF	Protein kinase binding (GO:0019901)	148/49	3.44×10^{-22}
	Kinase binding (GO:0019900)	124/418	2.94×10^{-18}
	Cadherin binding (GO:0045296)	101/313	1.19×10^{-17}
	RNA binding (GO:0003723)	274/1387	4.87×10^{-13}
	RNA polymerase II regulatory region sequence-specific DNA binding (GO:0000977)	116/460	1.11×10^{-11}
KEGG	Pathways in cancer	136/530	2.06×10^{-14}
	Focal adhesion	70/199	2.06×10^{-14}
	MAPK signaling pathway	86/295	1.89×10^{-12}
	PI3K-Akt signaling pathway	94/354	4.25×10^{-11}
	Human T-cell leukemia virus 1 infection	67/219	7.58×10^{-11}
WikiPathways	VEGFA-VEGFR2 Signaling Pathway WP3888	80/236	5.16×10^{-15}
	Focal Adhesion WP306	69/198	8.89×10^{-14}
	Integrated Breast Cancer Pathway WP1984	52/151	4.22×10^{-10}
	Cell Cycle WP179	44/120	9.84×10^{-10}
	Ebola Virus Pathway on Host WP4217	46/129	9.84×10^{-10}

On the top of the list of genes that are changed in liver metastasis (Table 6) is the term “VEGFA-VEGFR2 signaling pathway”. When the enrichment analysis for the 100 most up- or down-regulated genes (Table 2) in liver metastasis was done, the term “Complement and coagulation cascades” was found to be highly enriched with 13/79 genes being present on the list (data not shown). Genes specifically changed in liver metastasis only (data not shown) are reminiscent of processes taking place in the target organ according to the terms that are enriched and that include “Folate metabolism”, “Selenium micronutrient network”, “Fat digestion and absorption”, “Cholesterol metabolism”, “Phenylalanine metabolism” and fore-mentioned “Human complement system” and “Complement and coagulation cascades”.

Table 6. Gene ontology and pathway enrichment analysis of the genes differentially expressed in liver metastasis.

Category	Term	Count	Adj. p-Value
BP	Cellular protein metabolic process (GO:0044267)	76/484	7.17×10^{-10}
	Platelet degranulation (GO:0002576)	33/124	1.90×10^{-9}
	Regulated exocytosis (GO:0045055)	35/148	1.07×10^{-8}
	Negative regulation of cellular process (GO:0048523)	73/534	4.23×10^{-7}
	DNA metabolic process (GO:0006259)	51/314	4.31×10^{-7}
CC	Endoplasmic reticulum lumen (GO:0005788)	49/270	5.10×10^{-9}
	Focal adhesion (GO:0005925)	58/356	5.10×10^{-9}
	Secretory granule lumen (GO:0034774)	53/317	9.09×10^{-9}
	Perinuclear region of cytoplasm (GO:0048471)	53/378	3.82×10^{-6}
	Cytoplasmic vesicle lumen (GO:0060205)	26/129	8.41×10^{-6}
MF	Protein homodimerization activity (GO:0042803)	88/664	2.90×10^{-8}
	Metal ion binding (GO:0046872)	65/442	7.99×10^{-8}
	Transition metal ion binding (GO:0046914)	56/399	5.30×10^{-6}
	Kinase binding (GO:0019900)	56/418	2.01×10^{-5}
	Protein kinase binding (GO:0019901)	60/495	1.73×10^{-4}
KEGG	Cell cycle	31/124	7.94×10^{-9}
	Pathways in cancer	72/530	1.08×10^{-7}
	Complement and coagulation cascades	22/79	2.23×10^{-7}
	Focal adhesion	37/199	2.27×10^{-7}
	Human T-cell leukemia virus 1 infection	39/219	2.46×10^{-7}
WikiPathways	VEGFA-VEGFR2 Signaling Pathway WP3888	48/236	1.93×10^{-10}
	Cell Cycle WP179	31/120	2.20×10^{-9}
	Retinoblastoma Gene in Cancer WP2446	25/87	1.20×10^{-8}
	Nuclear Receptors Meta-Pathway WP2882	50/31	2.81×10^{-7}
	Human Complement System WP2806	24/97	4.75×10^{-7}

3.5. Prostate Cancer Metastasis Hub Genes and Their Involvement in Patient Disease-Free Survival

To detect the potential driving network of prostate cancer metastasis, hub genes among the 434 common genes of all metastatic sites were singled out and are shown in Figure 4. The disease-free survival analysis revealed the statistically significant involvement of the following genes (Figure 5): AURKA, BUB1, CCNB2, CDC20, CDKN3, CENPF, CHEK1, FOXM1, HMMR, MELK, PTTG1, TOP2A, TPX2, TRIP13, TYMS, UBE2C. Their biological roles are listed in Table 7 and among the enriched terms listed in Table 8 are “Cell-cycle” and “Microtubule cytoskeleton”. The analysis of mRNA expression for the first ten hub genes is shown in Figure 6, confirming their up-regulation in prostate cancer.

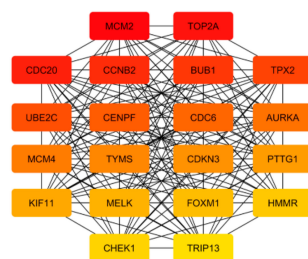


Figure 4. Hub genes that are found among 434 overlapping genes that are changed in metastases from all sites analyzed. The highest-ranked node is in red, and the lowest in yellow.

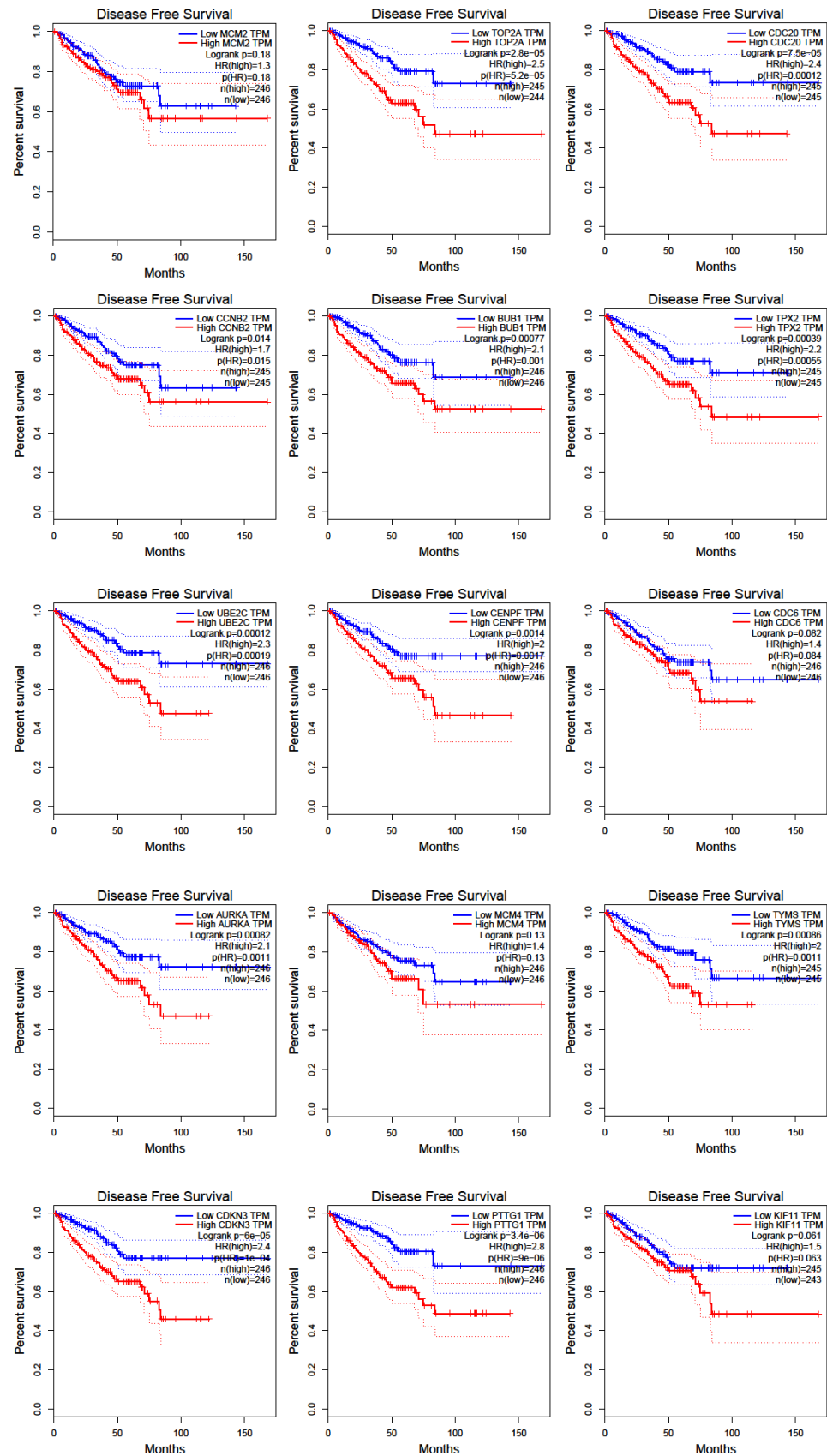


Figure 5. Cont.

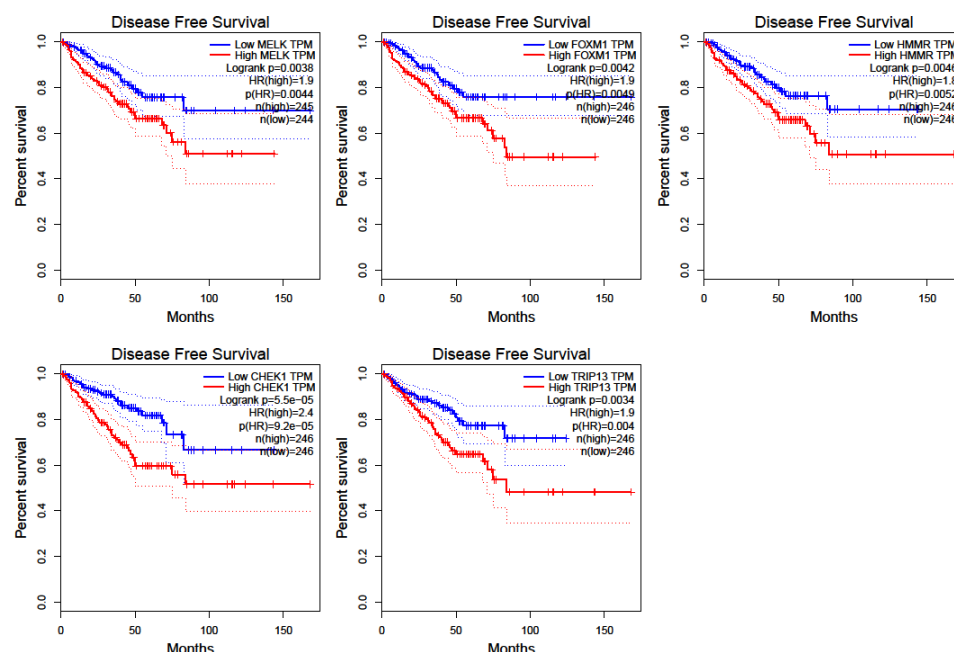


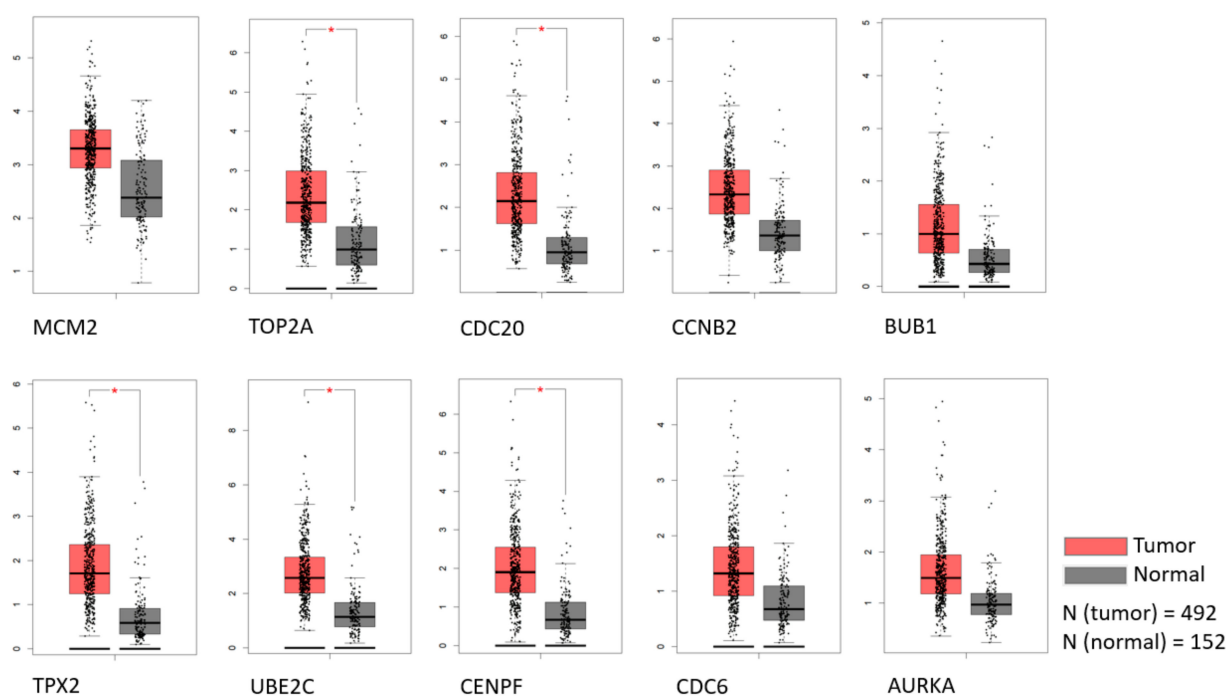
Figure 5. Disease-free survival for hub genes as retrieved by GEPIA software using TCGA data.

Table 7. Biological functions of 20 hub genes. The biological roles of the 20 core genes are listed.

Gene Symbol	Full Name	Function
MCM2	Minichromosome maintenance complex component 2	Involved in the initiation of eukaryotic genome replication
TOP2A	Topoisomerase II α	Controls the topology structure of DNA and cell cycle progression
CDC20	Cell division cycle 20	Regulatory protein interacting with several other proteins at multiple points in the cell cycle
CCNB2	Cyclin B2	Essential component of the cell cycle regulatory machinery
BUB1	BUB1 mitotic checkpoint serine/threonine kinase	Serine/threonine-protein kinase that plays a central role in mitosis
TPX2	TPX2 microtubule nucleation factor	Microtubule-associated protein linked to mitosis and spindle assembly
UBE2C	Ubiquitin-conjugating enzyme E2 C	Involved in ubiquitination; required for the destruction of mitotic cyclins and cell cycle progression
CENPF	Centromere protein F	Role in the centromere-kinetochore complex and chromosomal segregation
CDC6	Cell division cycle 6	Essential for the initiation of DNA replication
AURKA	Aurora kinase A	Cell cycle-regulated kinase involved in microtubule formation and/or stabilization at the spindle pole during chromosome segregation
MCM4	Minichromosome maintenance complex component 4	Essential for the initiation of eukaryotic genome replication
TYMS	Thymidylate synthetase	Catalyzes the methylation of deoxyuridylate to deoxythymidylate and maintains the dTMP pool critical for DNA replication and repair
CDKN3	Cyclin-dependent kinase inhibitor 3	Cyclin-dependent kinase inhibitor
PTTG1	PTTG1 regulator of sister chromatid separation	Homolog of yeast securin proteins, which prevent separins from promoting sister chromatid separation
KIF11	Kinesin family member 11	Motor protein that belongs to the kinesin-like protein family
MELK	Maternal embryonic leucine zipper kinase	Serine/threonine-protein kinase involved in various processes such as cell cycle regulation, self-renewal of stem cells, apoptosis, and splicing regulation
FOXM1	Forkhead box M1	Transcriptional activator involved in cell proliferation
HMMR	Hyaluronan (HA)-mediated motility receptor	Binds native and fragmented HA, promotes its uptake
CHEK1	Checkpoint kinase 1	Required for checkpoint mediated cell cycle arrest in response to DNA damage or the presence of unreplicated DNA
TRIP13	Thyroid hormone receptor interactor 13	Interacts with thyroid hormone receptors

Table 8. Gene ontology and pathway enrichment analysis of the hub genes.

Category	Term	Count	Adj. <i>p</i> -Value
BP	Mitotic cell cycle phase transition (GO:0044772)	9/221	7.22×10^{-11}
	Regulation of mitotic cell cycle phase transition (GO:1901990)	7/184	3.99×10^{-8}
	G1/S transition of the mitotic cell cycle (GO:0000082)	5/105	4.03×10^{-6}
	Regulation of mitotic sister chromatid separation (GO:0010965)	3/15	1.65×10^{-5}
	DNA metabolic process (GO:0006259)	6/314	1.65×10^{-5}
CC	Microtubule cytoskeleton (GO:0015630)	8/388	7.67×10^{-8}
	Spindle (GO:0005819)	6/186	4.15×10^{-7}
	Spindle pole (GO:0000922)	5/107	7.73×10^{-7}
	Condensed nuclear chromosome, centromeric region (GO:0000780)	2/12	6.23×10^{-5}
	Mitotic spindle (GO:0072686)	3/84	6.19×10^{-4}
MF	Histone serine kinase activity (GO:0035174)	2/7	0.0011
	Histone kinase activity (GO:0035173)	2/9	0.0011
	Kinase binding (GO:0019900)	5/418	0.0011
	Protein kinase binding (GO:0019901)	5/495	0.0018
	Protein serine/threonine kinase activity (GO:0004674)	4/368	0.0059
KEGG	Cell cycle	8/124	2.88×10^{-12}
	Oocyte meiosis	5/125	8.86×10^{-7}
	Human T-cell leukemia virus 1 infection	4/219	2.76×10^{-4}
	Progesterone-mediated oocyte maturation	3/99	4.42×10^{-4}
	Cellular senescence	3/160	0.0014
WikiPathways	Cell Cycle WP179	8/120	3.37×10^{-12}
	Gastric Cancer Network 1 WP2361	6/29	3.37×10^{-12}
	Retinoblastoma Gene in Cancer WP2446	5/87	2.25×10^{-7}
	Regulation of sister chromatid separation at the metaphase-anaphase transition WP4240	3/15	3.19×10^{-6}
	DNA Replication WP466	3/42	6.32×10^{-5}

**Figure 6.** The expression of the first 10 hub genes by rank in TCGA and GTEx datasets. Statistically significant differences are marked with an *.

4. Discussion

Metastasis formation is a complex process driven by a variety of genes and molecular events [3]. Meta-analysis on differential gene expression from primary tumors and metastasis are common for different cancer types. However, the analyses that stratify metastatic samples according to the secondary sites are rare with more interest shown in very recent

years [29–33]. To the best of my knowledge, the work that is presented here is the first such study for prostate cancer and its most common metastasis sites. These types of studies are important as they accumulate information that could be of interest when designing anti-metastatic therapies.

The main finding of the presented study is that a group of differentially expressed genes encoding for filaments or associated proteins is the most differentially expressed by fold change and the processes of focal adhesion and androgen receptor signaling are among the most changed in metastasis from all sites analyzed. Moreover, there is a substantial difference in expression programs from metastasis from different sites. In the following chapters, based on the results, several questions are considered: what are the site-specific transcriptional programs that predispose or characterize the metastasis from bone, lymph node, and liver and could potentially be used as targets to treat metastasis from those particular sites; what are the common genes that could be used as targets to treat metastasis from all sites; what are the strategies that are used by cancer cells to colonize different organs?

Although the lymph nodes are the first sites encountered by prostate cancer cells that enter the circulation system, the bones are the most common sites that are homing them [34]. This is very intriguing as this study shows that, among the three most common distal sites, metastasis found in bones underwent a much more profound change of transcriptional program (7871 genes with changed expression) in comparison to metastasis from lymph nodes (2509) and liver (1269). The question arises as to what facilitates the colonization of the bones when, despite the complete reorganization of the transcriptional program that is needed, they are still the first choice for prostate cancer cell homing? The suggested concept of pre-metastatic niche offers the explanation that the primary cancer cells, possibly through exosomes, prime the distal organs which increases chances and enables their homing [35]. However, the question is whether there is a predisposition already within primary prostate cancer cells and their transcriptional program that is kept and subsequently upgraded in metastatic cells that makes them prone to bone colonization (“seed pre-selection” [36]). From a list of differentially expressed genes, the driving events in bone-specific metastases that could be directing them to the target organ are extracted. Upregulation of SPP1 and downregulation of CHRDL1 and CNN1 (genes involved in bone biology) in metastasis from all sites analyzed are found which suggests they are changed early on and could belong to the genes that make prostate cancer metastatic cells bone-gravitating. The expression level of SPP1 is elevated in cancers, particularly those that spread preferentially to the skeleton. “Osteomimicry” of malignant cells is partially conferred by transmembrane receptors bound by SPP1. Binding of integrins on malignant cells by SPP1 results in activation of signaling cascades within the cell that promotes metastasis [37]. CHRDL1 gene encodes an antagonist of bone morphogenetic protein 4 and may play a role in embryonic bone formation, while overexpression of CNN1 in osteoblast lineage cells was shown to regulate bone mass [27]. Because of their prominent role in bone biology as listed above, these genes could contribute to the site-preference during the metastatic process. Also, an extensive change in transcription of immune cell-related genes (chemokines, T- and B-cells, and neutrophil-related genes) was recorded in genes differentially expressed in bone metastasis. This transformation supports the role of prostate cancer cell and immune system crosstalk which is crucial for the formation of metastasis in this organ [38]. The contribution of chemokines to the metastatic process has been well documented [39,40]. For example, the prostate cancer metastasis-promoting role of CXCL5 has been recently shown [41]. Some other chemokines from the list of differentially expressed genes (e.g. CCL5, CCR2, reviewed in [40]) are also implicated in the metastatic process from different cancer types. On the list of differentially expressed chemokines in bone metastasis (data not shown), 13 out of 14 chemokines or chemokine receptors with changed expression in bone metastasis only, are up-regulated, indicating a strong increase of activity in the network of chemokines with known (minor part) and yet to be investigated (major part) roles in prostate cancer

metastasis. This finding suggests that targeting the chemokine signaling pathway could alleviate the bone metastasis burden in prostate cancer patients.

As noted above, to colonize lymph nodes and liver, prostate cancer cells undergo changes in transcription that are several times less extensive in the number of affected genes than in bone metastasis. From this data, it could be suggested that the brute force that drives prostate cancer cells through circulation is probably more involved in regional lymph node and liver colonization than in bones. However, enrichment analysis of genes whose expression is changed in lymph nodes only revealed extensive changes in the expression of kinases, suggesting rewiring of signaling cascades. While the term “Focal adhesion” was on the top of the enrichment lists of genes shared among all metastasis, this list was extended to 60 genes, including 7 integrins, and was on the top of the list shared among bone and lymph node but not liver metastasis (data not shown). This indicates that bone and lymph node metastasis highly rewire the expression of adhesion molecules and related pathways, while for liver metastasis this change is much less prominent. Taken together, these results suggest that there are parts of focal adhesion (integrin) network that are commonly changed in prostate cancer metastasis from all analyzed sites, but also a part that is specific to metastasis from each site, giving them an integrin code that is, apparently, important during every step of the metastatic cascade [42] and a subject to a frequent change [43].

The observation from this work which indicates that the expression of genes encoding for microfilaments and intermediate filaments or associated proteins (MYH11, ACTG2, KRT15, NEFH, DES, CNN1, and PCP4) are the most extensively down-regulated in prostate cancer metastasis from all sites suggests fundamental reorganization of their cytoskeleton. KRT15 is downregulated in the progression of normal prostate tissue to prostate cancer and further to lymph node metastasis [44]. Other mentioned genes influence tumors either by inhibiting [45,46] or promoting their pathogenicity [47,48] or displaying a dual role [49,50]. Those studies investigated the roles of individual proteins, however, in this system, it is very likely that they act in concert which could be envisioned from their involvement in the same process of cytoskeleton assembly.

It is interesting to note that liver metastases are highly enriched for genes that are involved in the processes of a target organ. This phenomenon of metastatic cells adapting to the host site has been recently described [5], but the potential contamination with the host tissue should also be taken into account.

The role of androgen receptor signaling in prostate cancer progression is multilayered and has been extensively studied [51,52]. The change in androgen receptor signaling pathway (up-regulation of androgen receptor and changes in expression of related genes) that are documented here are in agreement with recent findings that elevation of androgen receptor promotes prostate cancer metastasis by induction of epithelial-mesenchymal transition [53]. Also, this result is in agreement with a study by Guo et al. [54] who suggest androgen receptor as one of the hub genes in metastatic prostate cancer. However, the study presented here encompasses a larger sample size and presents a more extended approach. In addition, herein differences in differential gene expression between different secondary sites are in focus which is, to the best of my knowledge, a unique approach for prostate cancer metastasis and not so common for other cancer types.

In this study, 20 genes were singled out as hub genes among those that change expression in all metastatic sites analyzed. For most of these genes involvement in disease-free survival was shown suggesting that these genes might be considered in potential targeted therapies.

Finally, heterogeneity of prostate cancer calls for studies that include an even larger number of samples than this study did. The experimental validation of these results would bring the confirmation of the importance of the genes that are suggested here to play a role in the prostate cancer metastatic process. Also, this analysis involved only the data for protein-coding genes and their subsequent mRNA expression. However, the roles of non-coding RNAs are also known to be highly important in prostate cancer progression,

both as regulatory elements and biomarkers [55,56]. It would be interesting to reveal their roles in prostate cancer metastasis from different secondary sites.

5. Conclusions

Although sharing changes in the expression of basic groups of genes belonging to the class of filaments and focal adhesions and androgen signaling pathway, metastasis from different sites differ profoundly in their transcriptional program. Based on this finding, it can be concluded that it is important to study separately cancer cells originating from different secondary sites because the results of gene expression data are expected to be skewed when metastasis samples are not stratified. In addition, data on the differentially expressed genes that are site-specific and common to all metastases provide potentially useful information for targeting metastatic cells. It would be interesting to see whether metastatic cells from different primary organs use similar strategies when colonizing the same secondary site. AURKA, BUB1, CCNB2, CDC20, CDKN3, CENPF, CHEK1, FOXM1, HMMR, MELK, PTTG1, TOP2A, TPX2, TRIP13, TYMS, UBE2C are the hub genes identified in this study that show involvement in the disease-free survival of prostate cancer patients.

Funding: This research was funded by MY ZABA START 2019 donation from Zagrebačka banka.

Institutional Review Board Statement: Not applicable.

Informed Consent Statement: Not applicable.

Acknowledgments: The author would like to thank Robert Bakarić and Andreja Ambriović Ristov for their advice, support, and critical reading of the manuscript.

Conflicts of Interest: The author declares no conflict of interest.

References


- Chaffer, C.L.; Weinberg, R.A. A perspective on cancer cell metastasis. *Science* **2011**, *331*, 1559. [CrossRef]
- Weber, G.F. Why does cancer therapy lack effective anti-metastasis drugs? *Cancer Lett.* **2013**, *328*, 207. [CrossRef]
- Zheng, G.; Ma, Y.; Zou, Y.; Yin, A.; Li, W.; Dong, D. HCMDB: The human cancer metastasis database. *Nucleic Acids Res.* **2018**, *46(D1)*, D950. [CrossRef]
- Hartung, F.; Wang, Y.; Aronow, B.; Weber, G.F. A core program of gene expression characterizes cancer metastases. *Oncotarget* **2017**, *8*, 10216. [CrossRef]
- Hartung, F.; Patil, A.; Meshram, R.J.; Weber, G.F. Gene expression signatures of site-specificity in cancer metastases. *Clin. Exp. Metastasis* **2019**, *37*, 159. [CrossRef] [PubMed]
- Rawla, P. Epidemiology of Prostate Cancer. *World J. Oncol.* **2019**, *10*, 63–89. [CrossRef] [PubMed]
- Dong, L.; Zieren, R.C.; Xue, W.; de Reijke, T.M.; Pienta, K.J. Metastatic prostate cancer remains incurable, why? *Asian J. Urol.* **2019**, *6*, 26–41. [CrossRef] [PubMed]
- Deng, Y.; Bi, R.; Zhu, Z.; Li, S.; Xu, B.; Rather, W.A.; Wang, C. A surveillance, epidemiology and end results database analysis of the prognostic value of organ-specific metastases in patients with advanced prostatic adenocarcinoma. *Oncol. Lett.* **2019**, *18*, 1057–1070. [CrossRef] [PubMed]
- Testa, U.; Castelli, G.; Pelosi, E. Cellular and Molecular Mechanisms Underlying Prostate Cancer Development: Therapeutic Implications. *Medicines* **2019**, *6*, 82. [CrossRef] [PubMed]
- Samaržija, I. Post-Translational Modifications that Drive Prostate Cancer Progression. *Biomolecules* **2021**, *11*, 247. [CrossRef] [PubMed]
- Barrett, T.; Wilhite, S.E.; Ledoux, P.; Evangelista, C.; Kim, I.F.; Tomashevsky, M.; Marshall, K.A.; Phillippy, K.H.; Sherman, P.M.; Holko, M.; et al. NCBI GEO: Archive for functional genomics data sets-Update. *Nucleic Acids Res.* **2013**, *41*, D991–D995. [CrossRef]
- Raudvere, U.; Kolberg, L.; Kuzmin, I.; Arak, T.; Adler, P.; Peterson, H.; Vilo, J. g:Profiler: A web server for functional enrichment analysis and conversions of gene lists. *Nucleic Acids Res.* **2019**, *47*, W191–W198. [CrossRef]
- Chandran, U.R.; Ma, C.; Dhir, R.; Bisceglia, M.; Lyons-Weiler, M.; Liang, W.; Michalopoulos, G.; Becich, M.; Monzon, F.A. Gene expression profiles of prostate cancer reveal involvement of multiple molecular pathways in the metastatic process. *BMC Cancer* **2007**, *12*, 64. [CrossRef] [PubMed]
- Taylor, B.S.; Schultz, N.; Hieronymus, H.; Gopalan, A.; Xiao, Y.; Carver, B.S.; Arora, V.K.; Kaushik, P.; Cerami, E.; Reva, B.; et al. Integrative Genomic Profiling of Human Prostate Cancer. *Cancer Cell* **2010**, *18*, 11–22. [CrossRef] [PubMed]
- Cai, C.; Wang, H.; He, H.H.; Chen, S.; He, L.; Ma, F.; Mucci, L.; Wang, Q.; Fiore, C.; Sowalsky, A.G.; et al. ERG induces androgen receptor-mediated regulation of SOX9 in prostate cancer. *J. Clin. Investig.* **2013**, *123*, 1109–1122. [CrossRef] [PubMed]

16. Böttcher, R.; Marije Hoogland, A.; Dits, N.; Verhoef, E.I.; Kweldam, C.; Waranecki, P.; Bangma, C.H.; van Leenders, G.J.L.H.; Jenster, G. Novel long non-coding RNAs are specific diagnostic and prognostic markers for prostate cancer. *Oncotarget* **2015**, *6*, 4036–4050. [CrossRef]
17. Kumar, A.; Coleman, I.; Morrissey, C.; Zhang, X.; True, L.D.; Gulati, R.; Etzioni, R.; Bolouri, H.; Montgomery, B.; White, T.; et al. Substantial interindividual and limited intraindividual genomic diversity among tumors from men with metastatic prostate cancer. *Nat. Med.* **2016**, *22*, 369–378. [CrossRef]
18. Toro-Domínguez, D.; Martorell-Marugán, J.; López-Domínguez, R.; García-Moreno, A.; González-Rumayor, V.; Alarcón-Riquelme, M.E.; Carmona-Sáez, P. ImaGEO: Integrative gene expression meta-analysis from GEO database. *Bioinformatics* **2019**, *35*, 880–882. [CrossRef]
19. Pirooznia, M.; Nagarajan, V.; Deng, Y. GeneVenn—A web application for comparing gene lists using Venn diagrams. *Bioinformatics* **2007**, *1*, 420–422. [CrossRef] [PubMed]
20. Chen, E.Y.; Tan, C.M.; Kou, Y.; Duan, Q.; Wang, Z.; Meirelles, G.V.; Clark, N.R.; Ma’ayan, A. Enrichr: Interactive and collaborative HTML5 gene list enrichment analysis tool. *BMC Bioinform.* **2013**, *14*, 128. [CrossRef] [PubMed]
21. Szklarczyk, D.; Gable, A.L.; Lyon, D.; Junge, A.; Wyder, S.; Huerta-Cepas, J.; Simonovic, M.; Doncheva, N.T.; Morris, J.H.; Bork, P.; et al. STRING v11: Protein-protein association networks with increased coverage, supporting functional discovery in genome-wide experimental datasets. *Nucleic Acids Res.* **2019**, *47*, D607–D613. [CrossRef] [PubMed]
22. Shannon, P.; Markiel, A.; Ozier, O.; Baliga, N.S.; Wang, J.T.; Ramage, D.; Amin, N.; Schwikowski, B.; Ideker, T. Cytoscape: A software Environment for integrated models of biomolecular interaction networks. *Genome Res.* **2003**, *13*, 2498–2504. [CrossRef] [PubMed]
23. Chin, C.H.; Chen, S.H.; Wu, H.H.; Ho, C.W.; Ko, M.T.; Lin, C.Y. cytoHubba: Identifying hub objects and sub-networks from complex interactome. *BMC Syst. Biol.* **2014**, *8* (Suppl. S4), S11. [CrossRef] [PubMed]
24. Tang, Z.; Li, C.; Kang, B.; Gao, G.; Li, C.; Zhang, Z. GEPIA: A web server for cancer and normal gene expression profiling and interactive analyses. *Nucleic Acids Res.* **2017**, *45*, W98–W102. [CrossRef]
25. Nakamura, F.; Hartwig, J.H.; Stossel, T.P.; Szymanski, P.T. Ca²⁺ and calmodulin regulate the binding of filamin A to actin filaments. *J. Biol. Chem.* **2005**, *280*, 32426–32433. [CrossRef] [PubMed]
26. Liu, T.; Li, B.; Zheng, X.F.; Jiang, S.D.; Zhou, Z.Z.; Xu, W.N.; Zheng, H.L.; Wang, C.D.; Zhang, X.L.; Jiang, L.S. Chordin-like 1 improves osteogenesis of bone marrow mesenchymal stem cells through enhancing BMP4-SMAD pathway. *Front. Endocrinol.* **2019**, *10*, 360. [CrossRef]
27. Su, N.; Chen, M.; Chen, S.; Li, C.; Xie, Y.; Zhu, Y.; Zhang, Y.; Zhao, L.; He, Q.; Du, X.; et al. Overexpression of H1 calponin in osteoblast lineage cells leads to a decrease in bone mass by disrupting osteoblast function and promoting osteoclast formation. *J. Bone Miner. Res.* **2013**, *28*, 660–671. [CrossRef]
28. Pathak, B.R.; Breed, A.A.; Nakhawa, V.H.; Jagtap, D.D.; Mahale, S.D. Growth inhibition mediated by PSP94 or CRISP-3 is prostate cancer cell line specific. *Asian J. Androl.* **2010**, *12*, 677–689. [CrossRef]
29. Yu, Z.; Zou, H.; Wang, H.; Li, Q.; Yu, D. Identification of Key Gene Signatures Associated With Bone Metastasis in Castration-Resistant Prostate Cancer Using Co-Expression Analysis. *Front. Oncol.* **2021**, *10*, 571524. [CrossRef] [PubMed]
30. Zhu, Z.; Wen, Y.; Xuan, C.; Chen, Q.; Xiang, Q.; Wang, J.; Liu, Y.; Luo, L.; Zhao, S.; Deng, Y.; et al. Identifying the key genes and microRNAs in prostate cancer bone metastasis by bioinformatics analysis. *FEBS Open Bio.* **2020**, *10*, 674–688. [CrossRef] [PubMed]
31. Xu, Z.; Ding, Y.; Lu, W.; Zhang, K.; Wang, F.; Ding, G.; Wang, J. Comparison of metastatic castration-resistant prostate cancer in bone with other sites: Clinical characteristics, molecular features and immune status. *PeerJ.* **2021**, *9*, e11133. [CrossRef]
32. Shamsara, E.; Shamsara, J. Bioinformatics analysis of the genes involved in the extension of prostate cancer to adjacent lymph nodes by supervised and unsupervised machine learning methods: The role of SPAG1 and PLEKHF2. *Genomics* **2020**, *112*, 3871–3882. [CrossRef]
33. Xu, N.; Chen, S.-H.; Lin, T.-T.; Cai, H.; Ke, Z.-B.; Dong, R.-N.; Huang, P.; Li, X.-D.; Chen, Y.-H.; Zheng, Q.-S. Development and validation of hub genes for lymph node metastasis in patients with prostate cancer. *J. Cell Mol. Med.* **2020**, *24*, 4402–4414. [CrossRef]
34. Wang, G.; Zhao, D.; Spring, D.J.; Depinho, R.A. Genetics and biology of prostate cancer. *Genes Dev.* **2018**, *32*, 1105–1140. [CrossRef]
35. Li, F.X.Z.; Liu, J.J.; Xu, F.; Lin, X.; Zhong, J.Y.; Wu, F.; Yuan, L.Q. Role of tumor-derived exosomes in bone metastasis (Review). *Oncol. Lett.* **2019**, *18*, 3935–3945. [CrossRef]
36. Gao, Y.; Bado, I.; Wang, H.; Zhang, W.; Rosen, J.M.; Zhang, X.H.F. Metastasis Organotropism: Redefining the Congenial Soil. *Dev. Cell* **2019**, *49*, 375–391. [CrossRef]
37. Kruger, T.E.; Miller, A.H.; Godwin, A.K.; Wang, J. Bone sialoprotein and osteopontin in bone metastasis of osteotropic cancers. *Crit. Rev. Oncol. Hematol.* **2014**, *89*, 330–341. [CrossRef]
38. Xiang, L.; Gilkes, D.M. The contribution of the immune system in bone metastasis pathogenesis. *Int. J. Mol. Sci.* **2019**, *20*, 999. [CrossRef]
39. Zlotnik, A.; Burkhardt, A.M.; Homey, B. Homeostatic chemokine receptors and organ-specific metastasis. *Nat. Rev. Immunol.* **2011**, *11*, 597–606. [CrossRef]
40. Borsig, L.; Wolf, M.J.; Roblek, M.; Lorentzen, A.; Heikenwalder, M. Inflammatory chemokines and metastasis-Tracing the accessory. *Oncogene* **2014**, *33*, 3217–3224. [CrossRef]

41. Roca, H.; Jones, J.D.; Purica, M.C.; Weidner, S.; Koh, A.J.; Kuo, R.; Wilkinson, J.E.; Wang, Y.; Daignault-Newton, S.; Pienta, K.J.; et al. Apoptosis-induced CXCL5 accelerates inflammation and growth of prostate tumor metastases in bone. *J. Clin. Investig.* **2018**, *128*, 248–266. [CrossRef] [PubMed]
42. Hamidi, H.; Ivaska, J. Every step of the way: Integrins in cancer progression and metastasis. *Nat. Rev. Cancer* **2018**, *18*, 533–548. [CrossRef]
43. Samaržija, I.; Dekanić, A.; Humphries, J.D.; Paradžik, M.; Stojanović, N.; Humphries, M.J.; Ambriović-Ristov, A. Integrin crosstalk contributes to the complexity of signalling and unpredictable cancer cell fates. *Cancers* **2020**, *12*, 1910. [CrossRef] [PubMed]
44. Schmidt, L.; Møller, M.; Haldrup, C.; Strand, S.H.; Vang, S.; Hedegaard, J.; Høyer, S.; Borre, M.; Ørntoft, T.; Sørensen, K.D. Exploring the transcriptome of hormone-naive multifocal prostate cancer and matched lymph node metastases. *Br. J. Cancer* **2018**, *119*, 1527–1537. [CrossRef] [PubMed]
45. Calmon, M.F.; Jeschke, J.; Zhang, W.; Dhir, M.; Siebenkäs, C.; Herrera, A.; Tsai, H.C.; O'Hagan, H.M.; Pappou, E.P.; Hooker, C.M.; et al. Epigenetic silencing of neurofilament genes promotes an aggressive phenotype in breast cancer. *Epigenetics* **2015**, *10*, 622–632. [CrossRef]
46. Kim, M.S.; Chang, X.; LeBron, C.; Nagpal, J.K.; Lee, J.; Huang, Y.; Yamashita, K.; Trink, B.; Ratovitski, E.A.; Sidransky, D. Neurofilament heavy polypeptide regulates the Akt- β -catenin pathway in human esophageal squamous cell carcinoma. *PLoS ONE* **2010**, *5*, e9003. [CrossRef]
47. Yoshimura, T.; Hamada, T.; Hijioka, H.; Souda, M.; Hatanaka, K.; Yoshioka, T.; Yamada, S.; Tsutsui, M.; Umekita, Y.; Nakamura, N.; et al. PCP4/PEP19 promotes migration, invasion and adhesion in human breast cancer MCF-7 and T47D cells. *Oncotarget* **2016**, *7*, 49065–49074. [CrossRef]
48. Arentz, G.; Chataway, T.; Price, T.J.; Izwan, Z.; Hardi, G.; Cummins, A.G.; Hardingham, J.E. Desmin expression in colorectal cancer stroma correlates with advanced stage disease and marks angiogenic microvessels. *Clin. Proteom.* **2011**, *8*, 16. [CrossRef]
49. Edfeldt, K.; Hellman, P.; Westin, G.; Stalberg, P. A plausible role for actin gamma smooth muscle 2 (ACTG2) in small intestinal neuroendocrine tumorigenesis. *BMC Endocr. Disord.* **2016**, *16*, 19. [CrossRef]
50. Wu, Y.; Liu, Z.G.; Shi, M.Q.; Yu, H.Z.; Jiang, X.Y.; Yang, A.H.; Fu, X.S.; Xu, Y.; Yang, S.; Ni, H.; et al. Identification of ACTG2 functions as a promoter gene in hepatocellular carcinoma cells migration and tumor metastasis. *Biochem. Biophys. Res. Commun.* **2017**, *491*, 537–544. [CrossRef]
51. Cioni, B.; Zwart, W.; Bergman, A.M. Androgen receptor moonlighting in the prostate cancer microenvironment. *Endocr. Relat. Cancer* **2018**, *25*, R331–R349. [CrossRef] [PubMed]
52. Xu, J.; Qiu, Y. Role of androgen receptor splice variants in prostate cancer metastasis. *Asian J. Urol.* **2016**, *3*, 177–184. [CrossRef] [PubMed]
53. Lin, C.Y.; Jan, Y.J.; Kuo, L.K.; Wang, B.J.; Huo, C.; Jiang, S.S.; Chen, S.C.; Kuo, Y.Y.; Chang, C.R.; Chuu, C.P. Elevation of androgen receptor promotes prostate cancer metastasis by induction of epithelial-mesenchymal transition and reduction of KAT5. *Cancer Sci.* **2018**, *109*, 3564–3574. [CrossRef] [PubMed]
54. Guo, L.; Lin, M.; Cheng, Z.; Chen, Y.; Huang, Y.; Xu, K. Identification of key genes and multiple molecular pathways of metastatic process in prostate cancer. *PeerJ* **2019**, *7*, e7899. [CrossRef]
55. Xu, Y.H.; Deng, J.L.; Wang, G.; Zhu, Y.S. Long non-coding RNAs in prostate cancer: Functional roles and clinical implications. *Cancer Lett.* **2019**, *464*, 37–55. [CrossRef] [PubMed]
56. Jiang, G.; Su, Z.; Liang, X.; Huang, Y.; Lan, Z.; Jiang, X. Long non-coding RNAs in prostate tumorigenesis and therapy (Review). *Mol. Clin. Oncol.* **2020**, *13*, 76. [CrossRef]

Article

External Validation of the Briganti Nomogram to Predict Lymph Node Invasion in Prostate Cancer—Setting a New Threshold Value

Bartosz Małkiewicz ^{1,*}, Kuba Ptaszkowski ², Klaudia Knecht ¹, Adam Gurwin ¹, Karol Wilk ¹, Paweł Kielb ¹, Krzysztof Dudek ³ and Romuald Zdrojowy ¹

- ¹ Department of Urology and Oncologic Urology, Wrocław Medical University, 50-556 Wrocław, Poland; klaudia.knecht@gmail.com (K.K.); gurwin.adam@gmail.com (A.G.); karolwilk@me.com (K.W.); pk.kielb@gmail.com (P.K.); romuald.zdrojowy@umed.wroc.pl (R.Z.)
- ² Department of Clinical Biomechanics and Physiotherapy in Motor System Disorders, Faculty of Health Science, Wrocław Medical University, Grunwaldzka 2, 50-355 Wrocław, Poland; kuba.ptaszkowski@umed.wroc.pl
- ³ Faculty of Mechanical Engineering, Wrocław University of Science and Technology, 50-370 Wrocław, Poland; krzysztof.dudek@pwr.edu.pl
- * Correspondence: bartosz.malkiewicz@umed.wroc.pl; Tel.: +48-506-158-136

Abstract: (1) Introduction: The study aimed to test and validate the performance of the 2012 Briganti nomogram as a predictor for pelvic lymph node invasion (LNI) in men who underwent radical prostatectomy (RP) with extended pelvic lymph node dissection (PLND) to examine their performance and to analyse the therapeutic impact of using a different nomogram cut-off. (2) Material and Methods: The study group consisted of 222 men with clinically localized prostate cancer (PCa) who underwent RP with ePLND between 01/2012 and 10/2018. Measurements included: preoperative PSA, clinical stage (CS), primary and secondary biopsy Gleason pattern, and the percentage of positive cores. The area under the curve (AUC) of the receiver operator characteristic analysis was appointed to quantify the accuracy of the primary nomogram model to predict LNI. The extent of estimation associated with the use of this model was graphically depicted using calibration plots. (3) Results: The median number of removed lymph nodes was 16 (IQR 12–21). A total of 53 of 222 patients (23.9%) had LNI. Preoperative clinical and biopsy characteristics differed significantly (all $p < 0.005$) between men with and without LNI. A nomogram-derived cut-off of 7% could lead to a reduction of 43% (95/222) of lymph node dissection while omitting 19% (10/53) of patients with LNI. The sensitivity, specificity, and negative predictive value associated with the 7% cut-off were 81.1%, 50.3%, and 96.3%, respectively. (4) Conclusions: The analysed nomogram demonstrated high accuracy for LNI prediction. A nomogram-derived cut-off of 7% confirmed good performance characteristics within the first external validation cohort from Poland.

Keywords: prostate cancer; radical prostatectomy; pelvic lymph node dissection; lymph node invasion; preoperative nomogram

Citation: Małkiewicz, B.; Ptaszkowski, K.; Knecht, K.; Gurwin, A.; Wilk, K.; Kielb, P.; Dudek, K.; Zdrojowy, R. External Validation of the Briganti Nomogram to Predict Lymph Node Invasion in Prostate Cancer—Setting a New Threshold Value. *Life* **2021**, *11*, 479. <https://doi.org/10.3390/life11060479>

Academic Editors: Ana Faustino and Paula A. Oliveira

Received: 9 May 2021

Accepted: 24 May 2021

Published: 25 May 2021

Publisher's Note: MDPI stays neutral with regard to jurisdictional claims in published maps and institutional affiliations.



Copyright: © 2021 by the authors. Licensee MDPI, Basel, Switzerland. This article is an open access article distributed under the terms and conditions of the Creative Commons Attribution (CC BY) license (<https://creativecommons.org/licenses/by/4.0/>).

1. Introduction

In Europe, prostate cancer (PCa) is the most common cancer in men, accounting for 24% of all cancers diagnosed in 2018, equivalent to 450,000 new cases [1]. Poland ranks first in the incidence rates for men and second in the list of causes of cancer deaths (approx. 9.5%) [2]. Despite the widespread use of screening tests by determining PSA's level, some patients are still diagnosed with a high local stage at diagnosis and are referred to as high risk on the D'Amico scale [3]. There is no doubt that radical treatment brings a much more significant benefit in overall survival and cancer-specific survival. Moreover, radical prostatectomy was most beneficial in patients with localised and locally advanced PCa [4,5]. Pelvic lymph node dissection (PLND) represents a vital staging procedure in identifying

patients with lymph node invasion (LNI) and should be performed in patients with intermediate or high-risk PCa and omitting patients with the low-risk disease [6]. It allows selecting lymph nodes affected by the neoplastic invasion out of all the collected ones [7]. However, this procedure carries a risk of complications; therefore, it should be avoided if the risk of LNI is low. The decision to undertake a given treatment strategy depends on the preoperative PSA level, clinical stage, Gleason grade, histopathological examination and currently supported by new imaging techniques, in particular multiparametric MRI. Since the primary tumour is the source of growth factors most likely responsible for the localization of distant metastases, it should be treated as effectively as possible, while minimizing any complications.

Several studies have shown that the use of extended lymphadenectomy (ePLND) is recommended for each PLND indication [8–10]. To date, several predictive models have been developed to determine the risk of LNI in patients undergoing ePLND. The two most used (2021 Briganti and MSKCC) have been externally validated [11,12]. The developed predictive models require periodic checks to ensure their current patients' accuracy. The result is a very accurate nomogram after internal validation. However, the lack of external validation is an obstacle to implementing the nomogram into broad clinical practice [13,14]. It is also impossible to obtain older patient data due to the different, more favourable grading of PCa in modern patients [15,16]. Finally, according to the European Association of Urology guidelines, ePLND should be performed for patients when the predicted probability of LNI exceeds 5% in Briganti calculation. However, in a few recent reports, 7% was suggested as an optimal cut-off with similar sensitivity and specificity, and a higher number of patients for whom PLND could be safely omitted [6,17]. Our study aimed to update and verify the nomogram predicting LNI on a different external patient data set and to find the most accurate cut-off for performing ePLND.

2. Materials and Methods

The data of 638 patients who underwent radical prostatectomy with ePLND due to a high-risk prostate cancer according to the d'Amico scale (PSA > 20 ng/mL, clinical stage \geq T2c or biopsy Gleason sum 8–10) have been retrospectively studied. The collected data comes from 01/2012 to 10/2018 from the Clinical Department of Urology and Urology Oncology in Wrocław. Overall, 222 patients met the criteria—they had information on preoperative PSA, age, Gleason score, clinical stage, and had at least 8 fully described sections taken during ePLND.

The clinical stage of the tumour was assessed according to the updated TNM classification from 2016; the prostate biopsy was obtained by TRUS-guided systemic biopsy, and PSA was determined before the DRE examination [18]. Dedicated uropathologists performed the pathologic analysis of the biopsy and post-operative specimens following the International Society of Urological Pathology's modifications in 2014 [19,20]. All specimens were collected and tested under the Stanford protocol guidelines, and their staging was determined according to the American Committee's guidelines for the Staging System for Prostate Cancer [21,22]. Patients were preoperatively examined for metastases using abdominal CT with contrast and bone scintigraphy. An updated Briganti nomogram was calculated for each subject in this group based on age, PSA, TNM stage, Gleason score, and the percentage of samples taken [23].

Open radical prostatectomy was performed with the ascending technique, and in laparoscopic cases, transperitoneal access was used. The extent of the lymph node dissection was the same regardless of the surgical technique (open or laparoscopic). Extended pelvic lymphadenectomy (ePLND) involves removing fatty tissue from the obturator fossa area (along the obturator nerve and the external iliac vein) along the internal and external iliac arteries, extending to the distal segment of the common iliac artery. The lateral border is the pelvic wall, and the middle is the perivesical fat. The distal margin is the deep femoral vein. Each station is collected separately according to its anatomical location for selective histopathological examination [24].

This retrospective study was conducted in agreement with the Declaration of Helsinki of 1975, revised in 2013, and approved by the Ethics Committee of Wrocław Medical University (KB/545/2020).

3. Statistical Analysis

Descriptive statistics focus on the frequencies and proportions of categorical variables. Means, medians, and interquartile ranges are presented for continuously coded variables. The Chi-square and t-tests for the independent sample were used to compare the statistical significance of differences, respectively, of proportions and means. Analyses focused on testing the accuracy and calibration of a previously updated and internally validated nomogram to predict the likelihood of LNI in ePLND. Therefore, this nomogram was externally validated using predefined regression coefficients. The area under the curve (AUC) of the receiver operator characteristic analysis was used to quantify the model accuracy for LNI prediction. The extent of the overestimation or underestimation was investigated graphically in random calibration plots. Like Briganti, the specificity, sensitivity, and negative predictive value (NPV) were systematically assessed for each LNI probability threshold obtained from the nomogram [25].

All tests were two-sided with statistical significance set at $p < 0.05$. The analyses were performed using the statistical package for R (R base for statistical calculations, version 2.1.13).

4. Results

The characteristics of 222 patients and the primary cohort, consisting of the base for the nomogram, are presented in comparative Table 1. Additionally, the table's data have been divided according to the occurrence of lymph node involvement (LNI) in the study group. Overall, LNI was found in 23.9% of patients ($n = 53$). The mean PSA value for patients with lymph node involvement was 24 ng/mL compared to 12.2 ng/mL without LNI, IQR: 12.7–33.8 vs. 7.2–17.6, respectively, with $p < 0.001$. Overall, patients with LNI had a higher clinical stage (T3) than those without, 41.5% vs. 13.1%, respectively ($p < 0.001$). Measurement of the biopsy secondary Gleason pattern also showed higher values in patients with LNI (52.8%) than without (21.9%, $p < 0.001$). The mean number of positive cores (6 vs. 5, $p = 0.001$), as well as the mean percentage of positive cores (50% vs. 42%, $p < 0.001$), were significantly higher in patients with LNI. The description of other pathological features is also listed in Table 1.

The accuracy of the external validation performed was estimated at 0.734 ($n = 222$). Figure 1 shows the ROC calibration curve, demonstrating the dependence of specificity (X-axis) on sensitivity (Y-axis). A designated segment at an angle of 45° defines the ideal relationship between specificity and sensitivity for a given test. Points above this segment suggest that sensitivity is superior to specificity, which means that there are too many false positives versus false negatives. The opposite dependence occurs in the case of points located below this section. The entire calibration curve for our external validation of the nomogram runs above it, which means that at the moment, with the help of the nomogram, we are incorrectly finding too many false LNIs. However, the degree of over-detection is low due to the entire assay's high accuracy.

Table 2 shows the probability of LNI occurrence resulting from applying the Briganti nomogram in the cohort where external validation was performed. For each cut-off point of the nomogram, the actual number of men with and without LNI was calculated. In addition, the sensitivity, specificity, positive predictive value (PPV), and negative predictive value (NPV) for the individual cut-off values of the nomogram were characterized. ePLND could be omitted in 95 men (42.8%), but this group would include 10 patients with LNI (18.9% of all LNI patients) using the nomogram cut-off of 7%. The sensitivity and specificity of the 7% cut-off were 81.1% and 50.3%, respectively, and NPV and PPV were 96.3% and 33.9%, respectively.

Table 1. Clinical and pathological data of primary and current study cohorts [25].

	Comparison between Primary and Current Study Cohorts:			Comparison within Study Cohort:		
	Primary (2006–2010) [25]	Current (2012–2018)	<i>p</i>	LNI (–)	LNI (+)	<i>p</i>
No (%)	588 (–)	222 (–)		169 (76.1)	53 (23.9)	
Age, years						
Median	66	65	<0.001	64	66	0.045
IQR	60–70	60–68		59–68	62–70	
PSA, ng/mL						
Median	6.3	13.6	<0.001	12.2	24.0	<0.001
IQR	4.8–8.9	7.6–21.1		7.2–17.6	12.7–33.8	
No. of biopsy cores taken						
Median	17	12	<0.001	12	12	0.639
IQR	13–24	12–12		12–12	10–12	
No. of positive biopsy cores						
Median	6	5	<0.001	5	6	0.001
IQR	3–10	3–8		3–7	4–10	
Perc. of positive biopsy cores						
Median	36	42	0.296	42	50	<0.001
IQR	17–61	25–66		25–58	33–91	
Clinical stage:						
T1	373 (63.4)	10 (4.5)	<0.001	8 (4.7)	2 (3.8)	<0.001
T2	184 (31.3)	168 (75.7)		139 (82.2)	29 (54.7)	
T3	31 (5.3)	44 (19.8)		22 (13.1)	22 (41.5)	
Primary biopsy Gleason pattern:						
≤3	488 (83.0)	155 (69.8)	<0.001	130 (76.9)	25 (47.2)	<0.001
≥4	100 (17.0)	67 (30.2)		39 (23.1)	28 (52.8)	
Secondary biopsy Gleason pattern:						
≤3	406 (69.0)	157 (70.7)	0.707	132 (78.1)	25 (47.2)	<0.001
≥4	182 (31.0)	65 (29.3)		37 (21.9)	28 (52.8)	
Clinical risk classification:						
Low		16 (7.8)		15 (9.6)	1 (2.0)	<0.001
Intermediate		45 (22.0)		44 (28.2)	1 (2.0)	
High		144 (70.2)		97 (62.2)	47 (96.0)	
Pathological stage:						
T2	431 (73.3)	108 (48.6)	<0.001	103 (60.9)	5 (9.4)	<0.001
T3a	97 (16.5)	48 (21.6)		33 (19.5)	15 (28.3)	
T3b	58 (9.9)	66 (29.7)		33 (19.5)	33 (62.3)	
T4	2 (0.3)	0 (0.0)		0 (0.0)	0 (0.0)	
Pathological primary Gleason pattern:						
≤3		141 (63.5)		119 (70.4)	25 (47.2)	0.003
≥4		81 (36.5)		50 (29.6)	28 (52.8)	
Pathological secondary Gleason pattern:						
≤3		142 (64.0)		119 (70.4)	23 (43.4)	<0.001
≥4		80 (36.0)		50 (29.6)	30 (56.6)	
Number of positive lymph nodes						
Median	2	2	<0.001	0	2	<0.001
IQR	1–3	1–5		0–0	1–5	
Number of lymph nodes removed						
Median	19	16	<0.001	15	20	<0.001
IQR	15–25	12–21		10–20	16–26	
Biopsy Gleason Grading Group						
1		76 (34.2)		64 (37.9)	12 (22.7)	<0.001
2		52 (23.4)		46 (27.2)	6 (11.3)	
3		29 (13.1)		22 (13.0)	7 (13.2)	
4–5		65 (29.3)		37 (21.9)	28 (52.8)	
Pathological Gleason Grading Group						
1		26 (11.7)		26 (15.4)	0 (0.0)	<0.001
2		58 (26.1)		49 (29.0)	9 (17.0)	
3		58 (26.1)		44 (26.0)	14 (26.4)	
4–5		80 (36.1)		50 (29.6)	30 (56.6)	

n (%) or median [IQR], IQR: interquartile range, LNI: lymph node invasion, PSA: prostate-specific antigen.

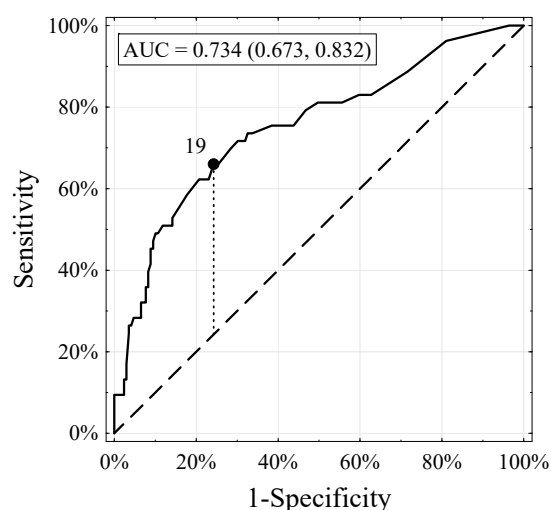


Figure 1. Receiver–operator characteristic (ROC) and area under the curve of the updated Briganti nomogram in 222 patients with risk of LNI.

Table 2. Analyses of the Nomogram-Derived Cut-Offs of the Externally Validated Updated LNI Nomogram.

Cut-off, %	TN + FN	TN	FN	TP + FP	FP	TP	NPV	PPV	TPR	TNR
1	6 (3.6)	6 (3.6)	0 (0)	216 (97.3)	163 (96.4)	53 (100)	100	24.5	100	3.6
2	34 (15.3)	32 (18.9)	2 (3.8)	188 (84.7)	137 (81.1)	51 (96.2)	94.1	27.1	96.2	18.9
3	54 (24.3)	48 (28.4)	6 (11.3)	168 (75.7)	121 (71.6)	47 (88.7)	88.9	28.0	88.7	28.4
4	73 (32.9)	64 (37.9)	9 (17.0)	150 (67.6)	106 (62.7)	44 (83.0)	97.4	29.3	83.0	37.6
5	77 (34.7)	68 (40.2)	9 (17.0)	145 (65.3)	101 (59.8)	44 (83.0)	97.2	30.3	83.0	40.2
6	85 (38.3)	75 (44.4)	10 (18.9)	137 (61.7)	94 (55.6)	43 (81.1)	96.9	31.4	81.1	44.4
7	95 (42.8)	85 (50.3)	10 (18.9)	127 (57.2)	84 (49.7)	43 (81.1)	96.3	33.9	81.1	50.3
8	101 (45.5)	90 (53.3)	11 (20.8)	121 (54.5)	79 (46.7)	42 (79.2)	95.6	34.7	79.2	53.3
9	108 (48.6)	95 (56.2)	13 (24.5)	114 (51.4)	74 (43.8)	40 (75.5)	96.3	35.1	75.5	56.2
10	112 (50.5)	99 (58.6)	13 (24.5)	110 (49.5)	70 (41.4)	40 (75.5)	95.0	36.4	75.5	58.6
15	133 (59.9)	118 (69.8)	15 (28.3)	89 (40.1)	51 (30.2)	38 (71.7)	93.7	42.7	71.7	69.8
20	154 (69.4)	134 (79.3)	20 (37.7)	68 (30.6)	35 (20.7)	33 (62.3)	93.3	48.5	62.3	79.3
25	170 (76.6)	145 (85.8)	25 (47.2)	51 (23.0)	24 (14.2)	27 (50.9)	92.5	52.9	51.9	85.8
30	179 (80.6)	152 (89.9)	27 (50.9)	43 (19.4)	17 (10.1)	26 (49.1)	91.6	60.5	49.1	89.9

Exemplary cutoffs with calculated ability to identify patients with ($n = 53$) or without ($n = 169$) pathologically confirmed LNI. TN + FN: patients below recommended ePLND cut-off, TN: patients below cut-off without pathologic LNI, FN: patients below cut-off with pathologic LNI, TP + FP: patients above recommended ePLND cut-off, FP: patients above cut-off without pathologic LNI, TP: patients above cut-off with pathologic LNI, NPV: negative predictive value, PPV: positive predictive value, TPR: sensitivity, TNR: specificity.

5. Discussion

According to the latest EAU guidelines, the ePLND template is recommended whenever PLND is required [8–10,26]. During ePLND, at least 13 lymph nodes should be removed and investigated to achieve optimal staging accuracy. In cases with 13 or more lymph nodes examined, the rate of metastatic involvement is twice as high as in lower lymph node counts [27]. Moreover, it has been proven that the more lymph nodes are removed, the more accurate the staging will be [8,28]. In our study, the median value of removed lymph nodes was 16, which allowed for an accurate assessment. There are different LNI predictive nomograms [11,29–32]. Our research performed an external validation of the Briganti nomogram for the Polish cohort [23]. Thus far, it has not been checked and formalized for the Polish centre’s needs. Our main goal was to optimize the local cohort nomogram in patients after radical prostatectomy. We tested different cut-off values that could be used to define with the highest accuracy patients in whom ePLND should be executed.

It is important to avoid unnecessary lymphadenectomy due to its intra- and postoperative complications. ePLND extends surgery time by an average of 90 min, which increases

blood loss and the risk of ischemic complications [28,33]. It can also cause obturator nerve injury, life-threatening bleeding due to iliac vessels laceration, ureteral injury, deep venous thrombosis, pulmonary embolism, and lymphocele [34,35]. The latest reports indicate the need to change the cut-off value for performing ePLND at RP from 5% to 7%, resulting from the nomogram [17]. Using a 7% nomogram cut-off in Diamand et al.'s study allows the avoidance of 55.9% of PLNDs, while omitting less than 2.6% of patients with LNI [36]. Venclovas et al.'s nomogram-derived cut-off of 7% is associated with a risk of missing LNI in 4%, avoiding unnecessary surgeries in 47% [17]. However, Hansen et al. decide to use a 4% cut-off to reduce 48% of lymph node dissection, while omitting 10% of patients with LNI [37].

Performed analyses showed some critical findings. Firstly, patients undergoing ePLND in different clinical centres may show very different clinical stages and pathological neoplastic changes. Two components are particularly noticeable compared to the primary medium where the Briganti nomogram was developed [23]. In our clinic, the frequency of LNI 23.9% compared to only 8.3% in the original series shows that some centres operate on patients at a higher stage of advancement than others. This fact may significantly affect the effectiveness of the prediction tools used, as in some centres, less aggressive tumours are removed. Secondly, we recorded a higher degree of malignancy in the Gleason primary and secondary patterns than in Briganti's group. In conclusion, our data clearly show that similar cohorts of men with prostate cancer may differ in terms of tumour characteristics, which means that external, cohort-specific validation is required before using a prognostic tool in routine clinical practice.

After testing as part of our external validation on an independent cohort, the nomogram's predicted accuracy was 73.4%, preferably compared to the 87.6% obtained by Briganti's internal validation team. The similar overall accuracy of the internal and external validation results indicates that, despite significant discrepancies in biopsy advancement and LNI operations frequency, this nomogram can adjust to these differences with a slight loss of accuracy. It follows that the nomogram's overall accuracy can be expected to remain similar, even if the target population differs from the original cohort. However, differences indicate that the initially optimal cut-off value will not be ideal for other cohorts.

We analysed many different potential cut-off values, comparing them with the results obtained by Briganti's team, to determine the best one for our cohort. In the original series, a threshold of 5% was adopted. In the studied group, the value that separates patients in whom ePLND should be performed from patients in whom ePLND should be omitted is 7%. This value is the optimal compromise between the number of avoided ePLNDs (42.8% of all patients) compared to the number of missed LNI patients. (18.9% of all LNI patients) [38]. Alternatively, using the proposed initial 5% cut-off, we would have to perform ePLND on a much larger number of men (66.3% vs. 57.2%), and only a small number of patients with LNI would benefit from it (false negative 17% vs. 19%). Despite our choice of a cut-off value of 7%, different sites may choose a different cut-off point that is optimal for their cohort. If the acceptable compromise between the number of ePLNDs performed and the missed LNIs is considered too high, a lower cut-off should be chosen. Conversely, a higher cut-off value may be considered when dealing with a population of patients with better prognostic characteristics and a less malignant course.

The study's overall accuracy is one of the few critical benchmarks in the predictive tool. Calibration or correlation between predicted and observed indicators represents another key volatility. In particular, the first one shows the operation of the prognostic tool for a specific risk group in the studied population. In the key range of values, it can assess, in detail, the relationship between the observed LNI risk and the predicted one using the nomogram. This range is 0–10%, and within its range, there should be a cut-off point at which ePLND will not be performed. More than 10% of specialists, based on the patient's clinical picture, would be inclined to perform this procedure. Therefore, the nomogram's proper calibration is the most essential for this key cut-off range. It includes the grey area of the uncertainty of the need to perform the ePLND. It is noteworthy that the nomogram's

calibration was not perfect and revealed an overestimation in terms of the predicted LNI probability. It was insignificant, which indicates the predictive stability of LNI occurrence using this nomogram. This discovery requires meticulous consideration, indicating the appropriate cut-off value. Therefore, it is essential to remember and carefully analyse the potential source of a possible error and be cautious when making final clinical decisions.

Despite its value, our study is not without limitations. First of all, the population compared to external validation in this study was smaller than in the development cohort of the updated LNI nomogram, which includes patients admitted to one Polish tertiary centre. As discussed earlier, validations from numerous institutions, preferably international, could lead to obtain more generalized conclusions. The previous analysis of the multi-institutional cohort, showed significant differences in accuracy between the various external validations [39]. Nevertheless, there may be problems with the data from many institutions, especially in predicting LNI, before lymphadenectomy. It is important to mention that, despite the known perception of performing ePLND instead of PLND, the standards or scope of this procedure can be different [10].

Furthermore, due to the scientific development on PLND over the years, the calendar year of the operation performed may affect the number of lymph nodes collected [40]. Surgical methods can also vary (open prostatectomy vs. laparoscopic prostatectomy), which is relevant for drawing conclusions [41,42]. Even though every surgeon decided on the same ePLND scope, differences in lymph node detection can still be noticed as a result of various operation methods or specialist's experience [43].

There may also be differences with the templates that were used in ePLND. Mattei and colleagues carefully checked the prostate's primary lymphatic landing site, founding that only 63% of the lymph nodes will be removed during classical ePLND [44]. In addition to this extent, a resection of the lymph nodes alongside the common iliac arteries to the crossing of the ureter could improve the percentage to 75%. Consequently, another external validation may result in different estimated accuracy. Moreover, patients were somehow pre-selected for ePLND before RP due to the previous nomogram. Despite this fact, the updated nomogram can still be verified in the current patient cohort. Lastly, our study's retrospective character is another limitation that may have impacted the results.

6. Conclusions

In conclusion, the external validation of the Briganti nomogram on the Polish cohort shows good accuracy and precise calibration. The cut-off value of the data calculated by the nomogram was optimized to 7%, giving better results than the proposed threshold of 5%. Additional external validation studies should be performed, and the predictive value adjusted to the local cohort.

Author Contributions: Conceptualization, B.M. and K.K.; methodology, B.M., P.K. and K.W.; software, K.D. and K.P.; validation, B.M., K.K. and A.G.; formal analysis, B.M., K.P. and K.D.; investigation, B.M. and P.K.; resources, B.M. and K.W.; data curation, K.K., A.G. and K.W.; writing—original draft preparation, B.M., K.K. and A.G.; Writing—Review and editing, B.M., R.Z.; visualization, A.G.; supervision, R.Z.; project administration, B.M.; funding acquisition, B.M. and K.P. All authors have read and agreed to the published version of the manuscript.

Funding: This research has been supported by a research grants from the Wrocław Medical University (STM.E060.20.132 and SUB.C090.21.045).

Institutional Review Board Statement: This retrospective study was conducted in agreement with the declaration of Helsinki of 1975, revised in 2013 and approved by the Ethics Committee of Wrocław Medical University (KB/545/2020). Regional Health authorities deleted from the database available for analysis any subject identifiers, aiming at maintaining data anonymity and confidentiality. Thus, none of the patients could be identified, either in this study or in the entire extracted database.

Informed Consent Statement: Due to the retrospective nature of this study and maintaining data anonymity and confidentiality, patient consent was waived.

Data Availability Statement: The datasets analysed are available from the corresponding author on reasonable request.

Conflicts of Interest: The authors declare no conflict of interest.

References




1. Rawla, P. Epidemiology of Prostate Cancer. *World J. Oncol.* **2019**, *10*, 63–89. [CrossRef] [PubMed]
2. Jassem, J.; Kordek, R. *Onkologia*; Via Medica: Gdansk, Poland, 2019.
3. D’Amico, A.V.; Whittington, R.; Bruce Malkowicz, S.; Schultz, D.; Blank, K.; Broderick, G.A.; Tomaszewski, J.E.; Renshaw, A.A.; Kaplan, I.; Beard, C.J.; et al. Biochemical outcome after radical prostatectomy, external beam radiation therapy, or interstitial radiation therapy for clinically localized prostate cancer. *J. Am. Med. Assoc.* **1998**, *280*, 969–974. [CrossRef] [PubMed]
4. Wilt, T.J.; Brawer, M.K.; Jones, K.M.; Barry, M.J.; Aronson, W.J.; Fox, S.; Gingrich, J.R.; Wei, J.T.; Gilhooly, P.; Grob, B.M.; et al. Radical Prostatectomy versus Observation for Localized Prostate Cancer. *N. Engl. J. Med.* **2012**, *367*, 203–213. [CrossRef]
5. Bill-Axelsson, A.; Holmberg, L.; Ruutu, M.; Garmo, H.; Stark, J.R.; Busch, C.; Nordling, S.; Häggman, M.; Andersson, S.O.; Bratell, S.; et al. Re: Radical prostatectomy versus watchful waiting in early prostate cancer. *J. Urol.* **2011**, *186*, 1708–1717. [CrossRef]
6. Mottet, N.; van den Bergh, R.C.N.; Briers, E.; Van den Broeck, T.; Cumberbatch, M.G.; De Santis, M.; Fanti, S.; Fossati, N.; Gandaglia, G.; Gillessen, S.; et al. EAU-EANM-ESTRO-ESUR-SIOG Guidelines on Prostate Cancer—2020 Update. Part 1: Screening, Diagnosis, and Local Treatment with Curative Intent. *Eur. Urol.* **2021**, *79*, 243–262. [CrossRef] [PubMed]
7. Burkhard, F.C.; Studer, U.E. The role of lymphadenectomy in high risk prostate cancer. *World J. Urol.* **2008**, *26*, 231–236. [CrossRef] [PubMed]
8. Masterson, T.A.; Bianco, F.J.; Vickers, A.J.; Diblasio, C.J.; Fearn, P.A.; Rabbani, F.; Eastham, J.A.; Scardino, P.T. The association between total and positive lymph node counts, and disease progression in clinically localized prostate cancer. *J. Urol.* **2006**, *175*, 1320–1325. [CrossRef]
9. Touijer, K.; Rabbani, F.; Otero, J.R.; Secin, F.P.; Eastham, J.A.; Scardino, P.T.; Guillonneau, B. Standard Versus Limited Pelvic Lymph Node Dissection for Prostate Cancer in Patients with a Predicted Probability of Nodal Metastasis Greater Than 1%. *J. Urol.* **2007**, *178*, 120–124. [CrossRef]
10. Briganti, A.; Blute, M.L.; Eastham, J.H.; Graefen, M.; Heidenreich, A.; Karnes, J.R.; Montorsi, F.; Studer, U.E. Pelvic Lymph Node Dissection in Prostate Cancer. *Eur. Urol.* **2009**, *55*, 1251–1265. [CrossRef]
11. Briganti, A.; Chun, F.K.H.; Salonia, A.; Zanni, G.; Scattoni, V.; Valiquette, L.; Rigatti, P.; Montorsi, F.; Karakiewicz, P.I. Validation of a Nomogram Predicting the Probability of Lymph Node Invasion among Patients Undergoing Radical Prostatectomy and an Extended Pelvic Lymphadenectomy. *Eur. Urol.* **2006**, *49*, 1019–1026. [CrossRef]
12. Walz, J.; Bladou, F.; Rousseau, B.; Laroche, J.; Salem, N.; Gravis, G.; Briganti, A.; Chun, F.K.H.; Karakiewicz, P.I.; Fournier, G. Head to head comparison of nomograms predicting probability of lymph node invasion of prostate cancer in patients undergoing extended pelvic lymph node dissection. *Urology* **2012**, *79*, 546–551. [CrossRef] [PubMed]
13. Shariat, S.F.; Karakiewicz, P.I.; Suardi, N.; Kattan, M.W. Comparison of nomograms with other methods for predicting outcomes in prostate cancer: A critical analysis of the literature. *Clin. Cancer Res.* **2008**, *14*, 4400–4407. [CrossRef] [PubMed]
14. Kattan, M.W. Factors affecting the accuracy of prediction models limit the comparison of rival prediction models when applied to separate data sets. *Eur. Urol.* **2011**, *59*, 566–567. [CrossRef] [PubMed]
15. Budäus, L.; Spethmann, J.; Isbarn, H.; Schmitges, J.; Beesch, L.; Haese, A.; Salomon, G.; Schlomm, T.; Fisch, M.; Heinzer, H.; et al. Inverse stage migration in patients undergoing radical prostatectomy: Results of 8916 European patients treated within the last decade. *BJU Int.* **2011**, *108*, 1256–1261. [CrossRef]
16. Gallina, A.; Chun, F.K.H.; Suardi, N.; Eastham, J.A.; Perrotte, P.; Graefen, M.; Hutterer, G.; Huland, H.; Klein, E.A.; Reuther, A.; et al. Comparison of stage migration patterns between Europe and the USA: An analysis of 11 350 men treated with radical prostatectomy for prostate cancer. *BJU Int.* **2008**, *101*, 1513–1518. [CrossRef]
17. Venclovas, Z.; Muilwijk, T.; Matjosaitis, A.J.; Jievaltas, M.; Joniau, S.; Milonas, D. Head-to-Head Comparison of Two Nomograms Predicting Probability of Lymph Node Invasion in Prostate Cancer and the Therapeutic Impact of Higher Nomogram Threshold. *J. Clin. Med.* **2021**, *10*, 999. [CrossRef]
18. Brierley, J.D.; Gospodarowicz, M.K.; Wittekind, C. *TNM Classification of Malignant Tumours, 8th ed*; The Union for International Cancer Control: Geneva, Switzerland, 2017.
19. Epstein, J.I.; Egevad, L.; Amin, M.B.; Delahunt, B.; Srigley, J.R.; Humphrey, P.A. The 2014 international society of urological pathology (ISUP) consensus conference on gleason grading of prostatic carcinoma definition of grading patterns and proposal for a new grading system. *Am. J. Surg. Pathol.* **2016**, *40*, 244–252. [CrossRef]
20. Gleason, D.F.; Mellinger, G.T.; Ardring, L.J. Prediction of prognosis for prostatic adenocarcinoma by combined histological grading and clinical staging. *J. Urol.* **1974**, *111*, 58–64. [CrossRef]
21. McNeal, J.E.; Redwine, E.A.; Freiha, F.S.; Stamey, T.A. Zonal distribution of prostatic adenocarcinoma. Correlation with histologic pattern and direction of spread. *Am. J. Surg. Pathol.* **1988**, *12*, 897–906. [CrossRef]
22. Greene, K.L.; Page, D.L.; Fleming, I.D. *AJCC Cancer Staging Manual*, 6th ed.; Springer: New York, NY, USA, 2002.

23. Briganti, A.; Joniau, S.; Gontero, P.; Abdollah, F.; Passoni, N.M.; Tombal, B.; Marchioro, G.; Kneitz, B.; Walz, J.; Frohneberg, D.; et al. Identifying the best candidate for radical prostatectomy among patients with high-risk prostate cancer. *Eur. Urol.* **2012**, *61*, 584–592. [CrossRef]
24. Steuber, T.; Schlomm, T.; Heinzer, H.; Zacharias, M.; Ahyai, S.; Chun, K.F.; Haese, A.; Klutmann, S.; Köllermann, J.; Sauter, G.; et al. [F18]-fluoroethylcholine combined in-line PET-CT scan for detection of lymph-node metastasis in high risk prostate cancer patients prior to radical prostatectomy: Preliminary results from a prospective histology-based study. *Eur. J. Cancer* **2010**, *46*, 449–455. [CrossRef]
25. Briganti, A.; Larcher, A.; Abdollah, F.; Capitanio, U.; Gallina, A.; Suardi, N.; Bianchi, M.; Sun, M.; Freschi, M.; Salonia, A.; et al. Updated nomogram predicting lymph node invasion in patients with prostate cancer undergoing extended pelvic lymph node dissection: The essential importance of percentage of positive cores. *Eur. Urol.* **2012**, *61*, 480–487. [CrossRef]
26. Heidenreich, A.; Bellmunt, J.; Bolla, M.; Joniau, S.; Mason, M.; Matveev, V.; Mottet, N.; Schmid, H.P.; Van Der Kwast, T.; Wiegel, T.; et al. EAU guidelines on prostate cancer. Part 1: Screening, diagnosis, and treatment of clinically localised disease. *Eur. Urol.* **2011**, *59*, 61–71. [CrossRef] [PubMed]
27. Barth, P.J.; Gerharz, E.W.; Ramaswamy, A.; Riedmiller, H. The influence of lymph node counts on the detection of pelvic lymph node metastasis in prostate cancer. *Pathol. Res. Pract.* **1999**, *195*, 633–636. [CrossRef]
28. Zheng, Y.; Gao, Y.; Cheng, Y.; Qi, F.; Zou, Q. Whether extended pelvic lymph node dissection should be performed in prostate cancer: The present evidence from a systematic review and meta-analysis. *Precis. Med. Sci.* **2020**, *9*, 23–30. [CrossRef]
29. Godoy, G.; Chong, K.T.; Cronin, A.; Vickers, A.; Laudone, V.; Touijer, K.; Guillonneau, B.; Eastham, J.A.; Scardino, P.T.; Coleman, J.A. Extent of pelvic lymph node dissection and the impact of standard template dissection on nomogram prediction of lymph node involvement. *Eur. Urol.* **2011**, *60*, 195–201. [CrossRef]
30. Eisenhauer, E.A.; Therasse, P.; Bogaerts, J.; Schwartz, L.H.; Sargent, D.; Ford, R.; Dancey, J.; Arbuck, S.; Gwyther, S.; Mooney, M.; et al. New response evaluation criteria in solid tumours: Revised RECIST guideline (version 1.1). *Eur. J. Cancer* **2009**, *45*, 228–247. [CrossRef]
31. Cagiannos, I.; Karakiewicz, P.; Eastham, J.A.; Otori, M.; Rabbani, F.; Gerigk, C.; Reuter, V.; Graefen, M.; Hammerer, P.G.; Erbersdobler, A.; et al. A preoperative nomogram identifying decreased risk of positive pelvic lymph nodes in patients with prostate cancer. *J. Urol.* **2003**, *170*, 1798–1803. [CrossRef] [PubMed]
32. Gandaglia, G.; Ploussard, G.; Valerio, M.; Mattei, A.; Fiori, C.; Fossati, N.; Stabile, A.; Beauval, J.B.; Malavaud, B.; Roumiguié, M.; et al. A Novel Nomogram to Identify Candidates for Extended Pelvic Lymph Node Dissection Among Patients with Clinically Localized Prostate Cancer Diagnosed with Magnetic Resonance Imaging-targeted and Systematic Biopsies. *Eur. Urol.* **2019**, *75*, 506–514. [CrossRef]
33. Fossati, N.; Willemsse, P.P.M.; Van den Broeck, T.; van den Bergh, R.C.N.; Yuan, C.Y.; Briers, E.; Bellmunt, J.; Bolla, M.; Cornford, P.; De Santis, M.; et al. The Benefits and Harms of Different Extents of Lymph Node Dissection During Radical Prostatectomy for Prostate Cancer: A Systematic Review. *Eur. Urol.* **2017**, *72*, 84–109. [CrossRef]
34. Fujimoto, N.; Shiota, M.; Tomisaki, I.; Minato, A.; Yahara, K. Reconsideration on clinical benefit of pelvic lymph node dissection during radical prostatectomy for clinically localized prostate cancer. *Urol. Int.* **2019**, *103*, 125–136. [CrossRef]
35. Di Pierro, G.B.; Grande, P.; Wirth, J.G.; Danuser, H.; Mattei, A. Extended pelvic lymph node dissection at the time of robot-assisted radical prostatectomy: Impact of surgical volume on efficacy and complications in a single-surgeon series. *J. Can. Urol. Assoc.* **2015**, *9*, 107–113. [CrossRef]
36. Diamand, R.; Oderda, M.; Albisinni, S.; Fourcade, A.; Fournier, G.; Benamran, D.; Iselin, C.; Fiard, G.; Descotes, J.L.; Assenmacher, G.; et al. External validation of the Briganti nomogram predicting lymph node invasion in patients with intermediate and high-risk prostate cancer diagnosed with magnetic resonance imaging-targeted and systematic biopsies: A European multicenter study. *Urol. Oncol. Semin. Orig. Investig.* **2020**, *38*, 847.e9–847.e16. [CrossRef]
37. Hansen, J.; Rink, M.; Bianchi, M.; Kluth, L.A.; Tian, Z.; Ahyai, S.A.; Shariat, S.F.; Briganti, A.; Steuber, T.; Fisch, M.; et al. External validation of the updated briganti nomogram to predict lymph node invasion in prostate cancer patients undergoing extended lymph node dissection. *Prostate* **2013**, *73*, 211–218. [CrossRef]
38. Mohler, J.; Armstrong, A.; Bahnson, R.; D’Amico, A. NCCN clinical practice guidelines in oncology: Prostate cancer. *J. Natl. Compr. Cancer Netw.* **2010**, *8*, 162–200. [CrossRef] [PubMed]
39. Chun, F.K.H.; Briganti, A.; Graefen, M.; Porter, C.; Montorsi, F.; Haese, A.; Scattoni, V.; Borden, L.; Steuber, T.; Salonia, A.; et al. Development and External Validation of an Extended Repeat Biopsy Nomogram. *J. Urol.* **2007**, *177*, 510–515. [CrossRef]
40. Mazzola, C.; Savage, C.; Ahallal, Y.; Reuter, V.E.; Eastham, J.A.; Scardino, P.T.; Guillonneau, B.; Touijer, K.A. Nodal counts during pelvic lymph node dissection for prostate cancer: An objective indicator of quality under the influence of very subjective factors. *BJU Int.* **2012**, *109*, 1323–1328. [CrossRef]
41. Feifer, A.H.; Elkin, E.B.; Lowrance, W.T.; Denton, B.; Jacks, L.; Yee, D.S.; Coleman, J.A.; Laudone, V.P.; Scardino, P.T.; Eastham, J.A. Temporal trends and predictors of pelvic lymph node dissection in open or minimally invasive radical prostatectomy. *Cancer* **2011**, *117*, 3933–3942. [CrossRef]
42. Prasad, S.M.; Keating, N.L.; Wang, Q.; Pashos, C.L.; Lipsitz, S.; Richie, J.P.; Hu, J.C. Variations in Surgeon Volume and Use of Pelvic Lymph Node Dissection with Open and Minimally Invasive Radical Prostatectomy. *Urology* **2008**, *72*, 652–653. [CrossRef]

43. Briganti, A.; Capitanio, U.; Chun, F.K.H.; Gallina, A.; Suardi, N.; Salonia, A.; Da Pozzo, L.F.; Colombo, R.; Di Girolamo, V.; Bertini, R.; et al. Impact of Surgical Volume on the Rate of Lymph Node Metastases in Patients Undergoing Radical Prostatectomy and Extended Pelvic Lymph Node Dissection for Clinically Localized Prostate Cancer. *Eur. Urol.* **2008**, *54*, 794–802. [CrossRef]
44. Mattei, A.; Fuechsel, F.G.; Bhatta Dhar, N.; Warncke, S.H.; Thalmann, G.N.; Krause, T.; Studer, U.E. The Template of the Primary Lymphatic Landing Sites of the Prostate Should Be Revisited: Results of a Multimodality Mapping Study. *Eur. Urol.* **2008**, *53*, 118–125. [CrossRef] [PubMed]

Article

Prostate Cancer Diagnostic Algorithm as a “Road Map” from the First Stratification of the Patient to the Final Treatment Decision

Hana Sedláčková ¹, Olga Dolejšová ¹, Milan Hora ¹, Jiří Ferda ², Ondřej Hes ³, Ondřej Topolčan ⁴, Radka Fuchsová ⁴ and Radek Kučera ^{4,5,*}

- ¹ Department of Urology, Faculty of Medicine in Pilsen, University Hospital, 305 99 Pilsen, Czech Republic; sedlackovah@fnplzen.cz (H.S.); dolejsovao@fnplzen.cz (O.D.); horam@fnplzen.cz (M.H.)
- ² Department of Medical Imaging, Faculty of Medicine in Pilsen, University Hospital, 304 60 Pilsen, Czech Republic; ferda@fnplzen.cz
- ³ Department of Pathology, Faculty of Medicine in Pilsen, University Hospital, 305 99 Pilsen, Czech Republic; HES@fnplzen.cz
- ⁴ Department of Immunochemistry Diagnostics, Faculty of Medicine in Pilsen, University Hospital, 305 99 Pilsen, Czech Republic; topolcan@fnplzen.cz (O.T.); fuchsovar@fnplzen.cz (R.F.)
- ⁵ Institute of Pharmacology and Toxicology, Medical Faculty in Pilsen, Charles University, 304 60 Pilsen, Czech Republic
- * Correspondence: KUCERAR@fnplzen.cz; Tel.: +420-603456958

Citation: Sedláčková, H.; Dolejšová, O.; Hora, M.; Ferda, J.; Hes, O.; Topolčan, O.; Fuchsová, R.; Kučera, R. Prostate Cancer Diagnostic Algorithm as a “Road Map” from the First Stratification of the Patient to the Final Treatment Decision. *Life* **2021**, *11*, 324. <https://doi.org/10.3390/life11040324>

Academic Editors: David Mann and Ana Faustino

Received: 28 February 2021

Accepted: 6 April 2021

Published: 7 April 2021

Publisher’s Note: MDPI stays neutral with regard to jurisdictional claims in published maps and institutional affiliations.



Copyright: © 2021 by the authors. Licensee MDPI, Basel, Switzerland. This article is an open access article distributed under the terms and conditions of the Creative Commons Attribution (CC BY) license (<https://creativecommons.org/licenses/by/4.0/>).

Abstract: The diagnostics of prostate cancer are currently based on three pillars: prostate biomarker panel, imaging techniques, and histological verification. This paper presents a diagnostic algorithm that can serve as a “road map”: from initial patient stratification to the final decision regarding treatment. The algorithm is based on a review of the current literature combined with our own experience. Diagnostic algorithms are a feature of an advanced healthcare system in which all steps are consciously coordinated and optimized to ensure the proper individualization of the treatment process. The prostate cancer diagnostic algorithm was created using the prostate specific antigen and in particular the Prostate Health Index in the first line of patient stratification. It then continued on the diagnostic pathway via imaging techniques, biopsy, or active surveillance, and then on to the treatment decision itself. In conclusion, the prostate cancer diagnostic algorithm presented here is a functional tool for initial patient stratification, comprehensive staging, and aggressiveness assessment. Above all, emphasis is placed on the use of the Prostate Health Index (PHI) in the first stratification of the patients as a predictor of aggressiveness and clinical stage of prostate cancer (PCa). The inclusion of PHI in the algorithm significantly increases the accuracy and speed of the diagnostic procedure and allows to choose the optimal pathway just from the beginning. The use of advanced diagnostic techniques allows us to move towards a more advanced level of cancer care. This diagnostics algorithm has become a standard of care in our hospital. The algorithm is continuously validated and modified based on our results.

Keywords: prostate cancer; diagnostic algorithm; prostate health index; biopsy; Gleason score; magnetic resonance; positron emission tomography; diagnosis; imaging; prostate-specific membrane antigen

1. Introduction

Prostate cancer (PCa) is the most frequent malignant disease to occur in men. According to The International Agency for Research on Cancer (IARC), 1,414,259 new cases of PCa were reported and 375,304 men died of PCa worldwide in 2020 [1]. PCa’s incidence and mortality are connected to the human development index (HDI). The disease is most prevalent in developed countries, while its mortality rate is highest in low-HDI countries [2]. The risk of PCa increases with age. The majority of PCa cases are diagnosed

in men older than 65 [3]. PCa is a highly heterogeneous disease, ranging from a clinically insignificant manifestation that requires only active surveillance, to a highly aggressive castration-resistant type of tumor that requires a quick and radical course of action. Differences in the incidence rate of PCa worldwide primarily reflect differences in the use of diagnostic testing. Accurate diagnostics and PCa staging are imperative for the selection of the most appropriate therapeutic strategy [4].

The diagnostics of PCa are currently based on three pillars: prostate biomarker panel, imaging techniques, and histological verification. This paper presents a diagnostic algorithm that can serve as a “road map” delineating the course of treatment: from initial patient stratification to the final decision regarding treatment. The algorithm is based on a review of the current literature combined with our own experience.

2. Diagnostic Algorithm

2.1. PCa Diagnostic Algorithm—A Tool for Patient Stratification, Staging and Aggressiveness Assessment

The first algorithm was created a few years ago. Since then, the algorithm has been supplemented every year with new knowledge and new diagnostic procedures introduced into clinical practice. This was done to ensure that the algorithm continues to reflect the most current procedures that are applied in our university hospital.

Diagnostic algorithms are a feature of an advanced healthcare system in which all steps are consciously coordinated and optimized to ensure the proper individualization of the treatment process. The PCa diagnostic algorithm was created using the prostate specific antigen (PSA) and in particular the Prostate Health Index (PHI) in the first line of patient stratification. It then continued on the diagnostic pathway via imaging techniques, biopsy, or active surveillance, and then on to the treatment decision itself (Figure 1).

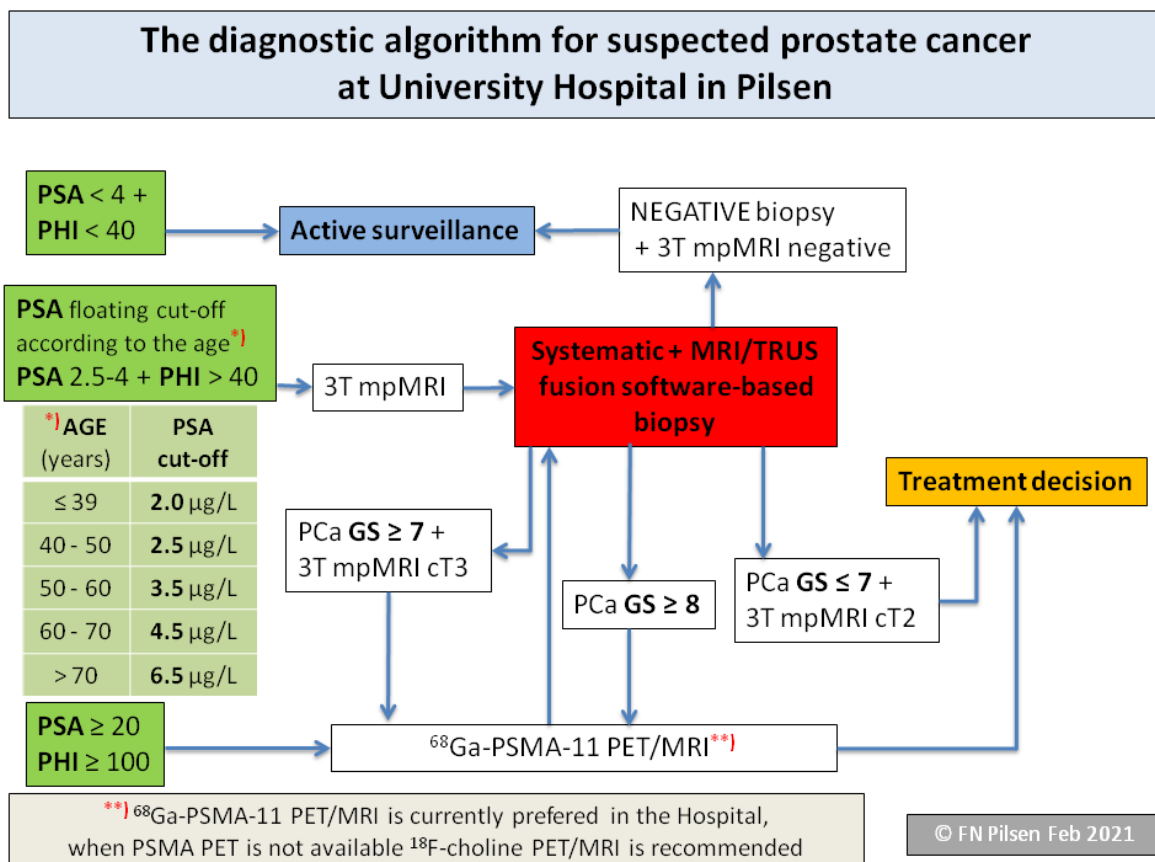


Figure 1. Prostate cancer diagnostic algorithm.

The first step is to have patients stratified into three groups according to PSA and PHI levels. If the PSA and PHI levels are low, patients are rated as benign: they will still be monitored and will be tested again, usually after six months.

If the level of PSA is above the reference ranges for the patient's age group, and/or the PHI level is over 40, the second step is to perform imaging techniques. We use multi-parametric magnetic resonance imaging (mpMRI) to localize the lesion, but also to evaluate a more detailed anatomy before surgery. We performed ^{68}Ga -PSMA-11 PET/MRI as part of the comprehensive staging in a selected group of patients before radical prostatectomy, as well as in primary diagnostics before histological verification. This is done in cases where there is a strong suspicion that the patient has a high-risk of developing PCa, or has locally advanced PCa and the extensive staging leads to a change in treatment management. In the middle of the algorithm, the current status of the PCa is proved using biopsy, in order to achieve that each patient with suspected PCa undergoes an mpMRI.

The biopsy holds a key position located in the middle of the algorithm. In order to achieve the best results in histological verification of significant PCa, we perform an MRI/transrectal ultrasound-guided (TRUS) fusion software-based targeted biopsy of the prostate. If the man is biopsy naïve, an additional systematic biopsy will be performed to determine the extent of the tumor and to help in planning the surgery–nerve sparing or not.

Finally, at the end of the algorithm, a treatment decision is made. Based on the results of histology, evaluated using the Gleason score and the imaging examinations, the appropriate method of treatment is selected according to the stage of the disease. As a relatively new approach, active surveillance is also incorporated into the algorithm.

2.2. The Algorithm Is Based on Our Experience, Results and Knowledge

It has been our experience that the value of PHI level can be used for validation in patients after radical prostatectomy. A total of 787 patients were examined and subsequently operated from 1/2013 to 12/2019. A definitive Gleason score was determined. PHI values were compared with definitive staging and grading. The study confirmed a very good ability of PHI to distinguish $\text{GS} < 7$ (low aggressiveness) and $\text{GS} \geq 7$ (higher aggressiveness) prostate tumors and thus, PHI was added to the first line of biochemical assessment of the tumor aggressiveness [5].

We have performed 3T mpMRI to detect PCa lesions as a standard method from 2012. This step also decreases the over diagnosis of PCa. From 1/2018 to 2/2020, 150 patients underwent ^{68}Ga -PSMA-11 PET/MRI as part of comprehensive staging; this examination is the only one under the clinical trial in our country.

Magnetic resonance imaging and targeted biopsy (MRI/TBx) were performed from 1/2017 to 12/2019 in the examination of 450 patients.

2.3. PHI as a Tool for the First (Initial) Stratification of the Patient

PCa diagnostics using biomarkers started in the 1980s with the total PSA (tPSA) measurement. Total PSA has a limited sensitivity and specificity for PCa detection [6]. Seeking better sensitivity and specificity, free PSA (fPSA) was introduced and then (2)proPSA. These developments enabled physicians not only to start using biomarkers, but also to calculate parameters; namely, the percentage of fPSA ($\% \text{freePSA} = (\text{fPSA}/\text{tPSA}) * 100$) and Prostate Health Index, PHI ($\text{PHI} = (([-2])\text{proPSA}/\text{fPSA}) \times \sqrt{\text{tPSA}}$). These parameters, PHI especially, contributed to PCa aggressiveness assessment using biochemical methods [7]. One of the largest recent studies carried out by PROMETHEUS, a Multicentric European Study, confirmed PHI as one of the strongest predictors of PCa, correlating with the Gleason Score (GS). In our own studies, firstly monocentric [5,8] and later on multicentric (with our partners) [9,10], we proved the PHI's ability to distinguish between PCa $\text{GS} < 7$ (low aggressiveness) and $\text{GS} \geq 7$ (higher aggressiveness).

2.4. The Key Role of Imaging Techniques in Staging and Surgical Navigation

A pathway with mpMRI combining T2-weighted, dynamic contrast-enhanced (DCE) and diffusion weighted imaging (DWI) has been shown to be accurate in significant PCa. Prostate anatomy is best assessed by T1 and T2 weighted images, with the DCE and DWI contributing functional information. There is also evidence that mpMRI tends to detect higher risk disease, which makes it attractive as a potential triage test [11]. mpMRI in the diagnostics of PCa is very often used for its high sensitivity and specificity. Sensitivity increases especially with tumor size and aggressiveness. The results are excellent, especially for significant tumors: tumor volume ≥ 0.5 mL or GS ≥ 7 [12]. Imaging with mpMRI plays two roles in PCa diagnostics. Firstly, it functions as a secondary screening test, exempting men with nonsuspicious tests from biopsy. MRI reduced the need for biopsy by 68% in men with PSA 3.0 $\mu\text{g/L}$. The second function of MRI is to provide an image of the lesion(s), so that sampling can be more precise [11].

As part of the unification of the MRI description, the European Society for Uroradiology (ESUR) introduced the PI-RADS (Prostate imaging reporting and data system) classification system. This prostate sector diagram employs forty-one sectors/regions: thirty-eight for the prostate, two for the seminal vesicles and one for the external urethral sphincter [13,14].

PET/CT with radiolabeled choline analogs is widely used in clinical practice for prostate cancer staging. ^{18}F -fluoroethylcholine PET demonstrated higher accuracy than MRI for the detection of primary prostate cancer; specificity was however limited by choline uptake in benign lesions [15]. Since 2012, ^{18}F - and ^{68}Ga -labeled inhibitors of prostate-specific membrane antigen (PSMA) entered early clinical development for PET imaging of PCa and showed immediate promise for sensitive and specific identification of local and distant sites of disease [16,17]. Results from ^{68}Ga -PSMA-11 PET/MRI and PET/CT in Figures 2–4. To summarize, according to the available systematic reviews and clinical trials, the sensitivity and specificity in primary staging of PCa using PSMA ligands is usually above 40% and over 85%, respectively. The impact on therapy planning was also investigated, performing PET/CT or, less frequently, PET/MRI using PSMA ligands, the therapeutic procedure changes in approximately 21% of patients in the primary staging [18,19].

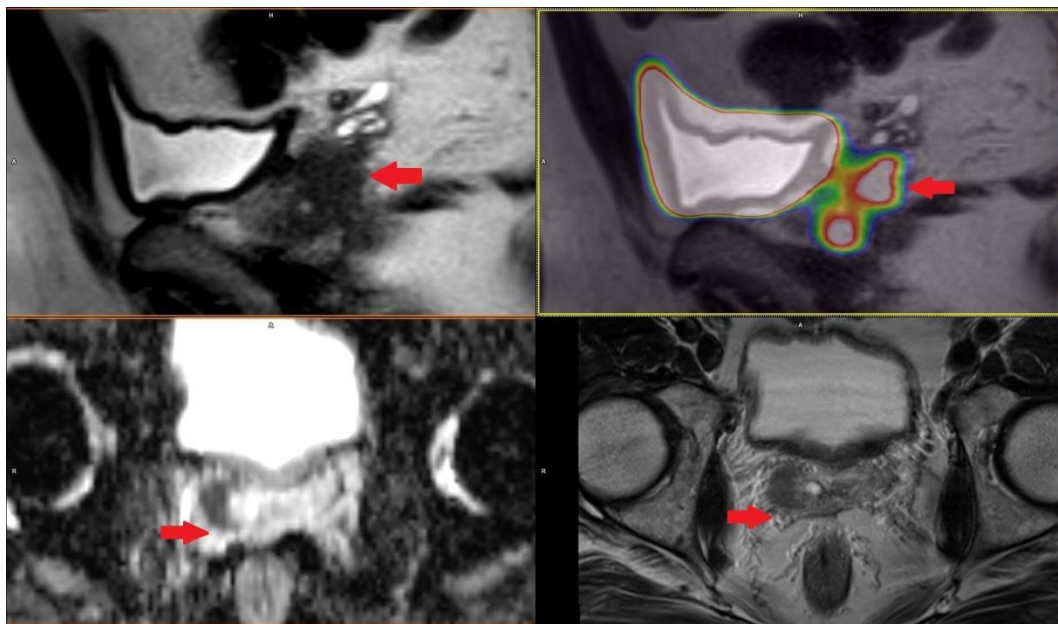


Figure 2. Patient with prostate cancer GS 7 (4 + 3) in right lobe with right seminal vesicle invasion cT3b iPSA 4.17 PHI 64.93 in ^{68}Ga -PSMA-11 PET/MRI.



Figure 3. Patient with lymph nodes metastases in prostate cancer GS 9 (4 + 5) iPSA 22.85 PHI 130.63 in [^{68}Ga]-PSMA-11 PET/MRI.

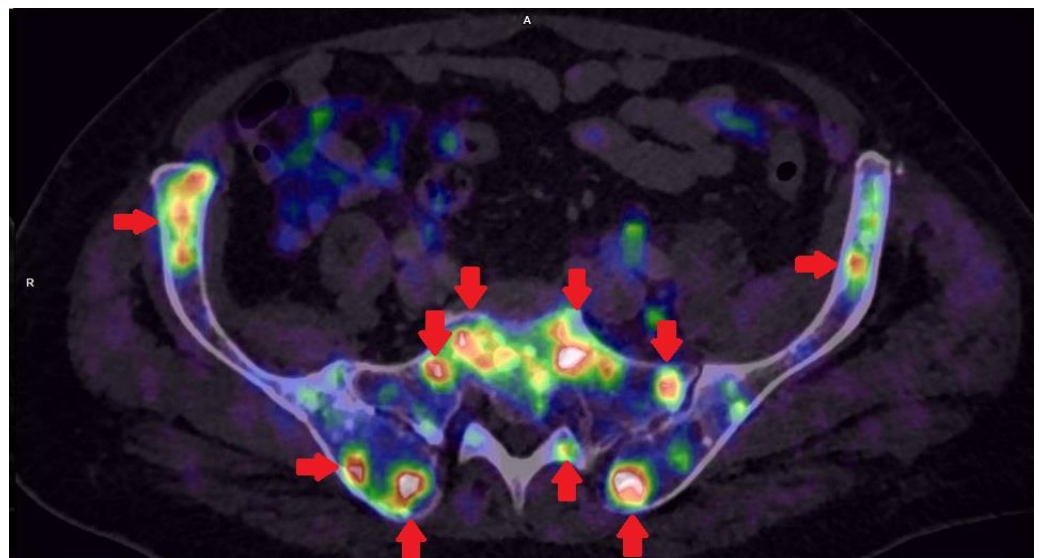


Figure 4. Patient with multiple bones metastases in prostate cancer GS 8 (4 + 4) iPSA 45.33 PHI 176.8 in [^{68}Ga]-PSMA-11 PET/CT.

2.5. The Basic Role of the Biopsy in Tumor Aggressiveness Assessment

A necessary condition for the initiation of PCa therapy is PCa histological verification using biopsy. The transrectal ultrasound (TRUS) navigated biopsy is used as a basic procedure [20]. The second option is the cognitive biopsy in which the result of the imaging technique, most often mpMRI, is known. Currently, the preferred procedure is the fusion biopsy, where images from mpMRI and TRUS are merged by software [20,21]. MRI information can be used to guide prostate biopsy cores, especially MRI/TRUS fusion software-based targeted biopsy of the prostate (MRI-TBx) to suspicious areas in the prostate. MRI-TBx has a higher detection rate for significant PCa and a lower detection rate for insignificant PCa compared with T-Bx [22]. Nonetheless, some lesions might also be missed on MRI-guided biopsies and these are the patients who pose a diagnostic challenge. With the introduction of ^{68}Ga -PSMA, ligands which exhibit almost exclusive expression in the prostate and increased expression in PCa are more often detected [23]. PSMA-PET/MRI in combination with a newly developed fusion biopsy system-PET/TRUS and PET/MRI/TRUS fusion-proved to be a valuable tool for the detection of PCa in patients following a prior negative prostate biopsy and is therefore attracting increasing attention [24].

Based on biopsies, the Gleason score (GS) has been used since the 1960s as the main grading system for PCa cell assessment. The GS ranges from 1 to 10 and was considered a main factor when a treatment plan was determined. This was the case until 2016 when the

International Society of Urological Pathology (ISUP) revised the PCa grading system and a new scale, the 5 ISUP Grades, was established [25].

2.6. Active Surveillance—A Suitable Procedure for Tumors with Low Aggressiveness

With more and more advanced diagnostic methods and increasingly accurate assessment of tumor aggressiveness, new approaches such as active surveillance can be applied instead of urgent surgery [26]. Active surveillance is an excellent example of how the medical paradigm has slowly changed during recent years. As aggressiveness is the main predictive factor for subsequent treatment management in the case of PCa, the main current task is to make precise and timely aggressiveness assessments [27]. Considering the side effects of radical prostatectomy (incontinence or sexual dysfunction), which is indicated in the case of highly aggressive PCa ($GS \geq 7$), active surveillance seems to be the suitable option for PCa with low aggressiveness ($GS < 7$).

3. Discussion

The above-described PCa diagnostic algorithm has a few limitations. One major difficulty may arise when using highly specific imaging methods with the latest radiotracers; these, however, are not widely available. Nonetheless, the algorithm was designed precisely with the aim of incorporating these state-of-the-art diagnostic methods and implementing them in clinical practice in order to achieve a clear indication.

Hybrid imaging using PET and MRI has been intentionally incorporated into the algorithm. MRI is perfect for the imaging of both the prostate, especially for targeted prostate biopsy, and for the detection of lymph node metastases. It has an irreplaceable role in preoperative lymph node staging. Having used the [^{68}Ga]-PSMA-11 as the latest radiotracer with very promising results, we believe that thus performed staging is highly specialized and yields the best results. [^{68}Ga]-labelled PSMA ligand could be superior to choline tracers in its ability to obtain high contrast. PSMA tracer can detect lesions characteristic of PCa with improved contrast when compared to the standard [^{18}F]-fluoromethylcholine, especially at low PSA levels. A significant advantage of [^{68}Ga]-PSMA-11 is that lesions characteristic of lymph node metastases are frequently presented in very high contrast when compared to choline. The superior contrast in [^{68}Ga]-PSMA-11 has also been demonstrated in most skeletal metastases [28].

Due to the low availability of PET/MRI scanners, PET/CT can be used instead. When this is the case, however, we lose the possibility of using images for targeted prostate biopsy and we are forced to perform further examinations in the form of at least mpMRI of the prostate, which delays further treatment decisions and initiations. Furthermore, the hybrid imaging method PET/MRI has the advantage of a reduced radiation dose compared to PET/CT.

Even though the PSMA-PET scan has shown considerable early promise, its availability is limited and incurs considerable cost. Furthermore, since prostate cancer patients commonly undergo mpMRI of the prostate, there is the possibility of a one-stop staging modality in the form of a whole-body MRI (wb-MRI). According to EAU guidelines, wb-MRI is more sensitive than conventional imaging methods and is more sensitive than choline PET/CT in its detection of bone metastases. Nevertheless, choline PET/CT had the highest specificity for diagnostic evaluation [29]. Wb-MRI with DWI is an effective method for overall staging in PCa, as it can detect metastases in normal-sized lymph nodes and early intramedullary bone metastases before the appearance of cortical destruction or reactive processes [30]. The LOCATE trial designed to compare the detection of prostate cancer using conventional imaging methods with wb-MRI will certainly yield promising results [31]. Due to the fact that a whole-body MRI is not a standard imaging method in our hospital, this alternative is not applicable in our case. Currently, mpMRI is the standard method for prostate imaging and it plays an important role in the detection, targeted biopsy, local staging, and risk classification of prostate cancers. Many studies have compared the bi-parametric MRI imaging protocol consisting of T2-weighted imaging and

DWI with a standard multi-parametric imaging protocol for the detection of PCa. There is no significant difference regarding the detection of PCa [32–34].

Our hospital is committed to performing mpMRI. This is based on knowledge gained from experience: DCE can in some cases help detect prostate cancer in both PZ and TZ. It is sometimes referred to as a “backup” sequence, especially if DWI/ADC is degraded by artifacts [35]. In PI-RADS version 2.1, DCE is used to differentiate scores of 3 and 4 in the peripheral zone. If we have a DWI score of 3 and early saturation is present, the finding is upgraded to a score of 4, which may help achieve a more accurate aggressiveness classification and individualized treatment of prostate cancer [13].

4. Conclusions

The PCa diagnostic algorithm presented here is a functional tool for initial patient stratification, comprehensive staging and aggressiveness assessment.

The use of advanced diagnostic techniques allows us to move towards to a more advanced level of cancer care that is more beneficial for patients. This diagnostics algorithm has become a standard of care in our hospital. The algorithm is continuously validated and modified based on our results.

Author Contributions: Conceptualization, H.S. and O.D.; methodology, R.K.; resources, R.F.; data curation, J.F.; writing—original draft preparation, H.S.; writing—review and editing, O.H. and R.K.; visualization, H.S. and O.D.; supervision, O.T. and M.H. All authors have read and agreed to the published version of the manuscript.

Funding: Supported by Ministry of Health, Czech Republic—conceptual development of research organization (Faculty Hospital in Pilsen-FNPI, 00669806) and BBMRI-CZ: Biobank network—a versatile platform for the research of the etiopathogenesis of diseases CZ.02.1.01/0.0/0.0/16_013/0001674.

Institutional Review Board Statement: Not applicable.

Informed Consent Statement: Not applicable.

Conflicts of Interest: The authors declare no conflict of interest.

References








1. Database. Available online: <https://Gco.Iarc.Fr/Today/Data/Factsheets/Cancers/27-Prostate-Fact-Sheet.Pdf> (accessed on 30 January 2020).
2. Kucera, R.; Pecan, L.; Topolcan, O.; Dahal, A.R.; Costigliola, V.; Giordano, F.A.; Golubnitschaja, O. Prostate Cancer Management: Long-Term Beliefs, Epidemic Developments in the Early Twenty-First Century and 3PM Dimensional Solutions. *EPMA J.* **2020**, *11*, 399–418. [CrossRef]
3. Catalona, W.J. Prostate Cancer Screening. *Med. Clin. N. Am.* **2018**, *102*, 199–214. [CrossRef] [PubMed]
4. Nevo, A.; Navaratnam, A.; Andrews, P. Prostate Cancer and the Role of Biomarkers. *Abdom. Radiol.* **2020**, *45*, 2120–2132. [CrossRef]
5. Dolejšova, O.; Kucera, R.; Fuchsova, R.; Topolcan, O.; Svobodova, H.; Hes, O.; Eret, V.; Pecan, L.; Hora, M. The Ability of Prostate Health Index (PHI) to Predict Gleason Score in Patients with Prostate Cancer and Discriminate Patients Between Gleason Score 6 and Gleason Score Higher Than 6—A Study on 320 Patients After Radical Prostatectomy. *Technol. Cancer Res. Treat.* **2018**, *17*, 153303381878737. [CrossRef]
6. Wilt, T.J.; Jones, K.M.; Barry, M.J.; Andriole, G.L.; Culkin, D.; Wheeler, T.; Aronson, W.J.; Brawer, M.K. Follow-up of Prostatectomy versus Observation for Early Prostate Cancer. *N. Engl. J. Med.* **2017**, *377*, 132–142. [CrossRef] [PubMed]
7. Maxeiner, A.; Kilic, E.; Matalon, J.; Friedersdorff, F.; Miller, K.; Jung, K.; Stephan, C.; Busch, J. The Prostate Health Index PHI Predicts Oncological Outcome and Biochemical Recurrence after Radical Prostatectomy—Analysis in 437 Patients. *Oncotarget* **2017**, *8*, 79279–79288. [CrossRef] [PubMed]
8. Ferda, J.; Ferdová, E.; Baxa, J.; Fínek, J.; Topolčan, O. ¹⁸F-Fluorocholine PET/MRI in Restaging of Prostatic Carcinoma in Relation to PSA Level and Detection of Active Disease. *Anticancer Res.* **2018**, *38*, 4139. [CrossRef]
9. Stejskal, J.; Adamcová, V.; Záleský, M.; Novák, V.; Čapoun, O.; Fiala, V.; Dolejšová, O.; Sedláčková, H.; Veselý, Š.; Zachoval, R. The Predictive Value of the Prostate Health Index vs. Multiparametric Magnetic Resonance Imaging for Prostate Cancer Diagnosis in Prostate Biopsy. *World J. Urol.* **2020**, 1–7. [CrossRef] [PubMed]
10. Novak, V.; Vesely, S.; Luksanová, H.; Prusa, R.; Capoun, O.; Fiala, V.; Dolejšová, O.; Sedlacková, H.; Kucera, R.; Stejskal, J.; et al. Preoperative Prostate Health Index Predicts Adverse Pathology and Gleason Score Upgrading after Radical Prostatectomy for Prostate Cancer. *BMC Urol.* **2020**, *20*, 144. [CrossRef]

11. Bergdahl, A.G.; Wilderäng, U.; Aus, G.; Carlsson, S.; Damber, J.-E.; Frånlund, M.; Geterud, K.; Khatami, A.; Socratous, A.; Stranne, J.; et al. Role of Magnetic Resonance Imaging in Prostate Cancer Screening: A Pilot Study within the Göteborg Randomised Screening Trial. *Eur. Urol.* **2016**, *70*, 566–573. [CrossRef] [PubMed]
12. Bratan, F.; Niaf, E.; Melodelima, C.; Chesnais, A.L.; Souchon, R.; Mège-Lechevallier, F.; Colombel, M.; Rouvière, O. Influence of Imaging and Histological Factors on Prostate Cancer Detection and Localisation on Multiparametric MRI: A Prospective Study. *Eur. Radiol.* **2013**, *23*, 2019–2029. [CrossRef]
13. Turkbey, B.; Rosenkrantz, A.B.; Haider, M.A.; Padhani, A.R.; Villeirs, G.; Macura, K.J.; Tempny, C.M.; Choyke, P.L.; Cornud, F.; Margolis, D.J.; et al. Prostate Imaging Reporting and Data System Version 2.1: 2019 Update of Prostate Imaging Reporting and Data System Version 2. *Eur. Urol.* **2019**, *76*, 340–351. [CrossRef]
14. Rowe, S.P.; Pienta, K.J.; Pomper, M.G.; Gorin, M.A. PSMA-RADS Version 1.0: A Step towards Standardizing the Interpretation and Reporting of PSMA-Targeted PET Imaging Studies. *Eur. Urol.* **2018**, *73*, 485–487. [CrossRef] [PubMed]
15. Giovacchini, G.; Giovannini, E.; Leoncini, R.; Riondato, M.; Ciarmiello, A. PET and PET/CT with Radiolabeled Choline in Prostate Cancer: A Critical Reappraisal of 20 Years of Clinical Studies. *Eur. J. Nucl. Med. Mol. Imaging* **2017**, *44*, 1751–1776. [CrossRef]
16. Rauscher, I.; Maurer, T.; Fendler, W.P.; Sommer, W.H.; Schwaiger, M.; Eiber, M. ⁶⁸Ga-PSMA Ligand PET/CT in Patients with Prostate Cancer: How We Review and Report. *Cancer Imaging* **2016**, *16*, 1–10. [CrossRef] [PubMed]
17. Fendler, W.P.; Schmidt, D.F.; Wenter, V.; Thierfelder, K.M.; Zach, C.; Stief, C.; Bartenstein, P.; Kirchner, T.; Gildehaus, F.J.; Gratzke, C.; et al. ⁶⁸Ga-PSMA-HBED-CC PET/CT Detects Location and Extent of Primary Prostate Cancer. *J. Nucl. Med.* **2016**, *57*, 1720–1725. [CrossRef] [PubMed]
18. Von Eyben, F.E.; Picchio, M.; von Eyben, R.; Rhee, H.; Bauman, G. ⁶⁸Ga-Labeled Prostate-Specific Membrane Antigen Ligand Positron Emission Tomography/Computed Tomography for Prostate Cancer: A Systematic Review and Meta-Analysis. *Eur. Urol. Focus* **2018**, *4*, 686–693. [CrossRef]
19. Roach, P.J.; Francis, R.; Emmett, L.; Hsiao, E.; Kneebone, A.; Hruby, G.; Eade, T.; Nguyen, Q.A.; Thompson, B.D.; Cusick, T.; et al. The Impact of ⁶⁸Ga-PSMA PET/CT on Management Intent in Prostate Cancer: Results of an Australian Prospective Multicenter Study. *J. Nucl. Med.* **2018**, *59*, 82–88. [CrossRef]
20. Ahmed, H.U.; El-Shater Bosaily, A.; Brown, L.C.; Gabe, R.; Kaplan, R.; Parmar, M.K.; Collaco-Moraes, Y.; Ward, K.; Hindley, R.G.; Freeman, A.; et al. Diagnostic Accuracy of Multi-Parametric MRI and TRUS Biopsy in Prostate Cancer (PROMIS): A Paired Validating Confirmatory Study. *Lancet* **2017**, *389*, 815–822. [CrossRef]
21. Kasivisvanathan, V.; Stabile, A.; Neves, J.B.; Giganti, F.; Valerio, M.; Shanmugabavan, Y.; Clement, K.D.; Sarkar, D.; Philippou, Y.; Thurtle, D.; et al. Magnetic Resonance Imaging-Targeted Biopsy Versus Systematic Biopsy in the Detection of Prostate Cancer: A Systematic Review and Meta-Analysis. *Eur. Urol.* **2019**, *76*, 284–303. [CrossRef]
22. Zettinig, O.; Shah, A.; Hennersperger, C.; Eiber, M.; Kroll, C.; Kübler, H.; Maurer, T.; Milletari, F.; Rackerseder, J.; Zu Berge, C.S.; et al. Multimodal Image-Guided Prostate Fusion Biopsy Based on Automatic Deformable Registration. *Int. J. Comput. Assist. Radiol. Surg.* **2015**, *10*, 1997–2007. [CrossRef]
23. Eiber, M.; Nekolla, S.G.; Maurer, T.; Weirich, G.; Wester, H.-J.; Schwaiger, M. ⁶⁸Ga-PSMA PET/MR with Multimodality Image Analysis for Primary Prostate Cancer. *Abdom. Imaging* **2015**, *40*, 1769–1771. [CrossRef] [PubMed]
24. Liu, C.; Liu, T.; Zhang, Z.; Zhang, N.; Du, P.; Yang, Y.; Liu, Y.; Yu, W.; Li, N.; Gorin, M.A.; et al. ⁶⁸Ga-PSMA PET/CT Combined with PET/Ultrasound-Guided Prostate Biopsy Can Diagnose Clinically Significant Prostate Cancer in Men with Previous Negative Biopsy Results. *J. Nucl. Med.* **2020**, *61*, 1314. [CrossRef] [PubMed]
25. Epstein, J.; Egevad, L.; Amin, M.; Delahunt, B.; Srigley, J.; Humphrey, P.; Al Hussain, T.; Algaba, F.; Aron, M.; Berman, D.; et al. The 2014 International Society of Urological Pathology (ISUP) Consensus Conference on Gleason Grading of Prostatic Carcinoma: Definition of Grading Patterns and Proposal for a New Grading System. *Am. J. Surg. Pathol.* **2016**, *40*, 244–252. [CrossRef]
26. Xu, J.; Bock, C.; Janisse, J.; Schwartz, K.L.; Triest, J.; Cher, M.L.; Goodman, M. Urologists' Perceptions of Active Surveillance and Their Recommendations for Low-Risk Prostate Cancer Patients. *Urology* **January 2021**, in press. [CrossRef]
27. Bul, M.; Zhu, X.; Valdagni, R.; Pickles, T.; Kakehi, Y.; Rannikko, A.; Bjartell, A.; van der Schoot, D.K.; Cornel, E.B.; Conti, G.N.; et al. Active Surveillance for Low-Risk Prostate Cancer Worldwide: The PRIAS Study. *Eur. Urol.* **2013**, *63*, 597–603. [CrossRef] [PubMed]
28. Afshar-Oromieh, A.; Zechmann, C.M.; Malcher, A.; Eder, M.; Eisenhut, M.; Linhart, H.G.; Holland-Letz, T.; Hadaschik, B.A.; Giesel, F.L.; Debus, J.; et al. Comparison of PET Imaging with a ⁶⁸Ga-Labelled PSMA Ligand and ¹⁸F-Choline-Based PET/CT for the Diagnosis of Recurrent Prostate Cancer. *Eur. J. Nucl. Med. Mol. Imaging* **2014**, *41*, 11–20. [CrossRef] [PubMed]
29. Mottet, N.; van den Bergh, R.C.N.; Briers, E.; Cornford, P.; De Santis, M.; Fanti, S.; Gillessen, S.; Grummet, J.; Henry, A.M.; Lam, T.B.; et al. EAU—ESTRO—ESUR—SIOG Guidelines on Prostate Cancer 2020. In *European Association of Urology Guidelines. 2020 Edition*; European Association of Urology Guidelines Office: Arnhem, The Netherlands, 2020.
30. Anttinen, M.; Ettala, O.; Malaspina, S.; Jambor, I.; Sandell, M.; Kajander, S.; Rinta-Kiikka, I.; Schildt, J.; Saukko, E.; Rautio, P.; et al. A Prospective Comparison of ¹⁸F-Prostate-Specific Membrane Antigen-1007 Positron Emission Tomography Computed Tomography, Whole-Body 1.5 T Magnetic Resonance Imaging with Diffusion-Weighted Imaging, and Single-Photon Emission Computed Tomography/Computed Tomography with Traditional Imaging in Primary Distant Metastasis Staging of Prostate Cancer (PROSTAGE). *Eur. Urol. Oncol.* **2020**, S2588931120300900. [CrossRef]

31. Adeleke, S.; Latifoltojar, A.; Sidhu, H.; Galazi, M.; Shah, T.T.; Clemente, J.; Davda, R.; Payne, H.A.; Chouhan, M.D.; Lioumi, M.; et al. Localising Occult Prostate Cancer Metastasis with Advanced Imaging Techniques (LOCATE Trial): A Prospective Cohort, Observational Diagnostic Accuracy Trial Investigating Whole-Body Magnetic Resonance Imaging in Radio-Recurrent Prostate Cancer. *BMC Med. Imaging* **2019**, *19*, 90. [CrossRef] [PubMed]
32. Campli, E.; Delli Pizzi, A.; Seccia, B.; Cianci, R.; d'Annibale, M.; Antonella, C.; Cinalli, S.; Castellan, P.; Navarra, R.; Iantorno, R.; et al. Diagnostic Accuracy of Biparametric vs Multiparametric MRI in Clinically Significant Prostate Cancer: Comparison between Readers with Different Experience. *Eur. J. Radiol.* **2018**, *101*, 17–23. [CrossRef]
33. Xu, L.; Zhang, G.; Shi, B.; Liu, Y.; Zou, T.; Yan, W.; Xiao, Y.; Xue, H.; Feng, F.; Lei, J.; et al. Comparison of Biparametric and Multiparametric MRI in the Diagnosis of Prostate Cancer. *Cancer Imaging* **2019**, *19*, 90. [CrossRef] [PubMed]
34. Alabousi, M.; Salameh, J.-P.; Gusenbauer, K.; Samoilov, L.; Jafri, A.; Yu, H.; Alabousi, A. Biparametric vs. Multiparametric Prostate Magnetic Resonance Imaging for the Detection of Prostate Cancer in Treatment-Naïve Patients: A Diagnostic Test Accuracy Systematic Review and Meta-Analysis. *BJU Int.* **2019**, *124*, 209–220. [CrossRef] [PubMed]
35. Pernický, J.; Tupý, R.; Cibulková, J.; Ferda, J. Changes in the prostate assessment using classification PI-RADS 2.1. *Ceska Radiol.* **2020**, *74*, 47–54.

Article

Long Noncoding RNA NEAT1 as a Potential Candidate Biomarker for Prostate Cancer

Diana Nitusca ¹, Anca Marcu ¹, Alis Dema ², Loredana Balacescu ³, Ovidiu Balacescu ³, Razvan Bardan ^{4,5}, Alin Adrian Cumpanas ^{4,5}, Ioan Ovidiu Sirbu ¹, Bogdan Petrut ⁶, Edward Seclaman ¹ and Catalin Marian ^{1,*}

¹ Department of Biochemistry and Pharmacology, “Victor Babeş” University of Medicine and Pharmacy, Pta Eftimie Murgu Nr. 2, 300041 Timișoara, Romania; nitusca.diana@umft.ro (D.N.); marcu.anca@umft.ro (A.M.); ovidiu.sirbu@umft.ro (I.O.S.); eseclaman@umft.ro (E.S.)

² Department of Pathology, “Victor Babeş” University of Medicine and Pharmacy, Pta Eftimie Murgu Nr. 2, 300041 Timișoara, Romania; dema.alis@umft.ro

³ Department of Genetics, Genomics and Experimental Pathology, The Oncology Institute “Prof. Dr. Ion Chiricuta”, 400015 Cluj-Napoca, Romania; lbalacescu@iocn.ro (L.B.); ovidiubalacescu@iocn.ro (O.B.)

⁴ Department of Urology, “Victor Babeş” University of Medicine and Pharmacy, Pta Eftimie Murgu Nr. 2, 300041 Timișoara, Romania; razvan.bardan@umft.ro (R.B.); cumpanas.alin@umft.ro (A.A.C.)

⁵ Urology Clinic, Timisoara Emergency County Hospital, 300723 Timisoara, Romania

⁶ Department of Urology, The Oncology Institute “Prof. Dr. Ion Chiricuta”, 400015 Cluj-Napoca, Romania; bogdan.petrut@umfluj.ro

* Correspondence: cmarian@umft.ro

Citation: Nitusca, D.; Marcu, A.; Dema, A.; Balacescu, L.; Balacescu, O.; Bardan, R.; Cumpanas, A.A.; Sirbu, I.O.; Petrut, B.; Seclaman, E.; et al. Long Noncoding RNA NEAT1 as a Potential Candidate Biomarker for Prostate Cancer. *Life* **2021**, *11*, 320. <https://doi.org/10.3390/life11040320>

Academic Editor: Ana Faustino and Paula A. Oliveira

Received: 18 March 2021

Accepted: 5 April 2021

Published: 6 April 2021

Publisher’s Note: MDPI stays neutral with regard to jurisdictional claims in published maps and institutional affiliations.

Abstract: *Background:* Prostate cancer (PCa) remains one of the leading causes of cancer-related mortality in men worldwide, mainly due to unsatisfactory diagnostic methods used at present, which lead to overdiagnosis, unnecessary biopsies and treatment, or misdiagnosis in early asymptomatic stages. New diagnostic biomarkers are needed for a correct and early diagnosis. Long noncoding RNAs (lncRNAs) have been broadly studied for their involvement in PCa biology, as well as for their potential role as diagnostic biomarkers. *Methods:* We conducted lncRNA profiling in plasma and microdissected formalin-fixed paraffin-embedded (FFPE) tissues of PCa patients and attempted validation for commonly dysregulated individual lncRNAs. *Results:* Plasma profiling revealed eight dysregulated lncRNAs, while microarray analysis revealed 717 significantly dysregulated lncRNAs, out of which only nuclear-enriched abundant transcript 1 (NEAT1) was commonly upregulated in plasma samples and FFPE tissues. NEAT1’s individual validation revealed statistically significant upregulation (FC = 2.101, $p = 0.009$). Receiver operating characteristic (ROC) analysis showed an area under the curve (AUC) value of 0.7298 for NEAT1 (95% CI = 0.5812–0.8785), suggesting a relatively high diagnostic value, thus having a potential biomarker role for this malignancy. *Conclusions:* We present herein data suggesting that NEAT1 could serve as a diagnostic biomarker for PCa. Additional studies of larger cohorts are needed to confirm our findings, as well as the oncogenic mechanism of NEAT1 in the development of PCa.

Keywords: prostate cancer; long noncoding RNA; NEAT1; laser capture microdissection



Copyright: © 2021 by the authors. Licensee MDPI, Basel, Switzerland. This article is an open access article distributed under the terms and conditions of the Creative Commons Attribution (CC BY) license (<https://creativecommons.org/licenses/by/4.0/>).

1. Introduction

Prostate cancer (PCa) currently represents one of the leading causes of cancer-related mortality among men worldwide [1], with an incidence rate of almost 60% over the age of 65 years [2]. Notwithstanding the great effort of the research field and the important contributions that modern medicine implemented over the past decades, the progress in reducing PCa mortality remains disputable to a certain extent [3].

The American Cancer Society predicts a total number of about 191,930 estimated new cases of PCa for 2020, with an increase of over 17,000 cases compared to the estimations of 2019 [4]. In addition, the mortality rate due to PCa is also expected to increase, with

33,330 estimated deaths in 2020 alone in the US, which surpasses the number of deaths from previous recent years. Worldwide statistics of PCa revealed that 3.8% of all deaths caused by cancer in men were due to PCa, with 358,989 deaths and 1,276,106 new cases in 2018 [5,6].

The high mortality rate could be at least partly explained due to the asymptomatic nature of PCa in the early stages, which leads to late diagnosis in most cases. Currently, several biomarkers are considered useful for PCa diagnosis and prognosis. However, only a few of them, such as prostate-specific antigen (PSA)-based, were Food and Drug Administration (FDA)-approved and used as PCa biomarkers in clinical use [7]. Nevertheless, even if PSA-based tests are useful for PCa diagnosis, due to their highly organ-specificity, PSA is not a cancer-specific biomarker, being also increased in benign prostatic hyperplasia (BPH) inflammation, body weight, lifestyle factors, or physical manipulation [8,9]. Consequently, the use of prostate-specific antigen (PSA) analysis, due to its low specificity for PCa, would adversely impact overdiagnosis, overtreatment, and unnecessary biopsies [10].

Therefore, the limitations of the diagnostic strategies that are currently used in matters of PCa require the identification of new approaches for novel diagnostic and prognostic biomarkers that could aid in the fine-tuning of conventional serum biomarkers [11]. The noninvasive liquid biopsy technique attempts to overcome the disadvantages and impediments of the current approaches, both for patient comfort and clinical utility [12]. DNA-, RNA-, and protein-based biomarkers represent promising candidates for future large-scale screenings, from which some already showed clinical relevance [13]. It is the case for prostate cancer antigen 3 (PCA3), a type of lncRNA, which outperformed PSA testing in matters of specificity [14].

lncRNAs are transcripts over 200 nucleotides in length, which are generally not translated into proteins [15]. They have shown to play different roles in physiology, such as development and differentiation, acting as transcription regulators. They function as enhancer RNAs, decoys, signals, guides in order to modulate transcription via chromatin remodeling, and sequestering regulatory factors [16,17]. Like other noncoding RNA species, lncRNAs are dysregulated in a vast number of medical conditions (i.e., psoriasis, Alzheimer's disease) and in cancer (breast cancer, colon cancer, PCa, etc.) [18–22]. They possess excellent features such as having specific prostate tissue expression and being localized to certain subcellular regions [23,24]. Moreover, various lncRNAs have shown to have a differential expression level compared to healthy controls (HCs), suggesting a likely diagnostic biomarker potential that could represent a novel, more optimized, and noninvasive approach for the diagnosis of PCa [25].

Herein, we performed lncRNA profiling in plasma and FFPE samples of PCa patients to analyze the lncRNA relative expression. We attempted to validate individual lncRNA NEAT1 as a diagnostic biomarker for PCa. Additionally, by using laser capture microdissection (LCM) as a valuable technology for limiting the heterogeneity from FFPE samples, we were capable of isolating only the desired areas of interest from a very diverse and heterogeneous tissue specimen.

2. Materials and Methods

2.1. Study Design

Our study design included a stage of lncRNA screening using both plasma and tissue samples, followed by two identification and validation stages on plasma samples. A flow-diagram representation of our study is shown in Figure 1.

Firstly, we conducted a lncRNA screening in plasma of 15 PCa patients and 15 healthy controls (HCs) and in 8 laser capture microdissected (LCM) FFPE tissues of PCa and adjacent normal tissues. Only NEAT1 was the commonly and significantly ($p < 0.05$) upregulated lncRNA among groups. It was further validated in an individual assay, consisting of the previous group of 15 patients with PCa and 15 HC plus an additional group of 37 PCa patients and 23 HC.

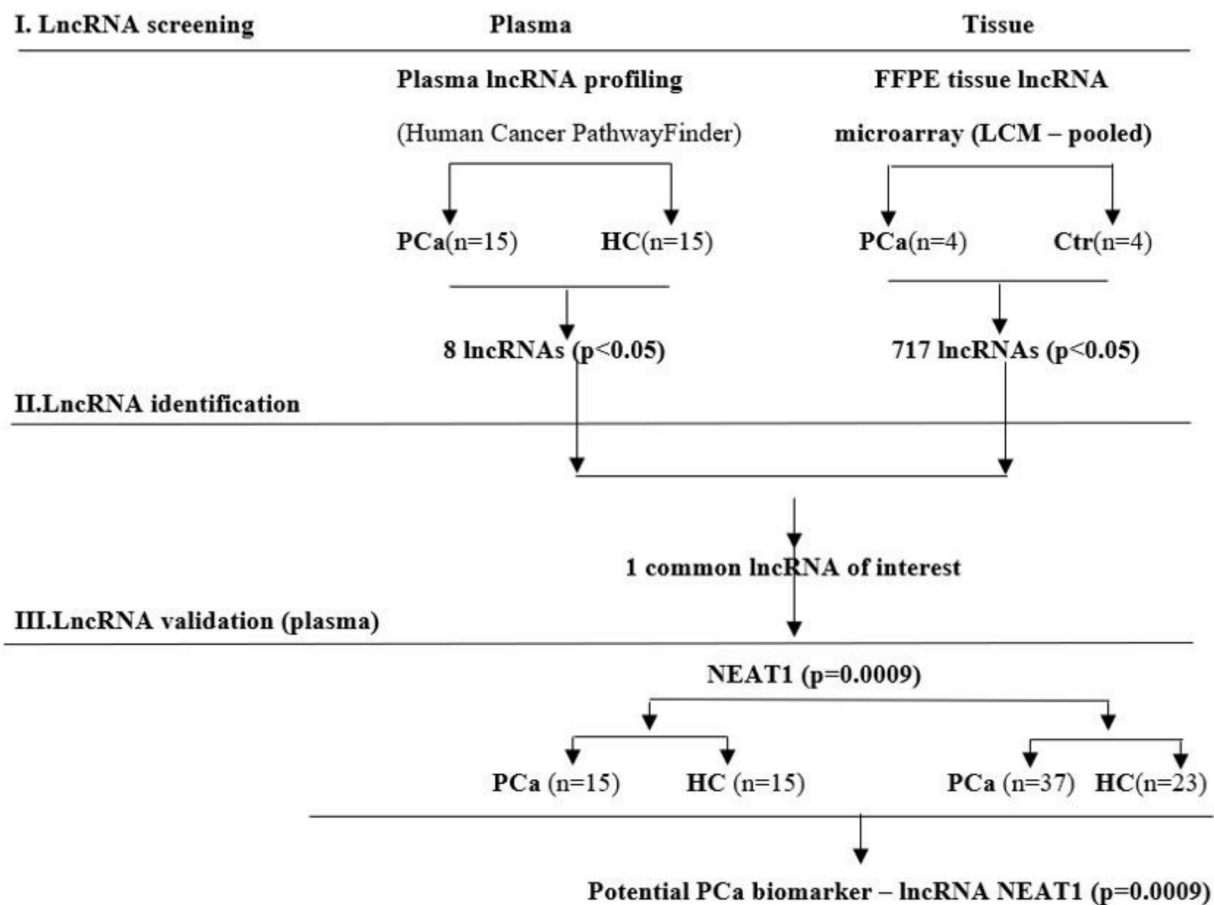


Figure 1. Flow-diagram of the study design used to screen, identify, and validate new lncRNA as prostate cancer (PCa) specific biomarkers.

Individual validation of NEAT1 was performed in two different groups of patients and controls, from two participating institutions: “Victor Babeş” University of Medicine and Pharmacy Timisoara (designated TM) and The Oncology Institute “Prof. Dr. Ion Chiricuta” (designated CJ).

2.2. Patients’ Characteristics and Plasma Samples

The biological samples (blood and tissues) used for screening stages were collected from the Urology Clinic of the Clinical Emergency County Hospital in Timisoara, Romania, while the plasma samples used for validation were provided by the Oncology Institute “Prof Dr. Ion Chiricuta” Cluj-Napoca. Patients admitted for the screening stage had undergone transrectal biopsies for histopathological diagnosis of PCa. Control samples were collected from healthy subjects, with no prostate disease, from the same hospital. All HCs had normal PSA levels (<4 ng/mL), verified by chemiluminescent microparticle immunoassay (Abbott Diagnostics, Chicago, IL, USA).

All subjects included in this study provided informed consent for the use of their biological samples. The study was approved by the Ethics Committee of the participating institutions, in accordance with the Declaration of Helsinki, and venous blood was collected in EDTA-containing tubes, as previously described [26]. Patients’ characteristics are briefly summarized in Table 1.

Table 1. Clinical and demographic characteristics of the subjects included in the study.

Characteristics	Training Lot		Validation Lot	
	Patients (n = 15)	Controls (n = 15)	Patients (n = 37)	Controls (n = 23)
Age (\pm SD)	67.2 (\pm 4.18)	51.3 (\pm 8.27)	65 (\pm 6.96)	58.2 (\pm 9.51)
PSA n (%)				
<4 ng/mL	0 (0.00)	15 (100.00)	2 (5.41%)	-
4–10 ng/mL	5 (33.33) *	0 (0.00)	20 (54.05 %)	-
\geq 10 ng/mL	9 (60.00) *	0 (0.00)	15 (40.54%)	-
Gleason score n (%)				
5–6	3 (20.00)		11 (29.7%)	
7	9 (60.00)		22 (59.4%)	
8–10	3 (20.00)		4 (10.9%)	

* Does not add up to 100% due to missing values.

2.3. Plasma lncRNA Screening

According to the manufacturer's instructions, total RNA was isolated from plasma using the miRNeasy Serum/Plasma Advanced Kit (Qiagen, Hilden, Germany). RNA concentration and quality were verified using a NanoDrop ND-1000 spectrophotometer (Thermo Fisher Scientific, Waltham, MA, USA). Reverse-transcription was performed using RT²-PreAMP cDNA Synthesis (Qiagen, Germany) to obtain the cDNA sequence, with a starting quantity of 60 ng RNA, according to the manufacturer's indications. cDNA was preamplified using specific primers, with the RT2 lncRNA PreAMP Primer Mix for Human Cancer PathwayFinder kit (Qiagen, Germany). Real-time PCR analysis for multiple lncRNAs was performed on a 7900 HT Real-Time PCR System (Thermo Fisher Scientific, USA), using RT2 lncRNA PCR Array Human Cancer PathwayFinder (Qiagen, Germany) combined with RT² SYBR Green qPCR Mastermix (Qiagen, Germany), for lncRNA profiling, following the manufacturer's protocol.

2.4. Plasma lncRNA Validation

Differentially expressed lncRNAs were further validated using TaqMan®Fast Advanced Master Mix (Thermo Fisher Scientific, USA) and specific primers. RNA was extracted from plasma using miRNeasy Serum/Plasma Advanced Kit (Qiagen, Germany), according to the manufacturer's instructions. Reverse-transcription was performed using SuperScript™ VILO™ cDNA Synthesis Kit (Thermo Fisher Scientific, USA). cDNA was subsequently used as a template in a Veriti 96-Well Thermal Cycler (Applied Biosystems, Foster, CA, USA) compatible with all kits used, following the manufacturer's suggestions. All samples were performed in triplicate.

2.5. lncRNA Analysis in FFPE Tissues

Eleven-year-old FFPE tissue samples of PCa from the Department of Pathology, University of Medicine and Pharmacy "Victor Babes" Timisoara, were sectioned (10 μ m in size), mounted on MMI RNase-free slides (MMI, Zurich, Switzerland), and microdissected using LCM technology, as previously described [26,27].

Total RNA was extracted from the tissue samples using miRNAeasy FFPE kit, with a melting protocol (Qiagen, Germany), according to the manufacturer's indications. Eight pooled tumor and normal adjacent samples, with enough RNA amount and good integrity evaluated by NanoDrop ND-1000 (Thermo Fischer Scientific, USA) and Agilent 2100 Bioanalyzer (Agilent Technologies, Santa Clara, CA, USA), were subjected to microarray analysis.

Each RNA sample (100 ng) was amplified and labeled with Cy3 using the Low Input Quick Amp Labeling Kit (Agilent Technologies). The Cy3-labeled cRNA probes were hybridized on SurePrint G3 Human GE v3 8 \times 60 K arrays (Agilent Technologies) for 17 h

at 65 °C. After washing, arrays were scanned with Agilent G2505C Microarray Scanner at 3 µm resolution and image files were processed with Agilent Feature Extraction software v. 11.5.1.1 (Agilent Technologies, Palo Alto, CA, USA).

2.6. Statistical Analysis

Results from the plasma lncRNA profiling step were analyzed using the statistical analysis platform GeneGlobe Data Analysis Center (Qiagen, Germany). Raw Cq values were preprocessed setting 37 as cutoff value and expression in at least 80% of samples. Ct values were normalized via an automatic selection of housekeeping genes. *ACTB* was used as endogenous control in plasma analysis for both profiling and validation. Relative quantities were log-transformed and compared (PCa vs. HC) among groups. The p-values were calculated using the Student's t-test of the replicate $2^{-\Delta\Delta CT}$ values. Individual lncRNAs were analyzed by the $\Delta\Delta Ct$ method for each gene in the PCa and HC groups.

Microarray data analysis was performed in R/Bioconductor. Raw median signals were filtered, background corrected and quantile normalized between arrays. The median value of all probes for each transcript was calculated. The differential expression was tested with limma package using the following criteria: absolute fold change >1.5 and $p < 0.05$.

3. Results

All subjects' clinical data are presented in Table 1. A certified pathologist analyzed the archived FFPE tissue samples to confirm PCa diagnosis, but no clinical and demographic characteristics are available for the eleven-year-old archived samples.

The results from the profiling step showed a total number of eight differentially expressed lncRNAs in plasma of PCa patients compared to healthy subjects, from which three were upregulated and five were downregulated, as shown in Table 2.

Table 2. Differentially expressed lncRNAs between PCa subjects and healthy controls (HCs).

LncRNA	Fold Change (FC)	p-Value
MIR7-3HG	130.67	0.011
NEAT1	66.94	0.029
RMRP	2.55	0.034
CAHM	−885.36	0.0009
CCAT1	−5.63	0.038
CCAT2	−88.02	0.0007
MRPL23-AS1	−7.40	0.017
XIST	−93.62	0.031

FFPE tissue microarray analysis revealed 717 lncRNAs that were markedly dysregulated in PCa samples versus controls (data not shown).

The comparison between FFPE tissues and plasma samples showed only one commonly upregulated lncRNA, NEAT1 ($p < 0.05$).

In the next step, NEAT1 was individually validated in plasma and tissue samples from both groups, as its expression was commonly and significantly upregulated in PCa subjects when compared to HC. In plasma samples from Group 1 (TM), although NEAT1 was upregulated (FC = 1.836), it did not reach statistical significance ($p = 0.351$). In contrast, in Group 2 (CJ), where the sample size was larger, NEAT1 was significantly upregulated (FC = 2.101, $p = 0.009$). Figure 2 shows the relative quantities for both groups.

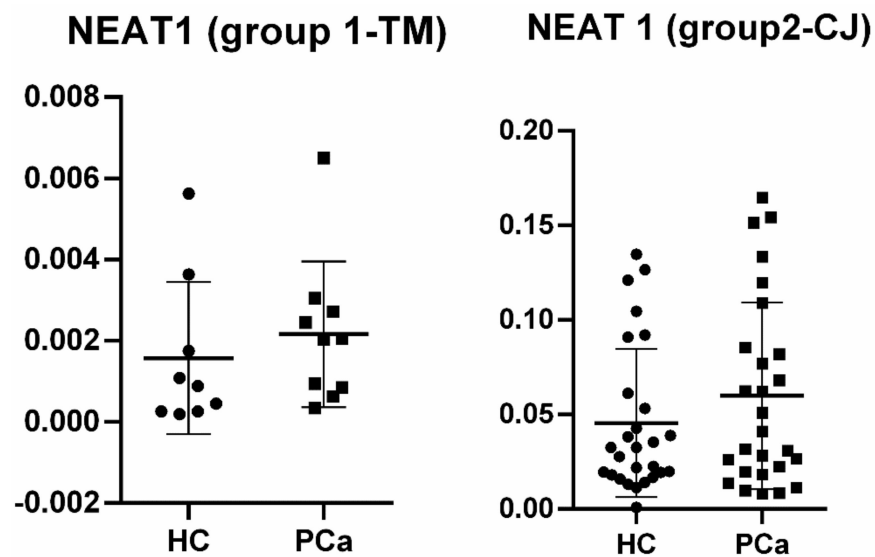


Figure 2. Relative quantities for NEAT1 in plasma of prostate cancer (PCa) patients vs. healthy controls (HCs) among groups.

ROC analysis for NEAT1 in Group 2 (CJ) revealed an area under the curve (AUC) of 0.7298 (95%CI = 0.5812–0.8785), suggesting, therefore, the biomarker potential for this type of lncRNA (Figure 3).

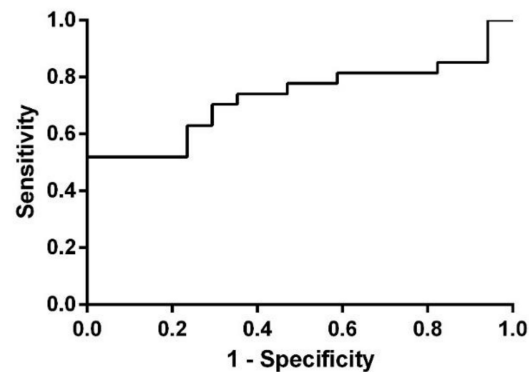


Figure 3. ROC analysis for NEAT1 in Group 2 (CJ).

4. Discussion

Our study aimed to investigate differentially expressed lncRNA species in PCa patients' plasma and LCM FFPE tissue samples, compared to healthy controls (HC), to determine lncRNAs as potential diagnostic biomarkers for PCa. The common lncRNA that was found to be dysregulated in both groups was nuclear-enriched abundant transcript 1 (NEAT1), and therefore, we conducted an individual analysis in order to validate this type of lncRNA as a biomarker for prostate malignancy. In Group 1 (TM), individual validation did not reach statistical significance ($p = 0.351$), most probably because of the low sample size, although it was upregulated with an almost two-fold increase in PCa samples when compared to HC. In Group 2 (CJ), NEAT1 revealed to be also upregulated (FC = 2.101), and this time, the result presented statistical significance ($p = 0.009$) and an AUC value of 0.7298 (95%CI = 0.5812–0.8785).

Our study went in the same direction as what was previously published in the literature. A report conducted by Li et al. (2018) proved the oncogenic role (and consequent overexpression) of NEAT1 and its functionality dependence on certain transcription factors [28]. To date, it is known that NEAT1 is an essential component for the structure of paraspeckles (nuclear domains that have a role in nuclear retaining of mRNA). This abundant 4kb lncRNA increased the numbers of paraspeckles when overexpressed and

eradicated them when depleted by RNAi, respectively [23]. Besides this architectural role, NEAT1 showed to be involved in various processes related to cancer, such as invasion, migration, proliferation, DNA damage, etc. [29], but the concrete tumorigenesis mechanism of NEAT1 remains unclear.

However, a new transcription regulation mechanism has been proposed, proving that the oncogenic role of NEAT1 is highly dependent on the transcriptional regulatory circuit NEAT1-CDC5L-AGRN. Cell division cycle 5-like protein (CDC5L) is essential for mitotic progression, and its target gene, AGRN, seems to be modulated by NEAT1, yielding this whole pathway critical for tumor growth [28].

Another oncogenic pathway for NEAT1 was proposed by Xiong et al. (2018), who showed that NEAT1 promotes PCa cell growth via the SRC3/IGF1R/AKT pathway. In this manner, NEAT1 interacts with steroid receptor co-activator3 (SRC3), therefore upregulating the phosphorylation of AKT and promoting PCa cell growth via IGF1R/AKT pathway. NEAT1 was consequently found to be overexpressed in PCa samples, together with SRC3 and IGF1R [30].

Yet, another study confirms the oncogenic potential of NEAT1, proving that it is the most upregulated lncRNA in PCa samples. In addition, NEAT1 showed to be recruited at the sites of PCa genes where it contributes, on an epigenetic level, to the promotion of tumorigenesis. The same study demonstrates that NEAT1 is a potential target for estrogen receptor alpha (ER α), suggesting that ER α could function as an alternate signaling pathway that can help refractory PCa bypass the classical androgen/androgen receptor (AR) axis [31].

In addition, responding to the emergent need of identifying mechanisms of lncRNAs, recent reports suggest that NEAT1 acts as a sponge for miR-98-5p to upregulate the oncogene HMGA2, proving that another novel regulatory pathway (NEAT1-miR-98-5p-HMGA2) could be crucial for PCa development [32].

Moreover, a pan-cancer analysis showed the same tendency of NEAT1 to be overexpressed in various types of cancer, besides PCa, such as stomach adenocarcinoma, hepatocellular liver carcinoma, kidney papillary cell carcinoma, and kidney clear cell carcinoma, although some contradictory evidence exists regarding its tumor suppressor role in promyelocytic leukemia [33,34].

To our knowledge, this is the first study that investigated the differential expression of NEAT1 in PCa FFPE tissues, using the LCM technique. Using this tool for isolating desired cell populations, we increased the biomarker specificity by limiting the sample heterogeneity, thus minimizing the risk of introducing noncancer cells that could interfere with the data obtained for the relative quantification of NEAT1 in FFPE PCa tissue samples. However, our study comprised a small sample size, which represents its main limitation, together with the lack of multiple comparison correction.

Taken together, these findings corroborate with previous reports stating that NEAT1 could be used as a biomarker for PCa diagnosis and should be perceived in the large context of biomarker discovery using novel and modern medical approaches. Undoubtedly, future studies comprising larger cohorts are compulsory for better understanding the roles and mechanisms of NEAT1 as an oncogene for PCa development, as well as the reliability of its overexpression in PCa samples (plasma, tissues, etc.) when compared to healthy subjects.

5. Conclusions

Our findings demonstrate that NEAT1 is significantly upregulated in PCa samples compared to HC, suggesting an oncogenic role for this particular type of lncRNA. Analyzed in an individual validation study, NEAT1 showed to have a relatively high diagnostic value and, therefore, could represent a promising and novel biomarker for PCa detection. However, these data need to be confirmed with the aid of additional studies encompassing larger cohort sizes that could ultimately lead to discovering the comprehensive oncogenic mechanism of NEAT1 regarding PCa biology.

Author Contributions: D.N., A.M., I.O.S., E.S. and C.M. participated in study design, performed LCM and gene expression analyses, data analysis, manuscript writing, and editing. A.D. performed the pathological diagnosis and participated in LCM analysis. L.B. and O.B. performed the microarray experiments, data analysis, and manuscript preparation. R.B., A.A.C. and B.P. recruited patients, participated in study design, data analysis, and manuscript preparation. All authors have read and agreed to the published version of the manuscript.

Funding: This research was funded by the Executive Unit for Financing Higher Education, Research, Development and Innovation of Romania (UEFISCDI), Grant Number PN-III-P4-IDPCE-2016-0371.

Institutional Review Board Statement: The study was conducted according to the guidelines of the Declaration of Helsinki, and approved by the Ethics Committees of the participating institutions (Clinical Emergency County Hospital in Timisoara, Code No. 71/05.08.2014 and Victor Babes University of Medicine and Pharmacy Timisoara, Code No. 9/13.05.2014 extended by Code No. 33_2017).

Informed Consent Statement: Informed consent was obtained from all subjects involved in the study. Written informed consent has been obtained from the patients to publish this paper.

Conflicts of Interest: The authors declare no conflict of interest.



References

- 2019 Prostate Cancer Statistics | Prolaris. Available online: <https://prolaris.com/2019/04/17/2019-prostate-cancer-statistics/> (accessed on 15 March 2020).
- SEER Cancer Statistics Review, 1975–2013; National Cancer Institute: Bethesda, MD, USA, 2016. Available online: https://seer.cancer.gov/csr/1975_2015/ (accessed on 15 March 2020).
- Potosky, A.L.; Feuer, E.J.; Levin, D.L. Impact of screening on incidence and mortality of prostate cancer in the US. *Epidemiol. Rev.* **2001**, *23*, 181–186. [CrossRef] [PubMed]
- Key Statistics for Prostate Cancer | Prostate Cancer Facts. Available online: <https://www.cancer.org/cancer/prostate-cancer/about/key-statistics.html> (accessed on 15 March 2020).
- Siegel, R.L.; Miller, K.D.; Jemal, A. Cancer statistics, 2020. *CA Cancer J. Clin.* **2020**, *70*, 7–30. [CrossRef] [PubMed]
- Pernar, C.H.; Ebot, E.M.; Wilson, K.M.; Mucci, L.A. The Epidemiology of Prostate Cancer. *NLM* **2018**, *8*, a030361. [CrossRef] [PubMed]
- Wolf, A.M.D.; Wender, R.C.; Etzioni, R.B.; Thompson, I.M.; D’Amico, A.V.; Volk, R.J.; Brooks, D.D.; Dash, C.; Guessous, I.; Andrews, K.; et al. American Cancer Society guideline for the early detection of prostate cancer: Update 2010. *CA Cancer J. Clin.* **2010**, *60*, 70–98. [CrossRef]
- Pienta, K.J. Critical appraisal of prostate-specific antigen in prostate cancer screening: 20 years later. *Urology* **2009**, *73*, S11–S20. [CrossRef]
- Parekh, N.; Lin, Y.; Marcella, S.; Kant, A.K.; Lu-Yao, G. Associations of lifestyle and physiologic factors with prostate-specific antigen concentrations: Evidence from the National Health and Nutrition Examination Survey (2001–2004). *Cancer Epidemiol. Biomark. Prev.* **2008**, *17*, 2467–2472. [CrossRef]
- Rodriguez, J.F.; Eggener, S.E. Prostate Cancer and the Evolving Role of Biomarkers in Screening and Diagnosis. *Radiol. Clin. N. Am.* **2018**, *56*, 187–196. [CrossRef]
- Ploussard, G.; De La Taille, A. Urine biomarkers in prostate cancer. *Nat. Rev. Urol.* **2010**, *7*. [CrossRef]
- Zainfeld, D.; Goldkorn, A. *Liquid Biopsy in Prostate Cancer: Circulating Tumor Cells and Beyond*; Springer International Publishing: Berlin/Heidelberg, Germany, 2018; pp. 87–104.
- Duffy, M.J. Can molecular markers now be used for early diagnosis of malignancy? *Clin. Chem.* **1995**, *41*, 1410–1413. [CrossRef]
- Merola, R.; Tomao, L.; Antenucci, A.; Sperduti, I.; Sentinelli, S.; Masi, S.; Mandoj, C.; Orlandi, G.; Papalia, R.; Guaglianone, S.; et al. PCA3 in prostate cancer and tumor aggressiveness detection on 407 high-risk patients: A National Cancer Institute experience. *J. Exp. Clin. Cancer Res.* **2015**, *34*, 1–6. [CrossRef]
- Ma, L.; Bajic, V.B.; Zhang, Z. On the classification of long non-coding RNAs. *RNA Biol.* **2013**, *10*, 925–933. [CrossRef] [PubMed]
- Rinn, J.L.; Kertesz, M.; Wang, J.K.; Squazzo, S.L.; Xu, X.; Bruggmann, S.A.; Goodnough, L.H.; Helms, J.A.; Farnham, P.J.; Segal, E.; et al. Functional Demarcation of Active and Silent Chromatin Domains in Human HOX Loci by Noncoding RNAs. *Cell* **2007**, *129*, 1311–1323. [CrossRef]
- Fang, Y.; Fullwood, M.J. Roles, Functions, and Mechanisms of Long Non-coding RNAs in Cancer. *Beijing Genom. Inst.* **2016**, *14*. [CrossRef]
- Sonkoly, E.; Bata-Csorgo, Z.; Pivarcsi, A.; Polyanka, H.; Kenderessy-Szabo, A.; Molnar, G.; Szentpali, K.; Bari, L.; Megyeri, K.; Mandi, Y.; et al. Identification and characterization of a novel, psoriasis susceptibility-related noncoding RNA gene, PRINS. *J. Biol. Chem.* **2005**, *280*, 24159–24167. [CrossRef]
- Faghihi, M.A.; Modarresi, F.; Khalil, A.M.; Wood, D.E.; Sahagan, B.G.; Morgan, T.E.; Finch, C.E.; St Laurent, G., 3rd; Kenny, P.J.; Wahlestedt, C. Expression of a noncoding RNA is elevated in Alzheimer’s disease and drives rapid feed-forward regulation of β -secretase. *Nat. Med.* **2008**, *14*, 723–730. [CrossRef]

20. Woo, C.J.; Kingston, R.E. HOTAIR Lifts Noncoding RNAs to New Levels. *Cell* **2007**, *129*, 1257–1259. [CrossRef]
21. Pibouin, L.; Villaudy, J.; Ferbus, D.; Muleris, M.; Prospéri, M.T.; Remvikos, Y.; Goubin, G. Cloning of the mRNA of overexpression in colon carcinoma-1: A sequence overexpressed in a subset of colon carcinomas. *Cancer Gene Cytogen* **2002**, *133*, 55–60. [CrossRef]
22. Ramnarine, V.R.; Kobelev, M.; Gibb, E.A.; Nouri, M.; Lin, D.; Wang, Y.; Buttyan, R.; Davicioni, E.; Zoubeidi, A.; Collins, C.C. *The Evolution of Long Noncoding RNA Acceptance in Prostate Cancer Initiation, Progression, and Its Clinical Utility in Disease Management*; Elsevier: Amsterdam, The Netherlands, 2019; Volume 76.
23. Clemson, C.M.; Hutchinson, J.N.; Sara, S.A.; Ensminger, A.W.; Fox, A.H.; Chess, A.; Lawrence, J.B. An Architectural Role for a Nuclear Noncoding RNA: NEAT1 RNA Is Essential for the Structure of Paraspeckles. *Mol. Cell* **2009**, *33*, 717–726. [CrossRef]
24. Srikantan, V.; Zou, Z.; Petrovics, G.; Xu, L.; Augustus, M.; Davis, L.; Livezey, J.R.; Connell, T.; Sesterhenn, I.A.; Yoshino, K.; et al. PCGEM1, a prostate-specific gene, is overexpressed in prostate cancer. *Proc. Natl. Acad. Sci. USA* **2000**, *97*, 12216–12221. [CrossRef]
25. Lee, B.; Mazar, J.; Aftab, M.N.; Qi, F.; Shelley, J.; Li, J.; Govindarajan, S.; Valerio, F.; Rivera, I.; Thurn, T.; et al. Long noncoding RNAs as putative biomarkers for prostate cancer detection. *J. Mol. Diagn.* **2014**, *16*, 615–626. [CrossRef]
26. Paunescu, I.A.; Bardan, R.; Marcu, A.; Nitusca, D.; Dema, A.; Negru, S.; Balacescu, O.; Balacescu, L.; Cumpănas, A.; Sirbu, I.O.; et al. Biomarker potential of plasma microRNA-150-5p in prostate cancer. *Medicina* **2019**, *55*, 564. [CrossRef] [PubMed]
27. Mihala, A.; Alexa, A.A.; Samoilă, C.; Dema, A.; Vizitiu, A.C.; Anghel, A.; Tamas, L.; Marian, C.; Sirbu, I.O. A pilot study on the expression of microRNAs resident on chromosome 21 in laser microdissected FFPE prostate adenocarcinoma samples. *Rom. J. Morphol. Embryol.* **2015**, *56*, 1063–1068.
28. Li, X.; Wang, X.; Song, W.; Xu, H.; Huang, R.; Wang, Y.; Zhao, W.; Xiao, Z.; Yang, X. Oncogenic properties of NEAT1 in prostate cancer cells depend on the CDC5L–AGRN transcriptional regulation circuit. *Cancer Res.* **2018**, *78*, 4138–4149. [CrossRef] [PubMed]
29. Fu, J.w.; Kong, Y.; Sun, X. Long noncoding RNA NEAT1 is an unfavorable prognostic factor and regulates migration and invasion in gastric cancer. *J. Cancer Res. Clin. Oncol.* **2016**, *142*, 1571–1579. [CrossRef]
30. Xiong, W.; Huang, C.; Deng, H.; Jian, C.; Zen, C.; Ye, K.; Zhong, Z.; Zhao, X.; Zhu, L. Oncogenic non-coding RNA NEAT1 promotes the prostate cancer cell growth through the SRC3/IGF1R/AKT pathway. *Int. J. Biochem. Cell Biol.* **2018**, *94*, 125–132. [CrossRef]
31. Chakravarty, D.; Sboner, A.; Nair, S.S.; Giannopoulou, E.G.; Li, R.; Hennig, S.; Mosquera, J.M.; Pauwels, J.; Park, K.; Kossai, M.; et al. The oestrogen receptor alpha-regulated lncRNA NEAT1 is a critical modulator of prostate cancer. *Nat. Commun.* **2014**, *5*, 5383. [CrossRef]
32. Guo, Z.; He, C.; Yang, F.; Qin, L.; Lu, X.; Wu, J. Long non-coding RNA-NEAT1, a sponge for miR-98-5p, promotes expression of oncogene HMGA2 in prostate cancer. *Biosci. Rep.* **2019**, *39*, 9. [CrossRef]
33. Zeng, C.; Xu, Y.; Xu, L.; Yu, X.; Cheng, J.; Yang, L.; Chen, S.; Li, Y. Inhibition of long non-coding RNA NEAT1 impairs myeloid differentiation in acute promyelocytic leukemia cells. *BMC Cancer* **2014**, *14*, 693. [CrossRef]
34. Li, S.; Li, J.; Chen, C.; Zhang, R.; Wang, K. Pan-cancer analysis of long non-coding RNA NEAT1 in various cancers. *Genes Dis.* **2018**, *5*, 27–35. [CrossRef]

Article

Analysis of Brain Functions in Men with Prostate Cancer under Androgen Deprivation Therapy: A One-Year Longitudinal Study

Vanessa Sánchez-Martínez ^{1,2} , Cristina Buigues ^{1,2}, Rut Navarro-Martínez ^{1,2,3}, Laura García-Villodre ^{1,2}, Noura Jekhalef ^{1,2}, María Serrano-Carrascosa ⁴, José Rubio-Briones ⁴ and Omar Cauli ^{1,2,*} 

¹ Department of Nursing, University of Valencia, 46010 Valencia, Spain; Vanessa.sanchez@uv.es (V.S.-M.); cristina.buigues@uv.es (C.B.); Rut.Navarro@uv.es (R.N.-M.); garcia_lauvil@gva.es (L.G.-V.); noujeg@alumni.uv.es (N.J.)

² Frailty and Cognitive Impairment Research Group (FROG), University of Valencia, 46010 Valencia, Spain

³ Haematology Department, Hospital General Universitario, 46014 Valencia, Spain

⁴ Department of Urology, Fundación IVO, 46009 Valencia, Spain; marietadelao77@gmail.com (M.S.-C.); jrubio@fivo.org (J.R.-B.)

* Correspondence: Omar.Cauli@uv.es

Citation: Sánchez-Martínez, V.; Buigues, C.; Navarro-Martínez, R.; García-Villodre, L.; Jekhalef, N.; Serrano-Carrascosa, M.; Rubio-Briones, J.; Cauli, O. Analysis of Brain Functions in Men with Prostate Cancer under Androgen Deprivation Therapy: A One-Year Longitudinal Study. *Life* **2021**, *11*, 227. <https://doi.org/10.3390/life11030227>

Academic Editors: Ana Faustino and Paula A. Oliveira

Received: 4 February 2021

Accepted: 9 March 2021

Published: 10 March 2021

Publisher's Note: MDPI stays neutral with regard to jurisdictional claims in published maps and institutional affiliations.

Abstract: The relationship between cognitive decline and androgen deprivation therapy (ADT) under luteinizing hormone-releasing hormone (LHRH) analogues is unclear, and there is a scarcity of longitudinal studies considering the interaction between cognition, depressive symptoms and sleep quality in men with prostate cancer (PCa) treated with ADT. This study aimed to determine if there were differences in the scores obtained in cognitive assessment, depressive symptoms, and sleep quality after one year of ADT and determine the interrelations between sleep, mood, and cognitive status. A prospective longitudinal observational study was designed, in which a cohort of men (mean age was 70.8 years) newly treated with androgen-deprivation therapy was assessed in the first six months of treatment and 12 months later. Analysis of cognitive function by the Mini-Mental State Examination (MMSE) scores indicated a significant ($p < 0.05$) increase after one year of treatment and by the Brief Scale for Cognitive Evaluation (BCog) scores indicated no changes in the scores before and after one year of treatment. Analysis of depressive symptoms with the Geriatric Depression Scale and sleep quality with the Athens Insomnia Scale (AIS) scores showed significant ($p < 0.05$) changes after one year of treatment with ADT, with men describing more depressive symptoms and more sleep disturbances. No statistically significant differences were found in the cognitive performance between men with impaired sleep or depression results and those without them. Our study showed no clinical evidence of the relationship between ADT under luteinizing hormone-releasing hormone (LHRH) analogues and cognitive deterioration in 1-year follow-up, but there are impairments in the sleep quality in men with PCa undergoing ADT and an increase in depressive symptoms which has important implications for clinicians as they would impair quality of life and adherence to treatment.

Keywords: neurotoxicity; testosterone; androgen-deprivation therapy; cognitive function; sleep; depression



Copyright: © 2021 by the authors. Licensee MDPI, Basel, Switzerland. This article is an open access article distributed under the terms and conditions of the Creative Commons Attribution (CC BY) license (<https://creativecommons.org/licenses/by/4.0/>).

1. Introduction

Prostate cancer (PCa) is the second most frequent cancer in men [1]. In 2017, its global estimated incidence was 1.3 million, and it caused 416,000 deaths [2], with marked differences in the rates across different regions and populations [1,3]. In Europe, it was estimated to represent 21.8% of the total cancer incidence and 10% of cancer deaths in 2018 [4]. The diagnosis of cancer is a stressful experience that significantly impacts all spheres of patients' lives, not only at the time of diagnosis but can be maintained for many years, even in those patients who have overcome the disease. However, not all

sequelae in the cognitive-emotional sphere are produced by the impact of the diagnosis and the associated psychological disorders. In recent years, increasing importance has been given to the toxicity produced by oncology treatments, whether acute or late-onset. This stands out, especially the appearance of a cognitive deterioration associated with the administration of oncological treatments [5–7]. PCa is an androgen-dependent disorder, so the standard treatment is based on hormonal therapy to reduce the production of hormones that enhance tumour growth, mainly androgen deprivation therapy (ADT), in the form of chemical castration [8,9] and other antiandrogens. However, it is not exempt from numerous and often debilitating physical and psychological adverse effects that may affect the quality of life [10–12]. These can be classified into nine groups: musculoskeletal changes, metabolic changes, cardiac disorders, nervous system disorders, vascular disorders, hepatobiliary disorders, reproductive system disorders, psychiatric disorders, and general disorders [11].

Cognitive symptoms, depression and sleep disturbances are considered particularly challenging side effects of ADT [13]. More than a decade ago, some reviews suggested that treatment with androgen deprivation therapy in men with PCa could lead to subtle cognitive decline [14,15]. Some studies reported declines in different cognitive domains, such as verbal memory, executive function, spatial memory or visuomotor skills, while others failed to demonstrate a relationship between cognition and ADT [16]. It has been argued that the adverse effects of ADT could be negatively influenced by factors such as older age and lower education level [17]. However, despite subsequent studies, reviews and meta-analyses, there is no accepted consensus that this connection actually exists, as reviews show conflicting results [16–22] and the analysis of cognitive functions under ADT with different psychometric tools and the comparisons of changes in different cognitive domains under ADT is necessary in order to tailor interventions to minimise the ADT-induced toxicity effects upon brain function over time.

Cognitive impairment could also be associated with other known psychiatric adverse effects of ADT in men with PCa, such as depression [22–24] and reduced sleep quality [25,26]. Depression has been documented to increase in men with PCa, with a prevalence between 10% and 40% [27,28] that might be related to multiple factors, such as age, comorbidities, socioeconomic status, erectile dysfunction or the disorder itself [28–30]. Treatment with ADT has been associated with a higher increase of the incidence of depression in this group [23,28], which could impact not only cognition and quality of life but also on PCa prognosis [22,28,31]. Moreover, depression could be underdiagnosed and so, undertreated [29]; this is more relevant considering that one of its outcomes is the risk of suicide, also described to be increased in men with PCa [28,32]. It is accepted that insomnia symptoms are frequently aggravated by cancer treatments and their side effects [33,34], but there is scarce evidence of the relationship between ADT and sleep disturbances. Some studies have concluded that poor sleep quality appears in approximately one-third of the men treated with ADT, but the underlying physiological mechanism is unclear [35,36]. Among other factors, it has been related to hot flashes, nicturia and emotional distress and to the pharmacological treatment of these adverse effects [26,37–39].

Cognitive decline, mood disorders and poor sleep quality are adverse effects that are not easily attributable to one root cause. To summarise the literature gaps, the link between cognitive decline and ADT is unclear, and there is a scarcity of longitudinal studies considering the interaction between cognition, depressive symptoms and sleep quality in men with PCa treated with ADT. For many clinical research types, such as the psycho-geriatric evaluation parameters under chronic pharmacological treatment, longitudinal studies provide a unique insight into variables' interactions that might not be possible in cross-sectional studies. They are beneficial when studying development lifespan issues such as cognitive function and associated factors.

In this context, this study aimed to study a cohort of men newly treated with ADT: to determine if, after one year of androgen deprivation therapy, there were differences between the baseline and the follow-up scores of the cognitive assessments; to measure

the influence of these treatments in the mood and sleep quality; and to determine the inter-relations between sleep, mood, cognitive status and other sociodemographic variables.

2. Methods

This is a prospective longitudinal observational study, in which a cohort of men newly treated with androgen-deprivation therapy with luteinizing hormone-releasing hormone (LHRH) analogues was assessed in the six months- to one year of treatment with LHRH analogues and at follow-up which was 12 months later (from the first evaluation). The trial was carried out in compliance with the guidelines of the Declaration of Helsinki, and the study protocol was approved by the local Ethics Committee (University of Valencia, Reference number: H1511682610849). All participants gave written informed consent before being enrolled in the study.

The participants were consecutively selected from an outpatient's oncology practice if they fulfilled the eligibility criteria. Data collection was made between January 2018 and March 2020. Men were included in the first six months of treatment with long-acting injectable androgen deprivation therapy based on LHRH analogue (leuprorelin or triptorelin) and if they agreed to participate by signing the informed consent form. Men could not participate if they were receiving any other chemotherapy treatment for prostate or any other cancer, or if they had any known cognitive deterioration due to other causes. We excluded all those men who had completed the baseline assessment and suffered any relevant change in their health status that could influence their sleep quality, mood, or cognitive performance.

2.1. Sample Size

The sample size was determined before the development of the study, so the statistical power was calculated for the main outcome of the study which is cognitive function. Accepting an alpha risk of 0.1 in a one-sided test with 33 subjects in the first group and 33 in the second, the statistical power was 90% to recognise as statistically significant the difference from 0.09 in the first group to 0.34 in the second group.

2.2. Sociodemographic and Clinical Variables

The sociodemographic variables considered were: age (both numerical and categorised into men younger and older than 75 years); education level (classified into four groups, according to the maximum education level completed: no studies, primary studies completed (until 14 years of age), secondary school or vocational studies, university degree); marital status; employment status; the form of cohabitation. The clinical variables were metastases; previous prostatectomy; ADT treatment (the LHRH analogues triptorelin or leuprorelin).

2.3. Outcome Variables

The Mini-Mental State Examination (MMSE) score was considered as a numerical and categorical variable: normal or impaired. Besides, the scores of its dimensions (orientation, spatial orientation, immediate recall, attention and calculation, delayed recall, language) were considered independently as numeric variables. The Brief Scale for Cognitive Evaluation (BCog) score and its dimensions (communication, attention, recent memory, concentration, remote memory, orientation, calculation and executive function) were considered numerical. The Athens Insomnia Scale (AIS) score (numeric and categorised into normal or impaired). The Geriatric Depression Scale (GDS) score (numeric and categorised into normal or impaired).

2.4. Psychological Assessments

The cognitive status was evaluated through two different brief cognitive assessments: the BCog and the MMSE. The short version of the GDS was used as a screening for depression, and the presence of insomnia was measured through the AIS.

The MMSE is a brief cognitive test widely used [40] since it was created in 1975 by Folstein et al. [41] and validated into Spanish by Lobo et al. in 1999 [42] with adequate psychometric properties. It comprises 30 items grouped into six dimensions: orientation, spatial orientation, registration, attention and calculation, recall and language. The test can be completed in five to 15 min, and it has two cut-off points, depending on the age of the person assessed.

The BCog is a short cognitive battery recently validated in Spain for the general population and people with schizophrenia [43]. It comprises eight dimensions (communication, attention, concentration, short and long-term memory, orientation, calculation and information processing) and can be completed in less than 15 min. Its internal consistency, calculated through Cronbach's alpha was 0.7 and its validity against the correlation with another brief cognitive test (Screening for Cognitive Impairment in Psychiatry), was 0.8.

The AIS is a self-report questionnaire used as a screening for sleep disturbances. Based on the International Classification of Diseases (ICD-10), the full scale is composed of eight items, with a score range from 0 to 24 (the cut-off point is six, and higher scores suggest a more serious problem) and it was validated by Soldatos et al. in 2000 [44]. The scale was validated into Spanish by Gómez-Benito et al. in 2011 [45] with acceptable psychometric properties (Cronbach's alpha was 0.86).

The abbreviated version of the GDS is a screening questionnaire developed by Yesavage et al. [46]. It is composed of 15 items, and it was validated into Spanish in 2002 by Martínez de la Iglesia et al. [47] with acceptable psychometric properties and with a cut-off point of five or more.

2.5. Statistical Analysis

Descriptive statistical analyses were carried out. Kolmogorov–Smirnov tests were made to determine which variables adapted to the normal distribution. Only the baseline and follow-up BCog scores and those of two of its subtests (calculation and remote memory) adapted the normal distribution, so most of the statistical analyses carried out were non-parametrical. Bivariate correlations were calculated, both parametrical (Pearson's) and non-parametrical (Spearman's). Partial correlations were calculated to control the influence of the age and education level in the outcome variables. T-tests, one-way analyses of variance (ANOVAs), Mann–Whitney's U tests and Kruskal–Wallis tests were carried out to determine if the differences between the values of the categorical variables were statistically significant. All the statistical tests were considered statistically significant at the level $p < 0.05$. The analyses were carried out using the IBM Statistical Package for Social Sciences SPSS (version 26.0; SPSS, Inc., Chicago, IL, USA).

3. Results

3.1. Characteristics of the Study Population

A sample of 44 men participated in the baseline assessment. Of them, 33 underwent the second assessment, so their results were analysed in this study. The reasons not to be reassessed were: three men refused to be screened for the second time, and eight suffered a health deterioration (for metastases requiring additional chemotherapy treatment or other reasons, such as cerebrovascular accidents) that could bias the results.

The mean age of the participants was 70.8 years, 13 (39.4%) men had completed compulsory education only (until 14 years of age), 27 (81.8%) were retired, 29 (87.9%) were married, and 24 (72.7%) lived only with their spouses. A total of 7 men had metastatic cancer, and 22 (66.7%) participants had previously a radical prostatectomy. Among men below age 75 years old, 71.4% had prostatectomy whereas among those aged 75 and over, 58.3% had prostatectomy. No significant differences were observed between prostatectomy and age group ($p = 0.44$, Chi-squared test). In the study sample, 11 patients were not submitted to a prostatectomy because 7 of them had bone-metastatic disease at diagnosis and 4 men received prostate brachytherapy as the main primary therapy. They were about to start or had started treatment with leuprorelin (9 men, 27.3%) or triptorelin (24 men)

in the six months previous to the baseline assessment. Sociodemographic and clinical data are provided in more detail in Table 1.

Table 1. Sociodemographic and clinical characteristics of the participants.

Variable	Values	Frequency (%); Mean (\pm SD)
Age	Under 75	21 (63.6%)
	75 or more	12 (36.4%)
Education level completed	None	6 (18.2%)
	Primary studies	13 (39.4%)
	Secondary studies	8 (24.2%)
	University studies	6 (18.2%)
Marital status	Married or in a relationship	29 (87.9%)
	Divorced	3 (9.1%)
Employment status	Other	1 (3%)
	Retired	27 (81.8%)
	Working	3 (9.1%)
Form of cohabitation	Other	3 (9.1%)
	Alone	3 (9.1%)
	With his wife or partner	24 (72.7%)
TNM stage	With his family	6 (18.2%)
	II	19 (57.6%)
	III	7 (21.2%)
Metastases	IV	7 (21.2%)
	No	26 (78.8%)
Prostatectomy	Yes	7 (21.2%)
	No	11 (33.3%)
PSA level at enrollment of the study	Yes	22 (66.6%)
Gleason score		1.86 (\pm 2.5)
ADT Drug		7.1 (\pm 1.0)
	Leuprorelin	9 (27.3%)
	Triptorelin	24 (72.7%)

SD: Standard deviation; TNM: Tumor, nodes, metastases; PSA: Prostate-specific antigen; ADT: Androgen-deprivation therapy.

3.2. Cognitive Evaluation, Depressive Symptoms and Insomnia Assessment in the Study Sample

The cognitive assessments showed different results (Table 2). On the one hand, the MMSE scores indicated a statistically significant increase after one year of treatment. On the other hand, the BCog scores indicated no statistically significant change in the scores before and after one year of treatment. The results obtained in the two assessments of the two cognitive tests applied were sensitive to the participants' age and education level, as the differences obtained in the scores were statistically different (all $p < 0.05$). The scores were statistically different in the two groups in the two assessments, being higher for the youngest men (for the MMSE $p < 0.05$, and the BCog $p < 0.001$) and the most educated group (for the MMSE $p < 0.05$, and the BCog $p < 0.01$). The changes in baseline and follow-up scores of the MMSE and the BCog were compared in the two age groups (under 75 years old and 75 or more). For the MMSE, an increase was found in the two age groups, being statistically significant for the oldest group ($p = 0.046$), but not statistically significant for the youngest ($p = 0.21$). The results obtained in the BCog test showed an increase in the youngest group ($p < 0.001$), but a non-statistically significant reduction in the oldest ($p = 0.79$). We also considered the subtraction (difference in the scores obtained in the baseline and follow-up) for the two cognitive assessments in the two age groups, but these differences were not statistically significant for any assessment. By categorizing the age of the participants at 65 years old, we observed again a significant worsening of sleep quality during follow-up ($p = 0.004$) and no significant differences for other parameters.

Table 2. Evolution of the cognitive performance, sleep disturbances and depressive symptoms over one year of treatment.

		Initial Assessment Median (IQR); Frequency (%); Mean (SD)	Follow-up Assessment Median (IQR); Frequency (%); Mean (SD)	<i>p</i> -Value
AIS	Score	2 (1–3.5)	4 (1–7.5)	<i>p</i> = 0.018 *
	Under 75 years old	2 (1–4.5)	3 (0.5–7)	0.51
	75 years old or more	2 (0–2.75)	5.5 (2.5–7.75)	0.009 *
	Normal	28 (84.8%)	21 (63.6%)	<i>p</i> = 0.001 *
GDS	Impaired	5 (15.2%)	12 (34.4%)	
	Score	2 (1–3.8)	2 (1–6)	<i>p</i> = 0.194
	Under 75 years old	2 (1–4)	1 (0.5–5.5)	0.77
	75 years old or more	1.5 (0.25–2.75)	3.5 (1.25–7)	0.074
MMSE	Normal	30 (90.9%)	23 (69.7%)	<i>p</i> = 0.164
	Impaired	3 (9.1%)	10 (30.3%)	
	Total score	28 (25–30)	29 (27–30)	<i>p</i> = 0.035 *
	Under 75 years old	30 (26.5–30)	29 (28–30)	<i>p</i> = 0.21
	75 years old or more	25.5 (25–28)	27 (26–29.75)	<i>p</i> = 0.046 *
	Orientation	5 (5–5)	5 (5–5)	<i>p</i> = 0.058
	Spatial orientation	5 (5–5)	5 (5–5)	<i>p</i> = 0.317
	Registration	3 (3–3)	3 (3–3)	<i>p</i> = 0.317
	Attention and calculation	5 (4–5)	5 (5–5)	<i>p</i> = 0.168
	Recall	3 (2–3)	3 (2–3)	<i>p</i> = 0.465
BCog	Language	9 (7–9)	9 (8–9)	<i>p</i> = 0.460
	Total score	68.6 (±14.5)	69 (±13)	<i>p</i> = 0.857
	Under 75 years old	74.14 (±12.78)	75.50 (± 11.29)	<i>p</i> < 0.001 *
	75 years old or more	58.96 (±12.28)	57.50(±6.23)	<i>p</i> = 0.79
	Communication	10 (7.9–12.5)	9 (6–11.5)	<i>p</i> = 0.177
	Attention	11 (10–12)	11 (10.5–12)	<i>p</i> = 0.550
	Recent memory	6 (5–7)	6 (5–7)	<i>p</i> = 0.717
	Concentration	4 (3–5)	3 (3–4.5)	<i>p</i> = 0.582
	Remote memory	20.4 (±7.3)	20.4 (± 7.1)	<i>p</i> = 0.979
	Orientation	8 (8–8)	8 (8–8)	<i>p</i> = 0.979
BCog	Calculation	4.2 (±2.3)	5.2 (±2.2)	<i>p</i> = 0.001 *
	Executive function	6 (4–7.5)	6 (4–7)	<i>p</i> = 0.333

SD: Standard deviation; IQR: Interquartile range; AIS: Athens Insomnia Scale; GDS: Geriatric Depression Scale; MMSE: Mini-Mental State Examination; BCog: Brief Scale for Cognitive Evaluation. The *p*-values were calculated through different statistical tests. T-tests were used for variables that adapted the normal distribution. Wilcoxon ranks tests were used for variables that did not adapt to the normal distribution.

The GDS and the AIS scores showed changes after one year of treatment with ADT, with men describing more depressive symptoms and more sleep disturbances. However, only the differences in the AIS were statistically significant (for the AIS *p* = 0.018; for the GDS *p* = 0.194). Detailed information is offered in Figures 1 and 2, and Table 2. The analysis considering age groups showed statistically significant differences for the AIS scores in the oldest group (*p* = 0.009).

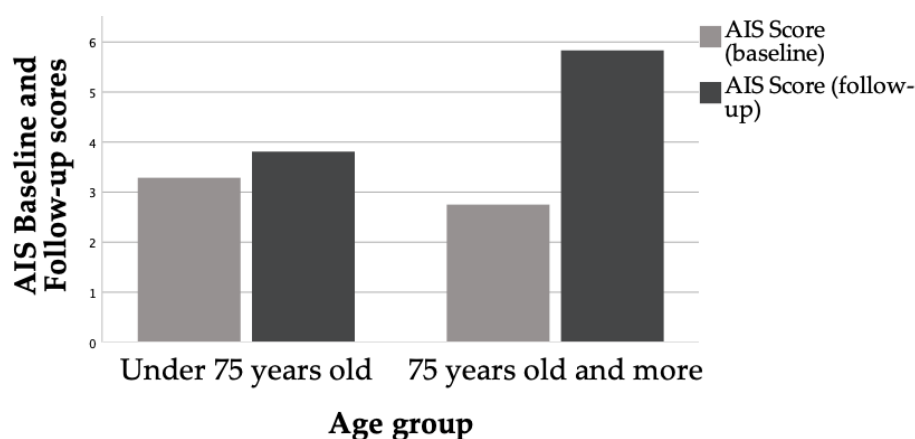


Figure 1. Evaluation of sleep quality at baseline and the follow-up according to age groups. AIS: Athens Insomnia Scale.

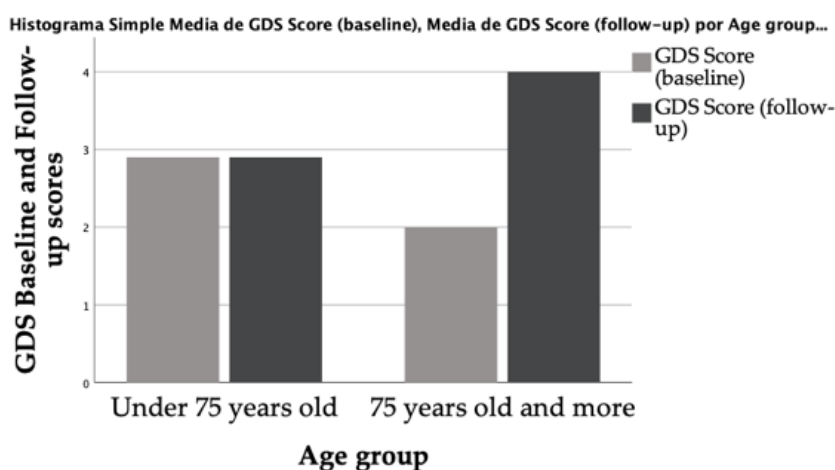


Figure 2. Evaluation of depressive symptoms at baseline and the follow-up according to age groups. GDS: Geriatric Depression Scale.

3.3. Association between Cognitive Evaluation, Depressive Symptoms and Insomnia

The participants obtained different scores in the cognitive tests according to their academic level. These differences were statistically significant for the total scores of the two tests and several of their subtests, with men who had higher academic levels obtaining higher scores. The other categorical variables (marital status, the form of cohabitation, working status, previous prostatectomy, presence of metastasis or ADT drug) did not relate to statistically significant differences in the total nor partial scores of the cognitive tests. There was not significant association between cognitive function at baseline or at follow-up and PSA level ($p = 0.63$ and $p = 0.64$ for MMSE scale; $p = 0.48$ in both cases for BCog scale). There was not significant association between cognitive function at baseline or at follow-up and Gleason score ($p = 0.27$ and $p = 0.47$ for MMSE scale; $p = 0.24$ and $p = 0.29$ for BCog scale). There was not significant association between cognitive function at baseline or at follow-up and TNM stages ($p = 0.45$ and $p = 0.46$ for MMSE scale; $p = 0.22$ and $p = 0.23$ for BCog scale). The presence of an impaired GDS or AIS scale scores did not relate to differences in the participants' scores in any of the assessments. There was not significant association between the score of depressive symptoms (GDS) at baseline or at follow-up and PSA level ($p = 0.17$ and $p = 0.81$, respectively). There was not significant association between the score of depressive symptoms (GDS) at baseline or at follow-up and Gleason score ($p = 0.26$ and $p = 0.59$, respectively). There was no significant association between the score of depressive symptoms (GDS) at baseline or at follow-up and TNM

stages ($p = 0.24$ and $p = 0.42$, respectively). There was no significant association between the score of sleep quality scale (AIS) at baseline or at follow-up and PSA level ($p = 0.31$ and $p = 0.65$, respectively). There was not significant association between the score of sleep quality scale (AIS) at baseline or at follow-up and Gleason score ($p = 0.53$ and $p = 0.69$, respectively). There was not significant association between the score of sleep quality scale (AIS) at baseline or at follow-up and TNM stages ($p = 0.66$ and $p = 0.83$, respectively).

Correlations were calculated to determine the interaction between the quantitative variables. Statistically significant correlations were found between the age and the baseline and the final scores of the two cognitive assessments, but not for the sleep disturbances or the depressive symptoms. Correlations were also found between the two cognitive tests' baseline and follow-up scores, both internal and crossed. These are shown in Tables 3 and 4. Neither the AIS nor the GDS scores showed correlations between them nor with any of the cognitive assessments.

Table 3. Correlations among quantitative variables (baseline assessment).

	Age 1st	MMSE 1st	BCog 1st	AIS 1st	GDS 1st
Age 1st		−0.39 *	−0.54 **	−0.16	−0.29
MMSE 1st	−0.39 *		0.72 ** <i>0.53 **</i>	−0.13 <i>−0.11</i>	0.2 <i>0.12</i>
BCog 1st	−0.54 **	0.72 ** <i>0.53 **</i>		−0.17 <i>−0.21</i>	0.11 <i>−0.07</i>
AIS 1st	−0.16	−0.13 <i>−0.11</i>	−0.17 <i>−0.21</i>		0.3 <i>0.53 **</i>
GDS 1st	−0.29	0.2 <i>0.12</i>	0.11 <i>−0.07</i>	0.3 <i>0.53 **</i>	

* The correlations were statistically significant $p < 0.05$, ** The correlations were statistically significant $p < 0.01$, The correlations controlled by age and education level are shown in italics. MMSE: Mini-Mental State Examination; BCog: Brief Scale for Cognitive Evaluation; AIS: Athens Insomnia Scale; GDS: Geriatric Depression Scale.

Table 4. Correlations among quantitative variables (follow-up assessment).

	Age 2nd	MMSE 2nd	BCog 2nd	AIS 2nd	GDS 2nd
Age 2nd		−0.44 *	−0.76 **	0.16	−0.04
MMSE 2nd	−0.44 *		0.48 ** <i>0.16</i>	0.22 <i>0.35</i>	0.15 <i>0.34</i>
BCog 2nd	−0.76 **	0.48 ** <i>0.16</i>		−0.12 <i>0.02</i>	0.13 <i>0.37*</i>
AIS 2nd	0.16	0.22 <i>0.35</i>	−0.12 <i>0.02</i>		0.29 <i>0.29</i>
GDS 2nd	−0.04	0.15 <i>0.34</i>	0.13 <i>0.37 *</i>	0.29 <i>0.29</i>	

* The correlations were statistically significant $p < 0.05$, ** The correlations were statistically significant $p < 0.01$, The correlations controlled by age and education level are shown in italics. MMSE: Mini-Mental State Examination; BCog: Brief Scale for Cognitive Evaluation; AIS: Athens Insomnia Scale; GDS: Geriatric Depression Scale.

Partial correlations were also calculated. When these correlations were controlled by age group and education level, some tests and scales' initial and final assessments showed statistically significant correlations (BCog, AIS and GDS). Moreover, a statistically significant correlation was found between the final score of the BCog and the GDS scale. These correlations are also shown in Tables 3 and 4.

The internal consistency and the internal correlations of the BCog were calculated in the two assessments. In the baseline assessment, the BCog Cronbach's alpha was 0.78, and 0.77 in the follow-up.

4. Discussion

In this longitudinal study, after one year of treatment with ADT with luteinizing hormone-releasing hormone (LHRH) analogues, the participants did not show a decline in their cognitive performance. By contrast, men in the youngest group improved their MMSE and BCog scores in the follow-up compared to the baseline assessment. A statistically significant decrease of the sleep quality was found, with more men exhibiting an impaired result of the AIS score. More men presented with an impaired GDS score in the follow-up assessment, but the differences were not statistically significant.

The BCog scores obtained in the two assessments by the youngest group of participants were comparable to those described for the general population. In contrast, the oldest group obtained lower scores than the participants with schizophrenia in which it was also validated [43]. There were differences between baseline and follow-up scores of the MMSE, with a discreet increase in the second assessment in the youngest group of participants. No statistically significant differences were found in the scores of the BCog. However, when considering the participants' ages, it was found that there was a decrease in the mean scores in older men while in younger men, the contrary happened. According to this data, the study participants did not decrease their cognitive performance, as happened in previous longitudinal studies [48–50]. These findings are valuable for clinical decision in men with PCa patients since the pharmacological treatment with LHRH analogues is the first-line treatment for many patients. The safety of their uses at least during one year over cognitive functions suggests it does not implicate any significant concern regarding this type of toxicity, assessed by two different cognitive assessment tools, and this could be important for some active patients. A small cognitive improvement was observed in specific cognitive domains.

A prospective controlled trial by Alibhai et al. assessed eight cognitive domains and found no adverse effects on cognitive function based on 12 months of ADT use in older men with PCa. In a cross-sectional study of 57 patients with non-metastatic PCa and 51 age-matched controls, ADT was not associated with alterations in cognitive function [51]. Another prospective controlled trial compared patients with non-metastatic PCa who initiated continuous ADT, patients with PCa who did not receive ADT, and healthy controls. Twelve months of ADT was found not to be associated with changes in self-reported cognitive concerns [52]. However, the data obtained from patient-reported outcome measures should be considered with caution because, being subjective, they are based on personal perceptions of cognitive function and may be affected by factors such as mood and fatigue. Objective tests remain the gold standard for measuring cognitive function, allowing the identification of treatment-related cognitive problems that can affect daily life. However, objective tests provide a useful measure of patients' perceptions of impairment and its impact on quality of life [53,54]. A US population-based analysis involving more than 100,000 men came to the same conclusion with information based on self-reported subjective evidence. ADT was not associated with an increased risk of cognitive impairment than patients with PCa who had not received ADT in the general population [55]. A systematic review and a meta-analysis of cognitive impairment in men with PCa receiving ADT also found no statistically significant risk of overall cognitive impairment after ADT [20,56]. As in these studies, we detected no statistically significant decreases of the cognitive performance in the sample, but this finding should be considered cautiously, as the decline of the scores might need a bigger sample size or a longer period to appear. Moreover, the age-associated physiological cognitive deterioration might synergize with the treatment with ADT.

In the present study, the AIS scores revealed a deterioration of the participants' sleep quality, with more men presenting an impaired result in the second assessment. This finding coincides with some previous research that assessed men with PCa [35,57] and people treated for other cancer types [39]. To the best of our knowledge, the evidence of sleep disorders and the methods to mitigate them in men treated with ADT is limited; in fact, it was not among the general side effects that we advised our patients about until now.

The relationship between lower testosterone concentrations and sleep disturbances is well established [58–60] and seems to be bidirectional, revealing a reduction of testosterone levels in young men samples with experimental sleep restriction [61,62]. However, some studies obtained different results in young men [63], and testosterone therapy showed a reduction in sleep duration in older men [64]. Men receiving ADT should be recommended to avoid known harms to sleep quality, together with the rest of the recommendations, like sleep hygiene measures or pharmacological treatment.

The GDS scores were higher in the second assessment, implying an increase of the men who had a positive screening for depressive symptoms, but the differences were not statistically significant. This finding contrasts with previous longitudinal studies that found a higher prevalence of depression in men treated with ADT [65–72], and in line with others, that did not confirm such a relationship [73,74]. Earlier studies suggested a relationship between borderline or lower testosterone levels and depressive symptoms in men [75–77], especially when the reduction of testosterone concentrations was longitudinal [78]. This longitudinal change might explain the trend of increasing depressive symptoms we observed in the sample studied, but the time interval between the baseline and the follow-up measurements might not have been enough to confirm statistically significant changes in the scores. Previous studies developed in the ageing population have proven the relevance of depressive symptoms in cognitive performance [79].

As previous research had concluded, in our study, men who were younger and had achieved higher education levels showed better cognitive performance [17]. No statistically significant differences were found in the cognitive performance between those who had impaired sleep or depression results and those who did not. Statistically significant correlations appeared between variables when partial correlations controlled by age and education level were calculated. The GDS follow-up score significantly correlated with the BCog score. We also found a correlation between the depressive symptoms and the sleep quality in the baseline assessment, but it was not confirmed in the follow-up.

To manage the potential impact of ADT in men and their partners' lives, previous studies have highlighted the need for a multidisciplinary approach through psychosocial interventions [38,80], educational interventions [81], and the role of exercise medicine [82,83]. As in the study of the ADT effects, there are significant gaps in the literature regarding the effectiveness of interventions to manage precise adverse effects of ADT, such as sleep deterioration [84]. We did not observe any differences regarding the outcomes of the study based on prior prostatectomy. However, we should be cautious about these results since the impact of general anaesthesia required for major surgery such as prostatectomy on cognitive impairment is controversial and complex [85,86]. Several studies have shown an association between exposure to surgery under general anaesthesia and the development of delayed neurocognitive recovery in only a subset of patients [85,87]. There are conflicting data on the relationship between exposure to anaesthesia and the development of long-term neurocognitive disorders, or the development of dementia in the patient population with normal preoperative cognitive function. Among patients, a prior prostatectomy was associated with impaired immediate and delayed verbal memory in one study [88], and a detailed analysis of different type of cognitive domains is required in longer follow-up studies in order to shed some light on this relevant issue.

This study has some strengths, as its longitudinal design. In this study, as suggested in previous studies [84,89], the cognitive assessment in men with PCa has been supplemented with other factors, like mood, age, education levels. Moreover, two different brief cognitive batteries were used, allowing the individual analysis of the specific cognitive functions, not only considering cognition as a whole. The scales used to measure depressive symptoms (GDS), and sleep disturbances (AIS) were validated for older men.

This study does have some limitations, too. The sample size was too small to infer about the statistical comparison between groups based on socio-demographic data and clinical findings. There were some heterogeneities in the prostate cancer burden such as patients previously having submitted to prostatectomy versus non prostatectomy group

or metastatic versus non-metastatic prostate cancer which could have limited the power of the difference analysis between groups. The sample was heterogeneous in age and education level, but these variables were considered confounding factors in the statistical analyses. Moreover, our findings' comparability may be limited due to the use of screening tests or batteries. The BCog scale was validated in a younger sample, but it showed acceptable results to measure cognition in older men, with adequate internal consistency in the baseline and the follow-up assessment. Even though we did not detect cognitive impairment by ADT in our series, it is crucial to take into account the possibility that some individuals with cognitive impairment present before ADT may suffer a worsening of their cognitive impairment or that studies with a follow-up longer than one-year could detect cognitive deficits under ADT in individuals with PCa. A further large-numbered study design should be required to support the conclusions of the study.

5. Conclusions

In this study, we did not find evidence of the relationship between ADT (under LHRH analogues) and cognitive deterioration in men with PCa despite using two different cognitive tests. Younger age and higher education level were correlated to higher scores in the cognitive tests. When controlled for age and education level, the follow-up scores of the BCog were found to be correlated to the depressive symptoms and to the sleep quality. Our results suggest changes in sleep quality in men with PCa undergoing ADT and a potential increase in depressive symptoms. We found a correlation between depressive symptoms and sleep quality. It is necessary to inform patients before the beginning of the treatment and adopt preventive measures to preserve their quality of life. More research is still needed.

Author Contributions: Conceptualization V.S.-M., R.N.-M., C.B., J.R.-B., O.C.; methodology C.B., R.N.-M., V.S.-M., O.C.; formal analysis, V.S.-M., N.J., L.G.-V., O.C.; investigation: C.B., R.N.-M., N.J., L.G.-V., V.S.-M., M.S.-C., O.C.; writing—original draft preparation, V.S.-M., O.C.; writing—review and editing V.S.-M., J.R.-B., O.C. All authors have read and agreed to the published version of the manuscript.

Funding: This research received research funding from University of Valencia (Valencia, Spain), “Accions especials d’investigació 2019 (Omar Cauli)”.

Institutional Review Board Statement: The study was conducted according to the guidelines of the Declaration of Helsinki, and approved by the Ethics Committee of University of Valencia Reference number: H1511682610849 (date of approval 7 February 2018).

Informed Consent Statement: Informed consent was obtained from all subjects involved in the study.

Data Availability Statement: The data presented in this study are available on request from the corresponding author.

Conflicts of Interest: The authors declare no conflict of interest.

References

1. Bray, F.; Ferlay, J.; Soerjomataram, I.; Siegel, R.L.; Torre, L.A.; Jemal, A. Global cancer statistics 2018: GLOBOCAN estimates of incidence and mortality worldwide for 36 cancers in 185 countries. *CA Cancer J. Clin.* **2018**, *68*, 394–424. [CrossRef]
2. Fitzmaurice, C.; Abate, D.; Abbasi, N.; Abbastabar, H.; Abd-Allah, F.; Abdel-Rahman, O.; Abdelalim, A.; Abdoli, A.; Abdollahpour, I.; Abdulle, A.S.M.; et al. Global, regional, and national cancer incidence, mortality, years of life lost, years lived with disability, and disability-adjusted life-years for 29 cancer groups, 1990 to 2017: A systematic analysis for the global burden of disease study. *JAMA Oncol.* **2019**, *5*, 1749–1768. [PubMed]
3. Pernar, C.H.; Ebot, E.M.; Wilson, K.M.; Mucci, L.A. The Epidemiology of Prostate Cancer. *Cold Spring Harb. Perspect. Med.* **2018**, *8*, a030361. [CrossRef] [PubMed]
4. Ferlay, J.; Colombet, M.; Soerjomataram, I.; Dyba, T.; Randi, G.; Bettio, M.; Gavin, A.; Visser, O.; Bray, F. Cancer incidence and mortality patterns in Europe: Estimates for 40 countries and 25 major cancers in 2018. *Eur. J. Cancer* **2018**, *103*, 356–387. [CrossRef]
5. Institute of Medicine (US) Committee on Psychosocial Services to Cancer Patients/Families in a Community Setting. *Cancer Care for the Whole Patient: Meeting Psychosocial Health Needs*; Adler, N.E., Page, A.E., Eds.; National Academies Press (US): Washington, DC, USA, 2008.

6. Kenyon, M.; Mayer, D.K.; Owens, A.K. Late and Long-Term Effects of Breast Cancer Treatment and Surveillance Management for the General Practitioner. *J. Obstet. Gynecol. Neonatal Nurs.* **2014**, *43*, 382–398. [CrossRef]
7. Okubo, R.; Wada, S.; Shimizu, Y.; Tsuji, K.; Hanai, A.; Imai, K.; Uchitomi, Y.; Fujiwara, Y.; Tsugane, S.; Matsuoka, Y.J. Expectations of and recommendations for a cancer survivorship guideline in Japan: A literature review of guidelines for cancer survivorship. *Jpn. J. Clin. Oncol.* **2019**, *49*, 812–822. [CrossRef]
8. Cornford, P.; Bellmunt, J.; Bolla, M.; Briers, E.; De Santis, M.; Gross, T.; Henry, A.M.; Joniau, S.; Lam, T.B.; Mason, M.D.; et al. EAU-ESTRO-SIOG Guidelines on Prostate Cancer. Part II: Treatment of Relapsing, Metastatic, and Castration-Resistant Prostate Cancer. *Eur. Urol.* **2017**, *71*, 630–642. [CrossRef] [PubMed]
9. Hofmann, M.R.; Hussain, M.; Dehm, S.M.; Beltran, H.; Wyatt, A.W.; Halabi, S.; Sweeney, C.; Scher, H.I.; Ryan, C.J.; Feng, F.Y.; et al. Prostate Cancer Foundation Hormone-Sensitive Prostate Cancer Biomarker Working Group Meeting Summary. *Urology* **2020**. [CrossRef]
10. Abrahamsson, P.-A. Potential Benefits of Intermittent Androgen Suppression Therapy in the Treatment of Prostate Cancer: A Systematic Review of the Literature. *Eur. Urol.* **2010**, *57*, 49–59. [CrossRef]
11. Edmunds, K.; Tuffaha, H.; A Galvão, D.; Scuffham, P.; Newton, R.U. Incidence of the adverse effects of androgen deprivation therapy for prostate cancer: A systematic literature review. *Support. Care Cancer* **2020**, *28*, 2079–2093. [CrossRef]
12. Fang, D.; Zhou, L. Androgen deprivation therapy in nonmetastatic prostate cancer patients: Indications, treatment effects, and new predictive biomarkers. *Asia-Pac. J. Clin. Oncol.* **2019**, *15*, 108–120. [CrossRef]
13. Elliott, S.; Latini, D.M.; Walker, L.M.; Wassersug, R.; Robinson, J.W. ADT Survivorship Working Group Androgen Deprivation Therapy for Prostate Cancer: Recommendations to Improve Patient and Partner Quality of Life. *J. Sex. Med.* **2010**, *7*, 2996–3010. [CrossRef]
14. Nelson, C.J.; Lee, J.S.; Gamboa, M.C.; Roth, A.J. Cognitive effects of hormone therapy in men with prostate cancer: A review. *Cancer* **2008**, *113*, 1097–1106. [CrossRef] [PubMed]
15. Kumar, R.J.; Barqawi, A.; Crawford, E.D. Preventing and treating the complications of hormone therapy. *Curr. Urol. Rep.* **2005**, *6*, 217–223. [CrossRef] [PubMed]
16. McHugh, D.J.; Root, J.C.; Nelson, C.J.; Morris, M.J. Androgen-deprivation therapy, dementia, and cognitive dysfunction in men with prostate cancer: How much smoke and how much fire? *Cancer* **2018**, *124*, 1326–1334. [CrossRef]
17. Jamadar, R.J.; Winters, M.J.; Maki, P.M. Cognitive changes associated with ADT: A review of the literature. *Asian J. Androl.* **2012**, *14*, 232–238. [CrossRef] [PubMed]
18. McGinty, H.L.; Phillips, K.M.; Jim, H.S.L.; Cessna, J.M.; Asvat, Y.; Cases, M.G.; Small, B.J.; Jacobsen, P.B. Cognitive functioning in men receiving androgen deprivation therapy for prostate cancer: A systematic review and meta-analysis. *Support. Care Cancer* **2014**, *22*, 2271–2280. [CrossRef]
19. Treanor, C.; Li, J.; Donnelly, M. Cognitive impairment among prostate cancer patients: An overview of reviews. *Eur. J. Cancer Care* **2017**, *26*. [CrossRef] [PubMed]
20. Sun, M.; Cole, A.P.; Hanna, N.; Mucci, L.A.; Berry, D.L.; Basaria, S.; Ahern, D.K.; Kibel, A.S.; Choueiri, T.K.; Trinh, Q.-D. Cognitive Impairment in Men with Prostate Cancer Treated with Androgen Deprivation Therapy: A Systematic Review and Meta-Analysis. *J. Urol.* **2018**, *199*, 1417–1425. [CrossRef]
21. Kluger, J.; Roy, A.; Chao, H.H. Androgen Deprivation Therapy and Cognitive Function in Prostate Cancer. *Curr. Oncol. Rep.* **2020**, *22*, 24. [CrossRef]
22. Lee, H.H.; Park, S.; Joung, J.Y.; Kim, S.H. How Does Androgen Deprivation Therapy Affect Mental Health Including Cognitive Dysfunction In Patients with Prostate Cancer? *World J. Men's Health* **2020**, *38*. [CrossRef]
23. Nead, K.T.; Sinha, S.; Yang, D.D.; Nguyen, P.L. Association of androgen deprivation therapy and depression in the treatment of prostate cancer: A systematic review and meta-analysis. *Urol. Oncol. Semin. Orig. Investig.* **2017**, *35*, 664.e1–664.e9. [CrossRef]
24. Cherrier, M.M.; Higano, C.S. Impact of androgen deprivation therapy on mood, cognition, and risk for AD. *Urol. Oncol. Semin. Orig. Investig.* **2020**, *38*, 53–61. [CrossRef]
25. Koskderelioglu, A.; Gedizlioglu, M.; Ceylan, Y.; Gunlusoy, B.; Kahyaoglu, N. Quality of sleep in patients receiving androgen deprivation therapy for prostate cancer. *Neurol. Sci.* **2017**, *61*, 1079–1451. [CrossRef] [PubMed]
26. Gonzalez, B.D.; Small, B.J.; Cases, M.G.; Williams, N.L.; Fishman, M.N.; Jacobsen, P.B.; Jim, H.S. Sleep disturbance in men receiving androgen deprivation therapy for prostate cancer: The role of hot flashes and nocturia. *Cancer* **2017**, *124*, 499–506. [CrossRef] [PubMed]
27. Donovan, K.A.; Walker, L.M.; Wassersug, R.J.; Thompson, L.M.A.; Robinson, J.W. Psychological effects of androgen-deprivation therapy on men with prostate cancer and their partners. *Cancer* **2015**, *121*, 4286–4299. [CrossRef] [PubMed]
28. Klaassen, Z.; Arora, K.; Wilson, S.N.; King, S.A.; Madi, R.; Neal, D.E.; Kurdyak, P.; Kulkarni, G.S.; Lewis, R.W.; Terris, M.K. Decreasing suicide risk among patients with prostate cancer: Implications for depression, erectile dysfunction, and suicidal ideation screening. *Urol. Oncol. Semin. Orig. Investig.* **2018**, *36*, 60–66. [CrossRef]
29. Watts, S.; Leydon, G.; Birch, B.; Prescott, P.; Lai, L.; Eardley, S.; Lewith, G. Depression and anxiety in prostate cancer: A systematic review and meta-analysis of prevalence rates. *BMJ Open* **2014**, *4*, e003901. [CrossRef]
30. Fervaha, G.; Izard, J.P.; Tripp, D.A.; Rajan, S.; Leong, D.P.; Siemens, D.R. Depression and prostate cancer: A focused review for the clinician. *Urol. Oncol. Semin. Orig. Investig.* **2019**, *37*, 282–288. [CrossRef] [PubMed]

31. Tucci, M.; Leone, G.; Buttigliero, C.; Zichi, C.; Di Stefano, R.F.; Pignataro, D.; Vignani, F.; Scagliotti, G.V.; Di Maio, M. Hormonal treatment and quality of life of prostate cancer patients: New evidences. *Minerva Urol. Nefrol. Ital. J. Urol. Nephrol.* **2017**, *70*, 144–151.
32. Rhee, H.; Gunter, J.H.; Heathcote, P.; Ho, K.; Stricker, P.; Corcoran, N.M.; Nelson, C.C. Adverse effects of androgen-deprivation therapy in prostate cancer and their management. *BJU Int.* **2014**, *115*, 3–13. [CrossRef] [PubMed]
33. Davidson, J.R.; MacLean, A.W.; Brundage, M.D.; Schulze, K. Sleep disturbance in cancer patients. *Soc. Sci. Med.* **2002**, *54*, 1309–1321. [CrossRef]
34. Howell, D.; Oliver, T.K.; Keller-Olaman, S.; Davidson, J.R.; Garland, S.; Samuels, C.; Savard, J.; Harris, C.; Aubin, M.; Olson, K.; et al. Sleep disturbance in adults with cancer: A systematic review of evidence for best practices in assessment and management for clinical practice. *Ann. Oncol.* **2014**, *25*, 791–800. [CrossRef] [PubMed]
35. Savard, J.; Hervouet, S.; Ivers, H. Prostate cancer treatments and their side effects are associated with increased insomnia. *Psycho-Oncology* **2012**, *22*, 1381–1388. [CrossRef] [PubMed]
36. Delpachitra, S.; Campbell, A.; Wibowo, E. Preference for sleep management strategies among prostate cancer patients: An Aotearoa/New Zealand perspective☆. *Cancer Treat. Res. Commun.* **2020**, *25*, 100219. [CrossRef]
37. Hanisch, L.J.; Gooneratne, N.S.; Soin, K.; Gehrman, P.R.; Vaughn, D.J.; Coyne, J.C. Sleep and daily functioning during androgen deprivation therapy for prostate cancer. *Eur. J. Cancer Care* **2010**, *20*, 549–554. [CrossRef] [PubMed]
38. Casey, R.G.; Corcoran, N.M.; Goldenberg, S.L. Quality of life issues in men undergoing androgen deprivation therapy: A review. *Asian J. Androl.* **2012**, *14*, 226–231. [CrossRef]
39. Savard, J.; Ivers, H.; Savard, M.-H.; Morin, C.M. Cancer treatments and their side effects are associated with aggravation of insomnia: Results of a longitudinal study. *Cancer* **2015**, *121*, 1703–1711. [CrossRef] [PubMed]
40. Trivedi, D. Cochrane Review Summary: Mini-Mental State Examination (MMSE) for the detection of dementia in clinically unevaluated people aged 65 and over in community and primary care populations. *Prim. Health Care Res. Dev.* **2017**, *18*, 527–528. [CrossRef] [PubMed]
41. Folstein, M.F.; Folstein, S.E.; McHugh, P.R. «Mini-mental state». A practical method for grading the cognitive state of patients for the clinician. *J. Psychiatr. Res.* **1975**, *12*, 189–198. [CrossRef]
42. Lobo, A.; Saz, P.; Marcos, G.; D  a, J.L.; de la C  mara, C.; Ventura, T.; Morales, F.; Fernando, L.; Monta  es, J.A.; Aznar, S. Revalidation and standardisation of the cognition mini-exam (first Spanish version of the Mini-Mental Status Examination) in the general geriatric population. *Med. Clin.* **1999**, *112*, 767–774.
43. S  nchez-Mart  nez, V.; Sales-Orts, R. Design and validation of a brief scale for cognitive evaluation in people with a diagnosis of schizophrenia (BCog-S). *J. Psychiatr. Ment. Health Nurs.* **2020**, *27*, 543–552. [CrossRef] [PubMed]
44. Soldatos, C.R.; Dikeos, D.G.; Paparrigopoulos, T.J. Athens Insomnia Scale: Validation of an instrument based on ICD-10 criteria. *J. Psychosom. Res.* **2000**, *48*, 555–560. [CrossRef]
45. G  mez-Benito, J.; Ruiz, C.; Guilera, G. A Spanish version of the athens insomnia scale. *Qual. Life Res.* **2011**, *20*, 931–937. [CrossRef] [PubMed]
46. Yesavage, J.A.; Brink, T.; Rose, T.L.; Lum, O.; Huang, V.; Adey, M.; Leirer, V.O. Development and validation of a geriatric depression screening scale: A preliminary report. *J. Psychiatr. Res.* **1982**, *17*, 37–49. [CrossRef]
47. Mart  nez de la Iglesia, J.; On  s Vilches, M.C.; Due  as Herrero, R.; Albert Colomer, C.; Aguado Tabern  , C.; Luque Luque, R. Versi  n espa  ola del cuestionario de Yesavage abreviado (GDS) para el despistaje de depresi  n en mayores de 65 a  os: Adaptaci  n y validaci  n. *Medifam* **2002**, *12*, 26–40. [CrossRef]
48. Chao, H.H.; Uchio, E.; Zhang, S.; Hu, S.; Bednarski, S.R.; Luo, X.; Rose, M.; Concato, J.; Li, C.-S.R. Effects of androgen deprivation on brain function in prostate cancer patients—A prospective observational cohort analysis. *BMC Cancer* **2012**, *12*, 371. [CrossRef]
49. Alibhai, S.M.; Mph, N.T.; Duff-Canning, S.; Breunis, H.; Tannock, I.F.; Naglie, G.; Fleshner, N.E.; Krahn, M.D.; Warde, P.; Marzouk, S.; et al. Effects of long-term androgen deprivation therapy on cognitive function over 36 months in men with prostate cancer. *Cancer* **2016**, *123*, 237–244. [CrossRef]
50. Morote, J.; Tabernerero,   .J.;   lvarez-Ossorio, J.; Ciria, J.; Dom  nguez-Escrig, J.; Vazquez, F.; Angulo, J.; L  pez, F.; De La Iglesia, R.; Romero, J. Cognitive function in patients on androgen suppression: A prospective, multicentric study. *Actas Urol. Esp.* **2018**, *42*, 114–120. [CrossRef]
51. Joly, F.; Alibhai, S.; Galica, J.; Park, A.; Yi, Q.-L.; Wagner, L.; Tannock, I. Impact of Androgen Deprivation Therapy on Physical and Cognitive Function, as Well as Quality of Life of Patients With Nonmetastatic Prostate Cancer. *J. Urol.* **2006**, *176*, 2443–2447. [CrossRef]
52. Marzouk, S.; Naglie, G.; Tomlinson, G.; Canning, S.D.; Breunis, H.; Timilshina, N.; Alibhai, S.M. Impact of Androgen Deprivation Therapy on Self-Reported Cognitive Function in Men with Prostate Cancer. *J. Urol.* **2018**, *200*, 327–334. [CrossRef]
53. Hutchinson, A.D.; Hosking, J.R.; Kichenadasse, G.; Mattiske, J.K.; Wilson, C. Objective and subjective cognitive impairment following chemotherapy for cancer: A systematic review. *Cancer Treat Rev.* **2012**, *38*, 926–934. [CrossRef]
54. Wefel, J.S.; Vardy, J.; Ahles, T.; Schagen, S.B. International Cognition and Cancer Task Force recommendations to harmonise studies of cognitive function in patients with cancer. *Lancet Oncol.* **2011**, *12*, 703–708. [CrossRef]
55. Shahinian, V.B.; Kuo, Y.-F.; Freeman, J.L.; Goodwin, J.S. Risk of the “Androgen Deprivation Syndrome” in Men Receiving Androgen Deprivation for Prostate Cancer. *Arch. Intern. Med.* **2006**, *166*, 465–471. [CrossRef] [PubMed]

56. Ryan, C.; Wefel, J.S.; Morgans, A.K. A review of prostate cancer treatment impact on the CNS and cognitive function. *Prostate Cancer Prostatic Dis.* **2019**, *23*, 207–219. [CrossRef]
57. Ivers, H.; Lacombe, L.; Fradet, Y.; Savard, J.; Simard, S.; Hervouet, S. Insomnia in men treated with radical prostatectomy for prostate cancer. *Psycho-Oncology* **2004**, *14*, 147–156. [CrossRef]
58. Barrett-Connor, E.; Dam, T.-T.; Stone, K.; Harrison, S.L.; Redline, S.; Orwoll, E.; Osteoporotic Fractures in Men Study Group. The Association of Testosterone Levels with Overall Sleep Quality, Sleep Architecture, and Sleep-Disordered Breathing. *J. Clin. Endocrinol. Metab.* **2008**, *93*, 2602–2609. [CrossRef]
59. Liu, P.Y. A Clinical Perspective of Sleep and Andrological Health: Assessment, Treatment Considerations, and Future Research. *J. Clin. Endocrinol. Metab.* **2019**, *104*, 4398–4417. [CrossRef] [PubMed]
60. Morssinkhof, M.; Van Wylick, D.; Priester-Vink, S.; Van Der Werf, Y.; Heijer, M.D.; Heuvel, O.V.D.; Broekman, B. Associations between sex hormones, sleep problems and depression: A systematic review. *Neurosci. Biobehav. Rev.* **2020**, *118*, 669–680. [CrossRef]
61. Leproult, R. Effect of 1 Week of Sleep Restriction on Testosterone Levels in Young Healthy Men. *JAMA* **2011**, *305*, 2173–2174. [CrossRef]
62. Schmid, S.M.; Hallschmid, M.; Jauch-Chara, K.; Lehnert, H.; Schultes, B. Sleep timing may modulate the effect of sleep loss on testosterone. *Clin. Endocrinol.* **2012**, *77*, 749–754. [CrossRef]
63. Smith, I.; Salazar, I.; Roychoudhury, A.; St-Onge, M.-P. Sleep restriction and testosterone concentrations in young healthy males: Randomized controlled studies of acute and chronic short sleep. *Sleep Health* **2019**, *5*, 580–586. [CrossRef]
64. Liu, P.Y.; Yee, B.; Wishart, S.M.; Jimenez, M.; Jung, D.G.; Grunstein, R.R.; Handelsman, D.J. The Short-Term Effects of High-Dose Testosterone on Sleep, Breathing, and Function in Older Men. *J. Clin. Endocrinol. Metab.* **2003**, *88*, 3605–3613. [CrossRef]
65. Lee, M.; Jim, H.S.; Fishman, M.; Zachariah, B.; Heysek, R.; Biagioli, M.; Jacobsen, P.B. Depressive symptomatology in men receiving androgen deprivation therapy for prostate cancer: A controlled comparison. *Psycho-Oncology* **2015**, *24*, 472–477. [CrossRef] [PubMed]
66. Dinh, K.T.; Reznor, G.; Muralidhar, V.; Mahal, B.A.; Nezoslosky, M.D.; Choueiri, T.K.; Hoffman, K.E.; Hu, J.C.; Sweeney, C.J.; Trinh, Q.D.; et al. Association of Androgen Deprivation Therapy With Depression in Localised Prostate Cancer. *J. Clin. Oncol. Off. J. Am. Soc. Clin. Oncol.* **2016**, *34*, 1905–1912. [CrossRef] [PubMed]
67. Chung, S.-D.; Kao, L.-T.; Lin, H.-C.; Xirasagar, S.; Huang, C.-C.; Lee, H.-C. Patients receiving androgen deprivation therapy for prostate cancer have an increased risk of depressive disorder. *PLoS ONE* **2017**, *12*, e0173266. [CrossRef]
68. Zhang, Z.; Yang, L.; Xie, D.; Shi, H.; Li, G.; Yu, D. Depressive symptoms are found to be potential adverse effects of androgen deprivation therapy in older prostate cancer patients: A 15-month prospective, observational study. *Psycho-Oncology* **2017**, *26*, 2238–2244. [CrossRef] [PubMed]
69. Gagliano-Jucá, T.; Trivison, T.G.; Nguyen, P.L.; Kantoff, P.W.; Taplin, M.-E.; Kibel, A.S.; Manley, R.; Hally, K.; Bearup, R.; Beleva, Y.M.; et al. Effects of Androgen Deprivation Therapy on Pain Perception, Quality of Life, and Depression in Men With Prostate Cancer. *J. Pain Symptom Manag.* **2018**, *55*, 307–317. [CrossRef] [PubMed]
70. Thomas, H.R.; Chen, M.-H.; D’Amico, A.V.; Bennett, C.L.; Kattan, M.W.; Sartor, O.; Stein, K.; Nguyen, P.L. Association Between Androgen Deprivation Therapy and Patient-reported Depression in Men With Recurrent Prostate Cancer. *Clin. Genitourin. Cancer* **2018**, *16*, 313–317. [CrossRef]
71. Tully, K.H.; Nguyen, D.-D.; Herzog, P.; Jin, G.; Noldus, J.; Nguyen, P.L.; Kibel, A.S.; Sun, M.; McGregor, B.; Basaria, S.; et al. Risk of Dementia and Depression in Young and Middle-aged Men Presenting with Nonmetastatic Prostate Cancer Treated with Androgen Deprivation Therapy. *Eur. Urol. Oncol.* **2021**, *4*, 66–72. [CrossRef]
72. Deka, R.; Rose, B.S.; Bryant, A.K.; Sarkar, R.R.; Nalawade, V.; McKay, R.; Murphy, J.; Simpson, D.R. Androgen deprivation therapy and depression in men with prostate cancer treated with definitive radiation therapy. *Cancer* **2019**, *125*, 1070–1080. [CrossRef] [PubMed]
73. Hervouet, S.; Savard, J.; Ivers, H.; Savard, M.-H. Depression and androgen deprivation therapy for prostate cancer: A prospective controlled study. *Health Psychol.* **2013**, *32*, 675–684. [CrossRef]
74. Tripp, D.A.; Verreault, P.; Tong, S.; Izard, J.; Black, A.; Siemens, D.R. Biopsychosocial impact of prostate cancer and androgen-deprivation therapy. *Can. Urol. Assoc. J.* **2017**, *11*, 338–343. [CrossRef]
75. Seidman, S.N. Androgens and the aging male. *Psychopharmacol. Bull.* **2007**, *40*, 205–218.
76. Westley, C.J.; Amdur, R.L.; Irwig, M.S. High Rates of Depression and Depressive Symptoms among Men Referred for Borderline Testosterone Levels. *J. Sex. Med.* **2015**, *12*, 1753–1760. [CrossRef]
77. Fischer, S.; Ehlert, U.; Castro, R.A. Hormones of the hypothalamic-pituitary-gonadal (HPG) axis in male depressive disorders—A systematic review and meta-analysis. *Front. Neuroendocr.* **2019**, *55*, 100792. [CrossRef]
78. Kische, H.; Pieper, L.; Venz, J.; Klotsche, J.; März, W.; Koch-Gromus, U.; Pittrow, D.; Lehnert, H.; Silber, S.; Stalla, G.; et al. Longitudinal change instead of baseline testosterone predicts depressive symptoms. *Psychoneuroendocrinology* **2018**, *89*, 7–12. [CrossRef]
79. Panza, F.; D’Introno, A.; Colacicco, A.M.; Capurso, C.; Del Parigi, A.; Caselli, R.J.; Frisardi, V.; Scapicchio, P.; Chiloiro, R.; Scafato, E.; et al. Temporal Relationship between Depressive Symptoms and Cognitive Impairment: The Italian Longitudinal Study on Aging. *J. Alzheimer’s Dis.* **2009**, *17*, 899–911. [CrossRef]

80. Weber, B.A.; Sherwill-Navarro, P. Psychosocial consequences of prostate cancer: 30 years of research. *Geriatr. Nurs.* **2005**, *26*, 166–175. [CrossRef] [PubMed]
81. Templeton, H.; Coates, V. Evaluation of an evidence-based education package for men with prostate cancer on hormonal manipulation therapy. *Patient Educ. Couns.* **2004**, *55*, 55–61. [CrossRef] [PubMed]
82. Cormie, P.; Zopf, E.M. Exercise medicine for the management of androgen deprivation therapy-related side effects in prostate cancer. *Urol. Oncol. Semin. Orig. Investig.* **2020**, *38*, 62–70. [CrossRef]
83. Teleni, L.; Chan, R.J.; Chan, A.; Isenring, E.A.; Vela, I.; Inder, W.J.; McCarthy, A.L. Exercise improves quality of life in androgen deprivation therapy-treated prostate cancer: Systematic review of randomised controlled trials. *Endocr. Relat. Cancer* **2015**, *23*, 101–112. [CrossRef]
84. Harvey, P.D. Clinical applications of neuropsychological assessment. *Dialog Clin. Neurosci.* **2012**, *14*, 91–99.
85. Belrose, J.C.; Noppens, R.R. Anesthesiology and cognitive impairment: A narrative review of current clinical literature. *BMC Anesthesiol.* **2019**, *19*, 1–12. [CrossRef] [PubMed]
86. Yiannopoulou, K.G.; Anastasiou, A.I.; Kontoangelos, K.; Papageorgiou, C.; Anastasiou, I.P. Cognitive and Psychological Impacts of Different Treatment Options for Prostate Cancer: A Critical Analysis. *Curr. Urol.* **2020**, *14*, 169–177. [CrossRef]
87. Gonzalez, B.D.; Jim, H.S.; Booth-Jones, M.; Small, B.J.; Sutton, S.K.; Lin, H.-Y.; Park, J.Y.; Spiess, P.E.; Fishman, M.N.; Jacobsen, P.B. Course and Predictors of Cognitive Function in Patients With Prostate Cancer Receiving Androgen-Deprivation Therapy: A Controlled Comparison. *J. Clin. Oncol.* **2015**, *33*, 2021–2027. [CrossRef] [PubMed]
88. Jim, H.S.L.; Small, B.J.; Patterson, S.; Salup, R.; Jacobsen, P.B. Cognitive impairment in men treated with luteinizing hormone-releasing hormone agonists for prostate cancer: A controlled comparison. *Support. Care Cancer* **2009**, *18*, 21–27. [CrossRef] [PubMed]
89. Mundell, N.L.; Daly, R.M.; MacPherson, H.; Fraser, S.F. Cognitive decline in prostate cancer patients undergoing ADT: A potential role for exercise training. *Endocr. Relat. Cancer* **2017**, *24*, R145–R155. [CrossRef]

MDPI
St. Alban-Anlage 66
4052 Basel
Switzerland
Tel. +41 61 683 77 34
Fax +41 61 302 89 18
www.mdpi.com

Life Editorial Office
E-mail: life@mdpi.com
www.mdpi.com/journal/life



MDPI
St. Alban-Anlage 66
4052 Basel
Switzerland
Tel: +41 61 683 77 34
www.mdpi.com



ISBN 978-3-0365-7084-6